

AFIT/DS/ENC/98J-1

Representations, Approximations, and Algorithms for
Mathematical Speech Processing

DISSERTATION
Laura R. C. Suzuki
Major, USAF

AFIT/DS/ENC/98J-1

19980629 028

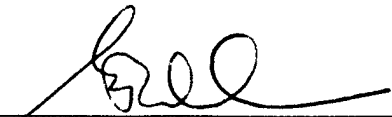
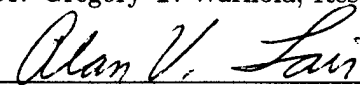
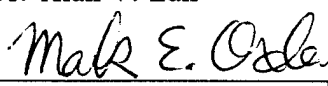

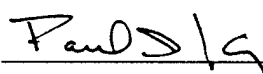
Approved for public release; distribution unlimited

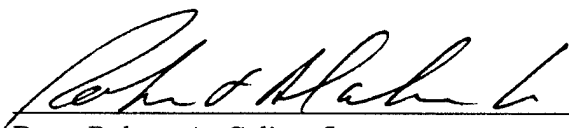
Representations, Approximations, and Algorithms for
Mathematical Speech Processing

Laura R. C. Suzuki, B.S., M.S.

Major, USAF

Approved:

 _____ Dr. Gregory T. Warhola, Research Advisor	<u>23 Apr 98</u>
 _____ Dr. Alan V. Lair	<u>4 Jun 98</u>
 _____ Dr. Mark E. Oxley	<u>23 April 98</u>
 _____ Dr. Martin P. DeSimio	<u>5 Jun 98</u>
 _____ Dr. Paul I. King, Dean's Representative	<u>4 Jun 98</u>



Dean Robert A. Calico, Jr
Graduate School of Engineering

AFIT/DS/ENC/98J-1

Representations, Approximations, and Algorithms for
Mathematical Speech Processing

DISSERTATION

Presented to the Faculty of the Graduate School of Engineering
of the Air Force Institute of Technology

Air University

In Partial Fulfillment of the
Requirements for the Degree of
Doctor of Philosophy
in Engineering

Laura R. C. Suzuki, B.S.,M.S.

Major, USAF

16 June 1998

Approved for public release; distribution unlimited

Abstract

Presented in this document is work leading to a mathematical frame tailored to speech processing. This development is based on work in three loosely-connected areas of mathematics.

The first area involves Carleson inequalities and representations in the Hardy spaces, $H_p(\mathbb{D})$, for $p > 1$. The main result of this work is the extension of a Carleson inequality theorem and a representation theorem based on it.

The second area involves mathematical frames. A frame for $L_2(\mathbb{R})$ is developed that is particularly useful for representing functions with time-varying features. Specific examples of this frame can be created adaptively to fit specific functions, for example, for use in data compression. Also in this area, a more general representation of the frame operator is presented. This alternate representation is particularly useful in that it allows for hybrid frame coefficient calculations, where the coefficients are found through a combination of iterative and exact techniques.

The third area, closely related to the first, concerns developing frames for the Hilbert space, $H_2(\mathbb{D})$. The representation theorem proven for the Hardy spaces, $H_p(\mathbb{D})$, is used to create frames for $H_2(\mathbb{D})$.

The results from these three areas are combined to create a class of frames for $L_2(\mathbb{R})$ which is well tailored to the characteristics of speech. Experiments were conducted using a computer program based on this class of frames to validate the applicability of this work to speech processing.

Acknowledgements

I wish to thank my research advisor, Dr Gregory T. Warhola, who stuck by me through some rough times. It would have been far easier for him to give up on me, but he did not.

I could not have completed this effort without the help of my research committee members, Dr Alan Lair, Dr Mark Oxley, Dr Marty Desimio, and Dr Paul King. Without their help and encouragement, I would have been unable to complete the final stage of this effort.

I owe a great deal of thanks to my husband, Yoshiaki, for keeping things running smoothly at home while I was preoccupied with research. My son Ian earned thanks by demanding some of my attention for himself, and thereby helping me to keep my life in balance.

Over the years, my fellow students have been a source of support, guidance, and inspiration. Having others around me "in the same boat" made it easier to keep my own stumbling stones and set-backs in the proper perspective. The ones ahead of me reminded me that the task at hand was achievable. Those behind me reminded me how far I had come. A few of those many students are Bruce Anderson, John and Cheryl Columbi, Kimberly Balkema Demoret, Amy Magnus, Rob Reid, Brian Smith, and Terry Wilson.

I owe special thanks to Dr Steve Rogers and Dr Matthew Kabrisky, who, although they were not on my committee, could always be counted on for support and encouragement.

Laura R. C. Suzuki

Table of Contents

	Page
Abstract	ii
Acknowledgements	iii
List of Figures	viii
List of Tables	xi
List of Symbols	xii
I. Introduction	1
II. Background	3
2.1 Speech	3
2.1.1 The speech production process	3
2.1.2 Speech production models	6
2.2 Human Hearing and Speech Perception	8
2.2.1 The physical auditory system	8
2.2.2 Simple auditory model	9
2.3 Distortion Measures	10
2.3.1 Descriptions of objective speech quality measures	10
2.3.2 Evaluations of objective speech quality measures	14
2.4 Important characteristics of speech	15
III. Representation of elements of the Hardy spaces, H_p	17
3.1 Introduction	17
3.2 Preliminaries	20
3.2.1 Hardy Spaces	20

	Page
3.2.2 The pseudo-hyperbolic metric, ρ	21
3.3 Lemmas concerning various inequalities	25
3.4 Supporting Lemmas and Theorems	28
3.5 Main result	40
3.6 Representation of elements of the Hardy spaces, $H_p(\mathbb{D})$	47
3.7 Summary	52
IV. Frames for $L_2(\mathbb{R})$ and a frame-like operator	53
4.1 Frame and frame operator properties	53
4.2 A frame for $L_2(\mathbb{R})$	58
4.3 A generalization of the frame operator.	65
4.4 Summary	73
V. Representation in $H_2(\mathbb{D})$	74
5.1 Blaschke Products	75
5.2 Frames for $H_2(\mathbb{D})$	76
5.3 Projections into the $H_2(\mathbb{D})$ frame	94
5.4 Summary	98
VI. Application to speech representation	99
6.1 A frame for speech	99
6.1.1 Description of the speech frame	99
6.1.2 Isometry between $H_2(\mathbb{D})$ and $L_2(\mathbb{R}^+)$	100
6.1.3 Frame for speech	102
6.1.4 Estimates for the bounds A and B	103
6.1.5 Frames from $H_2(\mathbb{D})$	105
6.2 Using the frame	109
6.2.1 Function represented by the sampled data	110
6.2.2 Dual frame to a windowed frame	111

	Page
6.2.3 Inner products with windowed frame elements	114
6.2.4 Representation of frame elements, $\psi_n B_n$	114
6.2.5 Choice of points $\{a_{n,k}\}$	115
6.3 The computer program	115
6.3.1 Basis set selection	116
6.3.2 Determination of offset times and analysis window sizes	116
6.3.3 A parameter for internal rescaling	117
6.3.4 Basis selection	117
6.3.5 Approximation coefficients	118
6.4 Summary	118
VII. Computer experiments	120
7.1 Fine-scale analyses	121
7.1.1 Description of fine-scale analyses	121
7.1.2 Discussion of results	123
7.2 Medium-scale analyses	150
7.2.1 Description of medium scale analyses	150
7.2.2 Discussion of results	152
7.3 Large-scale analysis	179
7.3.1 Description of large scale analyses	179
7.3.2 Discussion of results	182
7.4 Summary	198
VIII. Conclusions	199
Appendix A. A Space of Speech	201
A.1 Abstract Speech Space	201
A.1.1 Desired characteristics of the space	201
A.1.2 Description of the Abstract Speech Space, (S, d)	202

	Page
A.2 Linear System Background	211
A.2.1 Linear Systems	212
A.2.2 Linear System Representation of Speech	221
Appendix B. Additional proofs	224
B.1 Additional proofs from Chapter III	224
B.2 Proof of Theorem 3.6.1	232
Appendix C. Heuristic algorithm for finding glottal pulses	239
Bibliography	244

List of Figures

Figure		Page
1.	Glottal pulses	4
2.	Whispered excitation	5
3.	Formant structure and effects	6
4.	Simple speech production model	7
5.	Data used for fine-scale analysis	124
6.	Fourier transform of data used for fine-scale analysis	125
7.	Approximation sequence for phoneme /IY/	128
8.	Fourier transform of approximation sequence for phoneme /IY/	129
9.	Approximation sequence for phoneme /OY/	130
10.	Fourier transform of approximation sequence for phoneme /OY/	131
11.	Approximation sequence for phoneme /S/	132
12.	Fourier transform of approximation sequence for phoneme /S/	133
13.	Approximation sequence for <i>blocks</i>	134
14.	Fourier transform of approximation sequence for <i>blocks</i>	135
15.	Approximation sequence for <i>bumps</i>	136
16.	Fourier transform of approximation sequence for <i>bumps</i>	137
17.	Approximation sequence for <i>bumpstx</i>	138
18.	Fourier transform of approximation sequence for <i>bumpstx</i>	139
19.	Approximation sequence for <i>doppler</i>	140
20.	Fourier transform of approximation sequence for <i>doppler</i>	141
21.	Approximation sequence for <i>heavisine</i>	142
22.	Fourier transform of approximation sequence for <i>heavisine</i>	143
23.	Number of poles vs. L_2 error	144
24.	Data offset vs. L_2 error (/IY/, one pulse)	146
25.	Data offset vs. L_2 error (/OY/, one pulse)	147

Figure	Page
26. Data offset vs. L_2 error (/IY/, two pulses)	148
27. Data offset vs. L_2 error (/OY/, two pulses)	149
28. Speech data segments used in medium-scale analysis	152
29. Spectrograms of speech segments used in medium-scale analysis	153
30. Non-speech data segments used in medium-scale analysis	154
31. Poles chosen for approximations (phoneme /IY/, three pole approximations)	156
32. Poles chosen for approximations (phoneme /IY/, six pole approximations)	157
33. Poles chosen for approximations (phoneme /IY/, 10 pole approximations)	158
34. Poles chosen for approximations (phoneme /IY/, 32 pole approximations)	159
35. Poles chosen for approximations (phoneme /OY/, three pole approximations)	160
36. Poles chosen for approximations (phoneme /OY/, six pole approximations)	161
37. Poles chosen for approximations (phoneme /OY/, 10 pole approximations)	162
38. Poles chosen for approximations (phoneme /OY/, 32 pole approximations)	163
39. Number of iterations vs. normalized error (phoneme /IY/, three pole approximations)	164
40. Number of iterations vs. normalized error (phoneme /IY/, six pole approximations)	165
41. Number of iterations vs. normalized error (phoneme /IY/, 10 pole approximations)	166
42. Number of iterations vs. normalized error (phoneme /IY/, 32 pole approximations)	167
43. Number of iterations vs. normalized error (phoneme /OY/, three pole approximations)	168
44. Number of iterations vs. normalized error (phoneme /OY/, six pole approximations)	169
45. Number of iterations vs. normalized error (phoneme /OY/, 10 pole approximations)	170
46. Number of iterations vs. normalized error (phoneme /OY/, 32 pole approximations)	171

Figure	Page
47. Number of iterations vs. normalized error (phoneme /OY/, non-aligned) .	172
48. Number of iterations vs. normalized error (phoneme /OY/ reversed, non-aligned)	173
49. Number of iterations vs. normalized error (<i>Lenna</i> , non-aligned)	174
50. Number of iterations vs. normalized error (phoneme /OY/, aligned)	175
51. Error for approximations of various non-speech and speech samples	176
52. Segments used in <i>Lenna</i> and /OY/ (non-aligned)	177
53. Fourier transform of segments used in <i>Lenna</i> and /OY/ (non-aligned) . . .	178
54. Spectrograms of clean and noisy speech (<i>sa1</i>)	180
55. Spectrograms of clean and noisy speech (<i>sx194</i>)	181
56. Error for approximations of clean and noisy speech (<i>sa1</i> , 6 dB SNR) . . .	189
57. Error for approximations of clean and noisy speech (<i>sx194</i> , 6 dB SNR) . .	190
58. Error for approximations of clean and noisy speech (<i>sa1</i> , varying SNR) . .	191
59. Error for approximations of clean and noisy speech (<i>sx194</i> , varying SNR) .	192
60. Spectrograms of approximations of clean speech	193
61. Spectrograms of approximations of noisy speech	194
62. Spectrograms of approximations for different noise levels	195
63. Spectrograms of approximations of clean speech with differing window overlaps.	196
64. Time varying glottal excitation shape and impulse response	205
65. Weighting Function used in Glottal Pulse Finding Heuristic Algorithm . .	240
66. Glottal Pulses Found in Samples of Clean Speech	242
67. Glottal Pulses Found in Samples of Noisy Speech	243

List of Tables

Table		Page
1.	Minimum and maximum error for different analysis window offsets	145
2.	Compression ratios	182
3.	L_2 difference between clean speech and approximations	197

List of Symbols

Symbol	Description
$\partial\mathbb{D}$	Boundary of \mathbb{D} , i.e., the unit circle in \mathbb{C}
$\#\{\cdot\}$	Cardinality of set $\{\cdot\}$
$\lceil \cdot \rceil$	Ceiling function, i.e., the least integer upper bound
1_X	Characteristic function on the set X
\overline{X}	Closure of the set X
\mathbb{C}	The set of complex numbers
\mathbb{C}^+	The subset of \mathbb{C} such that for $z \in \mathbb{C}^+$, $\operatorname{Re}(z) > 0$
\mathbb{D}	Open unit disk in \mathbb{C}
$H_p(\mathbb{D})$	The Hardy space ($0 < p < \infty$) on \mathbb{D} with norm $\ f\ _p = \sup_{0 < r < 1} (\int_{\partial\mathbb{D}} f(rz) ^p d\sigma(z))^{1/p}$
$H_\infty(\mathbb{D})$	The Hardy space on \mathbb{D} with norm $\ f\ _\infty = \sup_{ z < 1} f(z) $
$H_2(\mathbb{C}^+)$	The Hilbert space on \mathbb{C}^+ with norm $\ f\ _{H_2(\mathbb{C}^+)}^2 = \lim_{x \rightarrow 0^+} \int_{-\infty}^{\infty} f(x + iy) ^2 dy$
$L_2(X)$	The Hilbert space of Lebesgue measurable, 2-integrable functions over X with norm $\ f\ _{L_2}^2 = \int_{t \in X} f(t) ^2 dt$
$L_p(X)$	The Banach space of Lebesgue measurable, p-integrable functions ($0 < p < \infty$) over X with norm $\ f\ _{L_p}^p = \int_{t \in X} f(t) ^p dt$
$L_\infty(X)$	The Banach space of Lebesgue measurable, essentially bounded functions over X with norm $\ f\ _{L_\infty} = \operatorname{ess\,sup}_{t \in X} f(t) $
$K(a, r)$	Pseudo-hyperbolic ball in \mathbb{D} about point a of radius r
ρ	Pseudo-hyperbolic metric on \mathbb{D}
\mathbb{R}	The set of real numbers
\mathbb{R}^+	The set of positive real numbers
\xrightarrow{u}	Uniform convergence
\mathbb{Z}	The set of integer numbers
\mathbb{Z}^+	The set of positive integer numbers, a.k.a., the natural numbers

Representations, Approximations, and Algorithms for Mathematical Speech Processing

I. Introduction

The motivation driving this work was the desire for a mathematical construct which is suitable for the representation of human speech. This goal resulted in mathematical work being done in three different areas of mathematics. Since the connection among these areas is not obvious, being defined by the desired representation for speech, an attempt will be made to provide a clear road map in this introduction.

The work presented in this document touches on three main areas, and culminates with a mathematical frame for $L_2(\mathbb{R})$ which is tailored to the representation of speech. The areas of work are representation of the Hardy spaces, $H_p(\mathbb{D})$, for $p > 1$, mathematical frames for $L_2(\mathbb{R})$, and mathematical frames for the Hardy space $H_2(\mathbb{D})$.

Since the concept of a mathematical frame, which is relatively new, is referred to frequently in this introduction, a brief description of a frame and why they are useful is appropriate here. A mathematical frame in a separable Hilbert space is a special kind of set of vectors which may be non-orthogonal and may be over-complete, i.e., linearly dependent. It is a spanning set in that any element of the Hilbert space may be represented as a linear combination of elements of the frame. While a frame may be over-complete, it cannot be too much so. A more rigorous definition of the frame and its associated frame operator are given in Definition 4.1.1.

I felt that a basic building block was needed for the desired speech representation. This building block should capture some of the basic characteristics of human speech over short periods of time. In addition, these building blocks should be compatible with the real world constraints imposed by the way speech is recorded for speech processing purposes. Such building blocks were found as the result of an extension to a representation theorem for the Hardy spaces, $H_p(\mathbb{D})$. These building blocks can be used via a frame for $H_2(\mathbb{D})$ based on them. By way of the Laplace transform, such a frame becomes a frame for $L_2(\mathbb{R}^+)$. As a result, a frame is developed which is tailored to the representation of short segments of recorded speech.

To represent longer segments of speech, the short-duration building blocks needed to be combined in some appropriate way. Independent of the $H_p(\mathbb{D})$ and $L_2(\mathbb{R}^+)$ representations above, a frame for $L_2(\mathbb{R})$ is developed based on a frame or set of frames for $L_2(\mathbb{R}^+)$. This construct has properties which make it suitable for effective speech processing.

Combining these two, one has a frame which can well represent the slowly time-varying, harmonic structure of speech, while still being able to represent the non-harmonic components of speech.

Additional results were found which aid in the numerical processing involved in finding frame representations of specific examples of recorded speech. An alternate representation of the frame operator is given which lends itself to more stable and efficient computation of frame representations. By viewing the operator as the sum of weighted projections onto subspaces, it becomes possible to recursively nest frames, allowing for more tractable inverse frame operator computations. This representation is especially useful in working with the above-mentioned speech frame for lengthy segments of speech.

To summarize, basic building blocks for speech representation are found via representations in $H_p(\mathbb{D})$. These building blocks are combined into a construct useful for speech representation using frames for $L_2(\mathbb{R}^+)$ and $L_2(\mathbb{R})$. The resulting construct – a frame suitable for speech representation – is made more practical by an alternate representation of frame operators which yields numerically more tractable frame calculations.

Chapter II discusses some useful background on speech and hearing – useful in that there are physiological considerations when developing speech representations for auditory use. Chapter III presents an extension to an $H_p(\mathbb{D})$ representation theorem. Chapter IV presents a frame for $L_2(\mathbb{R})$ as well as the alternate representation of the frame operator. The frame for $H_2(\mathbb{D})$ is presented in Chapter V. These results are combined in Chapter VI to yield a frame for speech processing. The results of experiments done with a computer implementation based on this construct are presented in Chapter VII.

II. Background

In order to work well with speech signals, one must have some understanding of how speech is created and perceived. This is particularly pertinent here since many of the “obvious” approaches to working with signals can lead to perceptually unacceptable results when applied to speech.

A review of the speech production process will now be given. Following that, some of the more successful speech production models will be reviewed. In addition, the human auditory system and its characteristics will be discussed along with some of the simple auditory models. Finally, existing distortion measures and their performances are discussed.

2.1 Speech

In order to represent speech well, one must have some understanding of how it is produced. This section describes the speech production process, the characteristics that this process imposes on speech and some of the simple, yet effective, speech production models.

Before beginning these discussions, it will be helpful to describe a very useful tool in speech analysis, the spectrogram. The spectrogram is a three-dimensional plot of time vs. frequency with the third dimension being the spectrum value at that time and frequency. The spectrum is the magnitude of the windowed Fourier transform. In a spectrogram, the magnitude is usually represented with color or gray-scale intensity, yielding two-dimensional pictures that are meaningful and easily interpreted. The primary reason for the usefulness of the spectrogram in speech analysis is that it, in a very real sense, mimics the frequency analysis which is done in the ear, which will be discussed in more detail later.

2.1.1 The speech production process [23]. The physical speech production process is quite complicated and involves the entire respiratory system. However, speech can, quite simply, be thought of as the output produced when a stream of air produced by the lungs is modified by the various parts of the vocal tract. Both the shaping of the vocal tract and the characteristics of the source air stream can be independently changed (to some extent). These changes modify the characteristics of the air stream, which carry the information that is contained in “speech.”

The whole vocal tract plays a part in the modifications to the air stream, but there are two main classes of modification. The first is *excitation*, the process by which frequency

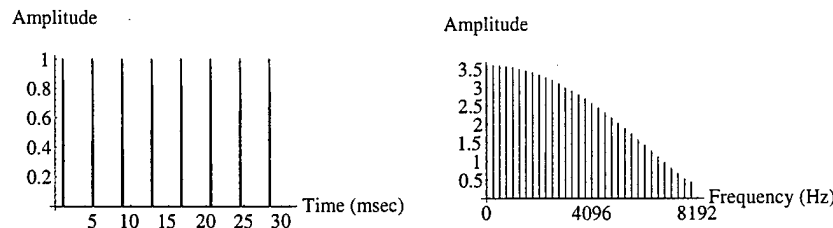


Figure 1. Simplified glottal pulses. (a) Amplitude vs. Time. (b) Spectrum Amplitude vs. Frequency

content is added. The second class of modification is caused by *linear filtering* (sometimes referred to as *modulation* [23]), by which the shape of the vocal tract induces changes in this frequency content. The nature of these changes as well as the nature of the underlying frequencies are what convey the information content in speech to the listener.

2.1.1.1 Excitation sources. The most important excitation source is the vocal cords. There are two main modes of excitation produced by the vocal cords. In the first, called *phonation*, the vocal cords repeatedly open and close. This interruption of the airflow produces air pulses, called *glottal pulses*. Usually, these pulses occur at regular intervals, but can become irregular, especially during unstressed portions of speech and near the ends of sentences. The shape of the glottal pulses varies greatly, from speaker to speaker, with pitch (fundamental voice frequency), etc. [23:115]. Because glottal pulses are usually regularly spaced, they add mainly harmonic frequency content to speech. Speech in which phonation takes place is called *voiced*, and that without, *unvoiced*. Figure 1 shows some simplified glottal pulses and the magnitude of their Fourier transform.

The second main mode of excitation from the vocal cords is called *whispering*. In this mode, the vocal cords are contracted, but not closed, so that only a small opening remains for the air to go through. This produces turbulence which causes wideband noise. This noise is the basis for whispered speech and for normal unvoiced speech. Figure 2 shows a simplification of such whispered excitation.

Phonation and whispering form the basis for most speech sounds. However, there are other sources of excitation in the vocal tract also. Three important ones are called *friction*, *compression*, and *vibration*, and are mainly used to form different consonants.

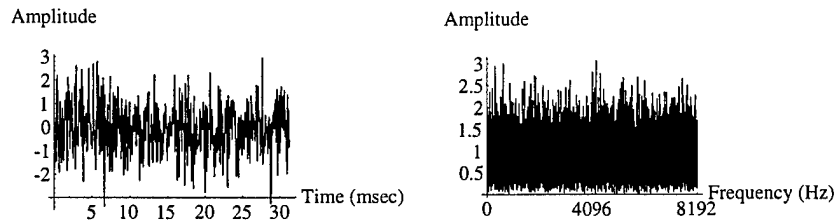


Figure 2. Whispered excitation. (a) Amplitude vs. Time. (b) Spectrum Amplitude vs. Frequency.

Frication is caused when the vocal tract is tightly constricted at some point other than at the vocal cords (e.g., tongue/roof-of-mouth, lips, etc.) The air flow past the constriction causes turbulence, which causes broadband noise (*fricative* sounds).

Compression is caused when the vocal tract is completely closed at some point other than at the vocal cords. The release of the pressure can be abrupt (*plosive* sounds) or can blend together with a following fricative (*affricative* sounds).

Vibration is caused by air being forced through a closure other than at the vocal cords. These vibrations add additional frequency content to the sound.

2.1.1.2 Frequency Modification. The frequency content of the sound is further modified by the shape of the vocal tract itself. The vocal tract transmits certain frequencies more efficiently than others, depending upon its shape. Relative peaks in frequency transmission are called *formants*. As the shape of the vocal tract is changed, the amount of each frequency which is passed changes also, which changes the sound of the speech. Figure 3 shows an example of a formant structure (shown in the Fourier domain) and the effect it has on the frequency content of a stream of glottal pulses.

This formant information is of primary importance in the perception of vowels, and vowels are conveyed almost solely in the formant information. However, it is also an important clue in the identity of consonants, because the consonant adjacent to a vowel affects the formant structure “at the edges” of the vowel [21]. This inter-modification of adjacent sounds is called *co-articulation*. So, although most languages transfer most of their information content in the consonants, the adjacent (linguistically less important [23]) vowels convey important clues about the identity of the consonants [23].

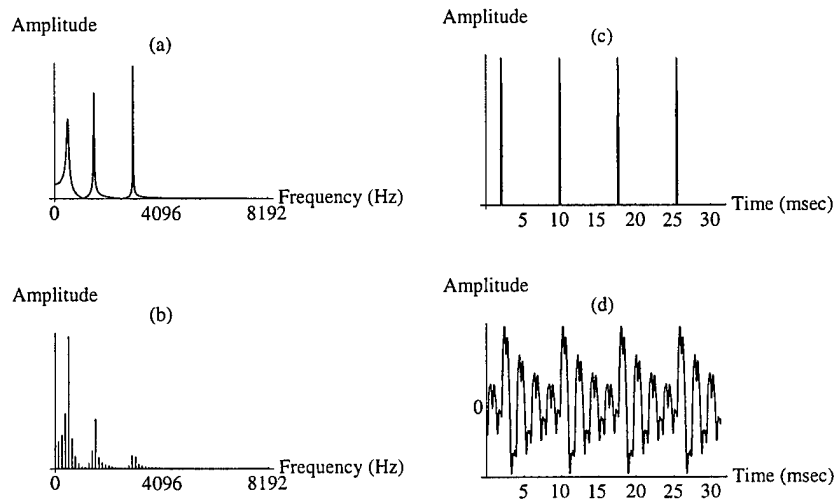


Figure 3. Formant structure and its effects on the frequency content in voiced speech. (a) Formant structure in frequency domain. (b) Effect on spectrum of simplified voiced excitation. (c) Original excitation. (d) Excitation after linear filtering.

While the speech production process is quite complex, some of the successful models of it are quite simple. The following section discusses some of the simpler speech production models and the simplifying assumptions employed to create them.

2.1.2 Speech production models. There are two differing philosophies on modeling speech production. One way is to model the actual vocal tract (shape, motions, etc.) and the motion of the air through it. This is quite difficult and computationally expensive, and until recently, the computing resources necessary to do such work were not readily available [13]. However, experience in speech synthesis has shown reasonably good results can be achieved by ignoring the actual vocal tract and the complexities of the air flow through it. Instead, the glottal excitation can be simplified to a one-dimensional input and the effects of the vocal tract simplified to the effects of a linear system on that input.

The simplest models take the form shown in Figure 4. Here, the excitation source input to the “black box” vocal tract is the air flow from the lungs after it has been excited by the vocal cords. Often, this glottal excitation is assumed to take the form of a train of pulses (for voiced speech) or white noise (for unvoiced speech), but current work continues in the development of new glottal excitation models [27]. The vocal tract is modeled as a causal, linear, time-invariant system, usually as one that can be represented by an all-pole

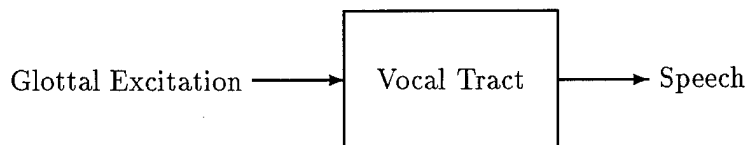


Figure 4. Simple speech production model. Vocal tract modeled as a linear system with an input of “glottal excitation” and producing as output, “speech.”

or a pole-zero model. The output (speech) from a given input (excitation) and fixed vocal tract configuration at time t is given by

$$s(t) = \int_0^t x(\tau)h(t - \tau) d\tau$$

where s is the speech signal, x is the excitation source, and h is the impulse response of the vocal tract. Notice that h is time-invariant, so to model speech (where the vocal tract varies with time) using this method would require that the output produced by different values of h be spliced together in some way.

It is more desirable to model the vocal tract as a time-varying linear system. For such a system, the output is given by

$$s(t) = \int_0^t x(\tau)v(t, \tau) d\tau$$

where x is as given before and $v(t, \tau)$ is the system response at time t to an impulse at time τ .

This type of model can quite easily model vowels and other vocalic sounds. In its simplest form, it is widely used for speech analysis and synthesis [23], although it does not provide for the cases where excitation occurs at additional points other than the vocal cords (e.g., fricatives), or where the air flow characteristics are significantly changed (e.g., plosives). An enhanced model is necessary to provide a more natural representation of these, but this is seldom done in practice, since good results have been achieved with the simpler model [23].

2.2 Human Hearing and Speech Perception

In order to develop an appropriate representation of speech, it is necessary to study some of the details of how the ear and brain process sound. This section discusses some of the information pertinent to the understanding of the human auditory system.

2.2.1 The physical auditory system [21, 23, 32, 28]. Sound (compression waves in air) enters the auditory system through the meatus (auditory canal). It is modified en route by the effects of the pinna (outer ear). These effects consist mainly of frequency filtering and amplitude reduction. The sound waves cause the tympanic membrane (ear drum) to vibrate. The ear drum is connected to the cochlea at the oval window through a linkage of three bones. These bones act as an impedance matching device which matches the acoustical impedance between air (outside the cochlea) and cochlear fluid.

The cochlea is a fluid-filled, spiral-shaped structure completely enclosed in bone except for two membrane-covered openings, the oval and round windows. It is divided along almost all its length by two membranes, the basilar membrane and Reissner's membrane. These divide the cochlea into three passages, the scala vestibuli, the scala media, and the scala tympani. The outer two of these three, the scala vestibuli and the scala tympani, are connected at the far end (farthest from the oval and round windows) at an opening called the helicotrema. The oval window interfaces with the scala vestibuli and the round window with the scala tympani.

Since the cochlea is enclosed in rigid bone except for the membrane covered oval and round windows, and is filled with an (almost) incompressible fluid, any vibration of the oval window must cause a corresponding vibration in the round window. That is, when the oval window is deflected inward, the round window is almost immediately deflected outward. Since the scala vestibuli and scala tympani are connected at the far end, vibrations of the oval window cause a corresponding vibrating displacement along the basilar membrane. Due to the nature of the auditory system, experiments to determine this displacement are quite difficult to conduct. However, the results of such experiments have shown that for a constant frequency tone (i.e., sinusoidal wave), the pattern of displacement is easy to categorize. The amplitude of displacement gradually increases to a maximum at a frequency-dependent distance along the basilar membrane, and then drops off more rapidly. The lower the frequency, the farther along the basilar membrane from the oval window this maximum occurs. Thus the frequency content of sound is distributed along the basilar membrane, in a manner similar to a spectrogram. The relationship between

displacement along the basilar membrane and frequency is roughly logarithmic above 800 Hz, and becomes more linear at lower frequencies.

Along the length of the basilar membrane, within the scala media, is a structure called the organ of Corti. The tectorial membrane also runs the length of the basilar membrane and lies above the organ of Corti. Hair cells projecting from the organ of Corti touch the tectorial membrane and shear between the tectorial and the basilar membrane cause the hair cells to move. This motion triggers nerve firings, the rates of which are somewhat (but not entirely) related to the amplitude of the vibrations.

Early experimenters working with cadavers came to the conclusion that the frequency selectivity of any given location on the basilar membrane was very low (i.e., any given location responded well to a broad range of frequencies); so theorists had trouble accounting for the rather good frequency resolution that is exhibited by most humans. More recent work with live animal subjects has revealed that the cochlea is not entirely a passive “spectrum analyzer.” It has been found that the auditory system actively tunes itself, so that in a living subject in good physiological condition, the frequency selectivity of a given location on the basilar membrane is much better than for one in poor physiological condition [21]. This active tuning mechanism, or at least its effects, must be accounted for in good models of the auditory system.

Since each location along the basilar membrane responds best to a different frequency, the location of maximum vibration is believed to be an important source of frequency information to the brain (the *place theory*). However, due to a phenomena called *phase locking*, which, for frequencies less than 5kHz, causes the nerve cells to fire at approximately the same phase of a sound wave every time, temporal information on the frequency is available also. That is, for given frequency f , all nerve cells corresponding to a frequency in a small neighborhood of f fire at the frequency f . The theory that this information is the primary source of frequency discrimination is called the *temporal theory*. Some research indicates that both place and temporal information is used [21, 23, 31].

2.2.2 Simple auditory model. Many of the most useful auditory models model the displacement of the basilar membrane generated by a sound as the output of an array of filter banks. Due to the causal nature of hearing and the finite time domain response possible in the auditory system, a type of filter chosen is a causal finite impulse response (FIR) filter. Much research has been done to determine the shapes of actual “auditory filters” at different locations along the basilar membrane [21].

Given the filter bank model of the cochlea, the displacement of the basilar membrane due to an input sound at a distance s from the cochlea base is given by

$$y_s(t) = (h_s * x)(t),$$

where y_s is the displacement as a function of time, t ; x is the input to the ear as a function of time; h_s is the impulse response corresponding to location s on the basilar membrane; and the asterisk is used to denote convolution.

The active tuning mechanism of the ear must also be modeled before nerve firing rates can be estimated. Although the actual mechanism by which the ear does this is not yet certain, it is sometimes modeled as a lateral inhibition network (LIN). In a LIN, strong activity in one neuron can inhibit weaker activity in adjacent neurons, causing the activity of these neurons to decrease even more.

2.3 Distortion Measures

Distortion and quality assessment measures are of great interest for many commercial applications. For this reason, much work has been put into developing and evaluating such measures, since accurate measures aid in the development of high quality transmission techniques.

Although the only generally accepted, general-purpose (i.e., can be used for any transmission technique) quality assessment measure is to have the system evaluated by a panel of trained listeners, this type of subjective measure is expensive and slow. Therefore, accurate objective measures, which can be automated, are being sought.

Below, different classes of objective quality measures are described and their performance reviewed. This information is used to help justify the structure of speech space in the following chapter.

2.3.1 Descriptions of objective speech quality measures. Objective speech quality measures in use today may be placed in four categories. The first category consists of measures that compare the actual waveforms of the original and distorted speech. This kind of measure is of use only when the distortion does not change the basic shape of the waveform. The second category consists of measures that compare parameters based on production models of speech. These can be applied to a wider range of distortion types, but may not work well on distortions that cannot be reproduced using the production model

basis of the measure. The next category consists of measures based on auditory models. These work well on a wide range of distortions but are computationally expensive. The last category consists of measures that combine multiple measures into one. The advantage here is that it is possible to combine different types of measures, that individually may not perform well, to yield superior performance.

A common enhancement of the above categories is to separate the speech into frequency bands and to perform the analysis on each frequency band separately. The results of each frequency band analysis can then be weighted independently. Additionally, all of these techniques can be further tailored by pre-classifying sounds (into, e.g., *fricative*, *vocalic*, and *nasal*) and using specific measures that perform well with the appropriate class [25].

An introduction to objective speech quality measures can be found in [25], where many of the older and recent measures (up through 1985) are described along with results of their extensive testing. Except where otherwise indicated, the descriptions below are based on those presented in [25], although the categorization is mine.

2.3.1.1 Waveform comparison measures. Waveform comparison techniques compare the waveforms of the original and distorted speech directly and attempt to assess the importance of the differences between them. Hence, this sort of objective measure is suitable for use only with distortions for which the waveform itself is well preserved. That is, if the waveform is not well preserved or is simply shifted in time, these measures may indicate large differences in perceptually identical speech.

One of the simplest objective quality measures is the ℓ_2 norm, given by

$$\|x_\phi - x_d\|^2 = \sum_n |x_\phi(n) - x_d(n)|^2,$$

where x_ϕ and x_d represent the sampled original and distorted signal, respectively. However, it yields quite poor results when applied to speech problems, and thus is never used. Specifically, the energy difference and perceptual difference are not correlated across a wide range of distortions.

Much more useful are variants of the signal-to-noise ratio (SNR). SNR measures compare the energy of the signal with the energy of the noise (defined as the difference

between the original and distorted signal). While the classical SNR, defined by

$$SNR = 10 \log_{10} \left[\frac{\sum_n x_\phi^2(n)}{\sum_n |x_\phi(n) - x_d(n)|^2} \right]$$

where x_ϕ is the original speech signal and x_d is the distorted speech, has been found to be of little use for speech quality, some segmental variants of the SNR are quite good. Particularly, the Frequency Weighted segmental SNR, where the SNR is calculated for different time segments and frequency bands, can be constructed to correlate quite well with perceptual quality. These variants are generally of the form

$$FW\ SNR = \frac{10}{M} \sum_{m=0}^{M-1} \left(\frac{\sum_j W(m, j) 10 \log_{10} [\sigma_{\phi, m, j}^2 / \sigma_{n, m, j}^2]}{\sum_j W(m, j)} \right)$$

where M is the number of segments, m is the segment index, j is the frequency band index, $W(m, j)$ is a weight for segment m and frequency band j , and $\sigma_{\phi, m, j}^2$ and $\sigma_{n, m, j}^2$ are the variances for band j and segment m of the original speech and noise, respectively.

2.3.1.2 Production model based comparison measures. Production model based techniques are generally based on the linear prediction coding (LPC) coefficients of the original and distorted speech. The importance of these differences is analyzed in various ways.

In the so-called LPC Parameter Measures, the speech is segmented in time, and parameters are calculated for the original and distorted speech based on the LPC coefficients calculated for each segment. These parameters are then compared for each segment according to

$$d(Q, p, m) = \left(\frac{1}{N} \sum_{k=1}^N |Q(k, m, \phi) - Q(k, m, \delta)|^p \right)^{1/p}$$

where $d(Q, p, m)$ is the distance for segment m using parameters defined by Q and power p for $1 < p < \infty$, N is the number of parameters, and $Q(k, m, \phi)$ and $Q(k, m, \delta)$ are the k th parameters for segment m of the original and distorted speech, respectively. The distances for each segment are combined according to

$$D(p) = \frac{\sum_{m=1}^M W(m) d(Q, p, m)}{\sum_{m=1}^M W(m)}, \quad (1)$$

where $D(p)$ is the overall measure, M is the number of segment, and $W(m)$ is the weight for segment m . Different measures can be easily developed by producing different parameter definitions.

The log-likelihood ratio measures use the LPC coefficients also, but in a different way. Here, the assumption is that the speech and distorted speech can both be represented well by the all-pole vocal tract transfer function model over short segments. The distance measure for segment m is given by

$$d(\vec{a}_d, \vec{a}_\phi, m) = \log \left(\frac{\vec{a}_d^T \mathbf{R}_\phi \vec{a}_d}{\vec{a}_\phi^T \mathbf{R}_\phi \vec{a}_\phi} \right),$$

where \vec{a}_d and \vec{a}_ϕ represent the LPC coefficients for the distorted and original speech, respectively, \mathbf{R}_ϕ represents the autocorrelation matrix of the original speech, and the superscript T denotes the transposition operation. It can be shown that the resulting value is never negative. These values are combined into an overall measure in a similar way to that done above in (1).

2.3.1.3 Auditory model-based comparison measures. The basis of auditory based comparison measures is generally the short-time spectrum (magnitude windowed Fourier spectrum) of the speech. The attitude of those in the speech quality field is best summarized by the following quote:

It is widely felt that distortions in the envelope of the short-time speech magnitude spectrum are the main determinants of speech quality. [25:pg 36]

This belief is fostered by the successes enjoyed using these techniques, which continues to fuel work in this area.

All of the methods discussed here use the magnitudes of the short-time spectrum to compute the measure. The reason that the short-time spectrum is considered an auditory model is that for many years (beginning in 1843 with Ohm's acoustic law [31]) the basilar membrane was considered to be performing something equivalent to a frequency analysis on incoming sound, which was considered to be well represented by a short-time Fourier spectrum. These measures are generally of the form

$$d(p, m) = \left| \frac{\sum_{k=1}^N W[V_\phi(m, k), V_d(m, k), k] |F(m, k)|^p}{\sum_{k=1}^N W[V_\phi(m, k), V_d(m, k), k]} \right|^{1/p}$$

where $d(p, m)$ is the distance for segment m using power p for $0 < p < \infty$, N is the number of frequency bands, $V_\phi(m, k)$ and $V_d(m, k)$ are the magnitude spectra for band k of the original and distorted speech, respectively, W is a weighting factor, and F is some measure of spectral difference. The measure F can take on many forms, linear or non-linear. As before, the segment differences can be combined according to (1) above.

A distinctly different and slightly more sophisticated method is the Weighted Slope Spectral Distance measure. In this technique, the rates of change (slopes) of different magnitude spectral bands are used in addition to the values of the bands themselves, to put more emphasis on the location of the spectral peaks than on their heights.

2.3.1.4 Composite comparison measures. Since objective measures perform with different degrees of accuracy on different types of distortions, it is logical to try to combine different measures together in hopes of seeing an overall improvement. Using a regression model describable as

$$\hat{y}_i = b_0 + \sum_{j=1}^k b_j x_{ij}$$

where x_{ij} is an objective variable, b_j is a regression coefficient, and \hat{y}_i is the estimate of composite acceptability. Quackenbush *et al* [25] tried various combinations of the previously described models as well as combinations of parametric models. They tuned the parameters for best performance on their database to provide upper bounds on model performance.

In [14], Hayashi and Kitawaki noted that for high quality speech, preferences are based on how easily noise that is just above the detection threshold can be detected in a given frequency band. They propose to measure this by linearly combining three different measures, the segmental SNR, the COSH (a measure of how closely the spectrum of the noise resembles the shape of the spectrum of the speech), and the similarity in the power envelopes of the source and noise in the time domain. They also use multiple regression analysis to optimize their performance.

2.3.2 Evaluations of objective speech quality measures. Over a 10 year period (1975-1985), Quackenbush *et al* [25] performed detailed analyses of many types of objective measures using a carefully constructed database. The basis against which they judged the objective measures was the results of a carefully conducted subjective listening test against the same database.

They examined standard measures in the field as well as newer ones and also developed some composite measures which combine various simpler measures, optimized for use with their extensive database. For each technique, they attempted to optimize performance on their database, in order to provide information on the upper bounds of performance. The figures of merit used to determine performance were an estimate of the correlation coefficient between the subjective and objective measures and an estimate of the variance of the error. The authors note that the computed values are of use only when comparing results from the same database.

Of the non-composite measures, the “best” results were obtained by a variant of the frequency variant segmental SNR. However, this technique is applicable only to a limited class of distortions, and so is of little interest in this study. Many of the spectral distance based measures did quite well, as did the LPC-based log-area ratio.

Of the composite measures, Quackenbush and his coworkers were able to design measures that did better than any of the simpler measures, with the exception of the limited-usefulness waveform comparison measures. Better results were achieved by combining dissimilar measures rather than similar ones. Despite this success, it must be noted that these composite measures were optimized on their specific database and may not perform as well on another.

For Hayashi and Kitawaki’s measure, they achieved excellent results when using all three measures, but much poorer results when using only one or two. This supports the idea that combining dissimilar methods can yield superior results [14].

2.4 Important characteristics of speech

In this section, the characteristics of speech that should be well represented and preserved in a “speech space” are stated. Information from the previous sections will be summarized and some new information will be introduced.

As seen from the success of the spectral-based distortion measures, the magnitude spectrum is an important feature of speech. Additional support for this view comes from [3, 29, 30], where the intelligibility degradation due to differing amounts of spectral smearing is studied.

Magnitude spectrum alone is not the sole determinant of speech quality, however; phase information is important, too. Leek and Summers [19] found that in subjects with normal hearing, spectral discrimination was slightly better with “peaked” waveforms (in

which the phase information resembles that of voiced speech) than with waveforms produced by other phase conditions. This lends support to the idea that high quality speech processing techniques should produce waveforms in which the phase as well as the magnitude spectrum resembles that of natural speech.

Likewise, the effective glottal excitation shape is important. To produce natural sounding speech, it is necessary to model voiced excitation as more than just a pulse train [6, 18].

Voice pitch is clearly important. Likewise, energy envelope (up to a multiplicative constant) has been shown to be of use in distortion measures [14].

However, preserving the exact waveform is not of great importance. If the waveform is perfectly preserved, then there is no perceptual difference, but the converse is not true.

To summarize, for this study, the important characteristics of speech are:

1. magnitude spectrum,
2. waveform characteristics (i.e., “peaked” waveforms for voiced speech),
3. glottal excitation shape,
4. voice pitch,
5. energy envelope shape.

Each of these characteristics can be quantified individually by representing them as parts of a simple speech production model. In “speech” produced from a suitable production model with representative input, each of these characteristics can be well preserved.

A space based on the idea of explicitly representing each of these key characteristics is presented in Appendix A. The main thrust of this dissertation diverged from the initial idea of working with such a space, and so the development of this space, while interesting, is no longer relevant to the main text. Instead, the path taken in this dissertation preserves these characteristics implicitly within the representation. That is, while the important characteristics are preserved, they cannot be readily determined from the form of the representations developed here. Because of this, the preservation of these key characteristics can only be shown through listening tests.

III. Representation of elements of the Hardy spaces, H_p

Work presented in this chapter shows the existence of a class of representations of elements of a Hardy space, $H_p(\mathbb{D})$, where \mathbb{D} is the open unit disk in \mathbb{C} . What will be presented here is a proof of an extension of a theorem by Luecking [20] dealing with Carleson inequalities in the Hardy spaces $H_p(\mathbb{D})$, which is the main result of this chapter. This theorem establishes forward and reverse Carleson inequalities where the sample points used in these inequalities are chosen from appropriate sets of a more general nature than those used in Luecking's theorem.

An additional result is an extension to a second theorem by Luecking which uses the Carleson inequalities to establish representations for elements of the Hardy spaces. This second extension, while trivial to prove given the work in [33], is the one that will be of primary importance in establishing a frame for $H_2(\mathbb{D})$, which is done in Chapter V. This frame for $H_2(\mathbb{D})$ is a key component in the frame designed in Chapter VI for speech representation.

In Section 3.1, some preliminary definitions and notations are given, followed by statements of the Carleson inequality theorem being extended and my extension to it. Sections 3.2 through 3.4 contain the necessary lemmas and theorems to prove the main result of this chapter, the proof of which is found in Section 3.5. The second result is stated and proven in Section 3.6.

In order to smooth the flow of the presentation, some of the proofs of lemmas and theorems stated in this chapter have been put in Appendix B.

3.1 Introduction

Definition 3.1.1 *Let \mathbb{D} be the open unit ball in \mathbb{C} . For $0 < p < \infty$, the Hardy space $H_p(\mathbb{D})$ is defined to be the space of analytic functions f on \mathbb{D} satisfying*

$$\|f\|_p = \|f\|_{H_p} = \sup_{0 < r < 1} \left(\int_{\partial \mathbb{D}} |f(rz)|^p d\sigma(z) \right)^{1/p} < \infty ,$$

where $\partial \mathbb{D}$ denotes the boundary of \mathbb{D} and σ denotes the normalized Lebesgue measure on $\partial \mathbb{D}$. The Hardy space $H_\infty(\mathbb{D})$ is defined to be the space of analytic functions f on \mathbb{D} satisfying

$$\|f\|_\infty = \|f\|_{H_\infty} = \sup_{|z| < 1} |f(z)| < \infty .$$

Definition 3.1.2 The pseudo-hyperbolic metric, denoted $\rho: \mathbb{D} \rightarrow \mathbb{D}$, is defined by

$$\rho(x, z) = \left| \frac{x - z}{1 - \bar{x}z} \right|.$$

The pseudo-hyperbolic ball about a of radius r , denoted $K(a, r)$, is given by

$$K(a, r) = \{z \in \mathbb{D} : \rho(a, z) < r\}.$$

Luecking's work was done in $H_p(\mathbb{D}^N)$, and so his definition of ρ is an extension of that used here. His theorem is as follows.

Theorem 3.1.3 (Luecking [20], [Thm 5.1]) Let $\{r_n\}$ be a sequence of numbers in the open interval $(0, 1)$ increasing to 1. Let the doubly indexed set $\{a_{n,k} \in \mathbb{C} \mid k = 1, \dots, k(n), n \in \mathbb{Z}^+\}$, be such that for each n, k , $|a_{n,k}| = r_n$ and for each n , $\partial(r_n \mathbb{D}^N) \subset \bigcup_{k=1}^{k(n)} K(a_{n,k}, \delta)$ for some fixed δ . If $p > 0$ and $\delta > 0$ is sufficiently small (where δ depends on p), then for some $0 < C < \infty$,

$$\|f\|_p^p \leq C \sup_n \sum_{k=1}^{k(n)} |f(a_{n,k})|^p (1 - r_n)^N$$

for every $f \in H_p(\mathbb{D}^N)$.

The proof of his theorem is followed by a statement to the effect that as long as the separation condition

$$\rho(a_{n,k}, a_{n,k'}) > \epsilon > 0 \quad \forall k \neq k'$$

for some $\epsilon > 0$ is satisfied, then the reverse inequality

$$\sup_n \sum_k |f(a_{n,k})|^p (1 - r_n)^N \leq C \|f\|_p^p, \quad f \in H_p(\mathbb{D}^N). \quad (2)$$

is true [20].

The extension to this theorem to follow, proven only for $p > 1$ and $N = 1$, loosens the constraint that the points $a_{n,k}$ lie on increasing radii with respect to n . Instead, it is allowed for each n , that the points $a_{n,k}$ lie in an appropriately constrained set, S_n . In addition, the intended use of this theorem requires the upper bound as given in (2), so that

that inequality is included in the theorem, together with constraints on δ to guarantee the existence of such an ϵ .

For ease in stating the many lemmas and theorems to come, the necessary constraints on the sets S_n to be used in the following theorem will be consolidated in the following condition.

Condition A *The sequence $\{S_n\}$ of compact subsets of \mathbb{D} satisfies Condition A if the following hold:*

1) *For each $n \in \mathbb{Z}^+$, there exists $\gamma_n \subset S_n$, where γ_n is a closed path with winding number $w(\gamma_n, 0) = 1$.*

2) *There exists a fixed $0 < \delta_r < 1$ such that for $r_n: [-\pi, \pi) \rightarrow [0, 1)$ and $M_n: [-\pi, \pi) \rightarrow [0, 1)$ defined according to*

$$M_n(\theta) = \sup\{|z| : z \in S_n \text{ and } \rho(z, s) < \delta_r \text{ for some } s = re^{i\theta} \in S_n\}$$

and

$$r_n(\theta) = \inf\{|z| : z \in S_n \text{ and } \rho(z, s) < \delta_r \text{ for some } s = re^{i\theta} \in S_n\},$$

with $\overline{M_n} \doteq \max_{\theta} M_n(\theta)$ and $\underline{r_n} \doteq \min_{\theta} r_n(\theta)$, we have

$$r_n \xrightarrow{u} 1$$

as $n \rightarrow \infty$,

$$\limsup_{n \rightarrow \infty} \frac{\overline{M_n} - r_n}{1 - \overline{M_n} \underline{r_n}} = C_s < 1 \quad (3)$$

and

$$\frac{M_n - r_n}{1 - M_n \underline{r_n}} \xrightarrow{u} 0 \quad (4)$$

as $n \rightarrow \infty$.

Some discussion of the implications of Condition A is in order. Since each set S_n contains a closed path γ_n with winding number $w(\gamma_n, 0) = 1$, we know that S_n surrounds

the origin. Since $r_n \xrightarrow{u} 1$, we know that eventually, the S_n are torus-like in that their center (about the origin) is hollow. Equation (4) implies that the sets S_n become thin along any radial from the origin and that the path γ_n does not vary “too much.”

The main result of this chapter is the following theorem, the proof of which is to be found in Section 3.5 below.

Theorem 3.1.4 *Fix $1 < p < \infty$. Suppose $\{S_n\}$ satisfies Condition A and let δ_r be defined as in Condition A.. Then there exist $0 < \epsilon \leq \delta < \min\{\delta_r, \frac{1}{3}\}$ and $0 < c \leq C < \infty$ such that whenever $\{a_{n,k}\}$ satisfies $a_{n,k} \in S_n$, $\rho(a_{n,k}, a_{n,j}) \geq \epsilon$ for all $j \neq k$, and $S_n \subseteq \bigcup_k K(a_{n,k}, \delta)$, the inequality*

$$c\|f\|_p^p \leq \sup_n \sum_{k=1}^{k(n)} |f(a_{n,k})|^p (1 - |a_{n,k}|) \leq C\|f\|_p^p \quad (5)$$

is true for all $f \in H_p(\mathbb{D})$.

The following section contains definitions and basic properties of the Hardy spaces and the metric ρ , which will be used extensively in the remainder of the chapter. Following that, Section 3.3 contains lemmas showing various inequalities that are necessary to complete the proofs to follow. Section 3.4 contains other interesting lemmas and theorems required to prove the main result, which is done in Section 3.5. Following this, Section 3.6 contains proofs of two theorems extended by Ward and Partington that make Theorem 3.1.4 useful in applications.

3.2 Preliminaries

This section contains definitions and proofs of some well known facts involving the Hardy spaces and the metric ρ .

3.2.1 Hardy Spaces. The following two theorems concerning Hardy spaces are given without proof, and can be found in, e.g., [12].

Theorem 3.2.1 (Hardy-Littlewood) *Let $0 < p \leq \infty$ and $f \in H_p(\mathbb{D})$. Define F by*

$$F(e^{i\theta}) = \sup_{0 \leq r < 1} |f(re^{i\theta})|.$$

Then $F \in L_p(\partial\mathbb{D})$ and $\|F\|_{L_p} \leq B_p \|f\|_{H_p}$ where $B_p < \infty$ depends only on p .

Theorem 3.2.2 *Let $0 < p \leq \infty$ and let $f \in H_p(\mathbb{D})$. Then $f(e^{i\theta}) \doteq \lim_{r \rightarrow 1} f(re^{i\theta})$ exists for almost every $\theta \in [-\pi, \pi)$ and $f \in L_p(\partial\mathbb{D})$. For $1 \leq p < \infty$, we have*

$$\|f\|_{H_p}^p = \|f\|_{L_p}^p = \frac{1}{2\pi} \int_{-\pi}^{\pi} |f(e^{i\theta})|^p d\theta ,$$

and for $p = \infty$, we have

$$\|f\|_{H_\infty} = \|f\|_{L_\infty} = \operatorname{ess\,sup}_{-\pi \leq \theta < \pi} |f(e^{i\theta})| .$$

3.2.2 The pseudo-hyperbolic metric, ρ . The metric ρ and the mapping ϕ_a (defined below) are, as will be seen, extremely useful in dealing with the Hardy spaces. Their important properties to be used here are given below.

Lemma 3.2.3 *For every $a \in \mathbb{D}$, $\phi_a: \mathbb{D} \rightarrow \mathbb{D}$, defined by*

$$\phi_a(z) = \frac{a - z}{1 - \bar{a}z}$$

is well-defined and bijective, with inverse $\phi_a^{-1} = \phi_a$.

Proof. Let $a \in \mathbb{D}$. We wish to show that for any $z \in \mathbb{D}$, that $\phi_a(z) \in \mathbb{D}$ also. To do this, it is necessary and sufficient to show that

$$|\phi_a(z)| = \left| \frac{a - z}{1 - \bar{a}z} \right| < 1 .$$

Calculating, we see

$$\begin{aligned} \left| \frac{a - z}{1 - \bar{a}z} \right|^2 &= \frac{(a - z)(\bar{a} - \bar{z})}{(1 - \bar{a}z)(1 - a\bar{z})} \\ &= \frac{|a|^2 + |z|^2 - 2\operatorname{Re}(a\bar{z})}{1 + |a|^2|z|^2 - 2\operatorname{Re}(a\bar{z})} . \end{aligned}$$

Since both the numerator and denominator are non-negative, to show that $|\phi_a(z)| < 1$, it is sufficient to show that $|a|^2 + |z|^2 < 1 + |a|^2|z|^2$, which is shown by

$$1 + |a|^2|z|^2 - |a|^2 - |z|^2 = (1 - |a|^2)(1 - |z|^2) > 0 ,$$

since $a, z \in \mathbb{D}$ implies $|a|, |z| < 1$. Therefore, ϕ_a is well-defined.

To see that ϕ_a is bijective, first note that it is its own inverse, that is, for any $z \in \mathbb{D}$,

$$\begin{aligned}\phi_a(\phi_a(z)) &= \phi_a\left(\frac{a-z}{1-\bar{a}z}\right) \\ &= \frac{a - \frac{a-z}{1-\bar{a}z}}{1 - \bar{a}\frac{a-z}{1-\bar{a}z}} \\ &= \frac{z(1-|a|^2)}{1-|a|^2} = z.\end{aligned}$$

This shows that ϕ_a is both injective and surjective. That it is injective is seen by the fact that it is invertible on its range (with inverse $\phi_a^{-1} = \phi_a$). That it is surjective is seen by the fact that for any $z \in \mathbb{D}$, $\phi_a(y) = z$ where $y \doteq \phi_a(z)$. Therefore, for any $a \in \mathbb{D}$, ϕ_a is bijective on \mathbb{D} . \square

Next, will be shown that ρ defines a metric on the set \mathbb{D} . To do this, we will first show one of the nice properties of ρ .

Lemma 3.2.4 *For any $a, x, z \in \mathbb{D}$,*

$$\rho(\phi_a(x), \phi_a(z)) = \rho(x, z).$$

Proof. By straight forward calculations,

$$\begin{aligned}\rho(\phi_a(x), \phi_a(z)) &= \left| \frac{\phi_a(x) - \phi_a(z)}{1 - \overline{\phi_a(x)}\phi_a(z)} \right| \\ &= \left| \frac{\frac{a-x}{1-\bar{a}x} - \frac{a-z}{1-\bar{a}z}}{1 - \frac{\bar{a}-\bar{x}}{1-\bar{a}\bar{x}} \frac{a-z}{1-\bar{a}z}} \right| \\ &= \frac{|(1-|a|^2)(z-x)|}{|(1-|a|^2)(1-\bar{x}z)|} \\ &= \frac{|x-z|}{|1-\bar{x}z|} = \rho(x, z).\end{aligned}$$

\square

The following proof that ρ is a metric is only difficult in that the typical techniques for showing the triangle inequality do not work.

Proposition 3.2.5 *The function ρ defines a metric on \mathbb{D} .*

Proof. The properties of symmetry and nonnegativity can be seen by inspection. The positivity property that $\rho(x, y) > 0$ when $x \neq y$ is trivial also. This leaves the triangle inequality, that is, for all $\tilde{x}, \tilde{y}, \tilde{z} \in \mathbb{D}$,

$$\rho(\tilde{x}, \tilde{z}) \leq \rho(\tilde{x}, \tilde{y}) + \rho(\tilde{y}, \tilde{z}) .$$

Using Lemma 3.2.4 and the equalities $\rho(a, b) = |\phi_a(b)|$ and $\phi_a(a) = 0$, this inequality is equivalent to

$$\rho(x, z) \leq |x| + |z| ,$$

where $x \doteq \phi_{\tilde{y}}(\tilde{x})$ and $z \doteq \phi_{\tilde{y}}(\tilde{z})$. Working with $(\rho(x, z))^2$, we see that

$$\begin{aligned} (\rho(x, z))^2 &= \frac{|x - z|^2}{|1 - \bar{x}z|^2} \\ &= \frac{(x - z)(\bar{x} - \bar{z})}{(1 - \bar{x}z)(1 - x\bar{z})} \\ &= \frac{|x|^2 + |z|^2 - 2|x||z|\cos\theta}{1 + |x|^2|z|^2 - 2|x||z|\cos\theta} , \end{aligned}$$

where $\theta \doteq \arg(\bar{x}z)$. Multiplying the right-hand side of the equation by $\frac{(|x|+|z|)^2}{(|x|+|z|)^2}$ we have

$$(\rho(x, z))^2 = (|x| + |z|)^2 \frac{|x|^2 + |z|^2 - 2|x||z|\cos\theta}{(|x| + |z|)^2(1 + |x|^2|z|^2 - 2|x||z|\cos\theta)} .$$

Note that showing that $\rho(x, z) \leq |x| + |z|$ is (of course) equivalent to showing $(\rho(x, z))^2 \leq (|x| + |z|)^2$, so to complete the proof, it is sufficient to show that

$$\frac{|x|^2 + |z|^2 - 2|x||z|\cos\theta}{(|x| + |z|)^2(1 + |x|^2|z|^2 - 2|x||z|\cos\theta)} \leq 1 .$$

Since both numerator and denominator of the fraction are positive, this can be done by showing $|x|^2 + |z|^2 - 2|x||z|\cos\theta \leq (|x| + |z|)^2(1 + |x|^2|z|^2 - 2|x||z|\cos\theta)$. Working with the quantity,

$$\begin{aligned} &(|x| + |z|)^2(1 + |x|^2|z|^2 - 2|x||z|\cos\theta) - (|x|^2 + |z|^2 - 2|x||z|\cos\theta) \\ &= |x||z|[(2 + |x||z|(|x| + |z|)^2) - 2((|x| + |z|)^2 - 1)\cos\theta] , \end{aligned}$$

we can see that for the triangle inequality to be true, we must have that $(2 + |x||z|(|x| + |z|)^2) - 2((|x| + |z|)^2 - 1) \cos \theta \geq 0$. Continuing,

$$\begin{aligned} & (2 + |x||z|(|x| + |z|)^2) - 2((|x| + |z|)^2 - 1) \cos \theta \\ & \geq (2 + |x||z|(|x| + |z|)^2) - 2|((|x| + |z|)^2 - 1) \cos \theta| \\ & \geq (2 + |x||z|(|x| + |z|)^2) - 2|(|x| + |z|)^2 - 1|. \end{aligned}$$

In the case where $|x| + |z| \leq 1$, this is easily shown by

$$\begin{aligned} (2 + |x||z|(|x| + |z|)^2) - 2|(|x| + |z|)^2 - 1| &= (2 + |x||z|(|x| + |z|)^2) + 2((|x| + |z|)^2 - 1) \\ &= (|x||z| + 2)(|x| + |z|)^2 \geq 0. \end{aligned}$$

The case where $|x| + |z| > 1$ is slightly more difficult. Assuming $|x| + |z| > 1$, we have

$$\begin{aligned} (2 + |x||z|(|x| + |z|)^2) - 2|(|x| + |z|)^2 - 1| &= (2 + |x||z|(|x| + |z|)^2) - 2((|x| + |z|)^2 - 1) \\ &= 4 + (|x||z| - 2)(|x| + |z|)^2. \end{aligned}$$

To show that this right-hand side is non-negative, first define $C \doteq |x| + |z|$ and minimize the value of $4 + (|x||z| - 2)(|x| + |z|)^2 = 4 + (|x|(C - |x|) - 2)C^2$. Using the usual introductory calculus techniques, one can determine a candidate extreme point of $|x| = \frac{C}{2}$, which on further inspection is revealed to be a maximum. This implies that the minimum is at an end point of the allowable range of $|x|$, that is, at $|x| = 1$ or $|x| = C - 1$. By the symmetry of the function, the two endpoints yield equivalent minima, and so we find that

$$4 + (|x||z| - 2)(|x| + |z|)^2 \geq 4 - 3C^2 + C^3.$$

Solving for the minimal value of the right-hand side in the allowable range of C , we find a minima at $C = 2$, which gives

$$4 + (|x||z| - 2)(|x| + |z|)^2 \geq 4 - 12 + 8 = 0.$$

Therefore

$$(2 + |x||z|(|x| + |z|)^2) - 2((|x| + |z|)^2 - 1) \cos \theta \geq 0,$$

which implies

$$\frac{|x|^2 + |z|^2 - 2|x||z|\cos\theta}{(|x| + |z|)^2(1 + |x|^2|z|^2 - 2|x||z|\cos\theta)} \leq 1 ,$$

giving the desired inequality of

$$(\rho(x, z))^2 \leq (|x| + |z|)^2 .$$

Substituting to regain our original variables, we get

$$\begin{aligned} \rho(\phi_{\tilde{y}}(\tilde{x}), \phi_{\tilde{y}}(\tilde{z})) &\leq |\phi_{\tilde{y}}(\tilde{x})| + |\phi_{\tilde{y}}(\tilde{z})| \\ \rho(\tilde{x}, \tilde{z}) &\leq \rho(\tilde{x}, \tilde{y}) + \rho(\tilde{y}, \tilde{z}) . \end{aligned}$$

□

3.3 Lemmas concerning various inequalities

This section contains lemmas showing various inequalities that will be used in the more interesting lemmas and theorems to follow in Sections 3.4 and 3.5. The proofs of these lemmas are relegated to Appendix B.

First, throughout this chapter, it will be necessary to make estimates based on the Lebesgue measure of the set $K(a, r)$ in \mathbb{R}^2 , denoted $m(K(a, r))$, normalized by π so that $m(\mathbb{D}) = 1$. That is the topic of the following two lemmas. The nature of these sets often makes it easier to work with Euclidean balls instead, either larger or smaller, as appropriate. That is the reason for the following lemma. Lemma 3.3.2 concerns an alternate definition of the set $K(a, r)$.

Lemma 3.3.1 *Let $a \in \mathbb{D}$ and $r \in [0, 1)$. Let $B(a, \delta)$ be the Euclidean ball centered at a of radius δ , that is,*

$$B(a, \delta) = \{z \in \mathbb{D} : |z - a| < \delta\} .$$

The largest δ such that $B(a, \delta) \subseteq K(a, r)$ is given by

$$\delta = \frac{r(1 - |a|^2)}{(1 + r|a|)} .$$

The smallest δ such that $K(a, r) \subseteq B(a, \delta)$ is given by

$$\delta = \frac{r(1 - |a|^2)}{(1 - r|a|)}.$$

Proof. See Appendix B.

Lemma 3.3.2 For $a \in \mathbb{D}$, $r \in (0, 1)$, the set $K(a, r)$ is given by $K(a, r) = B(\tilde{a}, \tilde{r})$, where $\tilde{a} = a \left(\frac{1-r^2}{1-r^2|a|^2} \right)$ and $\tilde{r} = \left(\frac{r(1-|a|^2)}{1-r^2|a|^2} \right)$.

Proof. See Appendix B.

The following lemma is needed for various inequalities to come, and simply states how large $|z|$ can be, given $\rho(a, z) < \delta$.

Lemma 3.3.3 Let $\delta \in (0, 1)$ and let $w \in \mathbb{D}$. If $\rho(w, z) \leq \delta$ then

$$|z| \leq \frac{\delta + |w|}{1 + \delta|w|}$$

and if $w \neq 0$, this upper bound is achieved only at the point

$$z = \frac{w}{|w|} \left(\frac{\delta + |w|}{1 + \delta|w|} \right)$$

Proof. See Appendix B.

The following lemma is simply a “utility” lemma concerning set inclusion for use in a later proof.

Lemma 3.3.4 Let $z \in \mathbb{D}$ and $r \in (0, 1)$. If $a \in B(z, \frac{r(1-|z|^2)}{4})$, then $K(a, r/2) \subseteq K(z, r)$.

Proof. See Appendix B.

The following lemma will be of use in various proofs where a bound on the angle subtended by the set $K(a, \delta)$ (as measured from the origin) is needed.

Lemma 3.3.5 Fix $\delta \in (0, 1)$ and $C > 4$. Then there exists $r \in (0, 1)$ such that whenever $|a| \geq r$,

$$\Delta\theta \leq C \left(\frac{\delta}{1 - \delta^2} \right) (1 - |a|),$$

where $\Delta\theta$ is the angle subtended by $K(a, \delta)$ with respect to the origin.

Proof. See Appendix B.

The remaining lemmas in this section are self-explanatory. They all establish inequalities.

Lemma 3.3.6 Let $r \in (0, 1)$ and $a, z \in \mathbb{D}$ such that $\rho(a, z) \leq r$; then

$$\frac{1}{1 - |a||z|} \leq \frac{1 + r}{1 - |a|^2} \leq \frac{2}{1 - |a|^2}$$

and

$$\frac{1 - |a|^2}{r^2(1 - |a||z|)^2} \leq \frac{2}{(1 - r)} \frac{1}{m(K(a, r))}.$$

Proof. See Appendix B.

Lemma 3.3.7 For all $a \in \mathbb{D}$ and $r, \epsilon \in (0, 1)$,

$$\frac{1}{m(K(a, \epsilon r))} \leq \left(\frac{(1 - \epsilon r)^2}{\epsilon^2(1 - r)^2} \right) \frac{1}{m(K(a, r))}.$$

Proof. See Appendix B.

Lemma 3.3.8 Let $z, w \in \mathbb{D}$ such that $\rho(z, w) < \frac{1}{3}$, then $|z - w| < 1 - |z|$.

Proof. See Appendix B.

Lemma 3.3.9 Let $r, \delta \in (0, 1)$ and suppose for some $w, z \in \mathbb{D}$, that $\rho(w, z) \leq \delta$. Then

$$\frac{1}{m(K(z, r))} \leq \frac{16(1 - r^2\delta^2)^2}{(1 - \delta^2)^2(1 - r^2)^2} \frac{1}{m(K(w, r))}$$

and

$$\frac{1}{1 - |z|^2} \leq \left(\frac{1}{1 - \delta} \right) \frac{1}{|1 - \overline{w}z|}.$$

Proof. See Appendix B.

3.4 Supporting Lemmas and Theorems

The more significant lemmas and theorems needed to prove the main result are found in this section.

The next two lemmas deal with estimates of the value of f at a point a . They will be required later in the proof of the main result.

Lemma 3.4.1 *Fix $p \geq 1$. Then there exists $C < \infty$ depending only on r such that*

$$|f(a)|^p \leq C \int_{K(a,r)} |f(\zeta)|^p \frac{dm(\zeta)}{m(K(a,r))}$$

for all f analytic in \mathbb{D} , $a \in \mathbb{D}$, and $r \in (0, 1)$.

Proof. Let f be analytic in \mathbb{D} . From Cauchy's Theorem, we have that for all $r' \in (0, 1)$,

$$\begin{aligned} f(0) &= \frac{1}{2\pi i} \int_{|z|=r'} \frac{f(z)}{z} dz \\ &= \frac{1}{2\pi} \int_{-\pi}^{\pi} f(r' e^{i\theta}) d\theta. \end{aligned}$$

Integrating both sides with respect to $r' dr'$ we find

$$\begin{aligned} \int_0^r f(0) r' dr' &= \frac{1}{2\pi} \int_0^r \int_{-\pi}^{\pi} f(r' e^{i\theta}) d\theta r' dr' \\ r^2 f(0) &= \int_{r\mathbb{D}} f(\zeta) dm(\zeta) \end{aligned}$$

which give

$$f(0) = \frac{1}{r^2} \int_{r\mathbb{D}} f(\zeta) dm(\zeta).$$

This leads to

$$\begin{aligned} |f(0)| &= \frac{1}{r^2} \left| \int_{r\mathbb{D}} f(\zeta) dm(\zeta) \right| \\ &\leq \frac{1}{r^2} \int_{r\mathbb{D}} |f(\zeta)| dm(\zeta). \end{aligned}$$

In the case where $p > 1$, define q by $\frac{1}{q} \doteq 1 - \frac{1}{p}$. Invoking the Hölder inequalities, we see that

$$\begin{aligned} |f(0)| &\leq \frac{1}{r^2} \int_{r\mathbb{D}} |f(\zeta)| dm(\zeta) \\ &\leq \frac{1}{r^2} \left(\int_{r\mathbb{D}} 1^q dm(\zeta) \right)^{1/q} \left(\int_{r\mathbb{D}} |f(\zeta)|^p dm(\zeta) \right)^{1/p} \\ &\leq \frac{1}{r^2} (r^2)^{1/q} \left(\int_{r\mathbb{D}} |f(\zeta)|^p dm(\zeta) \right)^{1/p}. \end{aligned}$$

This leads to

$$|f(0)|^p \leq \frac{1}{r^{2p}} (r^2)^{p/q} \int_{r\mathbb{D}} |f(\zeta)|^p dm(\zeta).$$

Since $\frac{1}{p} + \frac{1}{q} = 1$, this gives

$$|f(0)|^p \leq \frac{1}{r^2} \int_{r\mathbb{D}} |f(\zeta)|^p dm(\zeta).$$

Now, to extend this to $|f(a)|$, let us define a new function, $g: \mathbb{D} \rightarrow \mathbb{C}$ according to $g(z) = f(\phi_a(z))$. By hypothesis, f is analytic. Also, $\phi_a: \mathbb{D} \rightarrow \mathbb{D}$ is analytic for all $a \in \mathbb{D}$. Therefore, g is analytic also, and we have

$$\begin{aligned} |g(0)|^p &\leq \frac{1}{r^2} \int_{r\mathbb{D}} |g(\zeta)|^p dm(\zeta) \\ |f(a)|^p &= |f(\phi_a(0))|^p \leq \frac{1}{r^2} \int_{r\mathbb{D}} |f(\phi_a(\zeta))|^p dm(\zeta). \end{aligned}$$

Making the substitution, $z = \phi_a(\zeta)$, and using the fact that $\phi_a^{-1} = \phi_a$, we get

$$|f(a)|^p \leq \frac{1}{r^2} \int_{K(a,r)} |f(z)|^p \frac{dm(z)}{|\phi'_a(\phi_a(z))|}.$$

The derivative of ϕ_a , denoted $\phi'_a: \mathbb{D} \rightarrow \mathbb{C}$, is given by

$$\phi'_a(z) = -\frac{(1 - |a|^2)}{(1 - \bar{a}z)^2},$$

and so $\phi'_a(\phi_a(z))$ is given by

$$\phi'_a(\phi_a(z)) = -\frac{(1 - \bar{a}z)^2}{(1 - |a|^2)}.$$

Returning to our inequality, we use this to find

$$\begin{aligned} |f(a)|^p &\leq \frac{1}{r^2} \int_{K(a,r)} |f(z)|^p \left| -\frac{(1 - |a|^2)}{(1 - \bar{a}z)^2} \right| dm(z) \\ &= \frac{1}{r^2} \int_{K(a,r)} |f(z)|^p \frac{(1 - |a|^2)}{|1 - \bar{a}z|^2} dm(z) \\ &\leq \frac{1}{r^2} \int_{K(a,r)} |f(z)|^p \frac{(1 - |a|^2)}{(1 - |z||a|)^2} dm(z). \end{aligned}$$

Because $\rho(a, z) < r$, by Lemma 3.3.6 we have

$$|f(a)|^p \leq C \int_{K(a,r)} |f(z)|^p \frac{dm(z)}{m(K(a, r))},$$

where $C = \frac{2}{1-r}$ depends on r but not a or f . □

The following lemma can be found in, e.g., [2].

Lemma 3.4.2 *Let f be analytic in \mathbb{D} and suppose that for some $a \in \mathbb{D}$ and $R \in (0, 1 - |a|)$, that $|f(z)| \leq M$ for all $z \in B(a, R)$. Then, for each $n = 1, 2, \dots$ and for every $z \in B(a, \frac{R}{2^n})$, $|f^{(n)}(z)| \leq M \left(\frac{2}{R}\right)^n$.*

The following lemma, to be used in the proof of the main theorem, is an elaboration of a step in the proof of a lemma in [20]. Note, that in the usage of the result in [20], the value of ϵ was not restricted. This implies that there may be a better proof of the lemma which will not incur a restriction on the value of ϵ .

Lemma 3.4.3 Fix $p > 0$ and $r \in (0, 1)$. Then there exists $C < \infty$ depending only on p and r such that

$$|f(z) - f(w)|^p \leq C\epsilon^p \int_{K(z,r)} |f(\zeta)|^p \frac{dm(\zeta)}{m(K(z,r))}$$

whenever $\rho(z, w) < \epsilon \leq \frac{1}{3}$ for all f analytic in \mathbb{D} .

Proof. Given r , from Lemma 3.3.1, we know that

$$B(z, R) \subset K(z, r) \subset \mathbb{D},$$

where $R \doteq r(1 - |z|^2)/2 \leq \frac{r(1-|z|^2)}{1+r|z|}$. Using Lemma 3.3.4 above, we know that for all $a \in B(z, R/2)$, the set inclusion $K(a, r/2) \subset K(z, r)$ holds, and so from Lemma 3.4.1, we have that for all $a \in \mathbb{D}$,

$$|f(a)|^p \leq C \int_{K(a, r/2)} |f(\zeta)|^p \frac{dm(\zeta)}{m(K(a, r/2))}.$$

where C depends on $r/2$ but not a or f . Using Lemmas 3.3.7 and 3.3.9, we then have

$$\begin{aligned} |f(a)|^p &\leq C \left(\frac{16(1 - (r/2)^2 \epsilon^2)^2}{(1 - \epsilon^2)^2 (1 - (r/2)^2)^2} \right) \int_{K(a, r/2)} |f(\zeta)|^p \frac{dm(\zeta)}{m(K(z, r/2))} \\ &\leq C \left(\frac{16(4 - r^2 \epsilon^2)^2}{(1 - \epsilon^2)^2 (4 - r^2)^2} \right) \left(\frac{(1 - r/2)^2}{(1/2)^2 (1 - r)^2} \right) \int_{K(a, r/2)} |f(\zeta)|^p \frac{dm(\zeta)}{m(K(z, r))} \\ &\leq C \left(\frac{16(4 - r^2 \epsilon^2)^2}{(1 - \epsilon^2)^2 (2 + r)^2} \right) \int_{K(z, r)} |f(\zeta)|^p \frac{dm(\zeta)}{m(K(z, r))}, \end{aligned}$$

where this last step incorporates the factor $(1 - r)^{-2}$ into C . Using that $\epsilon \leq \frac{1}{3}$, we calculate

$$|f(a)|^p \leq 81C \int_{K(z, r)} |f(\zeta)|^p \frac{dm(\zeta)}{m(K(z, r))},$$

to get a bound independent of ϵ . Incorporating the constant 81 into C , this gives

$$\sup_{a \in B(z, R/2)} |f(a)| \leq M$$

where

$$M = \left(C \int_{K(z,r)} |f(\zeta)|^p \frac{dm(\zeta)}{m(K(z,r))} \right)^{1/p}.$$

Since f is analytic in \mathbb{D} , it has a Taylor series expansion about z valid in the region $|z - w| < 1 - |z|$. From Lemma 3.3.8, we know that for our choice of ϵ , $\rho(z, w) < \epsilon$ implies $|z - w| < 1 - |z|$, and so we may write

$$f(w) = f(z) + \sum_{k=1}^{\infty} f^{(k)}(z) \frac{(w - z)^k}{k!}.$$

This implies that (using Lemma 3.4.2)

$$\begin{aligned} |f(w) - f(z)| &= \left| \sum_{k=1}^{\infty} f^{(k)}(z) \frac{(w - z)^k}{k!} \right| \\ &\leq \sum_{k=1}^{\infty} |f^{(k)}(z)| \left| \frac{(w - z)^k}{k!} \right| \\ &\leq \sum_{k=1}^{\infty} M \left(\frac{4}{R} \right)^k \frac{|w - z|^k}{k!} \\ &\leq \sum_{k=1}^{\infty} M \left(\frac{8}{r} \right)^k \left(\frac{|w - z|}{(1 - |z|^2)} \right)^k \frac{1}{k!}. \end{aligned}$$

Using Lemma 3.3.9, we have

$$\begin{aligned} |f(w) - f(z)| &\leq M \sum_{k=1}^{\infty} \left(\frac{8}{r} \right)^k \left(\frac{1}{(1 - \epsilon)} \frac{|w - z|}{|1 - \bar{w}z|} \right)^k \frac{1}{k!} \\ &\leq M \sum_{k=1}^{\infty} \left(\frac{8}{r} \right)^k \left(\frac{3}{2} \rho(w, z) \right)^k \frac{1}{k!} \\ &\leq M \sum_{k=1}^{\infty} \left(\frac{8}{r} \right)^k \left(\frac{3}{2} \right)^k \rho(w, z) \frac{1}{k!} \\ &\leq M \rho(w, z) (e^{\frac{12}{r}} - 1) \\ &\leq M \epsilon (e^{\frac{12}{r}} - 1), \end{aligned}$$

where the fact that $\epsilon \leq \frac{1}{3}$ is used to obtain a bound independent of ϵ . Therefore, after incorporating constants,

$$|f(z) - f(w)|^p \leq C\epsilon^p \int_{K(z,r)} |f(\zeta)|^p \frac{dm(\zeta)}{m(K(z,r))},$$

where C depends only on r and p . □

The following two lemmas simply show the existence and finite cardinality of the sets $\{a_{n,k}\}$ needed in the main result.

Lemma 3.4.4 *Let $S \subset \mathbb{D}$ be a compact set and let $\epsilon \in (0, 1)$ be given. If the indexed set $\{a_k\} \subseteq S$ has the property that $\rho(a_k, a_j) \geq 2\epsilon$ whenever $j \neq k$, then $\#\{a_k\} < \infty$.*

Proof. Since S is a compact subset of \mathbb{D} , there exists $M < 1$ such that $|z| \leq M$ for all $z \in S$. That is, $S \subseteq M\overline{\mathbb{D}}$.

The condition $\rho(a_k, a_j) \geq 2\epsilon$ excludes the possibility of any a_j being in $K(a_k, 2\epsilon)$ ($j \neq k$) so the sets $K(a_j, \epsilon)$, $j = 1, 2, \dots$ are pairwise disjoint. For $a_k \in S \subset M\overline{\mathbb{D}}$, the Lebesgue measure, $m(K(a_k, \epsilon))$, of this region is given by Lemma 3.3.2 according to

$$m(K(a_k, \epsilon)) = \frac{\epsilon^2(1 - |a_k|^2)^2}{(1 - \epsilon^2|a_k|^2)^2}.$$

Using the fact that $1 - |a_k|^2 \geq 1 - M^2$ and that $\frac{1}{1 - \epsilon^2|a_k|^2} \geq 1$, this gives a lower bound of

$$m(K(a_k, \epsilon)) \geq \epsilon^2(1 - M^2)^2 > 0.$$

Furthermore, for M sufficiently close to 1, we have

$$m(M\overline{\mathbb{D}} \cap K(a_k, \epsilon)) > \frac{1}{3}m(K(a_k, \epsilon)) > \frac{\epsilon^2(1 - M^2)^2}{3} > 0.$$

Since $m(M\overline{\mathbb{D}}) = M^2 < 1$, we have that at most a finite number of a_k satisfying the separation condition may be in $M\overline{\mathbb{D}}$ and hence in S . Therefore, $\#\{a_k\} < \infty$. □

Note that in the following lemma, it may be possible to replace the condition $\epsilon \leq \delta$ with a weaker one. However, even if it is possible, it would require a much more difficult proof, since the shape of the set, S , becomes important.

Lemma 3.4.5 *Let $S \subset \mathbb{D}$ be a compact set and let $0 < \epsilon \leq \delta < 1$ be given. Then there exists an indexed set, $\{a_k\} \subset S$, such that $\rho(a_k, a_j) \geq \epsilon$ for all $k \neq j$ and such that $S \subset \bigcup_k K(a_k, \delta)$. This set will also have the property that $\#\{a_k\} < \infty$.*

Proof. (By construction) Choose $a_1 \in S$. Iteratively choose $a_k \in S \setminus \bigcup_{i=1}^{k-1} K(a_i, \delta)$. By this choice, $\rho(a_k, a_i) \geq \delta \geq \epsilon$ for each $i = 1, 2, \dots, k-1$. By Lemma 3.4.4, we know that any set $\{a_n\}$ with the property that $\rho(a_k, a_j) \geq \epsilon$ for $k \neq j$ is finite, so that for some finite N , $S \setminus \bigcup_{k=1}^N K(a_k, \delta) = \emptyset$, which implies that $S \subset \bigcup_{k=1}^N K(a_k, \delta)$. \square

The next lemma simply removes some calculations from the proofs of the following theorem and the main result.

Lemma 3.4.6 *Let $\{S_n\}$ satisfy Condition A. Then $\frac{1-r_n}{1-M_n} \xrightarrow{u} 1$.*

Proof. For each $\theta \in [-\pi, \pi)$, we have

$$\begin{aligned} \frac{M_n(\theta) - r_n(\theta)}{1 - M_n(\theta)r_n(\theta)} &\geq \frac{M_n(\theta) - r_n(\theta)}{1 - r_n^2(\theta)} = \frac{(1 - r_n(\theta)) - (1 - M_n(\theta))}{(1 - r_n(\theta))(1 + r_n(\theta))} \\ &= \frac{1}{1 + r_n(\theta)} \left(1 - \frac{1 - M_n(\theta)}{1 - r_n(\theta)} \right) \geq 0. \end{aligned}$$

Using (4) from Condition A, this implies $\frac{1}{1+r_n} \left(1 - \frac{1-M_n}{1-r_n} \right) \xrightarrow{u} 0$. Since $\frac{1}{1+r_n} \xrightarrow{u} \frac{1}{2}$, we have that $\left(1 - \frac{1-M_n}{1-r_n} \right) \xrightarrow{u} 0$, which implies $\frac{1-M_n}{1-r_n} \xrightarrow{u} 1$. Therefore, $\frac{1-r_n}{1-M_n} \xrightarrow{u} 1$. \square

Lemma 3.4.7 *Let $\{S_n\}$ satisfy Condition A. Then*

$$\limsup_{n \rightarrow \infty} \frac{1 - \underline{r_n}}{1 - \overline{M_n}} \leq \frac{2}{1 - C_s}, \quad (6)$$

where $C_s < 1$ is defined as in Condition A.

Proof. Since $0 \leq \underline{r_n} \leq \overline{M_n} < 1$, we get

$$\frac{2(1 - \overline{M_n})}{1 - \underline{r_n}} \geq \frac{(1 - \overline{M_n})(1 + \underline{r_n})}{1 - \overline{M_n}\underline{r_n}} = 1 - \frac{\overline{M_n} - \underline{r_n}}{1 - \overline{M_n}\underline{r_n}},$$

and hence

$$\liminf_{n \rightarrow \infty} \frac{1 - \overline{M_n}}{1 - \underline{r_n}} \geq \frac{1}{2} \liminf_{n \rightarrow \infty} \left[1 - \frac{\overline{M_n} - \underline{r_n}}{1 - \overline{M_n}\underline{r_n}} \right]$$

$$\begin{aligned}
&= \frac{1}{2} \left[1 - \limsup_{n \rightarrow \infty} \frac{\overline{M_n} - r_n}{1 - \overline{M_n} r_n} \right] \\
&= \frac{1 - C_s}{2} > 0.
\end{aligned}$$

Therefore,

$$\limsup_{n \rightarrow \infty} \frac{1 - r_n}{1 - \overline{M_n}} \leq \frac{2}{1 - C_s}.$$

□

The following lemma shows that, instead of using the sequences of circles defined by $re^{i\theta}$ to determine the norm of a function $f \in H_p(\mathbb{D})$, as in

$$\|f\|_p^p = \lim_{r \rightarrow 1} \frac{1}{\pi} \int_{-\pi}^{\pi} |f(re^{i\theta})|^p d\theta,$$

that suitably chosen sequences of functions, $r_n(\theta)$ (not necessarily continuous curves), can be used instead, as in

$$\|f\|_p^p = \lim_{n \rightarrow \infty} \frac{1}{\pi} \int_{-\pi}^{\pi} |f(r_n(\theta)e^{i\theta})|^p d\theta.$$

Lemma 3.4.8 *Let $0 < p < \infty$ be fixed and for each $n \in \mathbb{Z}^+$, let $r_n: [-\pi, \pi) \rightarrow [0, 1)$ be Lebesgue measurable functions such that $r_n(\theta) \rightarrow 1$ a.e. on $[-\pi, \pi)$ as $n \rightarrow \infty$. Then*

$$\lim_{n \rightarrow \infty} \int_{-\pi}^{\pi} |f(r_n(\theta)e^{i\theta})|^p \frac{d\theta}{2\pi} = \lim_{r \rightarrow 1} \int_{-\pi}^{\pi} |f(re^{i\theta})|^p \frac{d\theta}{2\pi} = \|f\|_p^p$$

for all $f \in H_p(\mathbb{D})$.

Proof. Let $f \in H_p(\mathbb{D})$ and define \tilde{f} by $\tilde{f}(e^{i\theta}) = \lim_{r \rightarrow 1} f(re^{i\theta})$. From Theorem 3.2.2, we know that this limit exists a.e. on $\theta \in [-\pi, \pi)$, that is, $\tilde{f} \in L_p(\partial\mathbb{D})$, and also that $\|f\|_p^p = \frac{1}{2\pi} \int_{-\pi}^{\pi} |\tilde{f}(e^{i\theta})|^p d\theta$. From Theorem 3.2.1, we have that $F \in L_p(\partial\mathbb{D})$, where F is defined by

$$F(e^{i\theta}) = \sup_{0 \leq r < 1} |f(re^{i\theta})|.$$

Since $r_n(\theta) \rightarrow 1$ for a.e. $\theta \in [-\pi, \pi)$, we have that $f(r_n(\theta)e^{i\theta}) \rightarrow \tilde{f}(e^{i\theta})$ for a.e. $\theta \in [-\pi, \pi)$. Also, $|f(r_n(\theta)e^{i\theta})|$ is bounded above by $F(e^{i\theta})$. Therefore, by the Lebesgue

Dominated Convergence Theorem, we have that

$$\lim_{n \rightarrow \infty} \frac{1}{2\pi} \int_{-\pi}^{\pi} |f(r_n(\theta)e^{i\theta})|^p d\theta = \frac{1}{2\pi} \int_{-\pi}^{\pi} |\tilde{f}(e^{i\theta})|^p d\theta = \|f\|_p^p.$$

□

Although it is not obvious from its statement, what the following lemma shows is that given the constraint of $\rho(M_n, r_n) = \frac{M_n - r_n}{1 - M_n r_n} \xrightarrow{u} 0$, the quantity $[M_n - r_n](\theta)$ approaches 0 faster than the radius of the ball $B\left(M_n(\theta), \left[\frac{r(1 - M_n^2)}{(1 + rM_n)}\right](\theta)\right) \subset K(M_n(\theta), r)$. Later, this will allow us to get an upper bound on the number of points a_k that can lie within an appropriately defined set S_n , constrained by $\rho(a_k, a_j) > \epsilon$, that varies with ϵ instead of ϵ^2 . The corollary that follows is provided to make use of this lemma more obvious in the context in which it is used.

Lemma 3.4.9 *Let $\{S_n\}$ satisfy Condition A with r_n and M_n as defined in that condition. Fix $r \in (0, 1)$. Then*

$$\frac{M_n - r_n}{\left(\frac{r(1 - M_n^2)}{1 + rM_n}\right)} \xrightarrow{u} 0.$$

Proof. For each $\theta \in [-\pi, \pi)$,

$$\begin{aligned} \frac{M_n(\theta) - r_n(\theta)}{\left(\frac{r(1 - M_n^2(\theta))}{(1 + rM_n(\theta))}\right)} &= \frac{(M_n(\theta) - r_n(\theta))(1 + rM_n(\theta))}{r(1 - M_n^2(\theta))} \\ &= \frac{(M_n(\theta) - r_n(\theta))}{(1 - M_n(\theta)r_n(\theta))} \frac{(1 - M_n(\theta)r_n(\theta))}{(1 - M_n(\theta))} \frac{(1 + rM_n(\theta))}{r(1 + M_n(\theta))} \\ &\leq \frac{(M_n(\theta) - r_n(\theta))}{(1 - M_n(\theta)r_n(\theta))} \frac{(1 - r_n^2(\theta))}{(1 - M_n(\theta))} \frac{(1 + rM_n(\theta))}{r(1 + M_n(\theta))} \\ &= \frac{(M_n(\theta) - r_n(\theta))}{(1 - M_n(\theta)r_n(\theta))} \frac{(1 - r_n(\theta))}{(1 - M_n(\theta))} \frac{(1 + r_n(\theta))(1 + rM_n(\theta))}{r(1 + M_n(\theta))}. \end{aligned}$$

We have, from Lemma 3.4.6, that $\frac{(1 - r_n)}{(1 - M_n)} \xrightarrow{u} 1$, and by inspection, $\frac{(1 + r_n)(1 + rM_n)}{r(1 + M_n)} \xrightarrow{u} \frac{(1 + r)}{r}$, since $r_n \leq M_n < 1$ and $r_n \rightarrow 1$, so that $M_n \rightarrow 1$ as $n \rightarrow \infty$. By (4) of Condition A, we have that $\frac{(M_n - r_n)}{(1 - M_n r_n)} \xrightarrow{u} 0$. Therefore

$$\frac{M_n - r_n}{\left(\frac{r(1-M_n^2)}{(1+rM_n)}\right)} \xrightarrow{u} 0.$$

□

Lemma 3.4.10 will require two sets, $\angle S_n(\theta, \Delta\theta)$ and $\Delta\theta_n$, and one function, $\Delta\phi_n(s)$, which are rather geometric in nature and somewhat confusing. In order to improve the flow of the proof of Lemma 3.4.10, these sets will be defined and discussed here, before the statement of the lemma.

Let $\{S_n\}$ satisfy Condition A. Fix $0 < r < 1$ and $0 < t < 1$. Define $r'_n : [-\pi, \pi) \rightarrow [0, 1)$ by $r'_n(\theta) = \frac{r(1-M_n^2(\theta))}{1+rM_n(\theta)}$. The set $\angle S_n(\theta, \Delta\theta)$ is defined by

$$\angle S_n(\theta, \Delta\theta) = \{z \in S_n : |\theta - \arg z| < t\Delta\theta\}. \quad (7)$$

The set $\Delta\theta_n$ is defined by

$$\Delta\theta_n = \sup\{\Delta\theta : \angle S_n(\arg s, \Delta\theta) \subset B(s, r'_n(\arg s)) \text{ for all } s \in S_n\}. \quad (8)$$

Note that $\Delta\theta_n$ may not be defined for some n . The function $\Delta\phi_n : \mathbb{D} \rightarrow [0, \pi]$ is defined by

$$\Delta\phi_n(s) = \text{one-half the angle subtended by } B(s, r'_n(\arg s)) \text{ relative to the origin}. \quad (9)$$

To explain the significance of these sets, the set $\angle S_n(\theta, \Delta\theta)$ is the intersection between the set S_n and a wedge of the unit disk, \mathbb{D} , of angular width $2t\Delta\theta$ centered at angle θ . The value $\Delta\theta_n$ represents the largest angular half-width of the set $\angle S_n(\arg s, \Delta\theta)$ which is a subset of the set $K(s, r'_n(\arg s))$ for $s \in S_n$, regardless of which $s \in S_n$ is chosen.

Lemma 3.4.10 *Fix $0 < r < 1$ and $0 < t < 1$. Let $\{S_n\}$ satisfy Condition A. Define $r'_n : [-\pi, \pi) \rightarrow [0, 1)$ by $r'_n(\theta) = \frac{r(1-M_n^2(\theta))}{1+rM_n(\theta)}$. Define the sets $\angle S_n(\theta, \Delta\theta)$ and $\Delta\theta_n$ and the function $\Delta\phi_n(s)$ by (7), (8), and (9), respectively. Then there exists $N < \infty$ such that $\Delta\theta_n$ is well-defined and $\Delta\theta_n \geq t\Delta\phi_n(s)$ for every $n > N$ and $s \in S_n$.*

Proof. From Lemma 3.4.9 above, we know that $\frac{M_n - r_n}{r'_n} \xrightarrow{u} 0$. Therefore, there exists some N such that for every $n \geq N$, $\Delta\theta_n$ is well-defined. That is, for every $n \geq N$ and

$s \in S_n$, $\angle S_n(\theta, \Delta\theta) \subset B(s, r'_n(\arg s))$. Since $r_n \xrightarrow{u} 1$, $\frac{M_n - r_n}{r'_n} \xrightarrow{u} 0$, and $\frac{\sin \Delta\theta}{\Delta\theta} \rightarrow 1$ as $\Delta\theta \rightarrow 0$, we have that $\Delta\theta_n \rightarrow 2 \inf_{s \in S_n} \Delta\phi_n(s)$. Therefore, there exists some N such that for all $n > N$, $\Delta\theta_n \geq t \Delta\phi_n(s)$ for any $s \in S_n$. \square

This lemma is later used to establish a bound on the angle subtended on a given radius, r_n , by a ball, $K(z, s)$, about a point z on that radius.

Lemma 3.4.11 *Let $0 \leq s < r_n < 1$ and suppose $\rho(r_n, r_n e^{i\theta}) \leq s$. Then,*

$$\sin \theta \leq \frac{s}{(1 - s^2)} \frac{(1 - r_n^4)}{r_n}.$$

Proof. By the definition of ρ (See Definition 3.1.2), we see that

$$s \geq \rho(r_n, r_n e^{i\theta}) = \frac{|r_n - r_n e^{i\theta}|}{|1 - r_n^2 e^{i\theta}|},$$

which leads to

$$s^2 \geq \frac{2r_n^2(1 - \cos \theta)}{1 + r_n^4 - 2r_n^2 \cos \theta}.$$

Solving for $\cos \theta$, we find

$$\cos \theta \geq \frac{2r_n^2 - s^2(1 + r_n^4)}{2r_n^2(1 - s^2)},$$

which leads to

$$\begin{aligned} \sin^2 \theta &\leq 1 - \left(\frac{2r_n^2 - s^2(1 + r_n^4)}{2r_n^2(1 - s^2)} \right)^2 \\ &= \frac{s^2[4r_n^2(1 - r_n^2)^2 - s^2(1 - r_n^4)^2]}{4r_n^4(1 - s^2)^2} \\ &\leq \frac{s^2[4r_n^2(1 - r_n^4)^2 - s^2(1 - r_n^4)^2]}{4r_n^4(1 - s^2)^2} \\ &= \frac{s^2(4r_n^2 - s^2)(1 - r_n^4)^2}{4r_n^4(1 - s^2)^2} \\ &\leq \frac{s^2(4r_n^2)(1 - r_n^4)^2}{4r_n^4(1 - s^2)^2} \\ &= \frac{s^2(1 - r_n^4)^2}{r_n^2(1 - s^2)^2}. \end{aligned}$$

Therefore,

$$\sin \theta \leq \frac{s}{(1-s^2)} \frac{(1-r_n^4)}{r_n}.$$

□

The following theorem is an elaboration of a step in the proof of Theorem 3.1.3. In that proof, the step was not justified, and the ϵ dependency was not revealed. I can conceive of no way to remove the ϵ dependency completely, and this brings into doubt the validity of Theorem 3.1.3 for values $0 < p \leq 1$. I suspect is that it is correct for these values. However, the proof might have to be different.

Theorem 3.4.12 *Fix $0 < \epsilon < 1$ and $0 < s < 1$. Let $\{S_n\}$ satisfy Condition A. Then for every set $\{a_{n,k}\}$ such that $a_{n,k} \in S_n$ and $\rho(a_{n,k}, a_{n,j}) \geq \epsilon$ for all $j \neq k$, there exist positive constants M and C depending only on s and C_s , where C_s is as defined in Condition A, such that*

$$\sum_k \int_{K(a_{n,k}, s)} |f(\zeta)|^p dm(\zeta) \leq \frac{C}{\epsilon} \int_{A_n} |f(\zeta)|^p dm(\zeta) \quad (10)$$

is true for all $n > M$ and all $f \in H_p(\mathbb{D})$, where A_n is any annulus containing each set in the collection $\{K(a_{n,k}, s)\}_{k=1}^{k(n)}$.

Proof. First, an upper bound will be obtained on the number of sets $K(a_{n,k}, s)$ in which any point in annulus A_n can be contained. This upper bound will be used to limit the magnitude of the sum relative to the integral over A_n in (10).

The angle subtended by the set $B\left(M_n(\theta), \frac{\epsilon(1-M_n^2(\theta))}{(1+\epsilon M_n(\theta))}\right)$ relative to the point at the origin is asymptotically equal to $\frac{2\epsilon(1-M_n^2(\theta))}{M_n(\theta)(1+\epsilon M_n(\theta))}$. Given our constraint that $r_n \xrightarrow{u} 1$ and $\frac{M_n - r_n}{1 - M_n r_n} \xrightarrow{u} 0$ and $\frac{2\epsilon(1-M_n^2(\theta))}{M_n(\theta)(1+\epsilon M_n(\theta))} > \epsilon(1 - M_n^2(\theta))$, we can conclude from Lemma 3.4.10 that there exists some $M < \infty$ such that for all $n > M$ and each $a_{n,k} \in A_n$, the set $K(a_{n,k}, \epsilon) \supset B\left(z, \frac{\epsilon(1-M_n(\theta))}{(1+\epsilon M_n(\theta))}\right)$ covers a wedge of A_n of angular width greater than $\epsilon(1 - M_n^2(\theta)) \geq \epsilon(1 - \overline{M_n}^2) > 0$ from which all other $a_{n,k}$ are excluded.

Next, we need to determine the maximum number of $a_{n,k}$ that can be in the ball $K(z, s)$. This will be done by using the above exclusion angle and determining the maximum angle that can be covered on the “worst case” of $|z| = r_n$. Assume $s = \rho(r_n, r_n e^{i\theta})$. From Lemma 3.4.11, we then have, $\sin \theta \leq \frac{s}{(1-s^2)} \frac{(1-r_n^4)}{r_n}$. Since $\frac{1-r_n^4}{r_n} \rightarrow 0$ and $\sin \theta \approx \theta$

as $\theta \rightarrow 0$, we can assume that for M sufficiently large and all $n > M$, the inequality $\theta \leq \frac{2s}{(1-s^2)} \frac{(1-r_n^4)}{r_n}$ will be true. That is, the angle subtended by $K(z, s)$ will be less than $2\theta \leq \frac{4s}{(1-s^2)} \frac{(1-r_n^4)}{r_n}$.

We have bounded the angle subtended by the set $K(z, s) \cap A_n$ above and have bounded below the angle of S_n completely covered by the set $K(a_{n,k}, \epsilon)$. Therefore, we may obtain an upper bound on the number of points $a_{n,k}$ in the set $K(z, s)$ by the ratio of these two angles, given by

$$\begin{aligned} \frac{\left(\frac{4s}{(1-s^2)} \frac{(1-r_n^4)}{r_n} \right)}{\epsilon(1-M_n^{-2})} &= \frac{1}{\epsilon} \left(\frac{4s}{1-s^2} \right) \left(\frac{1-r_n^4}{r_n(1-M_n^{-2})} \right) \\ &\leq \frac{1}{\epsilon} \left(\frac{8s}{1-s^2} \right) \left(\frac{1-r_n}{r_n(1-M_n)} \right). \end{aligned}$$

Since $r_n \rightarrow 1$ and by Lemma 3.4.7, $\limsup_{n \rightarrow \infty} \frac{1-r_n}{1-M_n} \leq \frac{2}{1-C_s}$, we know that for M sufficiently large and all $n > M$, the inequality $\frac{1-r_n}{r_n(1-M_n)} \leq \frac{2}{1-C_s} + 1$ will be true. Therefore, for M sufficiently large, the number of points $a_{n,k}$ in the set $K(z, s)$, denoted N , is bounded above by

$$N \leq \frac{1}{\epsilon} \left(\frac{8s}{1-s^2} \right) \left(\frac{2}{1-C_s} + 1 \right).$$

This gives that for all n sufficiently large,

$$\sum_k \int_{K(a_k, s)} |f(\zeta)|^p dm(\zeta) \leq \frac{C}{\epsilon} \int_{A_n} |f(\zeta)|^p dm(\zeta),$$

where $C = \left(\frac{8s}{1-s^2} \right) \left(\frac{2}{1-C_s} + 1 \right)$ is independent of ϵ and A_n is any annulus which contains the set $\{K(a_{n,k}, s)\}$. \square

3.5 Main result

We can now prove the main result (Theorem 3.1.4). The method of proof is to show that there is a δ small enough for the desired inequalities to be true. This is done by showing the inequalities depend on δ and some constant C independent of δ , allowing δ to be chosen such that we have the desired result.

Proof (Theorem 3.1.4). By Lemma 3.4.5, for any set $\{S_n\}$ as defined in the statement of this theorem, there exists a double indexed set $\{a_{n,k}\}$ which satisfies the conditions that for each n , $\rho(a_{n,j}, a_{n,k}) \geq \epsilon$ for all $j \neq k$ and $S_n \subset \bigcup_{k=1}^{k(n)} K(a_{n,k}, \delta)$. By Lemma 3.4.4, we have that $\#\{a_{n,k}\}_{k=1}^{k(n)}$ will be finite for each n .

Assume that for each n , the set $\{a_{n,k}\}$ is ordered by the relation $\arg a_{n,j} \leq \arg a_{n,k}$ for all $j < k$. Form a set, $\tilde{\gamma}_n$, according to

$$\tilde{\gamma}_n = \bigcup_{j=1}^{k(n)} \{z : z = [(1-t)|a_{n,j}| + t|a_{n,j+1}|]e^{i[(1-t)\arg a_{n,j} + t\arg a_{n,j+1}]}, t \in [0, 1]\},$$

where $\arg a_{n,k(n)+1} \doteq \arg a_{n,1} + 2\pi$ and $|a_{n,k(n)+1}| \doteq |a_{n,1}|$.

Define a function, $\gamma_n : [-\pi, \pi) \rightarrow \mathbb{D}$ by $\gamma_n(\theta) = z$ for some $z \in \tilde{\gamma}_n$ such that $\arg z = \theta$. In the (at most a finite number of) cases where $\gamma_n(\theta)$ is ambiguously defined, its value may be chosen arbitrarily. The function γ_n is piecewise continuous and bounded on a finite interval, and is hence Lebesgue measurable.

Fix $s \in (0, 1)$. By Lemma 3.4.3, there exists a constant $C < \infty$ depending only on C_s , p , and s such that

$$|f(z) - f(\zeta)|^p \leq C\delta^p \int_{K(\zeta, s)} |f|^p \frac{dm}{m(K(\zeta, s))}$$

whenever $\rho(z, \zeta) < \delta < \min\{\delta_r, \frac{1}{3}\}$. Multiply each side of this inequality by $\chi_\delta(z, \zeta)/(\delta(1 - |\zeta|))$, where χ_δ is defined by

$$\chi_\delta(z, \zeta) = \begin{cases} 1 & \text{if } \rho(z, \zeta) < \delta \\ 0 & \text{otherwise} \end{cases}.$$

Let $z = \gamma_n(\theta)$ and integrate both sides of the inequality with respect to $d\theta$ to get

$$\begin{aligned} \int_{-\pi}^{\pi} \frac{\chi_\delta(\gamma_n(\theta), \zeta)}{\delta(1 - |\zeta|)} |f(\gamma_n(\theta)) - f(\zeta)|^p d\theta &\leq C\delta^p \int_{-\pi}^{\pi} \frac{\chi_\delta(\gamma_n(\theta), \zeta)}{\delta(1 - |\zeta|)} \int_{K(\zeta, s)} |f|^p \frac{dm}{m(K(\zeta, s))} d\theta \\ &\leq C\delta^p \int_{-\pi}^{\pi} \frac{\chi_\delta(\gamma_n(\theta), \zeta)}{\delta(1 - |\zeta|)} d\theta \int_{K(\zeta, s)} |f|^p \frac{dm}{m(K(\zeta, s))}. \end{aligned}$$

For any fixed $\zeta \in \mathbb{D}$ and for n sufficiently large, from Lemma 3.3.5 we have that there is a c' depending only on s such that the maximum subtended angle $\Delta\theta$ in which $\gamma_n(\theta)$ could be within $K(\zeta, s)$ is such that $\Delta\theta \leq \min\{c'(1 - |\zeta|), c'(1 - \underline{r}_n)\} \leq c'(1 - |\zeta|)$. Since

$\chi_\delta(\gamma_n(\theta), \zeta)$ can only be non-zero within this angle, and when it is non-zero, it takes on the value 1, we have

$$\int_{-\pi}^{\pi} \frac{\chi_\delta(\gamma_n(\theta), \zeta)}{\delta(1-|\zeta|)} d\theta \leq \int_0^{\Delta\theta} \frac{1}{\delta(1-|\zeta|)} d\theta \leq \frac{c'}{\delta}.$$

Incorporating c' into C , we have

$$\int_{-\pi}^{\pi} \frac{\chi_\delta(\gamma_n(\theta), \zeta)}{\delta(1-|\zeta|)} |f(\gamma_n(\theta)) - f(\zeta)|^p d\theta \leq C\delta^{p-1} \int_{K(\zeta, s)} |f|^p \frac{dm}{m(K(\zeta, s))}. \quad (11)$$

Next, define a positive Borel measure over \mathbb{D} , $\mu_n: \mathbb{D} \rightarrow \mathbb{R}^+$, by

$$\mu_n(z) = \sum_{k=1}^{k(n)} (1 - |a_{n,k}|) \delta_{a_{n,k}}(z)$$

where

$$\delta_{a_{n,k}}(z) = \begin{cases} 1 & \text{if } z = a_{n,k} \\ 0 & \text{otherwise} \end{cases}.$$

Integrate both sides of (11) over \mathbb{D} with respect to $d\mu_n(\zeta)$ to get

$$\begin{aligned} & \int_{\mathbb{D}} \int_{-\pi}^{\pi} \frac{\chi_\delta(\gamma_n(\theta), \zeta)}{\delta(1-|\zeta|)} |f(\gamma_n(\theta)) - f(\zeta)|^p d\theta d\mu_n(\zeta) \\ & \leq C\delta^{p-1} \int_{\mathbb{D}} \int_{K(\zeta, s)} |f(\xi)|^p \frac{dm(\xi)}{m(K(\zeta, s))} d\mu_n(\zeta) \\ & \leq C\delta^{p-1} \sum_{k=1}^{k(n)} \mu_n(a_{n,k}) \int_{K(a_{n,k}, s)} |f(\xi)|^p \frac{dm(\xi)}{m(K(a_{n,k}, s))} \\ & \leq C\delta^{p-1} \sum_{k=1}^{k(n)} \delta(1 - |a_{n,k}|) \int_{K(a_{n,k}, s)} |f(\xi)|^p \frac{dm(\xi)}{m(K(a_{n,k}, s))}. \end{aligned}$$

Since $\frac{1}{m(K(\xi, s))} = \frac{(1-s^2|a_{n,k}|^2)^2}{s^2(1-|a_{n,k}|^2)^2} \leq \frac{c'}{(1-|a_{n,k}|)^2}$, where $c' \doteq \frac{(1-s^2)^2}{s^2}$ depends only on s , we can incorporate constants to give

$$\begin{aligned} & \int_{\mathbb{D}} \int_{-\pi}^{\pi} \frac{\chi_\delta(\gamma_n(\theta), \zeta)}{\delta(1-|\zeta|)} |f(\gamma_n(\theta)) - f(\zeta)|^p d\theta d\mu_n(\zeta) \\ & \leq C\delta^{p-1} \sum_{k=1}^{k(n)} \frac{\delta}{(1-|a_{n,k}|)} \int_{K(a_{n,k}, s)} |f(\xi)|^p dm(\xi). \end{aligned}$$

By the definition of $\overline{M_n}$, we know that $\frac{1}{1-|a_{n,k}|} \leq \frac{1}{1-\overline{M_n}}$, giving

$$\int_{\mathbb{D}} \int_{-\pi}^{\pi} \frac{\chi_{\delta}(\gamma_n(\theta), \zeta)}{\delta(1-|\zeta|)} |f(\gamma_n(\theta)) - f(\zeta)|^p d\theta d\mu_n(\zeta) \leq \frac{C\delta^p}{1-\overline{M_n}} \sum_{k=1}^{k(n)} \int_{K(a_{n,k}, s)} |f(\xi)|^p dm(\xi).$$

Since s and ϵ are fixed and $K(a_{n,k}, \epsilon/2)$ are disjoint, by Theorem 3.4.12 we know there exists some constant c' depending only on s and C_s such that

$$\sum_{k=1}^{k(n)} \int_{K(a_{n,k}, s)} |f(\xi)|^p dm(\xi) \leq \frac{c'}{\epsilon} \int_{A_n(s)} |f(\xi)|^p dm(\xi),$$

where $A_n(s)$, defined by

$$A_n(s) = \{z \in \mathbb{D} : \underline{r_n} - 2s(1 - \underline{r_n}) \leq |z| \leq \overline{M_n} + 2s(1 - \overline{M_n})\},$$

is an annulus which contains each of the $K(a_{n,k}, s)$ for $k = 1, 2, \dots, k(n)$. Incorporating the constant c' into C , this gives

$$\begin{aligned} & \int_{\mathbb{D}} \int_{-\pi}^{\pi} \frac{\chi_{\delta}(\gamma_n(\theta), \zeta)}{\delta(1-|\zeta|)} |f(\gamma_n(\theta)) - f(\zeta)|^p d\theta d\mu_n(\zeta) \\ & \leq \frac{C\delta^p \epsilon^{-1}}{1-\overline{M_n}} \int_{A_n} |f(\xi)|^p dm(\xi) \\ & \leq \frac{C\delta^p \epsilon^{-1}}{1-\overline{M_n}} \int_{\underline{r_n}-2s(1-\underline{r_n})}^{\overline{M_n}+2s(1-\overline{M_n})} \frac{1}{\pi} \int_{-\pi}^{\pi} |f(re^{i\theta})|^p d\theta r dr \\ & \leq \frac{C\delta^p \epsilon^{-1}}{1-\overline{M_n}} \int_{\underline{r_n}-2s(1-\underline{r_n})}^{\overline{M_n}+2s(1-\overline{M_n})} 2\|f\|_p^p r dr \\ & \leq \frac{C\delta^p \epsilon^{-1}}{1-\overline{M_n}} \int_{\underline{r_n}-2s}^{\overline{M_n}+2s} 2\|f\|_p^p r dr \\ & \leq 2(1+4s)(1-\underline{r_n}) \frac{C\delta^p \epsilon^{-1}}{1-\overline{M_n}} \|f\|_p^p. \end{aligned}$$

Incorporating the constant $2(1+4s)$ into C gives

$$\int_{\mathbb{D}} \int_{-\pi}^{\pi} \frac{\chi_{\delta}(\gamma_n(\theta), \zeta)}{\delta(1-|\zeta|)} |f(\gamma_n(\theta)) - f(\zeta)|^p d\theta d\mu_n(\zeta) \leq C\delta^p \epsilon^{-1} \frac{1-\underline{r_n}}{1-\overline{M_n}} \|f\|_p^p. \quad (12)$$

Now it is necessary to break apart the left-hand side integral. We raise each side of (12) to the $1/p$ power and invoke Minkowski's inequality to get

$$\begin{aligned} \left[\int_{\mathbb{D}} \int_{-\pi}^{\pi} \frac{\chi_{\delta}(\gamma_n(\theta), \zeta)}{\delta(1-|\zeta|)} |f(\gamma_n(\theta))|^p d\theta d\mu_n(\zeta) \right]^{1/p} &= \left[\int_{\mathbb{D}} \int_{-\pi}^{\pi} \frac{\chi_{\delta}(\gamma_n(\theta), \zeta)}{\delta(1-|\zeta|)} |f(\zeta)|^p d\theta d\mu_n(\zeta) \right]^{1/p} \\ &\leq C\delta\epsilon^{-1/p} \left(\frac{1-r_n}{1-M_n} \right)^{1/p} \|f\|_p. \end{aligned} \quad (13)$$

Applying Fubini's theorem to the first integral of (13), we have

$$\begin{aligned} &\int_{\mathbb{D}} \int_{-\pi}^{\pi} \frac{\chi_{\delta}(\gamma_n(\theta), \zeta)}{\delta(1-|\zeta|)} |f(\gamma_n(\theta))|^p d\theta d\mu_n(\zeta) \\ &= \int_{-\pi}^{\pi} \int_{\mathbb{D}} \frac{\chi_{\delta}(\gamma_n(\theta), \zeta)}{\delta(1-|\zeta|)} |f(\gamma_n(\theta))|^p d\mu_n(\zeta) d\theta \\ &= \int_{-\pi}^{\pi} \sum_{k=1}^{k(n)} \mu_n(a_{n,k}) \frac{\chi_{\delta}(\gamma_n(\theta), a_{n,k})}{\delta(1-|a_{n,k}|)} |f(\gamma_n(\theta))|^p d\theta \\ &= \int_{-\pi}^{\pi} \sum_{k=1}^{k(n)} \delta(1-|a_{n,k}|) \frac{\chi_{\delta}(\gamma_n(\theta), a_{n,k})}{\delta(1-|a_{n,k}|)} |f(\gamma_n(\theta))|^p d\theta \\ &= \sum_{k=1}^{k(n)} \int_{-\pi}^{\pi} \chi_{\delta}(\gamma_n(\theta), a_{n,k}) |f(\gamma_n(\theta))|^p d\theta. \end{aligned}$$

Since the sets $K(a_{n,k}, \delta)$ overlap and cover S_n , which “surrounds” the origin, we have that

$$\begin{aligned} \int_{\mathbb{D}} \int_{-\pi}^{\pi} \frac{\chi_{\delta}(\gamma_n(\theta), \zeta)}{\delta(1-|\zeta|)} |f(\gamma_n(\theta))|^p d\theta d\mu_n(\zeta) &= \sum_{k=1}^{k(n)} \int_{-\pi}^{\pi} \chi_{\delta}(\gamma_n(\theta), a_{n,k}) |f(\gamma_n(\theta))|^p d\theta \\ &\geq \int_{-\pi}^{\pi} |f(\gamma_n(\theta))|^p d\theta. \end{aligned} \quad (14)$$

Working now with the second integral of (13), we have

$$\int_{\mathbb{D}} \int_{-\pi}^{\pi} \frac{\chi_{\delta}(\gamma_n(\theta), \zeta)}{\delta(1-|\zeta|)} |f(\zeta)|^p d\theta d\mu_n(\zeta) = \int_{\mathbb{D}} |f(\zeta)|^p \int_{-\pi}^{\pi} \frac{\chi_{\delta}(\gamma_n(\theta), \zeta)}{\delta(1-|\zeta|)} d\theta d\mu_n(\zeta).$$

As before, the subtended angle $\Delta\theta$ for which $\chi_{\delta}(\gamma_n(\theta), \zeta)$ is non-zero is bounded above by $c'(1-|\zeta|)$. Therefore,

$$\int_{-\pi}^{\pi} \frac{\chi_{\delta}(\gamma_n(\theta), \zeta)}{\delta(1-|\zeta|)} d\theta \leq \frac{c'}{\delta}.$$

This gives

$$\begin{aligned}
\int_{\mathbb{D}} \int_{-\pi}^{\pi} \frac{\chi_{\delta}(\gamma_n(\theta), \zeta)}{\delta(1-|\zeta|)} |f(\zeta)|^p d\theta d\mu_n(\zeta) &\leq \frac{c'}{\delta} \int_{\mathbb{D}} |f(\zeta)|^p d\mu_n(\zeta) \\
&\leq \frac{c'}{\delta} \sum_{k=1}^{k(n)} \mu_n(a_{n,k}) |f(a_{n,k})|^p \\
&\leq \frac{c'}{\delta} \sum_{k=1}^{k(n)} \delta(1-|a_{n,k}|) |f(a_{n,k})|^p \\
&\leq c' \sum_{k=1}^{k(n)} (1-|a_{n,k}|) |f(a_{n,k})|^p. \tag{15}
\end{aligned}$$

Substituting (14) and (15) back into (13) gives

$$\begin{aligned}
&\left[\int_{-\pi}^{\pi} |f(\gamma_n(\theta))|^p d\theta \right]^{1/p} - c' \left[\sum_{k=1}^{k(n)} (1-|a_{n,k}|) |f(a_{n,k})|^p \right]^{1/p} \\
&\leq C\delta\epsilon^{-1/p} \left(\frac{1-r_n}{1-\overline{M}_n} \right)^{1/p} \|f\|_p,
\end{aligned}$$

which implies

$$\begin{aligned}
&\left[\int_{-\pi}^{\pi} |f(\gamma_n(\theta))|^p d\theta \right]^{1/p} - c' \sup_n \left[\sum_{k=1}^{k(n)} (1-|a_{n,k}|) |f(a_{n,k})|^p \right]^{1/p} \\
&\leq C\delta\epsilon^{-1/p} \left(\frac{1-r_n}{1-\overline{M}_n} \right)^{1/p} \|f\|_p,
\end{aligned}$$

and also

$$\begin{aligned}
&\left[\int_{-\pi}^{\pi} |f(\gamma_n(\theta))|^p d\theta \right]^{1/p} - C\delta\epsilon^{-1/p} \left(\frac{1-r_n}{1-\overline{M}_n} \right)^{1/p} \|f\|_p \\
&\leq c' \sup_n \left[\sum_{k=1}^{k(n)} (1-|a_{n,k}|) |f(a_{n,k})|^p \right]^{1/p}.
\end{aligned}$$

Since this is true for each n , it is true in the limit. Using Lemmas 3.4.8 and 3.4.7 to take the limit of the left-hand side as $n \rightarrow \infty$, we obtain

$$\liminf_{n \rightarrow \infty} \left[\left[\int_{-\pi}^{\pi} |f(\gamma_n(\theta))|^p d\theta \right]^{1/p} - C\delta\epsilon^{-1/p} \left(\frac{1-r_n}{1-\overline{M}_n} \right)^{1/p} \|f\|_p \right]$$

$$\begin{aligned}
&= \|f\|_p - \limsup_{n \rightarrow \infty} \left[C \delta \epsilon^{-1/p} \left(\frac{1 - r_n}{1 - \overline{M}_n} \right)^{1/p} \|f\|_p \right] \\
&= \|f\|_p - C \delta \epsilon^{-1/p} \|f\|_p \limsup_{n \rightarrow \infty} \left(\frac{1 - r_n}{1 - \overline{M}_n} \right)^{1/p} \\
&\geq \|f\|_p - C \delta \epsilon^{-1/p} \left(\frac{2}{1 - C_s} \right)^{1/p} \|f\|_p .
\end{aligned}$$

Since C is independent of δ and $p > 1$, we may choose δ and ϵ so that

$$C \delta \epsilon^{-1/p} \left(\frac{2}{1 - C_s} \right)^{1/p} < 1 ,$$

giving

$$c \|f\|_p \leq \sup_n \left[\sum_{k=1}^{k(n)} (1 - |a_{n,k}|) |f(a_{n,k})|^p \right]^{1/p} ,$$

where $c > 0$ depends on C_s , δ , and p but not on f , $\{S_n\}$, or $\{a_{n,k}\}$. Thus we have proven the left-hand inequality of (5).

The proof of the right-hand inequality of (5) is much easier. From Lemma 3.4.1 above, we have that there exists a constant, C , depending only on ϵ such that

$$|f(a_{n,k})|^p \leq C \int_{K(a_{n,k}, (\epsilon/2))} |f(\zeta)|^p \frac{dm(\zeta)}{m(K(a_{n,k}, (\epsilon/2)))} .$$

Therefore,

$$\sum_{k=1}^{k(n)} |f(a_{n,k})|^p (1 - |a_{n,k}|) \leq C \sum_{k=1}^{k(n)} (1 - |a_{n,k}|) \int_{K(a_{n,k}, (\epsilon/2))} |f(\zeta)|^p \frac{dm(\zeta)}{m(K(a_{n,k}, (\epsilon/2)))} .$$

Since

$$\frac{1}{m(K(a_{n,k}, (\epsilon/2)))} \leq \frac{1}{(\epsilon/2)^2 (1 - |a_{n,k}|)^2} \leq \frac{1}{(\epsilon/2)^2 (1 - \overline{M}_n) (1 - |a_{n,k}|)} ,$$

we have

$$\sum_{k=1}^{k(n)} |f(a_{n,k})|^p (1 - |a_{n,k}|) \leq \frac{C}{(\epsilon/2)^2 (1 - \overline{M}_n)} \sum_{k=1}^{k(n)} \int_{K(a_{n,k}, (\epsilon/2))} |f(\zeta)|^p dm(\zeta) . \quad (16)$$

The $K(a_{n,k}, (\epsilon/2))$ are disjoint, and so we may bound the sum of integrals over them by an integral over an annulus containing them, giving

$$\sum_{k=1}^{k(n)} |f(a_{n,k})|^p (1 - |a_{n,k}|) \leq \frac{C}{(\epsilon/2)^2(1 - \overline{M}_n)} \int_{A_n} |f(\zeta)|^p dm(\zeta),$$

where

$$A_n = \left\{ z : r_n - \frac{(\epsilon/2)(1 - r_n^2)}{1 - (\epsilon/2)r_n} \leq |z| \leq \overline{M}_n + \frac{(\epsilon/2)(1 - \overline{M}_n^2)}{1 + (\epsilon/2)\overline{M}_n} \right\}.$$

Applying this inequality to (16), we get

$$\begin{aligned} \sum_{k=1}^{k(n)} |f(a_{n,k})|^p (1 - |a_{n,k}|) &\leq \frac{C}{(\epsilon/2)^2(1 - \overline{M}_n)} \int_{r_n - \frac{(\epsilon/2)(1 - r_n^2)}{1 - (\epsilon/2)r_n}}^{\overline{M}_n + \frac{(\epsilon/2)(1 - \overline{M}_n^2)}{1 + (\epsilon/2)\overline{M}_n}} \int_{-\pi}^{\pi} |f(\zeta)|^p \frac{d\theta}{\pi} r dr \\ &\leq \frac{C}{(\epsilon/2)^2(1 - \overline{M}_n)} \int_{r_n - \frac{(\epsilon/2)(1 - r_n^2)}{1 - (\epsilon/2)r_n}}^{\overline{M}_n + \frac{(\epsilon/2)(1 - \overline{M}_n^2)}{1 + (\epsilon/2)\overline{M}_n}} 2 \|f\|_p^p r dr \\ &\leq \frac{C}{(\epsilon/2)^2(1 - \overline{M}_n)} \left(1 + \frac{4(\epsilon/2)}{1 - (\epsilon/2)}\right) (1 - r_n) \|f\|_p^p. \end{aligned}$$

Incorporating the constants based on ϵ into C , we get

$$\sum_{k=1}^{k(n)} |f(a_{n,k})|^p (1 - |a_{n,k}|) \leq C \frac{(1 - r_n)}{(1 - \overline{M}_n)} \|f\|_p^p.$$

By Lemma 3.4.7, we know that (6) holds, and so there exists some constant $c < \infty$ such that $\frac{(1 - r_n)}{(1 - \overline{M}_n)} \leq c$ for all n . Incorporating this constant, c , into C gives

$$\sum_{k=1}^{k(n)} |f(a_{n,k})|^p (1 - |a_{n,k}|) \leq C \|f\|_p^p,$$

proving the right-hand inequality of (5). \square

3.6 Representation of elements of the Hardy spaces, $H_p(\mathbb{D})$

Discussed in this section are two theorems which make it possible to use the results of Theorem 3.1.4 to find representations for elements of the Hardy spaces, $H_p(\mathbb{D})$. Theorem 3.6.1 is due to Bonsall and is found in [5: Theorem 1]. It was later extended by Dudley

Ward and Partington in [33:Theorem 3]. A proof for Theorem 3.6.1, an elaboration of that given in [33], is given in Appendix B, since it is so long.

Theorem 3.6.4 is the one of interest here. It relates the the Carleson inequalities established in Theorem 3.1.4 to norms of sequences of coefficients used to represent functions in $H_p(\mathbb{D})$. It is a rather trivial extension, based on Theorem 3.1.4, of [33:Theorem 5], which is itself an extension of [20:Theorem 5.5].

Theorem 3.6.1 (Ward and Partington, [33]) *Let X be a Banach space and define $X_1 \subset X$ by $X_1 = \{f \in X : \|f\| \leq 1\}$. For $n \in \mathbb{Z}^+$, let E_n be a finite subset of X with $\#(E_n) = k(n)$. Let the set E be defined by $E = \bigcup_n E_n$ and the set $E_{1,p}$ by*

$$E_{1,p} = \{h \in X : h = \sum_{n=1}^N \sum_{k=1}^{k(n)} \lambda_{n,k} u_{n,k}, \sum_{n=1}^N \left(\sum_{k=1}^{k(n)} |\lambda_{n,k}|^p \right)^{1/p} \leq 1, u_{n,k} \in E_n, N < \infty\}.$$

Let $\Lambda(E, f)$ be defined by

$$\Lambda(E, f) = \{\lambda = \{\lambda_{n,k}\} : f = \sum_{n,k} \lambda_{n,k} u_{n,k}, u_{n,k} \in E_n\}.$$

Let m, M, p , and q be positive constants with $\frac{1}{p} + \frac{1}{q} = 1$. Then the following statements are equivalent.

1. For each $\Phi \in X^*$,

$$m\|\Phi\| \leq \sup_n \left\{ \left(\sum_{k=1}^{k(n)} |\Phi(u_{n,k})|^q \right)^{1/q} : u_{n,k} \in E_n \right\} \leq M\|\Phi\|.$$

2. $mX_1 \subset \overline{E_{p,1}}$ and for each $h \in E_{p,1}$, where $h = \sum_{j=1}^N x_j$, and $x_j = \sum_{k=1}^{k(j)} \alpha_{j,k} u_{j,k}$, with $\sum_{j=1}^N \left(\sum_{k=1}^{k(j)} |\alpha_{j,k}|^p \right)^{1/p} \leq 1$, we have $\sum_{j=1}^N \|x_j\| \leq M$.

3. For each $f \in X$, $\Lambda(E, f)$ is non-empty and

$$\frac{\|f\|}{M} \leq \inf\{\|\lambda\|_{1,p} : \lambda \in \Lambda(E, f)\} \leq \frac{\|f\|}{m}.$$

Proof. See Appendix B.

Before stating Theorem 3.6.4, two lemmas needed in its proof will be stated and proved. The following lemma will be necessary to show that the conditions of Theorem 3.6.1 are met.

Lemma 3.6.2 Fix $a \in \mathbb{D}$, let $q \in (1, \infty)$, and define $\psi_a : \mathbb{D} \rightarrow \mathbb{C}$ by

$$\psi_a(z) = \frac{(1 - |a|)^{1/q}}{1 - \bar{a}z}. \quad (17)$$

Then $\psi_a \in H_p(\mathbb{D})$, where $\frac{1}{p} \doteq 1 - \frac{1}{q}$.

Proof. Since ψ_a is a rational function with a single pole at $z = \frac{a}{|a|^2} \notin \bar{\mathbb{D}}$, it is analytic in \mathbb{D} and so has a Maclaurin series expansion which is valid in all of \mathbb{D} . This expansion can be calculated to be

$$\psi_a(z) = (1 - |a|)^{1/q} \sum_{j=0}^{\infty} (\bar{a})^j z^j. \quad (18)$$

To see that $\psi_a \in H_p$, it is sufficient to show that

$$(1 - |a|)^{1/q} \sum_{j=0}^{\infty} |(\bar{a})^j|^p < \infty.$$

Calculating,

$$\begin{aligned} (1 - |a|)^{1/q} \sum_{j=0}^{\infty} |(\bar{a})^j|^p &= (1 - |a|)^{1/q} \sum_{j=0}^{\infty} (|a|^p)^j \\ &= \frac{(1 - |a|)^{1/q}}{1 - |a|^p} < \infty. \end{aligned}$$

□

This lemma provides the link between the sampled values in the inequalities of the main result, Theorem 3.1.4, and the functional values needed to prove Theorem 3.6.4 based on the results of Theorem 3.6.1.

Lemma 3.6.3 Let $a \in \mathbb{D}$ and $p \in (1, \infty)$. Define q by $\frac{1}{q} \doteq 1 - \frac{1}{p}$. Let $F \in H_p(\mathbb{D})^* \cong H_q(\mathbb{D})$. Choose $f \in H_q(\mathbb{D})$ such that

$$F(\phi) = \lim_{r \rightarrow 1^-} \int_{\partial \mathbb{D}} \phi(rz) \overline{f(rz)} d\sigma(z)$$

for all $\phi \in H_p(\mathbb{D})$. Let $\psi_a \in H_p(\mathbb{D})$ be as defined in (17). Then,

$$F(\psi_a) = (1 - |a|)^{1/q} \overline{f(a)}.$$

Proof. Since $f \in H_q(\mathbb{D})$, it may be expressed as a Maclaurin series, that is, $f(z) = \sum_{j=0}^{\infty} \gamma_j z^j$ for some choice of $\{\gamma_j\}_{j=0}^{\infty}$. Using the Maclaurin series for ψ_a given in (18), we have that the action of F on ψ_a is given by

$$\begin{aligned} F(\psi_a) &= \lim_{r \rightarrow 1^-} \int_{\partial \mathbb{D}} \overline{f(rz)} \psi_a(rz) d\sigma(z) \\ &= \lim_{r \rightarrow 1^-} \int_{\partial \mathbb{D}} \overline{\left(\sum_{j=0}^{\infty} \gamma_j (rz)^j \right)} \left((1 - |a|)^{1/q} \sum_{k=0}^{\infty} (\overline{a})^k (rz)^k \right) d\sigma(z) \\ &= (1 - |a|)^{1/q} \lim_{r \rightarrow 1^-} \int_{\partial \mathbb{D}} \sum_{j=0}^{\infty} \sum_{k=0}^{\infty} \overline{\gamma_j} \overline{a}^k r^{j+k} \overline{z}^j z^k d\sigma(z) \\ &= (1 - |a|)^{1/q} \lim_{r \rightarrow 1^-} \sum_{j=0}^{\infty} \overline{\gamma_j} \overline{a}^j r^{2j} \\ &= (1 - |a|)^{1/q} \sum_{j=0}^{\infty} \overline{\gamma_j} \overline{a}^j \\ &= (1 - |a|)^{1/q} \overline{f(a)}. \end{aligned}$$

□

As mentioned earlier, Theorem 3.6.4 is an extension of [20:Theorem 5.5]. Previously, [20:Theorem 5.5] was extended by Ward and Partington (see [33:Theorem 5]) to include specific upper and lower bounds. Below in Theorem 3.6.4, [33:Theorem 5] is modified to allow the set $\{a_{n,k}\}$ to satisfy the conditions of the main result, Theorem 3.1.4. The proof of Theorem 3.6.4 is unchanged from that given in [33:Theorem 5]. While this theorem is easily proven, this result is the one which will be of direct use in developing frames in Chapter V.

The representations proven in this theorem are defined with the use of sequences in $\ell_{1,p}$ for $1 < p < \infty$, defined as

$$\ell_{1,p} = \left\{ \{\lambda_{n,k}\}_{\substack{k=1,\dots,k(n) \\ n=1,\dots}} \in \mathbb{C} : \sum_{n=1}^{\infty} \left(\sum_{k=1}^{k(n)} |\lambda_{n,k}|^p \right)^{1/p} < \infty \right\}.$$

Theorem 3.6.4 *Let $\{S_n\}$, $\{a_{n,k}\}$, δ , ϵ , and q be as in Theorem 3.1.4 (where q replaces p). Then every $f \in H_p(\mathbb{D})$ has the form*

$$f(z) = \sum_{n,k} \lambda_{n,k} \frac{(1 - |a_{n,k}|)^{1/q}}{(1 - \overline{a_{n,k}}z)},$$

where $\frac{1}{p} \doteq 1 - \frac{1}{q}$, $\lambda = \{\lambda_{n,k}\} \in \ell_{1,p}$ and

$$c\|f\|_p \leq \inf_{\lambda \in \Lambda_p(f)} \|\lambda\|_{1,p} \leq C\|f\|_p$$

for some $0 < c \leq C < \infty$ independent of f .

Proof. This proof follows that in [33].

It is necessary to show the existence of some $k, K > 0$ such that for all $f \in H_p(\mathbb{D})$,

$$k\|f\|_p \leq \inf_{\lambda \in \Lambda_p(f)} \|\lambda\|_{1,p} \leq K\|f\|_p.$$

To do this, we will invoke Theorem 3.6.1.

First, note that $H_p(\mathbb{D})$ is a Banach space, with dual space $H_p(\mathbb{D})^* \cong H_q(\mathbb{D})$. Let $\Phi \in H_p(\mathbb{D})^*$ with corresponding $\phi \in H_q(\mathbb{D})$, and define $\psi_{n,k}$ by

$$\psi_{n,k}(z) = \frac{(1 - |a_{n,k}|)^{1/q}}{1 - \overline{a_{n,k}}z}.$$

We know that $\psi_{n,k} \in H_p(\mathbb{D})$ by Lemma 3.6.2, and from Lemma 3.6.3, we know that

$$\Phi(\psi_{n,k}) = (1 - |a_{n,k}|)^{1/q} \overline{\phi(a_{n,k})}$$

From Theorem 3.1.4, we know that for our choice of $a_{n,k}$ and for some choice of $0 < m, M < \infty$, we have

$$m\|\phi\| \leq \sup_n \left(\sum_{k=1}^{k(n)} |\phi(a_{n,k})|^q (1 - |a_{n,k}|) \right)^{1/q} \leq M\|\phi\|$$

which gives

$$m\|\phi\| \leq \sup_n \left(\sum_{k=1}^{k(n)} |\Phi(\psi_{n,k})|^q \right)^{1/q} \leq M\|\phi\| .$$

Having established this, Theorem 3.6.1, Part 1, applies, and so from Part 3 of the same theorem we have

$$\frac{1}{M}\|f\|_p \leq \inf_{\lambda \in \Lambda_p(f)} \|\lambda\|_{1,p} \leq \frac{1}{m}\|f\|_p .$$

□

3.7 Summary

In this chapter, Theorem 3.1.4 was proven, which provided bounds on weighted sums of sampled values of elements of the Hardy spaces, $H_p(\mathbb{D})$, for $1 < p < \infty$. This result was combined with the results in [33] to achieve a representation for elements of these Hardy spaces, as given in Theorem 3.6.4. It is this representation, applied to elements of the Hardy space $H_2(\mathbb{D})$ (itself also a Hilbert space), which will be used in the chapters to come in developing a frame suitable for speech representation.

IV. Frames for $L_2(\mathbb{R})$ and a frame-like operator

Presented in this chapter is a frame for $L_2(\mathbb{R})$ which is based on a frame or frames for $L_2(\mathbb{R}^+)$ and on hard, decaying exponential windows. This frame has a great deal of versatility, since it allows for frame design based on data-specific criteria. This is the first main result of this chapter. This result (Theorem 4.2.4) will be used in the development of the frame for speech representation, which is presented in Chapter VI.

A second main result of this chapter is the development of an operator akin to the frame operator. This operator is based on projections onto subspaces instead of frame elements. The usual frame operator is a special case of this more general operator. There are many practical applications for this operator, since its inverse can be calculated in a manner similar to that of the usual frame operator. One of the applications is to find representations based on the aforementioned frame for $L_2(\mathbb{R})$. This result (Theorem 4.3.1) is used in the calculation of frame representations in the speech frame in the computer program described in Chapter VI.

In Section 4.1, frames and the frame operator are defined and some useful properties are presented. Section 4.2 presents a general class of frames for $L_2(\mathbb{R})$, and Section 4.3 presents the subspace-based, frame-like, operator.

4.1 Frame and frame operator properties

Some of the theorems presented in this section will not be needed until the next chapter. However, it is convenient to group these basic theorems here. Frame properties dealing exclusively with the frame elements used in the next chapter will be presented there.

Definition 4.1.1 *Let \mathcal{H} be a separable Hilbert space and let $\{\phi_n\} \subset \mathcal{H}$ be an indexed, countable set. Suppose there exists constants $0 < A \leq B < \infty$ such that for every $f \in \mathcal{H}$,*

$$A\|f\|^2 \leq \sum_n |\langle f, \phi_n \rangle|^2 \leq B\|f\|^2$$

where $\langle \cdot, \cdot \rangle$ is the inner product defined on \mathcal{H} and $\|f\| = \langle f, f \rangle^{\frac{1}{2}}$. Then the set $\{\phi_n\}$ is called a frame for \mathcal{H} with frame bounds A and B . If $A = B$ the frame is called tight. If the set ceases to be a frame when a single element is excluded, the frame is called exact.

The operator $F: \mathcal{H} \rightarrow \mathcal{H}$ defined by

$$Ff = \sum_n \langle f, \phi_n \rangle \phi_n \quad (19)$$

is called the frame operator.

The following two theorems are well known and are presented without proof. They can be found in, e.g., [4].

Theorem 4.1.2 *Let $\{\phi_n\}$ be a frame in Hilbert space \mathcal{H} with frame bounds A and B . Then the frame operator $F: \mathcal{H} \rightarrow \mathcal{H}$ is invertible and the set $\{\tilde{\phi}_n\} = \{F^{-1}\phi_n\}$ is also a frame for \mathcal{H} , called the dual frame to $\{\phi_n\}$, with frame bounds $\frac{1}{B}$ and $\frac{1}{A}$. Also, every $f \in \mathcal{H}$ may be represented by*

$$f = \sum_n \langle f, \tilde{\phi}_n \rangle \phi_n = \sum_n \langle f, \phi_n \rangle \tilde{\phi}_n. \quad (20)$$

These representations are called the frame expansion and dual frame expansion, respectively, of f .

Theorem 4.1.3 *Let $\{\phi_n\}$ be an exact frame in Hilbert space \mathcal{H} with dual frame $\{\tilde{\phi}_n\}$. Then, $\{\phi_n\}$ and $\{\tilde{\phi}_n\}$ are biorthonormal. That is, for all n, m ,*

$$\langle \phi_n, \tilde{\phi}_m \rangle = \delta_{m,n},$$

where $\delta_{m,n}$ is the Kronecker delta.

The following theorem shows that a frame for a subspace can be used to define the orthogonal projection onto that subspace.

Theorem 4.1.4 *Let \mathcal{H} be a Hilbert space, $V \subset \mathcal{H}$ be a subspace, and $\{\phi_k\}$ and $\{\tilde{\phi}_k\}$ be a frame and a dual frame in V , respectively. Then, the orthogonal projection onto V , $P_V: \mathcal{H} \rightarrow V$, is given by*

$$P_V f = \sum_k \langle f, \phi_k \rangle \tilde{\phi}_k = \sum_k \langle f, \tilde{\phi}_k \rangle \phi_k$$

where $f \in \mathcal{H}$. That is, the projection onto the subspace V is given by the frame expansion in that subspace.

Proof. Let $f \in \mathcal{H}$. We have that $f = P_V f + P_{V^\perp} f$, where V^\perp is the orthogonal complement of V in \mathcal{H} . Since $P_V f \in V$, we may write

$$P_V f = \sum_k \langle P_V f, \phi_k \rangle \tilde{\phi}_k = \sum_k \langle P_V f, \tilde{\phi}_k \rangle \phi_k .$$

Since $P_{V^\perp} f \in V^\perp$ and $V^\perp \perp V$, we know that for all k ,

$$\langle P_{V^\perp} f, \phi_k \rangle = \langle P_{V^\perp} f, \tilde{\phi}_k \rangle = 0 .$$

This gives

$$P_V f = \sum_k (\langle P_V f, \phi_k \rangle + \langle P_{V^\perp} f, \phi_k \rangle) \tilde{\phi}_k = \sum_k (\langle P_V f, \tilde{\phi}_k \rangle + \langle P_{V^\perp} f, \tilde{\phi}_k \rangle) \phi_k ,$$

leading directly to

$$P_V f = \sum_k \langle f, \phi_k \rangle \tilde{\phi}_k = \sum_k \langle f, \tilde{\phi}_k \rangle \phi_k .$$

□

The proof of the following lemma is fairly straight forward. It is necessary to prove Theorem 5.2.7 in the next chapter.

Lemma 4.1.5 *Let $\{\psi_n\} \cup \{\phi_n\}$ be an exact frame for a Hilbert space \mathcal{H} such that $V = \text{span}\{\psi_n\}$ and $W = \text{span}\{\phi_n\}$, where $V \perp W$. Then the dual frame is given by $\{\tilde{\psi}_n\} \cup \{\tilde{\phi}_n\}$, where $\{\tilde{\psi}_n\}$ and $\{\tilde{\phi}_n\}$ are the dual frames in V and W of $\{\psi_n\}$ and $\{\phi_n\}$, respectively. If A_V and B_V are the frame bounds of $\{\psi_n\}$ in V and A_W and B_W are the frame bounds of $\{\phi_n\}$ in W , then $\min\{A_V, A_W\}$ and $\max\{B_V, B_W\}$ are the frame bounds of $\{\psi_n\} \cup \{\phi_n\}$ in \mathcal{H} .*

Proof. Let $\{\tilde{\psi}_n\} \cup \{\tilde{\phi}_n\}$ be the dual frame to $\{\psi_n\} \cup \{\phi_n\}$. Since $\{\psi_n\} \cup \{\phi_n\}$ is exact in \mathcal{H} , we know immediately that $\{\psi_n\}$ and $\{\phi_n\}$ are exact in V and W , respectively. By the properties of the frame and dual frame, for every $f \in \mathcal{H}$, we have

$$\begin{aligned} f &= \sum_n \langle f, \phi_n \rangle \tilde{\phi}_n + \sum_n \langle f, \psi_n \rangle \tilde{\psi}_n \\ &= \sum_n \langle f, \tilde{\phi}_n \rangle \phi_n + \sum_n \langle f, \tilde{\psi}_n \rangle \psi_n . \end{aligned}$$

Since $\tilde{\psi}_k \in V \subseteq \mathcal{H}$, we see that

$$\tilde{\psi}_k = \sum_n \langle \tilde{\psi}_k, \phi_n \rangle \tilde{\phi}_n + \sum_n \langle \tilde{\psi}_k, \psi_n \rangle \tilde{\psi}_n.$$

Since $\{\psi_n\}$ and $\{\phi_n\}$ span orthogonal subspaces, we know that $\langle \tilde{\psi}_k, \phi_m \rangle = 0$ for all k and m . By the exactness of the frames, we know that $\langle \tilde{\psi}_k, \psi_n \rangle = \delta_{n,k}$. Therefore,

$$\tilde{\psi}_k = \tilde{\psi}_k$$

for all k . Likewise, $\tilde{\phi}_k = \tilde{\phi}_k$ for all k . Therefore, the dual frame to $\{\psi_n\} \cup \{\phi_n\}$ is $\{\tilde{\psi}_n\} \cup \{\tilde{\phi}_n\}$ where $\{\tilde{\psi}_n\}$ and $\{\tilde{\phi}_n\}$ are the dual frames in V and W to $\{\psi_n\}$ and $\{\phi_n\}$, respectively.

To show the frame bounds, note that each $f \in \mathcal{H}$ can be uniquely written as $f = f_V + f_W$, where $f_V \in V$ and $f_W \in W$. Then,

$$\begin{aligned} \sum |\langle f, \psi_n \rangle|^2 + \sum |\langle f, \phi_n \rangle|^2 &= \sum |\langle f_V + f_W, \psi_n \rangle|^2 + \sum |\langle f_V + f_W, \phi_n \rangle|^2 \\ &= \sum |\langle f_V, \psi_n \rangle|^2 + \sum |\langle f_W, \phi_n \rangle|^2, \end{aligned}$$

which gives that

$$A_V \|f_V\|^2 + A_W \|f_W\|^2 \leq \sum |\langle f_V, \psi_n \rangle|^2 + \sum |\langle f_W, \phi_n \rangle|^2 \leq B_V \|f_V\|^2 + B_W \|f_W\|^2.$$

Since

$$\min\{A_V, A_W\} \|f\|^2 = \min\{A_V, A_W\} (\|f_V\|^2 + \|f_W\|^2) \leq A_V \|f_V\|^2 + A_W \|f_W\|^2$$

and

$$\max\{B_V, B_W\} \|f\|^2 = \max\{B_V, B_W\} (\|f_V\|^2 + \|f_W\|^2) \geq B_V \|f_V\|^2 + B_W \|f_W\|^2,$$

this gives

$$\min\{A_V, A_W\} \|f\|^2 \leq \sum |\langle f, \psi_n \rangle|^2 + \sum |\langle f, \phi_n \rangle|^2 \leq \max\{B_V, B_W\} \|f\|^2.$$

□

This next theorem reveals a useful property of the dual frame elements used in the next chapter. First, a definition is required.

Definition 4.1.6 Let $\{a_n\} \subset \mathcal{D}$ be an indexed set of points in some domain \mathcal{D} and let $\{f_n\}$ be an indexed set where for each n , $f_n : \mathcal{D} \rightarrow \mathbb{C}$. The set $\{f_n\}$ is called a set of interpolation functions on $\{a_n\}$ if for each n and each $m \neq n$, we have $f_n(a_n) \neq 0$ and $f_n(a_m) = 0$.

Theorem 4.1.7 Let $\{\phi_n\}$ be an exact frame in a Hilbert space \mathcal{H} of functions $f : \mathcal{D} \rightarrow \mathbb{C}$ and let $\{a_n\} \subset \mathcal{D}$. Suppose that for some $\{c_n\} \subset \mathbb{C}$, $c_n \neq 0$ for all n , we have $\langle f, \phi_n \rangle = c_n f(a_n)$ for all n and all $f \in \mathcal{H}$. Then $\{\tilde{\phi}_n\}$, the dual frame to $\{\phi_n\}$, will be of the form $\{\frac{1}{c_n} I_n\}$ where the set $\{I_n\}$ is a set of interpolation functions on the sample points $\{a_n\}$.

Proof. Because $\{\phi_n\}$ is an exact frame, from Theorem 4.1.3, we know that $\{\phi_n\}$ and $\{\tilde{\phi}_n\}$ are biorthonormal. Also, we have that $\langle \tilde{\phi}_m, \phi_n \rangle = c_n \tilde{\phi}_m(a_n)$, which implies $\tilde{\phi}_m(a_n) = \frac{\delta_{m,n}}{c_n}$. Therefore, $\{\tilde{\phi}_n\}$ is of the form of $\{\frac{1}{c_n} I_n\}$ where $\{I_n\}$ is a set of interpolating functions on the sample points $\{a_n\}$. \square

The following theorem is useful in that it gives an expression for the dual frame that does not depend on iterative methods. While its applicability may be limited, it is useful in the next chapter, where the projections involved are explicitly known.

Theorem 4.1.8 Let $\{\psi_k\}$ be an exact frame in a Hilbert space \mathcal{H} . Then, the dual frame, $\{\tilde{\psi}_k\}$, is given by

$$\tilde{\psi}_k = \frac{\psi_k - P_{S_k} \psi_k}{\langle \psi_k, \psi_k - P_{S_k} \psi_k \rangle} = \frac{\psi_k - P_{S_k} \psi_k}{\|\psi_k\|^2 - \langle \psi_k, P_{S_k} \psi_k \rangle},$$

where for each k , S_k is the space spanned by the set $\{\psi_j\}_{j \neq k}$ and the operator P_{S_k} is the orthogonal projection operator onto space S_k .

Proof. Since the frame $\{\psi_k\}$ is exact, from Theorem 4.1.3 we know it satisfies the property that $\langle \psi_j, \tilde{\psi}_k \rangle = \delta_{j,k}$ for all j, k . Since for all $j \neq k$ we have that $\psi_j \in S_k$ and since $S_k \perp (\psi_k - P_{S_k} \psi_k)$, we have the result by inspection. \square

Also note that the result of the previous theorem may be written as

$$\tilde{\psi}_k = \frac{\psi_k - \sum_j \langle \psi_k, \phi_j \rangle \phi_j}{\langle \psi_k, \psi_k - \sum_j \langle \psi_k, \phi_j \rangle \phi_j \rangle},$$

where $\{\phi_j\}$ is an orthonormal basis for the space S_k , or as

$$\tilde{\psi}_k = \frac{\psi_k - \sum_j \langle \psi_k, \tilde{\phi}_j \rangle \phi_j}{\langle \psi_k, \psi_k - \sum_j \langle \psi_k, \tilde{\phi}_j \rangle \phi_j \rangle},$$

where $\{\phi_j\}$ is a frame for S_k with dual frame $\{\tilde{\phi}_j\}$. Both of these representations may be useful in obtaining approximations to $\tilde{\psi}_k$.

4.2 A frame for $L_2(\mathbb{R})$.

In this section, a theorem showing a method to construct a frame for $L_2(\mathbb{R})$ from frames for $L_2(\mathbb{R}^+)$ using decaying exponential windows is proven. A decaying exponential window refers to a function, $f : \mathbb{R} \rightarrow \mathbb{C}$ of the form

$$f(x) = \begin{cases} e^{(\alpha+i\beta)(x-t)} & x \in J \\ 0 & \text{otherwise} \end{cases}, \quad (21)$$

where $\alpha, \beta, t \in \mathbb{R}$ and $J \subset \mathbb{R}$ is a bounded interval. This frame is useful in that the shifts of the windows (i.e., the locations of the bounded intervals on which the windows are non-zero) can vary to some extent, allowing for adaptive frames to be developed based on, e.g., a function that one wishes to represent well.

This first lemma will be needed to establish frame bounds.

Lemma 4.2.1 *Let $f \in L_2(J)$ where $J \subset [t_1, t_2]$ is a bounded interval, $t \in \mathbb{R}$, and $\alpha, \beta \in \mathbb{R}$. Then, $e^{(\alpha+i\beta)(\cdot-t)} f \in L_2(J)$ with*

$$\min\{e^{(t_1-t)\alpha}, e^{(t_2-t)\alpha}\} \|f\| \leq \|e^{(\alpha+i\beta)(\cdot-t)} f\| \leq \max\{e^{(t_1-t)\alpha}, e^{(t_2-t)\alpha}\} \|f\|.$$

Proof. That $e^{(\alpha+i\beta)(\cdot-t)} f \in L_2(J)$ is immediately obvious, since for a bounded interval J , $e^{(\alpha+i\beta)(\cdot-t)} \in L_2(J)$ is bounded above and below for all $t \in \mathbb{R}$. Examining $\|e^{(\alpha+i\beta)(\cdot-t)} f\|$, we see

$$\begin{aligned} \|e^{(\alpha+i\beta)(\cdot-t)} f\|^2 &= \int_J |e^{(\alpha+i\beta)(x-t)} f(x)|^2 dx \\ &= \int_J (e^{(x-t)\alpha})^2 |f(x)|^2 dx. \end{aligned}$$

Since the exponential function is monotonic on \mathbb{R} , we know that

$$\min\{e^{(t_1-t)\alpha}, e^{(t_2-t)\alpha}\}^2 |f(x)|^2 \leq (e^{(x-t)\alpha})^2 |f(x)|^2 \leq \max\{e^{(t_1-t)\alpha}, e^{(t_2-t)\alpha}\}^2 |f(x)|^2$$

for each $x \in J$. This leads immediately to

$$\min\{e^{(t_1-t)\alpha}, e^{(t_2-t)\alpha}\} \|f\| \leq \|e^{(\alpha+i\beta)(\cdot-t)} f\| \leq \max\{e^{(t_1-t)\alpha}, e^{(t_2-t)\alpha}\} \|f\|.$$

□

The following lemma will be useful when combining the results of Theorem 4.2.4 and Theorem 4.3.1, below, which is done in Chapter VI. It is placed here, in the context of similar lemmas, to make it more readily understood.

Lemma 4.2.2 *Let $\{\phi_j\}$ be a frame for $L_2(I)$ with frame bounds c and C , where $I \subset \mathbb{R}$. Then, for every bounded interval $J \subset [t_m, t_n] \subset I$ and for every $\alpha, \beta \in \mathbb{R}$, $\{e^{(\alpha+i\beta)(\cdot)} \phi_j\}$ is a frame for $L_2(J)$, with frame bounds $(\min\{e^{\alpha t_m}, e^{\alpha t_n}\})^2 c$ and $(\max\{e^{\alpha t_m}, e^{\alpha t_n}\})^2 C$.*

Proof. Let $f \in L_2(J)$. Then by Lemma 4.2.1, $e^{(\alpha-i\beta)(\cdot)} f \in L_2(J)$. Since $\{\phi_j\}$ is a frame for $L_2(I)$, it is a frame for $L_2(J)$ also, and so we may write

$$c \|e^{(\alpha-i\beta)(\cdot)} f\|^2 \leq \sum_j |\langle e^{(\alpha-i\beta)(\cdot)} f, \phi_j \rangle|^2 \leq C \|e^{(\alpha-i\beta)(\cdot)} f\|^2,$$

where the norms and inner products are those of $L_2(J)$. Again by Lemma 4.2.1, this gives

$$c \min\{e^{\alpha t_m}, e^{\alpha t_n}\}^2 \|f\|^2 \leq \sum_j |\langle f, e^{(\alpha+i\beta)(\cdot)} \phi_j \rangle|^2 \leq C \max\{e^{\alpha t_m}, e^{\alpha t_n}\}^2 \|f\|^2.$$

□

The following lemma would appear to be of little practical use, since it does not apply to a wide class of sequences $\{a_k\}$. However, it turns out to be a crucial lemma when proving Theorem 4.2.4.

Lemma 4.2.3 *Let $\{a_k\}$ be such that $\sum_{k=1}^{\infty} 2^k |a_k|^2 < \infty$. Then*

$$\left| \sum_{k=1}^{\infty} a_k \right|^2 \leq \sum_{k=1}^{\infty} 2^k |a_k|^2.$$

Proof. Let $\sum_{k=1}^{\infty} 2^k |a_k|^2 = x^2 < \infty$. The case where $x = 0$ is trivial. Otherwise, define a new sequence $b = \{|b_k|\}$ by $|b_k| = \frac{2^{k/2}}{x} |a_k|$. We know that $b \in \ell_2(\mathbb{Z}^+)$, since

$$\|b\|^2 \equiv \sum_{k=1}^{\infty} |b_k|^2 = \sum_{k=1}^{\infty} \frac{2^k}{x^2} |a_k|^2 = 1.$$

Define $c = \{2^{-k/2}\} \in \ell_2(\mathbb{Z}^+)$, with

$$\|c\|^2 \equiv \sum_{k=1}^{\infty} (2^{-k/2})^2 = \sum_{k=1}^{\infty} 2^{-k} = 1.$$

Since $b, c \in \ell_2(\mathbb{Z}^+)$, we know that $\langle b, c \rangle$ is well-defined, and is given by

$$\begin{aligned} \langle b, c \rangle &= \sum_{k=1}^{\infty} \left(\frac{2^{k/2}}{x} |a_k| \right) 2^{-k/2} \\ &= \frac{1}{x} \sum_{k=1}^{\infty} |a_k|. \end{aligned}$$

However, we also know that $|\langle b, c \rangle| \leq \|b\| \|c\| = 1$, which gives

$$\sum_{k=1}^{\infty} |a_k| \leq x.$$

Hence,

$$\left(\sum_{k=1}^{\infty} |a_k| \right)^2 \leq x^2 = \sum_{k=1}^{\infty} 2^k |a_k|^2.$$

Since the above argument also shows that $\sum_{k=1}^{\infty} a_k$ is absolutely convergent, we have that

$$\left| \sum_{k=1}^{\infty} a_k \right|^2 = \left(\sum_{k=1}^{\infty} a_k \right)^2 \leq \left(\sum_{k=1}^{\infty} |a_k| \right)^2 \leq \sum_{k=1}^{\infty} 2^k |a_k|^2.$$

□

The following theorem, a main result of this chapter, provides a way to construct frames for $L_2(\mathbb{R})$ using the decaying exponential windows defined in (21) and frames on $L_2(\mathbb{R}^+)$. (Note that it is not a misprint that $I_n = \infty$ is allowed in Theorem 4.2.4.)

In the following, $\mathbf{1}_X: \mathbb{R} \rightarrow \mathbb{R}$ is the characteristic function of the set $X \subset \mathbb{R}$. That is,

$$\mathbf{1}_X(t) = \begin{cases} 1 & t \in X \\ 0 & \text{otherwise} \end{cases}.$$

Theorem 4.2.4 Fix $0 < \epsilon \leq \delta < \infty$ and choose $\{t_n\}_{n \in \mathbb{Z}} \subset \mathbb{R}$ such that $t_n < t_{n+1}$ for all $n \in \mathbb{Z}$ and such that

$$|n - m|\epsilon \leq |t_n - t_m| \leq |n - m|\delta \quad (22)$$

for every $n, m \in \mathbb{Z}$. Choose $\{I_n\}_{n \in \mathbb{Z}} \subset \mathbb{R}^+$ such that for every n , $t_{n+1} - t_n \leq I_n \leq \infty$. For each n , let $\{\phi_{n,j}\}_{j \in \mathbb{Z}} \subset L_2(\mathbb{R}^+)$ be a frame for $L_2(\mathbb{R}^+)$ with frame bounds c and C . Let $\alpha, \beta \in \mathbb{R}$ be such that $\alpha < -\frac{\ln 2}{2\epsilon}$. Then the set $\{\mathbf{1}_{[t_n, t_n + I_n]} e^{(\alpha + i\beta)(\cdot - t_n)} \phi_{n,j}(\cdot - t_n)\}_{n,j \in \mathbb{Z}}$ is a frame for $L_2(\mathbb{R})$ with frame bounds

$$\frac{ce^{2\delta\alpha}(1 - (e^{2\delta\alpha})^{K_{\min}})}{1 - e^{2\delta\alpha}}$$

and

$$\frac{2C(1 - (2e^{2\epsilon\alpha})^{K_{\max}})}{1 - 2e^{2\epsilon\alpha}},$$

where K_{\min} , defined by

$$K_{\min} = \inf_n (\sup\{k : t_{n+k} - t_n \leq I_n\}),$$

represents the minimum (over n) number of intervals $[t_k, t_{k+1}]$, $k \in \mathbb{Z}$, completely covered by the interval $[t_n, t_n + I_n]$ and where K_{\max} , defined by

$$K_{\max} = \sup\{\sup\{k : t_{n+k-1} - t_n < I_n\} : n \in \mathbb{Z}\},$$

represents the maximum (over n) number of intervals $[t_k, t_{k+1}]$, $k \in \mathbb{Z}$, completely or partially covered by the interval $[t_n, t_n + I_n]$. Both K_{\min} and K_{\max} can be infinite.

Proof. To improve the readability of the proof, the proof that follows is done in detail for the simpler case where for each n , $I_n = t_{n+K} - t_n$ for some fixed $1 \leq K \leq \infty$ and where $\{\phi_{n,j}\}_{j \in \mathbb{Z}} = \{\phi_{m,j}\}_{j \in \mathbb{Z}}$ for all $m, n \in \mathbb{Z}$. For this constraint on $\{I_n\}$, we have that

$K_{\min} = K = K_{\max}$. The changes necessary for the more general case are tedious, but not difficult, and can be done by inspection.

Let $f \in L_2(\mathbb{R})$. For each $m \in \mathbb{Z}$, define $f_m \in L_2([t_m, t_{m+1}])$ by

$$f_m(t) = \begin{cases} f(t) & t_m \leq t < t_{m+1} \\ 0 & \text{otherwise} \end{cases}. \quad (23)$$

Clearly, $f = \sum_m f_m$ and since $f_m \perp f_n$ for all $m \neq n$, we have that $\|f\|^2 = \sum_m \|f_m\|^2$. Therefore, we may write

$$\begin{aligned} \sum_{n,j} |\langle f, \mathbf{1}_{[t_n, t_{n+K}]}(\cdot) e^{(\alpha+i\beta)(\cdot-t_n)} \phi_j(\cdot-t_n) \rangle|^2 \\ = \sum_{n,j} \left| \left\langle \sum_m f_m, \mathbf{1}_{[t_n, t_{n+K}]}(\cdot) e^{(\alpha+i\beta)(\cdot-t_n)} \phi_j(\cdot-t_n) \right\rangle \right|^2 \end{aligned} \quad (24)$$

$$\begin{aligned} &= \sum_{n,j} \left| \sum_m \langle f_m, \mathbf{1}_{[t_n, t_{n+K}]}(\cdot) e^{(\alpha+i\beta)(\cdot-t_n)} \phi_j(\cdot-t_n) \rangle \right|^2 \\ &= \sum_{n,j} \left| \sum_{m=n}^{n+K-1} \langle f_m, e^{(\alpha+i\beta)(\cdot-t_n)} \phi_j(\cdot-t_n) \rangle \right|^2 \\ &= \sum_{n,j} \left| \sum_{m=n}^{n+K-1} \langle e^{(\alpha-i\beta)(\cdot-t_n)} f_m, \phi_j(\cdot-t_n) \rangle \right|^2 \\ &\leq \sum_{n,j} \left(\sum_{m=n}^{n+K-1} |\langle e^{(\alpha-i\beta)(\cdot-t_n)} f_m, \phi_j(\cdot-t_n) \rangle| \right)^2. \end{aligned} \quad (25)$$

Provided the sum on the right-hand side is finite (which will later be seen to be true), we may use Lemma 4.2.3 in (25) to obtain

$$\begin{aligned} \sum_{n,j} |\langle f, \mathbf{1}_{[t_n, t_{n+K}]}(\cdot) e^{(\alpha+i\beta)(\cdot-t_n)} \phi_j(\cdot-t_n) \rangle|^2 \\ \leq \sum_{n,j} \sum_{m=n}^{n+K-1} 2^{m-n+1} |\langle e^{(\alpha-i\beta)(\cdot-t_n)} f_m, \phi_j(\cdot-t_n) \rangle|^2 \\ = \sum_{n,j} \sum_{k=0}^{K-1} 2^{k+1} |\langle e^{(\alpha-i\beta)(\cdot-t_n)} f_{n+k}, \phi_j(\cdot-t_n) \rangle|^2 \\ = \sum_{n,j} \sum_{k=0}^{K-1} 2^{k+1} |\langle e^{(\alpha-i\beta)(\cdot-t_{n-k})} f_n, \phi_j(\cdot-t_{n-k}) \rangle|^2 \end{aligned}$$

$$= \sum_n \sum_{k=0}^{K-1} 2^{k+1} \sum_j |\langle e^{(\alpha-i\beta)(\cdot-t_{n-k})} f_n, \phi_j(\cdot-t_{n-k}) \rangle|^2. \quad (26)$$

Since $\{\phi_j\}_{j \in \mathbb{Z}}$ is a frame for $L_2(\mathbb{R}^+)$, we may write

$$\sum_j |\langle e^{(\alpha-i\beta)(\cdot-t_{n-k})} f_n, \phi_j(\cdot-t_{n-k}) \rangle|^2 \leq C \|e^{(\alpha-i\beta)(\cdot-t_{n-k})} f_n\|^2.$$

From Lemma 4.2.1 and our choice of α , we have that

$$\|e^{(\alpha+i\beta)(\cdot-t_{n-k})} f_n\| \leq e^{(t_n-t_{n-k})\alpha} \|f_n\|,$$

and so

$$\sum_j |\langle e^{(\alpha-i\beta)(\cdot-t_{n-k})} f_n, \phi_j(\cdot-t_{n-k}) \rangle|^2 \leq C e^{2(t_n-t_{n-k})\alpha} \|f_n\|^2. \quad (27)$$

Returning to (26) and using (27), we have

$$\begin{aligned} \sum_{n,j} |\langle f, 1_{[t_n, t_{n+K}]}(\cdot) e^{(\alpha+i\beta)(\cdot-t_n)} \phi_j(\cdot-t_n) \rangle|^2 &\leq \sum_n \sum_{k=0}^{K-1} 2^{k+1} C e^{2(t_n-t_{n-k})\alpha} \|f_n\|^2 \\ &\leq C \sum_n \|f_n\|^2 \sum_{k=0}^{K-1} 2^{k+1} e^{2(t_n-t_{n-k})\alpha} \\ &\leq C \sum_n \|f_n\|^2 \sum_{k=0}^{K-1} 2^{k+1} e^{2\epsilon k \alpha}, \end{aligned}$$

where, for the last step, we have used $t_n - t_{n-k} \geq \epsilon k$ and $\alpha < 0$. Noting that for our choice of α and ϵ , the inequality $2e^{2\epsilon\alpha} < 1$ holds, we find

$$\begin{aligned} \sum_{k=0}^{K-1} 2^{k+1} e^{2\epsilon k \alpha} &= \sum_{k=0}^{\infty} 2^{k+1} e^{2\epsilon k \alpha} - \sum_{k=K}^{\infty} 2^{k+1} e^{2\epsilon k \alpha} \\ &= 2 \sum_{k=0}^{\infty} (2e^{2\epsilon\alpha})^k - 2^{K+1} e^{2\epsilon K \alpha} \sum_{k=0}^{\infty} (2e^{2\epsilon\alpha})^k \\ &= 2(1 - (2e^{2\epsilon\alpha})^K) \sum_{k=0}^{\infty} (2e^{2\epsilon\alpha})^k \\ &= \frac{2(1 - (2e^{2\epsilon\alpha})^K)}{1 - 2e^{2\epsilon\alpha}}. \end{aligned}$$

Using this, we may then write

$$\begin{aligned} \sum_{n,j} |\langle f, \mathbf{1}_{[t_n, t_n+K]}(\cdot) e^{(\alpha+i\beta)(\cdot-t_n)} \phi_j(\cdot-t_n) \rangle|^2 &\leq \frac{2(1-(2e^{2\epsilon\alpha})^K)}{1-2e^{2\epsilon\alpha}} \sum_n \|f_n\|^2 \\ &\leq \frac{2(1-(2e^{2\epsilon\alpha})^K)}{1-2e^{2\epsilon\alpha}} \|f\|^2, \end{aligned} \quad (28)$$

which establishes our upper bound. The lower bound is somewhat more straight forward. Beginning as before from the left-hand side of (24),

$$\begin{aligned} \sum_{n,j} |\langle f, \mathbf{1}_{[t_n, t_n+K]}(\cdot) e^{(\alpha+i\beta)(\cdot-t_n)} \phi_j(\cdot-t_n) \rangle|^2 \\ = \sum_n \sum_j |\langle \mathbf{1}_{[t_n, t_n+K]}(\cdot) e^{(\alpha-i\beta)(\cdot-t_n)} f, \phi_j(\cdot-t_n) \rangle|^2. \end{aligned}$$

Since $\{\phi_j\}_{j \in \mathbb{Z}}$ is a frame for $L_2(\mathbb{R}^+)$, we may write

$$\sum_{n,j} |\langle f, \mathbf{1}_{[t_n, t_n+K]}(\cdot) e^{(\alpha+i\beta)(\cdot-t_n)} \phi_j(\cdot-t_n) \rangle|^2 \geq c \sum_n \|\mathbf{1}_{[t_n, t_n+K]}(\cdot) e^{(\alpha-i\beta)(\cdot-t_n)} f\|^2.$$

Using f_m as defined in (23), this gives

$$\begin{aligned} \sum_{n,j} |\langle f, \mathbf{1}_{[t_n, t_n+K]}(\cdot) e^{(\alpha+i\beta)(\cdot-t_n)} \phi_j(\cdot-t_n) \rangle|^2 &\geq c \sum_n \left\| \sum_{m=n}^{n+K-1} e^{(\alpha-i\beta)(\cdot-t_n)} f_m \right\|^2 \\ &= c \sum_n \sum_{m=n}^{n+K-1} \|e^{(\alpha-i\beta)(\cdot-t_n)} f_m\|^2, \end{aligned}$$

since the functions $e^{(\alpha-i\beta)(\cdot-t_n)} f_m$ are orthogonal to each other. Then, by Lemma 4.2.1, we have

$$\begin{aligned} \sum_{n,j} |\langle f, \mathbf{1}_{[t_n, t_n+K]}(\cdot) e^{(\alpha+i\beta)(\cdot-t_n)} \phi_j(\cdot-t_n) \rangle|^2 &\geq c \sum_n \sum_{m=n}^{n+K-1} e^{2(t_{m+1}-t_n)\alpha} \|f_m\|^2 \\ &= c \sum_m \|f_m\|^2 \sum_{n=m-K+1}^m e^{2(t_{m+1}-t_n)\alpha} \\ &\geq c \sum_m \|f_m\|^2 \sum_{n=m-K+1}^m e^{2(m+1-n)\delta\alpha}, \end{aligned}$$

where the last step is valid because $\alpha < 0$ and (22). Continuing, we have

$$\begin{aligned}
\sum_{n,j} |\langle f, \mathbf{1}_{[t_n, t_{n+K}]}(\cdot) e^{(\alpha+i\beta)(\cdot-t_n)} \phi_j(\cdot-t_n) \rangle|^2 &\geq c \sum_m \|f_m\|^2 \sum_{k=0}^{K-1} e^{2(k+1)\delta\alpha} \\
&= c \sum_m \|f_m\|^2 \sum_{k=0}^{K-1} (e^{2\delta\alpha})^{k+1} \\
&= c \sum_m \|f_m\|^2 \frac{e^{2\delta\alpha}(1-(e^{2\delta\alpha})^K)}{1-e^{2\delta\alpha}} \\
&= \frac{ce^{2\delta\alpha}(1-(e^{2\delta\alpha})^K)}{1-e^{2\delta\alpha}} \|f\|^2, \tag{29}
\end{aligned}$$

which gives our lower bound. Bringing (28) and (29) together, we see

$$\begin{aligned}
&\frac{ce^{2\delta\alpha}(1-(e^{2\delta\alpha})^K)}{1-e^{2\delta\alpha}} \|f\|^2 \\
&\leq \sum_{n,j} |\langle f, \mathbf{1}_{[t_n, t_{n+K}]}(\cdot) e^{(\alpha+i\beta)(\cdot-t_n)} \phi_j(\cdot-t_n) \rangle|^2 \leq \frac{2(1-(2e^{2\epsilon\alpha})^K)}{1-2e^{2\epsilon\alpha}} \|f\|^2,
\end{aligned}$$

which completes the proof that $\{\mathbf{1}_{[t_n, t_{n+K}]} e^{(\alpha+i\beta)(\cdot-t_n)} \phi_{n,j}(\cdot-t_n)\}_{n,j \in \mathbb{Z}}$ is indeed a frame for $L_2(\mathbb{R})$. \square

4.3 A generalization of the frame operator.

Presented in this section is a generalization of the concept of a frame and frame operator. This particular generalization, the second main result of this chapter, is very useful in practical applications, such as those involving frames of the type proven in Theorem 4.2.4.

Let \mathcal{H} be a Hilbert space and let $\{\phi_k\}$ and $\{\tilde{\phi}_k\}$ be a frame and dual frame in \mathcal{H} . The representation to be developed is based on considering the operation $\langle f, \phi_k \rangle \phi_k$, which figures prominently in (19), to be a projection onto a subspace. Then, one may consider the mapping $\phi_k \mapsto \tilde{\phi}_k$ to be a linear transform between subspaces, giving an analogy to (20). In this way, it is possible to generalize *frame elements* to *frame subspaces*.

This has advantages in that it will allow the use of *nested frames*. That is, there is no constraint on how the orthogonal projections onto the subspaces are computed. In particular, given frames in the appropriate subspaces, the projection onto the subspace may be represented by its frame expansion, as in Theorem 4.1.4.

Any exact frame may be recast in this more generalized framework to give (possibly) faster calculations of coefficients in the frame expansion. The coefficients given in this case will be identical to those found by the usual methods. If the frame is not exact, it may still be possible to recast the frame such that identical coefficients are achieved, given careful construction of the subspaces.

Theorem 4.3.1 *For Hilbert space \mathcal{H} , let $\{V_j\} \subset \mathcal{H}$ be subspaces such that $\mathcal{H} = \sum_j V_j$, where the $\{V_j\}$ need not be mutually orthogonal. For each j , let $c_j \in \mathbb{R}^+$ and let $P_{V_j}: \mathcal{H} \rightarrow V_j$ be the orthogonal projection operator onto V_j . Suppose there exists $0 < A \leq B < \infty$ and such that for each $f \in \mathcal{H}$,*

$$A\|f\|^2 \leq \sum_j c_j \|P_{V_j} f\|^2 \leq B\|f\|^2. \quad (30)$$

Then, the operator $F: \mathcal{H} \rightarrow \mathcal{H}$ given by

$$Ff = \sum_j c_j P_{V_j} f \quad (31)$$

is bounded, self-adjoint, and invertible on its range. Define $T_{\tilde{V}_j}: V_j \rightarrow \tilde{V}_j$ by $T_{\tilde{V}_j} = F^{-1}$, where $\tilde{V}_j \subset \mathcal{H}$ is the range of $T_{\tilde{V}_j}$. Define $T_{V_j} \doteq T_{\tilde{V}_j}^$. Then, for all $f \in \mathcal{H}$, we have*

$$f = \sum_j c_j T_{\tilde{V}_j} P_{V_j} f = \sum_j c_j T_{V_j} P_{\tilde{V}_j} f.$$

Proof. This proof begins by showing that F is bounded.

$$\begin{aligned} \|F\| &= \sup_{\|f\|=\|g\|=1} |\langle Ff, g \rangle| \\ &= \sup_{\|f\|=\|g\|=1} \left| \left\langle \sum_j c_j P_{V_j} f, g \right\rangle \right| \\ &= \sup_{\|f\|=\|g\|=1} \left| \sum_j c_j \langle P_{V_j} f, g \rangle \right| \\ &= \sup_{\|f\|=\|g\|=1} \left| \sum_j c_j \langle P_{V_j} f, (\langle P_{V_j} f, g \rangle P_{V_j} f + (g - \langle P_{V_j} f, g \rangle P_{V_j} f)) \rangle \right|. \end{aligned} \quad (32)$$

Noting that $(g - \langle P_{V_j} f, g \rangle P_{V_j} f) \perp P_{V_j} f$, (32) becomes

$$\begin{aligned}
\|F\| &= \sup_{\|f\|=\|g\|=1} \left| \sum_j c_j \langle P_{V_j} f, \langle P_{V_j} f, g \rangle P_{V_j} f \rangle \right| \\
&= \sup_{\|f\|=\|g\|=1} \left| \sum_j c_j \overline{\langle P_{V_j} f, g \rangle} \langle P_{V_j} f, P_{V_j} f \rangle \right| \\
&= \sup_{\|f\|=\|g\|=1} \left| \sum_j c_j \overline{\langle P_{V_j} f, g \rangle} \|P_{V_j} f\|^2 \right| \\
&\leq \sup_{\|f\|=\|g\|=1} \sum_j c_j |\langle P_{V_j} f, g \rangle| \|P_{V_j} f\|^2.
\end{aligned}$$

Since $\|f\| = \|g\| = 1$ and for each j , P_{V_j} is an orthogonal projection, we know that $|\langle P_{V_j} f, g \rangle| \leq 1$, leading to

$$\begin{aligned}
\|F\| &\leq \sup_{\|f\|=\|g\|=1} \sum_j c_j \|P_{V_j} f\|^2 \\
&\leq \sup_{\|f\|=\|g\|=1} B \|f\|^2 = B.
\end{aligned}$$

Therefore, F is bounded and $\|F\| \leq B$.

To show that F is self-adjoint, let $f, g \in \mathcal{H}$ and recall that $\{c_j\} \subset \mathbb{R}$.

$$\begin{aligned}
\langle Ff, g \rangle &= \left\langle \sum_j c_j P_{V_j} f, g \right\rangle \\
&= \sum_j c_j \langle P_{V_j} f, g \rangle \\
&= \sum_j c_j \langle f, P_{V_j} g \rangle \\
&= \left\langle f, \sum_j c_j P_{V_j} g \right\rangle \\
&= \langle f, Fg \rangle,
\end{aligned}$$

where I have used the fact that projection operators are self-adjoint. Therefore, F is self-adjoint on \mathcal{H} .

Next, since F is linear, to show that F is invertible on its range it is sufficient to show that it is injective. So, assume that for some $f \in \mathcal{H}$, that $Ff = 0$. Using (30), elementary

calculations give

$$\begin{aligned}
\langle f, Ff \rangle &= \langle f, \sum_j c_j P_{V_j} f \rangle \\
&= \sum_j c_j \langle (P_{V_j} f + P_{V_j^\perp} f), P_{V_j} f \rangle \\
&= \sum_j c_j \langle P_{V_j} f, P_{V_j} f \rangle \\
&= \sum_j c_j \|P_{V_j} f\|^2 \\
&\geq A \|f\|^2,
\end{aligned}$$

Now, using the inequality $|\langle f, Ff \rangle| \leq \|f\| \|Ff\|$, we get

$$A \|f\| \leq \|Ff\|.$$

Therefore, $Ff = 0$ implies $f = 0$, and so F is injective and therefore invertible on its range.

Since F is invertible on its range, we may write

$$\begin{aligned}
f &= F^{-1} Ff = F^{-1} \sum_j c_j P_{V_j} f \\
&= \sum_j c_j F^{-1} P_{V_j} f.
\end{aligned}$$

Since P_{V_j} has a range of V_j , using the definition of $T_{\tilde{V}_j}$, we have

$$f = \sum_j c_j T_{\tilde{V}_j} P_{V_j} f.$$

That is, $I = \sum_j c_j T_{\tilde{V}_j} P_{V_j}$.

Next, write

$$\begin{aligned}
I &= I^* = \left(\sum_j c_j T_{\tilde{V}_j} P_{V_j} \right)^* \\
&= \sum_j c_j (T_{\tilde{V}_j} P_{V_j})^*.
\end{aligned} \tag{33}$$

The form of $(T_{\tilde{V}_j}P_{V_j})^*$ can be found by solving $\langle T_{\tilde{V}_j}P_{V_j}f, g \rangle = \langle f, (T_{\tilde{V}_j}P_{V_j})^*g \rangle$ for $f, g \in \mathcal{H}$.

$$\begin{aligned}\langle T_{\tilde{V}_j}P_{V_j}f, g \rangle &= \langle T_{\tilde{V}_j}P_{V_j}f, (P_{\tilde{V}_j} + P_{\tilde{V}_j^\perp})g \rangle \\ &= \langle T_{\tilde{V}_j}P_{V_j}f, P_{\tilde{V}_j}g \rangle + \langle T_{\tilde{V}_j}P_{V_j}f, P_{\tilde{V}_j^\perp}g \rangle.\end{aligned}\quad (34)$$

Since the range of $T_{\tilde{V}_j}$ is \tilde{V}_j and $\tilde{V}_j \perp \tilde{V}_j^\perp$, we have $\langle T_{\tilde{V}_j}P_{V_j}f, P_{\tilde{V}_j^\perp}g \rangle = 0$. Thus (34) becomes

$$\begin{aligned}\langle T_{\tilde{V}_j}P_{V_j}f, g \rangle &= \langle T_{\tilde{V}_j}P_{V_j}f, P_{\tilde{V}_j}g \rangle \\ &= \langle P_{V_j}f, T_{\tilde{V}_j}^*P_{\tilde{V}_j}g \rangle.\end{aligned}\quad (35)$$

Since $T_{V_j} \doteq T_{\tilde{V}_j}^*$, we have

$$\begin{aligned}\langle T_{\tilde{V}_j}P_{V_j}f, g \rangle &= \langle P_{V_j}f, T_{V_j}P_{\tilde{V}_j}g \rangle \\ &= \langle (P_{V_j} + P_{V_j^\perp} - P_{V_j^\perp})f, T_{V_j}P_{\tilde{V}_j}g \rangle \\ &= \langle (P_{V_j} + P_{V_j^\perp})f, T_{V_j}P_{\tilde{V}_j}g \rangle - \langle P_{V_j^\perp}f, T_{V_j}P_{\tilde{V}_j}g \rangle \\ &= \langle f, T_{V_j}P_{\tilde{V}_j}g \rangle - \langle P_{V_j^\perp}f, T_{V_j}P_{\tilde{V}_j}g \rangle.\end{aligned}$$

As before, since the range of T_{V_j} is V_j , we know that $\langle P_{V_j^\perp}f, T_{V_j}P_{\tilde{V}_j}g \rangle = 0$. Therefore,

$$\langle T_{\tilde{V}_j}P_{V_j}f, g \rangle = \langle f, T_{V_j}P_{\tilde{V}_j}g \rangle.$$

That is, $(T_{\tilde{V}_j}P_{V_j})^* = T_{V_j}P_{\tilde{V}_j}$. Using this in (33), we have

$$\begin{aligned}I = I^* &= \sum_j c_j (T_{\tilde{V}_j}P_{V_j})^* \\ &= \sum_j c_j T_{V_j}P_{\tilde{V}_j}.\end{aligned}$$

Therefore, for all $f \in \mathcal{H}$, we have

$$f = \sum_j c_j T_{\tilde{V}_j}P_{V_j}f = \sum_j c_j T_{V_j}P_{\tilde{V}_j}f,$$

□

In Theorem 4.3.4, it will be shown that the same iterative methods for determining the inverse of the operator F commonly used with the ordinary frame operator will also

work here. This work follows along the same path taken in, e.g., [9] and [11]. Two preliminary lemmas will make the proof of Theorem 4.3.4 easier.

The following lemma is very useful in establishing that the lower frame bound need not be known in order to use the iterative method described below in Theorem 4.3.4. That is, one need only know that a lower frame bound exists in order to use the iterative method and not the actual value of the lower frame bound.

Lemma 4.3.2 *Let \mathcal{H} , $\{V_j\}$, $\{c_j\}$, F , A , and B be as in Theorem 4.3.1. Let $A' \in (0, B]$. Define the operator $R: \mathcal{H} \rightarrow \mathcal{H}$ by $R = I - \frac{2}{A'+B}F$. Then $\|R\| < 1$.*

Proof. We will bound $\|R\|$ by noting that R , as the sum of two self-adjoint operators, is self-adjoint, and that for self-adjoint operators,

$$\|R\| = \sup_{\|f\|=1} |\langle Rf, f \rangle|.$$

Examining $\langle Rf, f \rangle$, we find that

$$\begin{aligned} \langle Rf, f \rangle &= \langle (I - \frac{2}{A'+B}F)f, f \rangle \\ &= \|f\|^2 - \frac{2}{A'+B} \langle Ff, f \rangle \\ &= \|f\|^2 - \frac{2}{A'+B} \sum_j c_j \|P_{V_j} f\|^2. \end{aligned}$$

Inequality (30) implies

$$\|f\|^2 - \frac{2B}{A'+B} \|f\|^2 \leq \langle Rf, f \rangle \leq \|f\|^2 - \frac{2A}{A'+B} \|f\|^2,$$

leading directly to

$$-\left(\frac{B-A'}{B+A'}\right) \|f\|^2 \leq \langle Rf, f \rangle \leq \left(\frac{B+A'-2A}{B+A'}\right) \|f\|^2.$$

By the restriction $0 < A \leq B < \infty$ and our choice of $A' \in (0, B]$, we know

$$0 \leq \left(\frac{B-A'}{B+A'}\right) < 1$$

and

$$-1 < \left(\frac{B + A' - 2A}{B + A'} \right) < 1.$$

Therefore,

$$|\langle Rf, f \rangle| \leq \max \left\{ \left(\frac{B - A'}{B + A'} \right), \left(\frac{B + A' - 2A}{B + A'} \right) \right\} \|f\|^2 < \|f\|^2.$$

Therefore,

$$\begin{aligned} \|R\| &= \sup_{\|f\|=1} |\langle Rf, f \rangle| \\ &\leq \max \left\{ \left(\frac{B - A'}{B + A'} \right), \left(\frac{B + A' - 2A}{B + A'} \right) \right\} < 1. \end{aligned} \quad (36)$$

□

Without much difficulty, it can be easily shown that the value of A' which minimizes the the bound on $\|R\|$ in (36) is $A' = A$, where A is the maximum value for which (30) holds. Since the rate of convergence of the iterative method to be presented in Theorem 4.3.4 is dependent on $\|R\|$, if A can be estimated, this estimate should be used. However, it is sufficient to show that $A > 0$ exists in order to guarantee convergence of the iterative method in Theorem 4.3.4 for any choice of $0 < A' \leq B$.

The previous lemma leads directly to a representation for F^{-1} .

Lemma 4.3.3 *Let \mathcal{H} , $\{V_j\}$, $\{c_j\}$, F , A , and B be as in Theorem 4.3.1 and let A' and R be as in Lemma 4.3.2. Then $F^{-1}: \mathcal{H} \rightarrow \mathcal{H}$ is given by*

$$F^{-1} = \frac{2}{A' + B} \sum_{n=0}^{\infty} R^n.$$

Proof. Note that $\frac{A'+B}{2}(I - R) = \frac{A'+B}{2}(I - (I - \frac{2}{A'+B}F)) = F$. Therefore, we may write

$$F^{-1} = \frac{2}{A' + B}(I - R)^{-1}.$$

From Lemma 4.3.2, we have that $\|R\| < 1$. Therefore, we may expand $(I - R)^{-1}$ in a Neumann series to get

$$F^{-1} = \frac{2}{A' + B}(I - R)^{-1} = \frac{2}{A' + B} \sum_{n=0}^{\infty} R^n .$$

□

We are now ready to present an iterative method for finding a representation for $f \in \mathcal{H}$.

Theorem 4.3.4 *Let \mathcal{H} and F be as in Theorem 4.3.1 and let R be as in Lemma 4.3.2. For $f \in \mathcal{H}$ and for each $N \in \mathbb{Z}^+$, define f_N by*

$$f_N = \frac{2}{A' + B} \sum_{n=0}^N R^n Ff .$$

Then,

$$f = \lim_{N \rightarrow \infty} f_N .$$

Proof. From Lemma 4.3.3, we have that $F^{-1} = \frac{2}{A' + B} \sum_{n=0}^{\infty} R^n$. Using this, we have

$$\begin{aligned} f = F^{-1}Ff &= \frac{2}{A' + B} \sum_{n=0}^{\infty} R^n Ff \\ &= \lim_{N \rightarrow \infty} \frac{2}{A' + B} \sum_{n=0}^N R^n Ff \\ &= \lim_{N \rightarrow \infty} f_N . \end{aligned}$$

□

If it is desired to explicitly define the spaces $\{\tilde{V}_j\}$ specified in the statement of Theorem 4.3.1, it is possible to apply the operator F^{-1} to a basis of each space V_j . That is, the action of $F^{-1}P_{V_j}$ is completely defined by its action on a basis of V_j .

4.4 Summary

In this chapter, I developed a frame for $L_2(\mathbb{R})$ based on a frame or frames for $L_2(\mathbb{R}^+)$ (Theorem 4.2.4). This frame can be particularly useful in dealing with $L_2(\mathbb{R})$ functions where characteristics of the functions change with respect to the independent variable. Although this frame is not peculiar to speech, it has properties that will make it especially useful in creating frames for speech, as will be done in Chapter VI.

Independent of this frame for $L_2(\mathbb{R})$, I developed an operator akin to the ordinary frame operator (Theorem 4.3.1). This operator, a generalization of the ordinary frame operator, can be used as a basis for faster and more versatile algorithms for finding frame representations. This alternate representation can be particularly useful in finding frame representations in frames which are not amenable to ordinary frame representation calculations. In particular, frames which are not over-complete but which contain many non-orthogonal elements may be used more effectively by being rearranged for more efficient use with the more general operator. This alternate representation will be used in the program described in Chapter VI, and was found to be quite helpful.

V. Representation in $H_2(\mathbb{D})$

Chapter III presented an extension of a representation theorem for elements of $H_p(\mathbb{D})$. That theorem proved that a representation exists, but it gave no way to find any such representation. Producing such a representation is the goal of this chapter.

This chapter is concerned with representations in $H_2(\mathbb{D})$, a Hilbert space, and so after some preliminaries, the more general Hardy spaces, $H_p(\mathbb{D})$, will be neglected in favor of $H_2(\mathbb{D})$. For convenience, in this chapter, the notation $\|\cdot\|$ will refer to the H_2 norm on \mathbb{D} . Also, since the work here will be in a Hilbert space, the functional evaluation $\psi[f]$ will be replaced notationally as the inner product $\langle f, \psi \rangle$.

There are two main results in this chapter, Theorems 5.2.7 and 5.2.10, both of which establish frames for $H_2(\mathbb{D})$. Theorem 5.2.10 is the more useful of the two, and is based more firmly than Theorem 5.2.7 on the results of Chapter III. These results will be combined with the frame developed in Chapter IV to create a frame for speech in Chapter VI.

Blaschke products will be defined in Section 5.1 and are of great use when working with representations involving the functions of the form given in (17), which was the form used in the representation of Chapter III. Some of the basic properties of Blaschke products will be presented.

Functions of the form of (17) are rational functions with a single pole in $\mathbb{C} \setminus \overline{\mathbb{D}}$ and no zeros, and so will be referred to as simple pole functions. Note that throughout this chapter and the chapters that follow, the form of simple pole functions which will be used is given by

$$\psi(z) = \frac{(1 - |a|^2)^{1/2}}{(1 - \bar{a}z)} \quad (37)$$

where $a \in \mathbb{D}$. This form varies from (17) used in Chapter III by a constant bounded between 1 and $\sqrt{2}$, and so this change presents no difficulties in using the results based on (17). The impetus behind this change is that for ψ of the form of (37), we have $\|\psi\| = 1$. An important characteristic of functions of the form of (37) (Lemma 3.6.3) is that for all $f \in H_2(\mathbb{D})$,

$$\langle f, \psi \rangle = f(a)(1 - |a|^2)^{1/2}. \quad (38)$$

Unfortunately, as is shown in Section 5.2, there is no set of simple pole functions that can be a frame for $H_2(\mathbb{D})$. Fortunately, as is also shown in Section 5.2, there are both

frames and orthonormal bases for $H_2(\mathbb{D})$ based on Gram-Schmidt orthonormalization of sets of simple pole functions. Section 5.3 gives an algorithm for finding approximations to elements of $H_2(\mathbb{D})$ using the frames presented in Section 5.2.

5.1 Blaschke Products

For our work, we will define Blaschke products to be functions of the form

$$B(z) = \prod_{k=1}^n \frac{(a_k - z)}{(1 - \overline{a_k}z)}, \quad (39)$$

where $1 \leq n \leq \infty$, $\{a_k\} \subset \mathbb{D}$, and $\sum_{k=1}^n (1 - |a_k|) < \infty$. This definition is identical (up to a constant of magnitude 1) to that given in [12].

The following lemma is given without proof. It summarizes some of the properties of the Blaschke products that will be needed in the proofs ahead. The details of the proof can be found in various places in, e.g., [12].

Lemma 5.1.1 *Let B be a Blaschke product. Then $B \in H_p(\mathbb{D})$ for each $0 < p \leq \infty$, $|B(z)| < 1$ for all $z \in \mathbb{D}$, $|B(e^{i\theta})| = 1$ for a.e. $\theta \in [-\pi, \pi)$ and $\|B\|_p = 1$.*

The next two lemmas illustrate some of the useful properties of the Blaschke products that will be used in various proofs.

Lemma 5.1.2 *Let B be a Blaschke product and $g \in H_p(\mathbb{D})$ for $p \geq 1$. Then $\|Bg\|_p = \|g\|_p$.*

Proof. Let

$$g(e^{i\theta}) \doteq \lim_{r \rightarrow 1} g(re^{i\theta}). \quad (40)$$

By Theorem 3.2.2, we have that for g defined in this way,

$$\|Bg\|_p^p = \frac{1}{2\pi} \int_{-\pi}^{\pi} |B(e^{i\theta})g(e^{i\theta})|^p d\theta.$$

However, from Lemma 5.1.1, we have that $|B(e^{i\theta})| = 1$ for a.e. $\theta \in [-\pi, \pi)$. Therefore,

$$\begin{aligned}
\|Bg\|_p^p &= \frac{1}{2\pi} \int_{-\pi}^{\pi} |g(e^{i\theta})|^p d\theta \\
&= \|g\|_p^p.
\end{aligned}$$

□

Lemma 5.1.3 *Let B be a Blaschke product and $f, g \in H_2(\mathbb{D})$. Then, $\langle Bf, Bg \rangle = \langle f, g \rangle$.*

Proof. Allowing $f(e^{i\theta})$ and $g(e^{i\theta})$ to be defined by the (possibly non-analytic) extensions of f and g to $\partial\mathbb{D}$ given above in (40), we have that

$$\begin{aligned}
\langle Bf, Bg \rangle &= \frac{1}{2\pi} \int_{-\pi}^{\pi} B(e^{i\theta}) f(e^{i\theta}) \overline{B(e^{i\theta}) g(e^{i\theta})} d\theta \\
&= \frac{1}{2\pi} \int_{-\pi}^{\pi} |B(e^{i\theta})|^2 f(e^{i\theta}) \overline{g(e^{i\theta})} d\theta \\
&= \frac{1}{2\pi} \int_{-\pi}^{\pi} f(e^{i\theta}) \overline{g(e^{i\theta})} d\theta \\
&= \langle f, g \rangle,
\end{aligned}$$

since by Lemma 5.1.1, we have that $|B(e^{i\theta})| = 1$ for a.e. $\theta \in [-\pi, \pi)$. □

The following theorem is vital to the work presented later. It appears in [12], where it is attributed to F. Riesz. It is presented here without proof.

Theorem 5.1.4 (F. Riesz) *Let $f \in H_p(\mathbb{D})$, $0 < p < \infty$, f not identically zero. Then f can be written in the form*

$$f = Bg,$$

where B is a Blaschke product and $g \in H_p(\mathbb{D})$ does not vanish.

5.2 Frames for $H_2(\mathbb{D})$

The results from Theorem 3.6.4 involved representations for $f \in H_p(\mathbb{D})$ of the form

$$f = \sum_{n,k} \lambda_{n,k} \psi_{n,k}, \quad (41)$$

with $\sum_n \left(\sum_{k=1}^{k(n)} |\lambda_{n,k}|^p \right)^{1/p} < \infty$, where $\{\lambda_{n,k}\} \subset \mathbb{C}$ is a doubly indexed set with $n \in \mathbb{Z}^+$ and $k = 1, \dots, k(n)$ and $k(n) < \infty$ for each n , and where

$$\psi_{n,k}(z) = \frac{(1 - |a_{n,k}|)^{1/p}}{1 - \overline{a_{n,k}}z},$$

for some set $\{a_{n,k}\} \subset \mathbb{D}$. Since I want to represent functions in $H_2(\mathbb{D})$ as a sum (41), I need to determine how to find the coefficients $\{\lambda_{n,k}\}$.

If the set $\{\psi_{n,k}\}$ were a frame, then this problem would be well understood. Unfortunately, as Theorem 5.2.1 shows, this is never the case.

Theorem 5.2.1 *There does not exist any set $\{a_k\} \subset \mathbb{D}$ such that the set $\{\psi_k\}$ is a frame for $H_2(\mathbb{D})$, where ψ_k is defined by*

$$\psi_k(z) = \frac{(1 - |a_k|^2)^{1/2}}{1 - \overline{a_k}z}.$$

Proof. Let $\{a_k\} \subset \mathbb{D}$ and assume $\sum_k (1 - |a_k|) < \infty$. By Lemma 5.1.1, we have that the Blaschke product B defined by (39) is analytic in \mathbb{D} with $\|B\| = 1$. From (38), we have

$$\langle B, \psi_k \rangle = (1 - |a_k|^2)^{1/2} B(a_k) = 0$$

for all k . This implies that

$$\sum_k |\langle B, \psi_k \rangle|^2 = 0.$$

Since $\|B\| = 1 \neq 0$ this implies that there does not exist $c > 0$ such that $c\|f\|^2 \leq \sum_k |\langle f, \psi_k \rangle|^2$ for all $f \in H_2(\mathbb{D})$. Therefore, if $\sum_k (1 - |a_k|) < \infty$, then $\{\psi_k\}$ is not a frame for $H_2(\mathbb{D})$.

Next, assume that $\sum_k (1 - |a_k|) = \infty$. Choose $f \in H_2(\mathbb{D})$ defined by $f(z) = 1$ for all $z \in \mathbb{D}$. For this choice of f , $\|f\| = 1$. Evaluating $\sum_k |\langle f, \psi_k \rangle|^2$ we see

$$\begin{aligned} \sum_k |\langle f, \psi_k \rangle|^2 &= \sum_k |(1 - |a_k|^2)^{1/2} f(a_k)|^2 \\ &= \sum_k (1 - |a_k|)(1 + |a_k|) \end{aligned}$$

$$\geq \sum_k (1 - |a_k|) = \infty .$$

Since $\|f\| = 1$, this implies there does not exist $C < \infty$ such that $\sum_k |\langle f, \psi_k \rangle|^2 \leq C \|f\|^2$ for all $f \in H_2(\mathbb{D})$. Therefore, if $\sum_k (1 - |a_k|) = \infty$, then $\{\psi_k\}$ is not a frame.

Since either $\sum_k (1 - |a_k|) < \infty$ or $\sum_k (1 - |a_k|) = \infty$, this implies that there does not exist a set $\{a_k\} \subset \mathbb{D}$ such that $\{\psi_k\}$ is a frame for $H_2(\mathbb{D})$. \square

Despite the fact that a set of simple poles, $\{\psi_k\}$, cannot be a frame for $H_2(\mathbb{D})$, an orthonormal basis for $H_2(\mathbb{D})$ can be created by performing the Gram-Schmidt orthonormalization process on $\{\psi_k\}$. In [22], Ninness and Gustafsson prove the following theorem.

Theorem 5.2.2 *Let $\{a_n\}_{n=1}^\infty \subset \mathbb{D}$ be such that $a_n \neq a_m$ for all $n \neq m$ and define $\{\phi_n\}_{n=1}^\infty \subset H_2(\mathbb{D})$ by*

$$\phi_n = \psi_n B_n ,$$

where

$$\psi_n(z) = \frac{(1 - |a_n|^2)^{1/2}}{1 - \overline{a_n}z} , \quad (42)$$

$$B_n(z) = \prod_{k=1}^{n-1} \left(\frac{a_k - z}{1 - \overline{a_k}z} \right) , \quad (43)$$

and $B_1 = 1$. The set $\{\phi_n\}_{n=1}^\infty$ is an orthonormal basis for $H_2(\mathbb{D})$ if and only if

$$\sum_{k=0}^\infty (1 - |a_k|) = \infty .$$

Proof. This proof follows the one given in [22], but I provide more detail. It consists of showing that the sequence $\{\phi_n\}$ is the result of performing the Gram-Schmidt orthonormalization process on the sequence $\{\psi_n\}$ and then showing the necessity and sufficiency of the condition $\sum_{k=0}^\infty (1 - |a_k|) = \infty$ to have a basis.

Define the result of the Gram-Schmidt orthonormalization process on $\{\psi_k\}$ to be $\{\phi_k\}$. Since $\|\psi_1\| = 1$, the first element of the orthonormalized sequence is given by

$\phi_1 = B_1\psi_1 = \psi_1$. It is easily shown using (38) together with (42) and (43) that

$$\begin{aligned}\psi_2 - \langle \psi_2, \phi_1 \rangle \phi_1 &= \frac{(\overline{a_1} - \overline{a_2})}{(1 - \overline{a_2}a_1)} \psi_2 B_2 \\ &= \overline{B_2(a_2)} \psi_2 B_2 .\end{aligned}$$

Since $\|\psi_n\| = 1$ and B_n is a Blaschke product, by Lemma 5.1.1, we have that $\|\psi_n B_n\| = 1$. Hence,

$$\begin{aligned}\|\psi_2 - \langle \psi_2, \phi_1 \rangle \phi_1\| &= \|\overline{B_2(a_2)} \psi_2 B_2\| \\ &= |\overline{B_2(a_2)}| ,\end{aligned}$$

implying that the next function in the orthonormal sequence, ϕ_2 , is given by

$$\phi_2 = \psi_2 B_2 .$$

Now assume that $\phi_k = \psi_k B_k$ for each $k = 1, \dots, n-1$. Applying the Gram-Schmidt process, we see

$$\begin{aligned}\psi_n(z) - \sum_{k=1}^{n-1} \langle \psi_n, \phi_k \rangle \phi_k(z) &= \psi_n(z) - \sum_{k=1}^{n-1} \overline{\langle \phi_k, \psi_n \rangle} \phi_k(z) \\ &= \psi_n(z) - \sum_{k=1}^{n-1} (1 - |a_n|^2)^{1/2} \overline{\phi_k(a_n)} \phi_k(z) \\ &= \frac{(1 - |a_n|^2)^{1/2}}{(1 - \overline{a_n}z)} \\ &\quad - \sum_{k=1}^{n-1} (1 - |a_n|^2)^{1/2} \frac{(1 - |a_k|^2)^{1/2}}{(1 - \overline{a_n}a_k)} \left[\prod_{j=1}^{k-1} \frac{(\overline{a_j} - \overline{a_n})}{(1 - \overline{a_n}a_j)} \right] \frac{(1 - |a_k|^2)^{1/2}}{(1 - \overline{a_k}z)} \left[\prod_{j=1}^{k-1} \frac{(a_j - a_n)}{(1 - \overline{a_j}z)} \right] \\ &= (1 - |a_n|^2)^{1/2} \left(\frac{1}{(1 - \overline{a_n}z)} - \sum_{k=1}^{n-1} \frac{(1 - |a_k|^2)}{(1 - \overline{a_n}a_k)(1 - \overline{a_k}z)} \left[\prod_{j=1}^{k-1} \frac{(\overline{a_j} - \overline{a_n})}{(1 - \overline{a_n}a_j)} \frac{(a_j - a_n)}{(1 - \overline{a_j}z)} \right] \right) \\ &= \frac{(1 - |a_n|^2)^{1/2}}{(1 - \overline{a_n}z) \left[\prod_{k=1}^{n-1} (1 - \overline{a_k}z)(1 - \overline{a_n}a_k) \right]} \left(\left[\prod_{j=1}^{n-1} (1 - \overline{a_j}z)(1 - \overline{a_n}a_j) \right] \right. \\ &\quad \left. - (1 - \overline{a_n}z) \sum_{k=1}^{n-1} (1 - |a_k|^2) \left[\prod_{j=k+1}^{n-1} (1 - \overline{a_n}a_j)(1 - \overline{a_j}z) \right] \left[\prod_{j=1}^{k-1} (\overline{a_j} - \overline{a_n})(a_j - z) \right] \right) \quad (44)\end{aligned}$$

For the next part of the calculation, combine the first term of the difference with the first term of the sum, giving

$$\begin{aligned}
\psi_n(z) - \sum_{k=1}^{n-1} \langle \psi_n, \phi_k \rangle \phi_k(z) &= \frac{(1 - |a_n|^2)^{1/2}}{(1 - \overline{a_n}z) \left[\prod_{k=1}^{n-1} (1 - \overline{a_k}z)(1 - \overline{a_n}a_k) \right]} \left((1 - \overline{a_1}z)(1 - \overline{a_n}a_1) \left[\prod_{j=2}^{n-1} (1 - \overline{a_j}z)(1 - \overline{a_n}a_j) \right] \right. \\
&\quad \left. - (1 - \overline{a_n}z)(1 - |a_1|^2) \left[\prod_{j=2}^{n-1} (1 - \overline{a_n}a_j)(1 - \overline{a_j}z) \right] \right. \\
&\quad \left. - (1 - \overline{a_n}z) \sum_{k=2}^{n-1} (1 - |a_k|^2) \left[\prod_{j=k+1}^{n-1} (1 - \overline{a_n}a_j)(1 - \overline{a_j}z) \right] \left[\prod_{j=1}^{k-1} (\overline{a_j} - \overline{a_n})(a_j - z) \right] \right) \\
&= \frac{(1 - |a_n|^2)^{1/2}}{(1 - \overline{a_n}z) \left[\prod_{k=1}^{n-1} (1 - \overline{a_k}z)(1 - \overline{a_n}a_k) \right]} \left((\overline{a_1} - \overline{a_n})(a_1 - z) \left[\prod_{j=2}^{n-1} (1 - \overline{a_j}z)(1 - \overline{a_n}a_j) \right] \right. \\
&\quad \left. - (1 - \overline{a_n}z) \sum_{k=2}^{n-1} (1 - |a_k|^2) \left[\prod_{j=k+1}^{n-1} (1 - \overline{a_n}a_j)(1 - \overline{a_j}z) \right] \left[\prod_{j=1}^{k-1} (\overline{a_j} - \overline{a_n})(a_j - z) \right] \right).
\end{aligned}$$

Note that the quantity $(\overline{a_1} - \overline{a_n})(a_1 - z)$ is a factor of each term in the sum. Factoring it out of the difference, we then have

$$\begin{aligned}
\psi_n(z) - \sum_{k=1}^{n-1} \langle \psi_n, \phi_k \rangle \phi_k(z) &= \frac{(1 - |a_n|^2)^{1/2} (\overline{a_1} - \overline{a_n})(a_1 - z)}{(1 - \overline{a_n}z) \left[\prod_{k=1}^{n-1} (1 - \overline{a_k}z)(1 - \overline{a_n}a_k) \right]} \left(\left[\prod_{j=2}^{n-1} (1 - \overline{a_j}z)(1 - \overline{a_n}a_j) \right] \right. \\
&\quad \left. - (1 - \overline{a_n}z) \sum_{k=2}^{n-1} (1 - |a_k|^2) \left[\prod_{j=k+1}^{n-1} (1 - \overline{a_n}a_j)(1 - \overline{a_j}z) \right] \left[\prod_{j=2}^{k-1} (\overline{a_j} - \overline{a_n})(a_j - z) \right] \right).
\end{aligned}$$

Carefully examining the difference, it can be seen that it is again in the form seen in (44). Since n is finite, we may iteratively continue this regrouping, to get

$$\begin{aligned}
\psi_n(z) - \sum_{k=1}^{n-1} \langle \psi_n, \phi_k \rangle \phi_k(z) &= \frac{(1 - |a_n|^2)^{1/2} \left[\prod_{k=1}^{n-1} (\overline{a_k} - \overline{a_n})(a_k - z) \right]}{(1 - \overline{a_n}z) \left[\prod_{k=1}^{n-1} (1 - \overline{a_k}z)(1 - \overline{a_n}a_k) \right]} \\
&= \left[\prod_{k=1}^{n-1} \frac{(\overline{a_k} - \overline{a_n})}{(1 - \overline{a_n}a_k)} \right] \frac{(1 - |a_n|^2)^{1/2}}{(1 - \overline{a_n}z)} \left[\prod_{k=1}^{n-1} \frac{(a_k - z)}{(1 - \overline{a_k}z)} \right] \\
&= \overline{B_n(a_n)} \psi_n(z) B_n(z).
\end{aligned}$$

Note that $B_n(a_n) \neq 0$ so long as $a_n \neq a_k$ for all $k = 1, \dots, n-1$. Therefore, the sequence $\{\phi_n\} = \{\psi_n B_n\}$ is the Gram-Schmidt orthonormalization of the sequence $\{\psi_n\}$.

To show the necessity of the condition that $\sum_{k=0}^{\infty} (1 - |a_n|) = \infty$, note that by Theorem 5.1.4, any $f \in H_2(\mathbb{D})$, f not identically zero, may be expressed as $f = gB$, where $g \in H_2(\mathbb{D})$ is non-vanishing and B is a Blaschke product. If we have chosen $\{a_n\}$ such that $\sum_{k=0}^{\infty} (1 - |a_n|) < \infty$, by Lemma 5.1.1, the Blaschke product defined by $\{a_n\}$, $B(z) = \prod_{k=1}^{\infty} \frac{(a_k - z)}{(1 - \bar{a}_k z)}$, is an element of $H_2(\mathbb{D})$ with $\|B\| = 1$. However, using (38), for each $k = 1, 2, \dots$, we have that

$$\langle B, \psi_k \rangle = (1 - |a_k|^2)^{1/2} B(a_k) = 0,$$

which shows that B is orthogonal to the space spanned by the $\{\psi_k\}$. However, $\{\phi_k\}$ is the orthonormalization of the set $\{\psi_k\}$, so that this also implies that B is orthogonal to the space spanned by the $\{\phi_k\}$. Hence, $\{\phi_k\}$ is not complete. Therefore, it is necessary that $\sum_{k=1}^{\infty} (1 - |a_n|) = \infty$ in order for $\{\phi_k\}$ to be an orthonormal basis for $H_2(\mathbb{D})$.

The sufficiency that $\sum_{k=1}^{\infty} (1 - |a_n|) = \infty$ in order for $\{\phi_k\}$ to be complete is seen by assuming that $\{\phi_k\}$ is not complete. This implies the existence of a function $f \in H_2(\mathbb{D})$, f not identically zero, such that $\langle f, \phi_k \rangle = 0$ for all $k = 1, 2, \dots$. Since each ψ_k is in the span of $\{\phi_n\}_{n=1}^k$, using (38) this likewise implies that $\langle f, \psi_k \rangle = (1 - |a_k|^2)^{1/2} f(a_k) = 0$ for all $k = 1, 2, \dots$. From Theorem 5.1.4, we know that for this to be true, f must be of the form

$$f = Bg,$$

where the Blaschke product B is defined by $B(z) = \prod_{j=1}^{\infty} \frac{(a_j - z)}{(1 - \bar{a}_j z)}$ and $g \in H_2(\mathbb{D})$ (g not necessarily non-vanishing in this case). By the definition of a Blaschke product, we have $\sum_{k=1}^{\infty} (1 - |a_n|) < \infty$. Hence, for every non-basis sequence $\{\phi_k\}$, we have that $\sum_{k=1}^{\infty} (1 - |a_n|) < \infty$. Therefore, $\sum_{k=1}^{\infty} (1 - |a_n|) = \infty$ is sufficient for $\{\phi_k\}$ to be complete. \square

Corollary 5.2.3 *For every finite set $\{a_k\}_{k=1}^K \subset \mathbb{D}$ such that $a_j \neq a_k$ for all $j \neq k$ and every Blaschke product B , the set $\{\psi_k B\}_{k=1}^K$ is linearly independent.*

Proof. From the proof of Theorem 5.2.2 above, we have that the set $\{\psi_k\}$ is linearly independent. To see the the set $\{\psi_k B\}_{k=1}^K$ is linearly independent, assume that

$$\sum_{k=1}^K c_k \psi_k B = 0$$

for some $\{c_k\}_{k=1}^K \subset \mathbb{C}$. Since B is a Blaschke product, it is 0 only at a countable number of points. So for a.e. choice of $z \in \mathbb{D}$, we have $B(z) \neq 0$. Evaluating the function at z , we see that

$$\sum_{k=1}^K c_k \psi_k(z) B(z) = B(z) \sum_{k=1}^K c_k \psi_k(z) = 0,$$

which yields

$$\sum_{k=1}^K c_k \psi_k(z) = 0.$$

Since this is true for almost every choice of $z \in \mathbb{D}$, this implies

$$\sum_{k=1}^K c_k \psi_k = 0.$$

However, the set $\{\psi_k\}_{k=1}^K$ is linearly independent, which implies that $c_k = 0$ for $1 \leq k \leq K$. Therefore, the set $\{\psi_k B\}_{k=1}^K$ is linearly independent also. \square

Corollary 5.2.4 *Let $\{a_n\} \subset \mathbb{D}$, $\{\psi_n\} \subset H_2(\mathbb{D})$ and $\{B_n\} \subset H_2(\mathbb{D})$ be as defined in Theorem 5.2.2 above, and let $1 \leq j < k < m < n < \infty$. Then $\psi_n B_m \perp \psi_k B_j$.*

Proof. Rearrange the sequence $\{a_i\}$ into a new sequence $\{b_n\}$ so that the desired functions $\psi_n B_m$ and $\psi_k B_j$ are the results of the Gram-Schmidt orthonormalization process on the new sequence. That is, create the sequence $\{b_n\} \subset \mathbb{D}$ from the old sequence $\{a_n\}$ according to $\{b_n\} = \{a_i\}_{i=1}^j + \{a_k\} + \{a_i\}_{i=j+1}^{k-1} + \{a_i\}_{i=k+1}^m + \{a_n\} + \{a_i\}_{i=m+1}^{n-1} + \{a_i\}_{i=n+1}^\infty$, where here, the $+$ operator indicates sequence concatenation. Then, this corollary follows immediately from the above theorem. \square

Theorem 5.2.5 *Let $\{a_{n,k}\}$ be such that $\sum_n \sum_{k=1}^{k(n)} (1 - |a_{n,k}|) = \infty$. Define $B_n \in H_2(\mathbb{D})$ by*

$$B_{n+1}(z) = B_n(z) \prod_{k=1}^{k(n)} \frac{(a_{n,k} - z)}{(1 - \overline{a_{n,k}} z)},$$

where $B_1 \doteq 1$. Then, for $F_n = \text{span}(\{a_{n,k} B_n\}_{k=1}^{k(n)})$, we have that $F_n \perp F_m$ for all $n \neq m$ and that $H_2(\mathbb{D}) = \overline{\bigoplus_{n=1}^\infty F_n}$.

Proof. From Corollary 5.2.4 above, we have immediately for each $m \neq n$ and each $1 \leq k_m \leq k(m)$ and $1 \leq k_n \leq k(n)$, that $\psi_{n,k_n} B_n \perp \psi_{m,k_m} B_m$. Therefore, the sets $\{\psi_{m,k} B_m\}_{k=1}^{k(m)}$ and $\{\psi_{n,k} B_n\}_{k=1}^{k(n)}$ span orthogonal subspaces. That is, $F_m \perp F_n$ for all $m \neq n$.

Next, note that for our choice of $\{a_{n,k}\}$, by Theorem 5.2.2, the span of the set $\{\psi_{n,k}\}$ is $H_2(\mathbb{D})$. Since each $\psi_{n,k}$ is in the space $\bigoplus_{j=1}^n F_n$, we have that $H_2(\mathbb{D}) = \overline{\bigoplus_{n=1}^{\infty} F_n}$. \square

Theorem 5.2.6 *Let the set $\{a_k\}_{k=1}^K \subset \mathbb{D}$ be such that $a_k \neq a_j$ for all $k \neq j$. Let $B \in H_2(\mathbb{D})$ be a Blaschke product with $B(a_k) \neq 0$ for each a_k . Define the set $\{\psi_k\}_{k=1}^K \subset H_2(\mathbb{D})$ by*

$$\psi_k(z) = \frac{(1 - |a_k|^2)^{1/2}}{(1 - \overline{a_k} z)}.$$

Then, the set $\{\psi_k B\}_{k=1}^K$ forms a frame for a subspace of $H_2(\mathbb{D})$, and its dual frame, $\{\widetilde{\psi_k B}\}_{k=1}^K$, is given by

$$\widetilde{\psi_k B}(z) = \psi_k(z) B(z) \frac{B_k(z)}{B_k(a_k)},$$

where the Blaschke product B_k is defined by

$$B_k(z) = \prod_{j=1, j \neq k}^K \frac{(a_j - z)}{(1 - \overline{a_j} z)}.$$

Proof. By Corollary 5.2.3, we have that the set $\{\psi_k B\}_{k=1}^K$ is linearly independent. Since it is a finite set, this implies that it is an exact frame in some subspace of $H_2(\mathbb{D})$, specifically, the subspace spanned by $\{\psi_k B\}_{k=1}^K$.

Using (38) and the result of Theorem 4.1.8 and Lemma 5.1.3, and noting that $\psi_k B_k B$ is the result of performing the Gram-Schmidt orthonormalization process on the set $\{\psi_k B\}$, with element $\psi_k B$ being the last one to be processed, we have

$$\begin{aligned} \widetilde{\psi_k B} &= \frac{\psi_k B B_k}{\langle \psi_k B, \psi_k B B_k \rangle} \\ &= \frac{\psi_k B B_k}{\langle \psi_k, \psi_k B_k \rangle} \\ &= \frac{\psi_k B B_k}{\psi_k(a_k) B_k(a_k) (1 - |a_k|^2)^{1/2}} \end{aligned}$$

$$= \psi_k B \frac{B_k}{B_k(a_k)}.$$

□

The following theorem gives a construction of a frame for $H_2(\mathbb{D})$. It is one of the main results of this chapter.

Theorem 5.2.7 *Let the set $\{a_{n,k}\}$ be defined such that Theorem 3.6.1 applies to the set $\{\psi_{n,k}\}$ where*

$$\psi_{n,k}(z) = \frac{(1 - |a_{n,k}|^2)^{1/2}}{1 - \overline{a_{n,k}}z}.$$

Additionally, assume that there exists $0 < m \leq M < \infty$ such that for each n ,

$$m\|\phi_n\| \leq \left(\sum_{k=1}^{k(n)} |\lambda_{n,k}|^2 \right)^{1/2} \leq M\|\phi_n\|$$

where $\phi_n = \sum_{k=1}^{k(n)} \lambda_{n,k} \psi_{n,k} B_n$ and where $B_n \in H_2(\mathbb{D})$ is defined recursively by

$$B_{n+1}(z) = B_n(z) \prod_{k=1}^{k(n)} \left(\frac{a_{n,k} - z}{1 - \overline{a_{n,k}}z} \right),$$

with $B_1(z) \doteq 1$. Then the set $\{\psi_{n,k} B_n\}$ is a frame for $H_2(\mathbb{D})$ with frame bounds $\frac{1}{M^2}$ and $\frac{1}{m^2}$ and with dual frame $\left\{ \frac{B_{n,k}}{B_{n,k}(a_{n,k})} \psi_{n,k} B_n \right\}$, where

$$B_{n,k}(z) = \prod_{j=1, j \neq k}^{k(n)} \left(\frac{a_{n,j} - z}{1 - \overline{a_{n,j}}z} \right).$$

Proof. For each n , define $F_n = \text{span}\{\psi_{n,k} B_n\}_{k=1}^{k(n)}$. From Theorem 5.2.6, we have that the set $\{\psi_{n,k} B_n\}_{k=1}^{k(n)}$ is an exact frame for F_n , with dual frame $\left\{ \psi_{n,k} B_n \frac{B_{n,k}}{B_{n,k}(a_{n,k})} \right\}_{k=1}^{k(n)}$.

Next, let $f_n \in F_n$. Since $\{\psi_{n,k} B_n\}_{k=1}^{k(n)}$ is a frame for F_n , we may express f_n as $f_n = \sum_{k=1}^{k(n)} \langle f_n, \psi_{n,k} B_n \rangle \psi_{n,k} B_n \frac{B_{n,k}}{B_{n,k}(a_{n,k})}$.

Choose $\{\lambda_{n,k}\}_{k=1}^{k(n)}$ aligned with $\{\langle f_n, \psi_{n,k} B_n \rangle\}_{k=1}^{k(n)}$ such that $\sum_{k=1}^{k(n)} |\lambda_{n,k}|^2 = 1$. Defining $\phi_n \in F_n$ by $\phi_n = \sum_{k=1}^{k(n)} \lambda_{n,k} \psi_{n,k} B_n$, we then have $\|\phi_n\| \leq \frac{(\sum_{k=1}^{k(n)} |\lambda_{n,k}|^2)^{1/2}}{m} = \frac{1}{m}$. Using

$|\langle f_n, \phi_n \rangle| \leq \|f_n\| \|\phi_n\| \leq \frac{\|f_n\|}{m}$ and the fact that for exact frames, the frame and its dual are biorthonormal, we have

$$\begin{aligned}
|\langle f_n, \phi_n \rangle| &= \left| \left\langle \sum_{k=1}^{k(n)} \langle f_n, \psi_{n,k} B_n \rangle \psi_{n,k} B_n \frac{B_{n,k}}{B_{n,k}(a_{n,k})}, \sum_{k'=1}^{k(n)} \lambda_{n,k'} \psi_{n,k'} B_n \right\rangle \right| \\
&= \left| \sum_{k=1}^{k(n)} \sum_{k'=1}^{k(n)} \langle f_n, \psi_{n,k} B_n \rangle \overline{\lambda_{n,k'}} \left\langle \psi_{n,k} B_n \frac{B_{n,k}}{B_{n,k}(a_{n,k})}, \psi_{n,k'} B_n \right\rangle \right| \\
&= \left| \sum_{k=1}^{k(n)} \langle f_n, \psi_{n,k} B_n \rangle \overline{\lambda_{n,k}} \right| \\
&= \left(\sum_{k=1}^{k(n)} |\langle f_n, \psi_{n,k} B_n \rangle|^2 \right)^{1/2} \left(\sum_{k=1}^{k(n)} |\lambda_{n,k}|^2 \right)^{1/2} \\
&= \left(\sum_{k=1}^{k(n)} |\langle f_n, \psi_{n,k} B_n \rangle|^2 \right)^{1/2}.
\end{aligned}$$

This leads us to

$$|\langle f_n, \phi_n \rangle| = \left(\sum_{k=1}^{k(n)} |\langle f_n, \psi_{n,k} B_n \rangle|^2 \right)^{1/2} \leq \frac{\|f_n\|}{m}. \quad (45)$$

Now choose $\phi_n \in F_n$, $\phi_n = \sum_{k=1}^{k(n)} \lambda_{n,k} \psi_{n,k} B_n$, such that ϕ_n is aligned with f_n and $\|\phi_n\| = 1$ (i.e., $\phi_n = \frac{f_n}{\|f_n\|}$). Using $|\langle f_n, \phi_n \rangle| = \|f_n\| \|\phi_n\| = \|f_n\|$ and $\left(\sum_{k=1}^{k(n)} |\lambda_{n,k}|^2 \right)^{1/2} \leq M \|\phi_n\| = M$, we have

$$\begin{aligned}
\frac{\|f_n\|}{M} = \frac{|\langle f_n, \phi_n \rangle|}{M} &= \frac{1}{M} \left| \left\langle \sum_{k=1}^{k(n)} \langle f_n, \psi_{n,k} B_n \rangle \psi_{n,k} B_n \frac{B_{n,k}}{B_{n,k}(a_{n,k})}, \sum_{k'=1}^{k(n)} \lambda_{n,k'} \psi_{n,k'} B_n \right\rangle \right| \\
&= \frac{1}{M} \left| \sum_{k=1}^{k(n)} \langle f_n, \psi_{n,k} B_n \rangle \overline{\lambda_{n,k}} \right| \\
&\leq \frac{1}{M} \left(\sum_{k=1}^{k(n)} |\langle f_n, \psi_{n,k} B_n \rangle|^2 \right)^{1/2} \left(\sum_{k=1}^{k(n)} |\lambda_{n,k}|^2 \right)^{1/2} \\
&= \left(\sum_{k=1}^{k(n)} |\langle f_n, \psi_{n,k} B_n \rangle|^2 \right)^{1/2}. \quad (46)
\end{aligned}$$

Combining (45) and (46), we see that for each n and any $f_n \in F_n$, we have

$$\frac{\|f_n\|^2}{M^2} \leq \sum_{k=1}^{k(n)} |\langle f_n, \psi_{n,k} B_n \rangle|^2 \leq \frac{\|f_n\|^2}{m^2}. \quad (47)$$

From Theorem 5.2.5, we have that $F_n \perp F_m$ for each $n \neq m$ and that $H_2(\mathbb{D}) = \bigoplus_{n=1}^{\infty} F_n$. Therefore, any $f \in H_2(\mathbb{D})$ may be written as

$$f = \sum_{n=1}^{\infty} f_n,$$

where $f_n = P_{F_n} f$ is the orthogonal projection of f onto the subspace F_n . By the orthogonality of the subspaces F_n , we may write $\|f\|^2 = \sum_{n=1}^{\infty} \|f_n\|^2$. Returning to (47), this gives

$$\frac{\|f\|^2}{M^2} = \sum_{n=1}^{\infty} \frac{\|f_n\|^2}{M^2} \leq \sum_{n=1}^{\infty} \sum_{k=1}^{k(n)} |\langle f_n, \psi_{n,k} B_n \rangle|^2 \leq \sum_{n=1}^{\infty} \frac{\|f_n\|^2}{m^2} = \frac{\|f\|^2}{m^2}.$$

Since for each n and k , we have $\langle f, \psi_{n,k} B_n \rangle = \langle f_n, \psi_{n,k} B_n \rangle$, we may then write

$$\frac{\|f\|^2}{M^2} \leq \sum_{n=1}^{\infty} \sum_{k=1}^{k(n)} |\langle f, \psi_{n,k} B_n \rangle|^2 \leq \frac{\|f\|^2}{m^2},$$

establishing our frame bounds. □

The following theorem shows that points $\{a_{n,k}\}$ chosen according to Theorem 3.1.4 are candidates from which to create an orthonormal basis for $H_2(\mathbb{D})$, as in Theorem 5.2.2. That is, $\sum_n \sum_{k=1}^{k(n)} (1 - |a_{n,k}|) = \infty$.

Theorem 5.2.8 *Let $\{a_{n,k}\}$ satisfy the conditions of Theorem 3.1.4 with δ , \underline{r}_n and \overline{M}_n as defined in that theorem. Then $\sum_n \sum_{k=1}^{k(n)} (1 - |a_{n,k}|) = \infty$.*

Proof. The method of proof will be to use the separation conditions from the statement of Theorem 3.1.4 to bound the desired sum. This will be done by using the value of the Euclidean radius of the pseudo-hyperbolic ball, $K(a, \delta)$.

Fix $n \in \mathbb{Z}$. By the construction of the set $\{\psi_{n,k}\}$, we can bound the sum $\sum_{k=1}^{k(n)}(1 - |a_{n,k}|)$ above and below according to

$$(1 - \overline{M}_n)k(n) \leq \sum_{k=1}^{k(n)}(1 - |a_{n,k}|) \leq (1 - \underline{r}_n)k(n).$$

To establish a lower bound on $k(n)$, note that by Lemma 3.3.2, the radius r of the ball $K(r_n, \delta)$ is given by $r = \frac{\delta(1-\underline{r}_n^2)}{1-\delta^2\underline{r}_n^2}$. This radius is the largest possible for balls $K(a_{n,k}, \delta)$ about points $\{a_{n,k}\}_{k=1}^{k(n)}$ corresponding to $\{\psi_{n,k}\}_{k=1}^{k(n)}$. Since we are looking for a lower bound for $k(n)$, we can determine the number of balls necessary to cover the set $\{\underline{r}_n e^{i\theta} : \theta \in [-\pi, \pi]\}$. This number will be approximately $\frac{2\pi\underline{r}_n}{2r}$, which gives

$$\begin{aligned} k(n) &\geq \frac{2\pi\underline{r}_n(1-\delta^2\underline{r}_n^2)}{2\delta(1-\underline{r}_n^2)} \\ &\geq \frac{\pi\underline{r}_n(1-\delta^2\underline{r}_n^2)}{\delta(1+\underline{r}_n)} \frac{1}{(1-\underline{r}_n)}. \end{aligned}$$

Since $\frac{\pi\underline{r}_n(1-\delta^2\underline{r}_n^2)}{\delta(1+\underline{r}_n)} \rightarrow \frac{\pi(1-\delta^2)}{2\delta}$ is bounded away from 0 and is finite, we know that for sufficiently large n , we may write

$$k(n) \geq \frac{B}{(1-\underline{r}_n)}$$

for some constant $B > 0$. This gives for sufficiently large n that

$$\frac{B(1-\overline{M}_n)}{(1-\underline{r}_n)} \leq \sum_{k=1}^{k(n)}(1 - |a_{n,k}|).$$

From Lemma 3.4.7, we have that $\liminf_{n \rightarrow \infty} \frac{1-\overline{M}_n}{1-\underline{r}_n} \geq \frac{1-C_s}{2} > 0$, which implies for sufficiently large n , we may write

$$0 < \frac{B(1-C_s)}{4} \leq \sum_{k=1}^{k(n)}(1 - |a_{n,k}|)$$

for every $n \geq N$. Therefore,

$$\sum_n \sum_{k=1}^{k(n)} (1 - |a_{n,k}|) = \infty.$$

□

A very desirable result would be to show that, for points $\{a_{n,k}\}$ chosen according to Theorem 3.1.4, the set $\{\psi_{n,k}B_n\}$ is a frame for $H_2(\mathbb{D})$. Unfortunately, this has not yet been shown, although I suspect it is true. However, a similar result has been shown (Theorem 5.2.10 below) that is suitable for the practical applications I have in mind. The following lemma is necessary to prove this result.

Lemma 5.2.9 *Let the sets $S_n \subset \mathbb{D}$ satisfy Condition A, and for each n , let $\{a_{n,k}\}_{k=1}^{k(n)} \subset S_n$ be chosen such that $\rho(a_{n,j}, a_{n,k}) \geq \epsilon > 0$ for each $j \neq k$ for some fixed ϵ . Then there exists $\delta > 0$ such that*

$$|B_{n,k}(a_{n,k})| \geq \delta$$

for each n and k , where

$$B_{n,k}(z) = \prod_{k'=1, k' \neq k}^{k(n)} \frac{a_{n,k'} - z}{1 - \overline{a_{n,k'}}z}.$$

Proof. From Lemma 3.4.10, we have for N sufficiently large, $\Delta\theta_n \doteq \epsilon(1 - \overline{M_n}^2) \leq |\theta_{n,j} - \theta_{n,k}|$, if $n \geq N$ and $j \neq k$, where $\theta_{n,k} \doteq \arg a_{n,k}$. It can be shown easily that $\rho(a, b) \geq \rho(c \frac{a}{|a|}, c \frac{b}{|b|})$ for every $a, b \in \mathbb{D}$ and every $0 \leq c \leq \min\{|a|, |b|\}$. Therefore,

$$\begin{aligned} |B_{n,k}(a_{n,k})| &= \prod_{k'=1, k' \neq k}^{k(n)} \rho(a_{n,k'}, a_{n,k}) \\ &\geq \prod_{k'=1, k' \neq k}^{k(n)} \rho\left(\frac{r_n}{|a_{n,k'}|} \frac{a_{n,k'}}{|a_{n,k'}|}, \frac{r_n}{|a_{n,k}|} \frac{a_{n,k}}{|a_{n,k}|}\right) \\ &= \prod_{k'=1, k' \neq k}^{k(n)} \left| \frac{r_n e^{i\theta_{n,k'}} - r_n e^{i\theta_{n,k}}}{1 - \overline{r_n}^2 e^{i(\theta_{n,k} - \theta_{n,k'})}} \right|. \end{aligned} \tag{48}$$

Using the identity

$$\left| \frac{a-b}{1-\bar{a}b} \right|^2 = 1 - \frac{(1-|a|^2)(1-|b|^2)}{|1-\bar{a}b|^2}$$

in (48), we get

$$|B_{n,k}(a_{n,k})|^2 \geq \prod_{k'=1, k' \neq k}^{k(n)} \left(1 - \frac{(1-r_n^2)^2}{|1-\underline{r}_n^2 e^{i(\theta_{n,k}-\theta_{n,k'})}|^2} \right). \quad (49)$$

Since both sides of (49) are strictly positive, elementary computations produce

$$\begin{aligned} 2 \ln |B_{n,k}(a_{n,k})| &\geq \sum_{k'=1, k' \neq k}^{k(n)} \ln \left(1 - \frac{(1-r_n^2)^2}{|1-\underline{r}_n^2 e^{i(\theta_{n,k}-\theta_{n,k'})}|^2} \right) \\ &= - \sum_{k'=1, k' \neq k}^{k(n)} \sum_{j=1}^{\infty} \frac{1}{j} \left(\frac{(1-r_n^2)^2}{|1-\underline{r}_n^2 e^{i(\theta_{n,k}-\theta_{n,k'})}|^2} \right)^j \\ &\geq - \sum_{k'=1, k' \neq k}^{k(n)} \sum_{j=1}^{\infty} \left(\frac{(1-r_n^2)^2}{|1-\underline{r}_n^2 e^{i(\theta_{n,k}-\theta_{n,k'})}|^2} \right)^j \\ &= - \sum_{k'=1, k' \neq k}^{k(n)} \frac{\left(\frac{(1-r_n^2)^2}{|1-\underline{r}_n^2 e^{i(\theta_{n,k}-\theta_{n,k'})}|^2} \right)}{1 - \left(\frac{(1-r_n^2)^2}{|1-\underline{r}_n^2 e^{i(\theta_{n,k}-\theta_{n,k'})}|^2} \right)} \\ &= - \sum_{k'=1, k' \neq k}^{k(n)} \frac{(1-r_n^2)^2}{|1-\underline{r}_n^2 e^{i(\theta_{n,k}-\theta_{n,k'})}|^2 - (1-r_n^2)^2} \\ &= - \sum_{k'=1, k' \neq k}^{k(n)} \frac{(1-r_n^2)^2}{2\underline{r}_n^2(1-\cos(\theta_{n,k}-\theta_{n,k'}))} \\ &\geq -2 \sum_{k=1}^{k(n)/2} \frac{(1-r_n^2)^2}{2\underline{r}_n^2(1-\cos(k\Delta\theta_n))}, \end{aligned} \quad (50)$$

where the last step uses the inequality $|\theta_{n,k}-\theta_{n,k'}| \leq |k-k'|\Delta\theta_n$. Note that, for any $\Delta\theta_n/2 < \phi \leq \pi$,

$$\frac{1}{1-\cos\phi} \leq \frac{2}{\Delta\theta_n} \int_{\phi-\Delta\theta_n/2}^{\phi} \frac{1}{1-\cos\theta} d\theta.$$

Therefore

$$\begin{aligned}
2 \sum_{k=1}^{k(n)/2} \frac{1}{1 - \cos(k\Delta\theta_n)} &\leq \frac{2}{\Delta\theta_n} \int_{\Delta\theta_n/2}^{2\pi - \Delta\theta_n/2} \frac{1}{1 - \cos\theta} d\theta \\
&= \frac{2}{\Delta\theta_n} (\cot(\Delta\theta_n/4) - \cot(\pi - \Delta\theta_n/4)) \\
&= \frac{4}{\Delta\theta_n} \cot(\Delta\theta_n/4) \\
&\leq \frac{16}{(\Delta\theta_n)^2} .
\end{aligned} \tag{51}$$

Incorporating (51) into (50), we have

$$\begin{aligned}
2 \ln |B_{n,k}(a_{n,k})| &\geq -\frac{16}{(\Delta\theta_n)^2} \frac{(1 - \underline{r}_n^2)^2}{2\underline{r}_n^2} \\
&= -\frac{16}{\epsilon^2(1 - \overline{M}_n^2)^2} \frac{(1 - \underline{r}_n^2)^2}{2\underline{r}_n^2} \\
&= -\frac{(1 - \underline{r}_n)^2}{(1 - \overline{M}_n)^2} \frac{8(1 + \underline{r}_n)^2}{\epsilon^2 \underline{r}_n^2 (1 + \overline{M}_n)^2} \\
&\geq -\left(\frac{1 - \underline{r}_n}{1 - \overline{M}_n}\right)^2 \frac{8}{\epsilon^2 \underline{r}_n^2} .
\end{aligned} \tag{52}$$

Since $\limsup_{n \rightarrow \infty} \frac{1 - \underline{r}_n}{1 - \overline{M}_n} \leq \frac{2}{1 - C_\epsilon}$ and $\underline{r}_n \rightarrow 1$, we know there exists some constant $C_\epsilon < \infty$ such that

$$\left(\frac{1 - \underline{r}_n}{1 - \overline{M}_n}\right)^2 \frac{8}{\epsilon^2 \underline{r}_n^2} \leq C_\epsilon \tag{53}$$

for all n . Incorporating (53) into (52), we get

$$2 \ln |B_{n,k}(a_{n,k})| \geq -C_\epsilon$$

for all n and k . This implies that

$$|B_{n,k}(a_{n,k})| \geq \delta > 0 .$$

where $\delta = e^{-C_\epsilon/2}$. □

Theorem 5.2.10 *Let the sets $S_n \subset \mathbb{D}$ satisfy Condition A, and for each n , let $\{b_{n,k}\}_{k=1}^{k(n)} \subset S_n$ be chosen so that there exists an $\epsilon > 0$ such that $\rho(b_{n,j}, b_{n,k}) \geq \epsilon > 0$ for each $j \neq k$. Fix $0 < M < \infty$. Define the set $\{a_{n,k}\}$ as a reindexing of the set $\{b_{n,k}\}$ such that for each n , $\{a_{n,k}\} \subset \{b_{n',k}\}$ for some n' and such that $k(n) \doteq \#\{a_{n,k}\} \leq M$. Then the set $\{\psi_{n,k}B_n\}$ is a frame for $H_2(\mathbb{D})$, where*

$$\psi_{n,k}(z) = \frac{(1 - |a_{n,k}|^2)^{1/2}}{1 - \overline{a_{n,k}}z} \quad (54)$$

and

$$B_{n+1}(z) = B_n(z) \prod_{k=1}^{k(n)} \frac{a_{n,k} - z}{1 - \overline{a_{n,k}}z}, \quad (55)$$

with $B_1(z) \doteq 1$.

Proof. The upper frame bounds are easy to find. First note that, by Theorem 5.2.5, the sets $\{\psi_{n,k}B_n\}$ and $\{\psi_{n',k}B_{n'}\}$ span orthogonal subspaces for every $n \neq n'$ and we may write

$$f = \sum_{n=1}^{\infty} f_n$$

where, for each n , f_n is in the span of $\{\psi_{n,k}B_n\}$. The orthogonality of the subspaces gives

$$\|f\|^2 = \sum_{n=1}^{\infty} \|f_n\|^2.$$

Thus, for each n ,

$$\begin{aligned} \sum_{k=1}^{k(n)} |\langle f, \psi_{n,k}B_n \rangle|^2 &= \sum_{k=1}^{k(n)} |\langle f_n, \psi_{n,k}B_n \rangle|^2 \\ &= \sum_{k=1}^{k(n)} |\langle \frac{f_n}{B_n}, \psi_{n,k} \rangle|^2, \end{aligned}$$

where the last equality uses the result of Lemma 5.1.3 and where the division by B_n is justified by noting that f_n is in the span of $\{\psi_{n,k}B_n\}$. However, the set $\{b_{n,k}\}$ satisfies the hypothesis of Theorem 3.1.4, which means that Theorem 3.6.1 applies. Since $\{a_{n,k}\} \subset$

$\{b_{n',k}\}$ for some n' , this implies that

$$\sum_{k=1}^{k(n)} |\langle f_n, \psi_{n,k} B_n \rangle|^2 = \sum_{k=1}^{k(n)} |\langle \frac{f_n}{B_n}, \psi_{n,k} \rangle|^2 \leq C \|\frac{f_n}{B_n}\|^2 = C \|f_n\|^2$$

for some fixed $C < \infty$. Therefore,

$$\sum_{n=1}^{\infty} \sum_{k=1}^{k(n)} |\langle f, \psi_{n,k} B_n \rangle|^2 \leq \sum_{n=1}^{\infty} C \|f_n\|^2 = C \|f\|^2.$$

This establishes the upper frame bound.

To establish the lower frame bound, note that for each n , f_n can be represented by

$$f_n = \sum_{k=1}^{k(n)} \langle f, \psi_{n,k} B_n \rangle \psi_{n,k} \frac{B_{n,k} B_n}{B_{n,k}(a_{n,k})},$$

where, for each n and k , $B_{n,k}$ is defined by

$$B_{n,k}(z) = \prod_{k'=1, k' \neq k}^{k(n)} \frac{a_{n,k'} - z}{1 - \overline{a_{n,k'}} z}.$$

Choose $\{\gamma_{n,k}\}$ such that $\sum_{k=1}^{k(n)} \gamma_{n,k} \psi_{n,k} B_n$ is aligned with f_n with $\|\sum_{k=1}^{k(n)} \gamma_{n,k} \psi_{n,k} B_n\| = 1$. Then

$$\begin{aligned} \|f_n\|^2 &= \left(\langle f_n, \sum_{k=1}^{k(n)} \gamma_{n,k} \psi_{n,k} B_n \rangle \right)^2 \\ &= \left(\sum_{k=1}^{k(n)} \langle f, \psi_{n,k} B_n \rangle \overline{\gamma_{n,k}} \right)^2 \\ &\leq \left(\sum_{k=1}^{k(n)} |\langle f, \psi_{n,k} B_n \rangle|^2 \right) \left(\sum_{k=1}^{k(n)} |\gamma_{n,k}|^2 \right), \end{aligned} \tag{56}$$

which implies

$$\frac{\|f_n\|^2}{\left(\sum_{k=1}^{k(n)} |\gamma_{n,k}|^2 \right)} \leq \sum_{k=1}^{k(n)} |\langle f, \psi_{n,k} B_n \rangle|^2.$$

Next we need to establish an upper bound, independent of n , for the quantity $\sum_{k=1}^{k(n)} |\gamma_{n,k}|^2$.

For each k' , we have

$$\begin{aligned} \left| \left\langle \sum_{k=1}^{k(n)} \gamma_{n,k} \psi_{n,k} B_n, \psi_{n,k'} \frac{B_n B_{n,k'}}{B_{n,k'}(a_{n,k'})} \right\rangle \right| &= |\gamma_{n,k'}| \leq \left\| \sum_{k=1}^{k(n)} \gamma_{n,k} \psi_{n,k} B_n \right\| \left\| \psi_{n,k'} \frac{B_n B_{n,k'}}{B_{n,k'}(a_{n,k'})} \right\| \\ &\leq \frac{1}{|B_{n,k'}(a_{n,k'})|}. \end{aligned}$$

Therefore,

$$\begin{aligned} \sum_{k=1}^{k(n)} |\gamma_{n,k}|^2 &\leq \sum_{k=1}^{k(n)} \frac{1}{|B_{n,k}(a_{n,k})|^2} \\ &\leq \frac{k(n)}{\min_k |B_{n,k}(a_{n,k})|^2} \\ &\leq \frac{M}{\min_k |B_{n,k}(a_{n,k})|^2}. \end{aligned} \tag{57}$$

From Lemma 5.2.9 above, we know that for each k and n and $\tilde{B}_{n,k}$ defined by

$$\tilde{B}_{n,k}(a_{n,k}) \doteq \prod_{k'=1, k' \neq k}^{k(n)} \frac{b_{n,k} - b_{n,k'}}{1 - \overline{b_{n,k}} b_{n,k'}},$$

that

$$|\tilde{B}_{n,k}(a_{n,k})| = \prod_{k'=1, k' \neq k}^{k(n)} \left| \frac{b_{n,k} - b_{n,k'}}{1 - \overline{b_{n,k}} b_{n,k'}} \right| \geq \delta > 0$$

for some fixed δ independent of n and k . Since each $\{a_{n,k}\} \subset \{b_{n',k}\}$, we have that $|B_{n,k}(a_{n,k})| \geq |\tilde{B}_{n',k'}(b_{n',k'})| \geq \delta$ for some n', k' . From (57),

$$\sum_{k=1}^{k(n)} |\gamma_{n,k}|^2 \leq \frac{M}{\delta^2}.$$

Combining this with (56), we get

$$\|f_n\|^2 \frac{\delta^2}{M} \leq \frac{\|f_n\|^2}{\left(\sum_{k=1}^{k(n)} |\gamma_{n,k}|^2\right)} \leq \sum_{k=1}^{k(n)} |\langle f, \psi_{n,k} B_n \rangle|^2$$

which gives the lower frame bound,

$$\|f\|^2 \frac{\delta^2}{M} \leq \sum_{n=1}^{\infty} \sum_{k=1}^{k(n)} |\langle f, \psi_{n,k} B_n \rangle|^2 .$$

□

5.3 Projections into the $H_2(\mathbb{D})$ frame

In this section, a method of projecting into the frame described in the previous section is given. One advantage of this algorithm is that it does not require the points $\{a_{n,k}\}$ to be fully determined *a priori*, which allows for adaptive frame selections.

In that sense, it is equivalent to the orthogonal matching pursuit algorithm described in [24]. However, the properties of the frame elements used here lead to a nicer representation in the sense that the exact forms resulting from the orthonormalization in the orthogonal matching pursuit are known.

The next lemma is needed to show that a division used in the algorithm is well-defined.

Lemma 5.3.1 *Let $\{a_k\}_{k=1}^K \subset \mathbb{D}$ be chosen such that $a_k \neq a_j$ for all $k \neq j$, and let $\{\psi_k\}_{k=1}^K$ be defined by*

$$\psi_k(z) = \frac{(1 - |a_k|^2)^{1/2}}{(1 - \overline{a_k}z)} .$$

Let S be the space spanned by $\{\psi_k\}_{k=1}^K$ and let S^\perp be the orthogonal complement to S in $H_2(\mathbb{D})$. Then, for any $f \in S^\perp$, f is of the form

$$f = Bg ,$$

where

$$B(z) = \prod_{k=1}^K \frac{(a_k - z)}{(1 - \overline{a_k}z)}$$

and $g \in H_2(\mathbb{D})$.

Proof. Since $f \in S^\perp$ and $S^\perp \perp S$, we know that $\langle f, \psi_k \rangle = 0$ for all $k = 1, \dots, K$. That is,

$$\langle f, \psi_k \rangle = (1 - |a_k|^2)^{1/2} f(a_k) = 0$$

for all a_k . Using Theorem 5.1.4, we get

$$f = Bg$$

for some $g \in H_2(\mathbb{D})$. □

Lemma 5.3.2 *Let $\{a_{n,k}\} \subset \mathbb{D}$ be chosen such that Theorem 5.2.7 or Theorem 5.2.10 applies and define $\{\psi_{n,k}\} \subset H_2(\mathbb{D})$ according to*

$$\psi_{n,k}(z) = \frac{(1 - |a_{n,k}|^2)^{1/2}}{(1 - \overline{a_{n,k}}z)}.$$

For each $n \in \mathbb{Z}^+$, let V_n be the subspace of $H_2(\mathbb{D})$ spanned by the set $\{\psi_{n,k}\}_{k=1}^{k(n)}$. Similarly, for each $n \in \mathbb{Z}^+$, let F_n be the subspace of $H_2(\mathbb{D})$ spanned by the set $\{\psi_{n,k}B_n\}_{k=1}^{k(n)}$, where

$$B_{n+1}(z) \doteq B_n(z) \prod_{k=1}^{k(n)} \frac{(a_{n,k} - z)}{(1 - \overline{a_{n,k}}z)},$$

and $B_1(z) \doteq 1$. If $f \in H_2(\mathbb{D})$ is chosen such that $f \perp F_m$ for each $m = 1, \dots, n-1$, then $P_{F_n}f$ is given by

$$P_{F_n}f = B_n P_{V_n} \frac{f}{B_n}.$$

Proof. Let $f \in H_2(\mathbb{D})$ be such that $f \perp F_m$ for each $m = 1, \dots, n-1$. By Lemma 5.3.1 above, this implies that f is of the form

$$f = gB_n$$

for some $g \in H_2(\mathbb{D})$. From Theorem 5.2.6, we know that $\{\psi_{n,k} B_n\}_{k=1}^{k(n)}$ is a frame in F_n with dual frame $\{\psi_{n,k} B_n \frac{B_{n,k}}{B_{n,k}(a_{n,k})}\}$ where $B_{n,k}$ is defined by

$$B_{n,k}(z) \doteq \prod_{j=1, j \neq k}^{k(n)} \frac{(a_{n,j} - z)}{(1 - \overline{a_{n,j}}z)}.$$

Theorem 4.1.4 gives that

$$\begin{aligned} P_{F_n} f &= \sum_{k=1}^{k(n)} \langle f, \psi_{n,k} B_n \rangle \psi_{n,k} B_n \frac{B_{n,k}}{B_{n,k}(a_{n,k})} \\ &= B_n \sum_{k=1}^{k(n)} \langle g B_n, \psi_{n,k} B_n \rangle \psi_{n,k} \frac{B_{n,k}}{B_{n,k}(a_{n,k})} \\ &= B_n \sum_{k=1}^{k(n)} \langle g, \psi_{n,k} \rangle \psi_{n,k} \frac{B_{n,k}}{B_{n,k}(a_{n,k})} \end{aligned}$$

which (using (20) and again Theorem 5.2.6) is of the form

$$\begin{aligned} P_{F_n} f &= B_n P_{V_n} g \\ P_{F_n} f &= B_n P_{V_n} \frac{f}{B_n}. \end{aligned}$$

□

Lemma 5.3.3 *Let $\{a_{n,k}\}$, $\{\psi_{n,k}\}$, $\{F_n\}$, and $\{V_n\}$ be as in Lemma 5.3.2. For $f \in H_2(\mathbb{D})$, define f_n by*

$$f_n = f_{n-1} - B_{n-1} P_{V_{n-1}} \frac{f_{n-1}}{B_{n-1}} \quad (58)$$

where $f_1 \doteq f$. Then, for each $n \geq 1$ and each $m = 1, \dots, n-1$, we have $f_n \perp F_m$.

Proof. (By induction) By Lemma 5.3.2 above, we have that $P_{F_1} f = B_1 P_{V_1} \frac{f_1}{B_1}$, which implies that for f_2 as defined, $f_2 \perp F_1$. Assume that for some n , we have $f_n \perp F_m$ for all $m = 1, \dots, n-1$. Then, $P_{F_n} f_n = B_n P_{V_n} \frac{f_n}{B_n}$, which implies that for f_{n+1} as defined, $f_{n+1} \perp F_n$. However, since by Theorem 5.2.5 we know $F_n \perp F_m$ for all $n \neq m$, we have $f_{n+1} \perp F_m$ for each $m = 1, \dots, n$. □

Theorem 5.3.4 *Let $\{a_{n,k}\}$, $\{\psi_{n,k}\}$, $\{F_n\}$, $\{V_n\}$, and $\{f_n\}$ be as in Lemma 5.3.3 above. For any $f \in H_2(\mathbb{D})$,*

$$f = \lim_{n \rightarrow \infty} \sum_{k=1}^n B_k P_{V_k} \frac{f_k}{B_k}.$$

Proof. From the definition of f_n in (58), we find that for each n ,

$$f = f_n + \sum_{k=1}^{n-1} B_k P_{V_k} \frac{f_k}{B_k}.$$

From Lemma 5.3.3, we know that $f_n \perp F_m$ for all $m = 1, \dots, n-1$. Also, since $P_{F_m} f_m = B_m P_{V_m} \frac{f_m}{B_m}$, we may write

$$f = f_n + \sum_{k=1}^{n-1} P_{F_k} f_k.$$

Since the right-hand summation is a sum of projections onto the orthogonal subspaces $\{F_k\}_{k=1}^n$, we have $f_n \perp \sum_{k=1}^{n-1} P_{F_k} f_k$. That is, f can be represented as the sum of orthogonal elements. Since such a decomposition is unique, and since $f_n \perp F_m$ for $m = 1, \dots, n-1$, we have

$$P_{S_n} f = \sum_{k=1}^n B_k P_{V_k} \frac{f_k}{B_k}$$

and

$$f_{n+1} = P_{S_n^\perp} f,$$

where $S_n = \bigoplus_{k=1}^n F_k$ and S_n^\perp is the orthogonal complement to S_n in $H_2(\mathbb{D})$. Since $\sum_{n=1}^\infty F_n = H_2(\mathbb{D})$, we have for every $f \in H_2(\mathbb{D})$, that $\lim_{n \rightarrow \infty} f_n = 0$. Therefore,

$$f = \lim_{n \rightarrow \infty} \sum_{k=1}^n B_k P_{V_k} \frac{f_k}{B_k}.$$

□

5.4 Summary

In this chapter, I presented two theorems (Theorems 5.2.7 and 5.2.10) which stated results about frames for $H_2(\mathbb{D})$. These frames are useful because they are created from frame elements which sample the values of element of $H_2(\mathbb{D})$ as specific points. This sampling property will be especially useful in practical applications where values of functions may be known only at specific sample points. These frames will be used in the development of frames tailored for speech in Chapter VI, where isometric isomorphisms between $H_2(\mathbb{D})$ and $L_2(\mathbb{R}^+)$ will be employed to use these results as building blocks for the $L_2(\mathbb{R})$ frame developed in Chapter IV.

I also developed a method by which representations in these $H_2(\mathbb{D})$ frames can be found, without having all of the frame elements determined *a priori*. This method is a specific implementation of an orthogonal matching pursuit algorithm, where the properties of the frame elements are used to get exact forms for the representation coefficients. These exact forms were used when possible in the computer program described in Chapter VI to give faster calculations and more precise values.

VI. *Application to speech representation*

The theory presented in Chapters III, IV, and V can be used together in the area of speech processing and representation. The goal of this chapter is to demonstrate an application of the theory to speech processors to make the connection.

Since this chapter is concerned with connecting several theorems together into an application, the main result of this chapter is not a theorem or theorems, but rather the sum total of the illustrated connections. This includes a frame tailored to speech processing and the description of an application program which finds approximations to speech based on this frame.

This chapter is organized into three sections – one dealing with theoretical considerations, the second with practical considerations, and the last describing the implementation of the computer program. Section 6.1 formulates a frame for speech based on the work in the previous chapters. An estimate is given for the norm of the frame-like operator, for use when projecting into the frame. Section 6.2 is concerned with the practical application aspects, such as the issue of having available only discretely sampled speech instead of continuous speech. Section 6.3 describes a computer program which uses the results of the other two sections. Specific attention is given to design considerations which required the program to vary from the theory.

6.1 *A frame for speech*

In this section, connections are established between the theory of the previous chapters and the properties of speech to create a frame tailored to speech. First, the frame to be created will be described, which will make clearer the necessary mathematical justification to follow. Second, the necessary proofs will be presented to justify the creation of the frame.

6.1.1 Description of the speech frame. As discussed in Chapter II, speech can be considered a slowly time-varying function. For harmonic speech, the speech signal can be approximated well by the response of a slowly time-varying system to a sequence of impulse functions, where the impulses are aligned with the glottal pulses in the speech. The decay of the vocal response is very rapid, so that the approximate start of the response for each impulse function (glottal pulse) is readily apparent.

This would appear to correspond well to a frame based on Theorem 4.2.4 with the frames used at each time shift being chosen to well represent the rapid decay of the impulse response. As shown below in Lemma 6.2.4, the basis functions of the frames defined in Theorems 5.2.7 and 5.2.10 can be transformed into decaying exponentials, which give a good representation of both the harmonic nature of harmonic speech and of the decay of the impulse response. Due to the rapid decay of the impulse response, it intuitively makes sense to limit the length of the basis function (given by I_n for each n) so that the number of intervals overlapping with interval $[t_n, t_n + I_n)$ for each n is small.

To define this frame, we will need to do several things. First, we will need to establish an isometric isomorphism between $H_2(\mathbb{D})$ and $L_2(\mathbb{R}^+)$, so that we may use the frame of Theorem 5.2.10 in the construction of the frame of Theorem 4.2.4. In order to use the iterative method given in Theorem 4.3.4 to find representations in this frame, it will be necessary to have a reasonable estimate for the upper bound B ; Theorem 6.1.3 solves this problem for the frame-like construct to be used. Next, we will need to define the sets S_n used in Theorem 3.1.4 and show that they satisfy the necessary conditions.

6.1.2 Isometry between $H_2(\mathbb{D})$ and $L_2(\mathbb{R}^+)$. The frames in Chapter V are based on the $H_2(\mathbb{D})$ representation given in Chapter III. To use these results with Theorem 4.2.4 we must connect the spaces $H_2(\mathbb{D})$ and $L_2(\mathbb{R}^+)$ in some way. In this section, we will demonstrate an isometric isomorphism between them.

Used as an intermediate space in this transform will be the Hardy space $H_2(\mathbb{C}^+)$, where $\mathbb{C}^+ \doteq \{z \in \mathbb{C} : \text{Re}(z) > 0\}$. While there is more than one way to define this space [12], we will use the following:

$$H_2(\mathbb{C}^+) = \{f \text{ analytic in } \mathbb{C}^+ : \lim_{x \rightarrow 0^+} \int_{-\infty}^{\infty} |f(x + iy)|^2 dy = \sup_{x > 0} \int_{-\infty}^{\infty} |f(x + iy)|^2 dy < \infty\}$$

with

$$\|f\|_{H_2(\mathbb{C}^+)}^2 = \lim_{x \rightarrow 0^+} \int_{-\infty}^{\infty} |f(x + iy)|^2 dy = \sup_{x > 0} \int_{-\infty}^{\infty} |f(x + iy)|^2 dy.$$

Note that it is not true that the supremum “occurs” as $x \rightarrow 0^+$ for all analytic functions with a bounded supremum on \mathbb{C}^+ . Therefore, the restriction that the supremum occur as $x \rightarrow 0^+$ must remain in the above definition.

As shown in Theorem 3.2.2 for functions in $H_2(\mathbb{D})$, a function $f \in H_2(\mathbb{C}^+)$ can be extended to the imaginary axis, where the extension is given by $f(iy) = \lim_{x \rightarrow 0^+} f(x + iy)$. The resulting function is in $L_2(i\mathbb{R})$ with $\|f\|_{L_2} = \|f\|_{H_2(\mathbb{C}^+)}$.

An isometric isomorphism between $H_2(\mathbb{C}^+)$ and $H_2(\mathbb{D})$ is given by $S: H_2(\mathbb{C}^+) \rightarrow H_2(\mathbb{D})$, defined by

$$Sf(z) = \frac{2\sqrt{\pi}f\left(\frac{1-z}{1+z}\right)}{1+z}, \quad f \in H_2(\mathbb{C}^+), \quad (59)$$

and inverted by

$$S^{-1}f(z) = \frac{f\left(\frac{1-z}{1+z}\right)}{\sqrt{\pi}(1+z)}, \quad f \in H_2(\mathbb{D}). \quad (60)$$

The Laplace transform, $\mathcal{L}: L_2(\mathbb{R}^+) \rightarrow H_2(\mathbb{C}^+)$ provides an isometric isomorphism between $L_2(\mathbb{R}^+)$ and $H_2(\mathbb{C}^+)$ when defined by

$$\mathcal{L}f(s) = \frac{1}{\sqrt{2\pi}} \int_0^\infty f(t)e^{-st} dt. \quad (61)$$

This definition varies by a constant from the usual one. Its inverse is defined by

$$\mathcal{L}^{-1}f(t) = \frac{1}{i\sqrt{2\pi}} \int_C f(s)e^{st} ds, \quad (62)$$

where C is a Bromwich path with real part greater than that of all of the singularities of f (i.e., to the right of all of the singularities of f).

Using the Laplace transform in (61) and the transform S defined in (59), we may define an isometric isomorphism $T: L_2(\mathbb{R}^+) \rightarrow H_2(\mathbb{D})$ by

$$T = S\mathcal{L}, \quad (63)$$

with $T^{-1} = \mathcal{L}^{-1}S^{-1}$. This transform will provide the connection between $L_2(\mathbb{R}^+)$ and $H_2(\mathbb{D})$ necessary to combine the results of Chapters III and V with the results in Chapter IV.

Given Theorem 6.1.1 below, we know that the transform $T^{-1}: H_2(\mathbb{D}) \rightarrow L_2(\mathbb{R}^+)$ will take frames of the type described in Chapter V into an equivalent frame in $L_2(\mathbb{R}^+)$. Since we have already assumed that speech is an element of $L_2(\mathbb{R}^+)$, one might ask: "Why not

simply use such a frame to find representations of speech?” The answer is that speech has additional properties which may not be well represented by such a frame. That is, while a sample of speech could be represented by its frame expansion in any frame, an approximation to a desired degree of accuracy may require more frame elements to be kept in some frames than in others. This is what motivates use of the frame described in Theorem 4.2.4.

6.1.3 Frame for speech. Having illustrated the isometric isomorphism T between the spaces $L_2(\mathbb{R}^+)$ and $H_2(\mathbb{D})$, we are ready to illustrate a frame tailored to speech processing. First, we will need the following, rather trivial, but useful, theorem.

Theorem 6.1.1 *Let \mathcal{H} and \mathcal{H}' be separable, isometric, Hilbert spaces and let $T: \mathcal{H} \rightarrow \mathcal{H}'$ be an isometric isomorphism between them. Let $\{\psi_k\}$ be a frame in \mathcal{H} with frame bounds A and B . Then $\{T\psi_k\}$ is a frame in \mathcal{H}' with frame bounds A and B .*

Proof. Since $\{\psi_k\}$ is a frame in \mathcal{H} , we may write

$$\begin{aligned} A\|f\|^2 &\leq \sum_k |\langle f, \psi_k \rangle|^2 \leq B\|f\|^2 \\ A\|Tf\|^2 &\leq \sum_k |\langle Tf, T\psi_k \rangle|^2 \leq B\|Tf\|^2 \end{aligned}$$

where we have used that $\|f\| = \|Tf\|$ and $\langle f, g \rangle = \langle Tf, Tg \rangle$ for all $f, g \in \mathcal{H}$. Since any $g \in \mathcal{H}'$ can be written as $g = TT^{-1}g$ and $T^{-1}g \in \mathcal{H}$, we have that

$$A\|TT^{-1}g\|^2 \leq \sum_k |\langle TT^{-1}g, T\psi_k \rangle|^2 \leq B\|TT^{-1}g\|^2,$$

which leads immediately to

$$A\|g\|^2 \leq \sum_k |\langle g, T\psi_k \rangle|^2 \leq B\|g\|^2.$$

□

We will now combine the major results of the previous chapters to create a frame tailored to speech representation. Having shown an isometric isomorphism between $L_2(\mathbb{R}^+)$ and $H_2(\mathbb{D})$, we may combine the results of Theorem 5.2.10, which provided a frame for $H_2(\mathbb{D})$, and Theorem 4.2.4, which provided a composite frame for $L_2(\mathbb{R})$ based on a frame

or frames for $L_2(\mathbb{R}^+)$. Assume a frame for $H_2(\mathbb{D})$ of the type defined in Theorem 5.2.10 (to be defined further in Section 6.1.5) and denote its representation in $L_2(\mathbb{R}^+)$ under the isomorphism given in (63) as $\{\phi_k\}$.

Theorem 4.2.4 provides a frame that is a set of translated and windowed frame elements from a frame or set of frames. Using the frame $\{\phi_k\}$ as the basis for this frame, we have a frame $\{\phi_{j,k}\}$, where the index j represents the j th translation.

Theorem 4.3.1 requires a set of subspaces $\{V_j\}$ for its use. Defining the subspaces V_j according to

$$V_j = \overline{\text{span}\{\phi_{j,k}\}_k},$$

we are poised to find representations in the frame $\{\phi_{j,k}\}$.

The next step is to examine how representations in this composite frame may be found. This will be done by using Theorem 4.3.1, which gives a generalization of the frame operator based on subspaces; Theorem 4.1.4, which gives a representation of projections onto subspaces; and Theorem 4.3.4, which gives an iterative solution for the desired representation in the generalized frame.

To do this, we must first define the projection operators P_{V_j} . Given that the set $\{\phi_{j,k}\}_k$ is a frame for the subspace V_j , Theorem 4.1.4 allows us to define the projection operator P_{V_j} by the frame expansion. That is, we define P_{V_j} by

$$P_{V_j}f = \sum_k \langle f, \tilde{\phi}_{j,k} \rangle \phi_{j,k},$$

where $\{\tilde{\phi}_{j,k}\}_k$ is the dual frame to $\{\phi_{j,k}\}_k$ in the subspace V_j .

Given a representation for the projection operators P_{V_j} , Theorem 4.3.4 provides an iterative solution for a representation of elements $f \in \mathcal{H}$, where $\mathcal{H} = \sum_j V_j$ and the subspaces V_j are not necessarily orthogonal. Approximations to f can be found by truncating the representation at some finite N .

6.1.4 Estimates for the bounds A and B . As shown in Theorem 4.3.4, the values of the true frame bounds A and B are not necessary in order for the iterative method of inverting the operator F (given in Theorem 4.3.4) to converge. For example, any B' where $B \leq B' < \infty$ will work in place of B and any A' where $0 < A' \leq B'$ will work in place

of A . However, faster convergence can be achieved by using good estimates A' and B' for bounds A and B , provided $0 < A' \leq A \leq B \leq B' < \infty$ can be shown to be true.

The following lemma will be useful in the proof of Theorem 6.1.3, which determines a good estimate of B . It determines an upper bound on the number of intervals $[t_n, t_n + I_n) \subset \mathbb{R}$ that can contain any point $t \in \mathbb{R}$, given constraints on the magnitude of the $\{I_n\}$ and on the spacing of the points $\{t_n\}$.

Lemma 6.1.2 *Let ϵ , δ , $\{t_n\}$, and $\{I_n\}$ be as in Theorem 4.2.4. Assume that there exists $0 < M < \infty$ such that $I_n \leq M$ for each $n \in \mathbb{Z}$. Define $X: \mathbb{R} \rightarrow \mathbb{Z}^+$ according to*

$$X(t) = \sum_n \mathbf{1}_{[t_n, t_n + I_n)}(t)$$

where $\mathbf{1}_I$ is the characteristic function over the interval I . Then $X(t) \leq \lceil \frac{M}{\epsilon} \rceil$ for all $t \in \mathbb{R}$, where $\lceil \cdot \rceil$ represents the least integer upper bound.

Proof. From the conditions of Theorem 4.2.4, we have $k\epsilon \leq t_{n+k} - t_n$ for every $k \in \mathbb{Z}^+$ and for all n . Choose $k = \lceil \frac{M}{\epsilon} \rceil$. Then $t_{n+k} - t_n \geq \epsilon \lceil \frac{M}{\epsilon} \rceil \geq M \geq I_n$. This implies that $[t_n, t_n + I_n)$ and $[t_{n+k}, t_{n+k} + I_{n+k})$ are disjoint. That is, any point $t \in \mathbb{R}$ can be contained in at most $\lceil \frac{M}{\epsilon} \rceil$ intervals, and so $X(t) \leq \lceil \frac{M}{\epsilon} \rceil$ for every $t \in \mathbb{R}$. \square

The following theorem will show that the quantity $\lceil \frac{M}{\epsilon} \rceil$ in the above lemma can be used to determine an upper bound on the quantity B in Theorem 4.3.1.

Theorem 6.1.3 *Let ϵ , $\{I_n\}$, and $\{\phi_{n,k}\}$ be as described in Theorem 4.2.4. For each j , define $V_j = \text{span}_k \{\phi_{j,k}\}$. Assume that for $0 < M < \infty$, that $I_n \leq M$ for each n . Let $\{c_j\} \subset \mathbb{R}^+$ and assume that $c_j \leq C < \infty$ for each j . Define the operator $F: L_2(\mathbb{R}) \rightarrow L_2(\mathbb{R})$ as in Theorem 4.3.1, by*

$$Ff = \sum_j c_j P_{V_j} f.$$

Then, for each $f \in L_2(\mathbb{R})$,

$$\sum_j c_j \|P_{V_j} f\|^2 \leq CM_\epsilon \|f\|^2,$$

where $M_\epsilon \doteq \lceil \frac{M}{\epsilon} \rceil$.

Proof. First, we know by Lemma 6.1.2, that there are at most M_ϵ intervals $[t_n, t_n + I_n)$ intervals which contain any point $t \in \mathbb{R}$. This gives that for each $m = 1, \dots, M_\epsilon$, the elements of the set $\{V_{m+kM_\epsilon}\}_{k \in \mathbb{Z}}$ are orthogonal subspaces, since the corresponding intervals on which they are defined are pairwise disjoint. Denote $W_m = \bigoplus_k V_{m+kM_\epsilon}$; we have that for each $f \in \mathcal{H}$, that

$$\begin{aligned} \|P_{W_m} f\|^2 &= \left\| \sum_k P_{V_{m+kM_\epsilon}} f \right\|^2 \\ &= \sum_k \|P_{V_{m+kM_\epsilon}} f\|^2. \end{aligned}$$

Using this, we find that

$$\begin{aligned} \sum_j c_j \|P_{V_j} f\|^2 &\leq C \sum_j \|P_{V_j} f\|^2 \\ &= C \sum_{m=1}^{M_\epsilon} \sum_{k \in \mathbb{Z}} \|P_{V_{m+kM_\epsilon}} f\|^2 \\ &= C \sum_{m=1}^{M_\epsilon} \left\| \sum_{k \in \mathbb{Z}} P_{V_{m+kM_\epsilon}} f \right\|^2 \\ &= C \sum_{m=1}^{M_\epsilon} \|P_{W_m} f\|^2 \\ &\leq C \sum_{m=1}^{M_\epsilon} \|f\|^2 \\ &= CM_\epsilon \|f\|^2. \end{aligned}$$

□

6.1.5 Frames from $H_2(\mathbb{D})$. Given the frame described in words in Section 6.1.3, it is still necessary to define the frames for $H_2(\mathbb{D})$ to be used in its construction. These will be formed in accordance with Theorem 3.1.4 with the sets S_n defined by

$$\begin{aligned} S_n = & \left\{ z \in \mathbb{C}^+ : z = \frac{1 - (x_n + iy)}{1 + (x_n + iy)}, -y_{max} \leq y \leq y_{max} \right\} \\ & \cup \left\{ z \in \mathbb{C}^+ : z = e^{i\theta} \left| \frac{1 - (x_n + iy_{max})}{1 + (x_n + iy_{max})} \right|, |\theta| > \arg \left(\frac{1 - (x_n + iy_{max})}{1 + (x_n + iy_{max})} \right) \right\} \quad (64) \end{aligned}$$

where $x_n \rightarrow 0^+$ and $0 \leq y_{max} < \infty$.

It is necessary to show that these curves indeed satisfy the constraints of Theorem 3.1.4. The following lemma will be of use.

Lemma 6.1.4 *Fix $x > 0$ and $\Delta y \in \mathbb{R}$. Then, for every $y \in \mathbb{R}$,*

$$\begin{aligned} \rho \left(\left(\frac{1 - (x + iy)}{1 + (x + iy)} \right), \left(\frac{1 - (x + i(y + \Delta y))}{1 + (x + i(y + \Delta y))} \right) \right) &= \rho \left(\left(\frac{1 - x}{1 + x} \right), \left(\frac{1 - (x + i\Delta y)}{1 + (x + i\Delta y)} \right) \right) \\ &= \left| \frac{\Delta y}{2x - i\Delta y} \right|. \end{aligned}$$

Proof. By the definition of ρ ,

$$\begin{aligned} &\rho \left(\left(\frac{1 - (x + iy)}{1 + (x + iy)} \right), \left(\frac{1 - (x + i(y + \Delta y))}{1 + (x + i(y + \Delta y))} \right) \right) \\ &= \left| \frac{\left(\frac{1 - (x + iy)}{1 + (x + iy)} \right) - \left(\frac{1 - (x + i(y + \Delta y))}{1 + (x + i(y + \Delta y))} \right)}{1 - \left(\frac{1 - (x + iy)}{1 + (x + iy)} \right) \left(\frac{1 - (x + i(y + \Delta y))}{1 + (x + i(y + \Delta y))} \right)} \right| \\ &= \left| \frac{(1 - (x + iy))(1 + (x + i(y + \Delta y))) - (1 - (x + i(y + \Delta y)))(1 + (x + iy))}{(1 + (x + iy))(1 + (x + i(y + \Delta y))) - (1 - (x + i(y + \Delta y)))(1 - (x + iy))} \right| \\ &= \left| \frac{\Delta y}{2x - i\Delta y} \right| \\ &= \rho \left(\left(\frac{1 - x}{1 + x} \right), \left(\frac{1 - (x + i\Delta y)}{1 + (x + i\Delta y)} \right) \right). \end{aligned}$$

□

The following theorem will show that the sets S_n defined in (64) are suitable for use with Theorem 3.1.4.

Theorem 6.1.5 *The sets S_n , defined in (64), satisfy Condition A with*

$$\limsup_{n \rightarrow \infty} \frac{\overline{M_n} - \underline{r_n}}{1 - \overline{M_n} \underline{r_n}} \leq \frac{y_{max}^2}{2 + y_{max}^2} < 1.$$

Proof. Given the restrictions of Condition A, by inspection of (64) it can be seen that

$$\underline{r_n} = \frac{1 - x_n}{1 + x_n} \tag{65}$$

and

$$\overline{M_n} = \left| \frac{1 - (x + iy_{max})}{1 + (x + iy_{max})} \right|. \quad (66)$$

Also by inspection, it can be seen that $x_n \rightarrow 0$ implies $\underline{r_n} \rightarrow 1$.

To show that $r_n \xrightarrow{u} 1$, note that $\underline{r_n} \leq r_n(\theta)$ for all $\theta \in [-\pi, \pi)$. Therefore, since $\underline{r_n} \rightarrow 1$ and $r_n(\theta) < 1$ for all n and $\theta \in [-\pi, \pi)$, we have $r_n \xrightarrow{u} 1$.

To see that $\limsup_{n \rightarrow \infty} \frac{\overline{M_n} - r_n}{1 - \overline{M_n} \underline{r_n}} \leq \frac{y_{max}^2}{2 + y_{max}^2}$, we use the values of $\overline{M_n}$ and $\underline{r_n}$ in (65) and (66) to get

$$\begin{aligned} \frac{\overline{M_n} - r_n}{1 - \overline{M_n} \underline{r_n}} &= \frac{\left| \frac{1 - (x_n + iy_{max})}{1 + (x_n + iy_{max})} \right| - \left(\frac{1 - x_n}{1 + x_n} \right)}{1 - \left| \frac{1 - (x_n + iy_{max})}{1 + (x_n + iy_{max})} \right| \left(\frac{1 - x_n}{1 + x_n} \right)} \\ &= \frac{(1 + x_n)|1 - (x_n + iy_{max})| - (1 - x_n)|1 + (x_n + iy_{max})|}{(1 + x_n)|1 + (x_n + iy_{max})| - (1 - x_n)|1 - (x_n + iy_{max})|} \\ &= \frac{\sqrt{1 - 2x_n^2 + 2y_{max}^2 + x_n^4 + 2x_n^2 y_{max}^2 + y_{max}^4} - (1 - x_n^2)}{2 + 2x_n^2 + y_{max}^2} \\ &\leq \frac{\sqrt{1 + 2x_n^2 + 2y_{max}^2 + x_n^4 + 2x_n^2 y_{max}^2 + y_{max}^4} - (1 - x_n^2)}{2 + 2x_n^2 + y_{max}^2} \\ &= \frac{(1 + x_n^2 + y_{max}^2) - (1 - x_n^2)}{2 + 2x_n^2 + y_{max}^2} \\ &= \frac{2x_n^2 + y_{max}^2}{2 + 2x_n^2 + y_{max}^2}. \end{aligned}$$

Therefore,

$$\begin{aligned} \limsup_{n \rightarrow \infty} \frac{\overline{M_n} - r_n}{1 - \overline{M_n} \underline{r_n}} &\leq \lim_{n \rightarrow \infty} \frac{2x_n^2 + y_{max}^2}{2 + 2x_n^2 + y_{max}^2} \\ &= \frac{y_{max}^2}{2 + y_{max}^2} < 1. \end{aligned}$$

To show that $\frac{\overline{M_n} - r_n}{1 - \overline{M_n} \underline{r_n}} \xrightarrow{u} 0$ as $n \rightarrow \infty$, first note that we need only be concerned with the region of the set given by $z = \frac{1 - (x_n + iy)}{1 + (x_n + iy)}$, $0 \leq y \leq y_{max}$, since S_n is symmetric and since the region of the set outside that given by $-y_{max} \leq y \leq y_{max}$ is simply a segment of a circle centered on the origin, for which $\frac{\overline{M_n} - r_n}{1 - \overline{M_n} \underline{r_n}}$ is identically zero. Note that for the remainder of the proof, the notation $\left[\frac{\overline{M_n} - r_n}{1 - \overline{M_n} \underline{r_n}} \right](\cdot)$ denotes $\frac{M_n(\cdot) - r_n(\cdot)}{1 - M_n(\cdot) \underline{r_n}(\cdot)}$. This is done for convenience in handling complicated arguments to the function $\frac{\overline{M_n} - r_n}{1 - \overline{M_n} \underline{r_n}}$.

Solving for y_ϵ such that $y_\epsilon > 0$ and $\rho(\frac{1-(x+iy)}{1+(x+iy)}, \frac{1-(x+i(y+y_\epsilon))}{1+(x+i(y+y_\epsilon))}) = \epsilon$, we have from Lemma 6.1.4 that

$$\epsilon = \left| \frac{y_\epsilon}{2x - iy_\epsilon} \right|,$$

which gives

$$y_\epsilon = \frac{2x\epsilon}{\sqrt{1-\epsilon^2}}.$$

Defining $\Delta y_n = y_\epsilon = \frac{2x_n\epsilon}{\sqrt{1-\epsilon^2}}$, we may determine the values of r_n and M_n evaluated at various points. By the nature of the sets S_n , for $\Delta y_n \leq y \leq y_{max}$,

$$r_n \left(\arg \left(\frac{1 - (x_n + iy)}{1 + (x_n + iy)} \right) \right) = \left| \frac{1 - (x_n + i(y - \Delta y_n))}{1 + (x_n + i(y - \Delta y_n))} \right| \quad (67)$$

and for $0 \leq y \leq \Delta y_n$,

$$r_n \left(\arg \left(\frac{1 - (x_n + iy)}{1 + (x_n + iy)} \right) \right) = \left| \frac{1 - x_n}{1 + x_n} \right|.$$

Likewise, for $0 \leq y \leq y_{max} - \Delta y_n$,

$$M_n \left(\arg \left(\frac{1 - (x_n + iy)}{1 + (x_n + iy)} \right) \right) = \left| \frac{1 - (x_n + i(y + \Delta y_n))}{1 + (x_n + i(y + \Delta y_n))} \right| \quad (68)$$

and for $y_{max} - \Delta y_n \leq y \leq y_{max}$,

$$M_n \left(\arg \left(\frac{1 - (x_n + iy_{max})}{1 + (x_n + iy_{max})} \right) \right) = \left| \frac{1 - (x_n + iy_{max})}{1 + (x_n + iy_{max})} \right|.$$

Examining the nature of the sets S_n in (64), we note that for $y_{max} - \Delta y_n < y \leq y_{max}$, we have

$$\left[\frac{M_n - r_n}{1 - M_n r_n} \right] \left(\arg \left(\frac{1 - (x_n + iy)}{1 + (x_n + iy)} \right) \right) \leq \left[\frac{M_n - r_n}{1 - M_n r_n} \right] \left(\arg \left(\frac{1 - (x_n + i(y_{max} - \Delta y_n))}{1 + (x_n + i(y_{max} - \Delta y_n))} \right) \right)$$

and for $0 \leq y \leq \Delta y_n$ we have

$$\left[\frac{M_n - r_n}{1 - M_n r_n} \right] \left(\arg \left(\frac{1 - (x_n + iy)}{1 + (x_n + iy)} \right) \right) \leq \left[\frac{M_n - r_n}{1 - M_n r_n} \right] \left(\arg \left(\frac{1 - (x_n + i\Delta y_n)}{1 + (x_n + i\Delta y_n)} \right) \right),$$

we need only consider the case of $\Delta y_n \leq y \leq y_{max} - \Delta y_n$. Evaluating $\frac{M_n - r_n}{1 - M_n r_n}$ at values in this range, using (67) and (68), we see that

$$\begin{aligned}
& \left[\frac{M_n - r_n}{1 - M_n r_n} \right] \left(\arg \left(\frac{1 - (x_n + iy)}{1 + (x_n + iy)} \right) \right) \\
&= \frac{\left| \frac{1 - (x_n + i(y + \Delta y_n))}{1 + (x_n + i(y + \Delta y_n))} \right| - \left| \frac{1 - (x_n + i(y - \Delta y_n))}{1 + (x_n + i(y - \Delta y_n))} \right|}{1 - \left| \frac{1 - (x_n + i(y + \Delta y_n))}{1 + (x_n + i(y + \Delta y_n))} \right| \left| \frac{1 - (x_n + i(y - \Delta y_n))}{1 + (x_n + i(y - \Delta y_n))} \right|} \\
&= \frac{\left(\sqrt{(1 - x_n^2 + (y + \Delta y_n)^2)^2 + 4x_n^2(y + \Delta y_n)^2} - \sqrt{(1 - x_n^2 + (y - \Delta y_n)^2)^2 + 4x_n^2(y - \Delta y_n)^2} \right) / (2(1 + x_n^2 + y^2 + (\Delta y_n)^2))}{\sqrt{(1 - x_n^2 + (y + \Delta y_n)^2)^2 + 4x_n^2 + 4x_n^2(y + \Delta y_n)^2} - \sqrt{(1 - x_n^2 + (y - \Delta y_n)^2)^2 + 4x_n^2}} \\
&\leq \frac{x_n^2 + 2y\Delta y_n}{1 + x_n^2 + y^2 + (\Delta y_n)^2} \\
&\leq x_n^2 + 2y_{max}\Delta y_n \\
&= x_n^2 + \frac{4x_n y_{max} \epsilon}{\sqrt{1 - \epsilon^2}} \\
&= x_n \left(x_n + \frac{4y_{max} \epsilon}{\sqrt{1 - \epsilon^2}} \right).
\end{aligned}$$

Since

$$\lim_{n \rightarrow \infty} x_n \left(x_n + \frac{4y_{max} \epsilon}{\sqrt{1 - \epsilon^2}} \right) = 0,$$

this gives that $\frac{M_n - r_n}{1 - M_n r_n} \xrightarrow{u} 0$ as $n \rightarrow \infty$. □

6.2 Using the frame

At this point, it is necessary to look at the requirements to actually use the frame designed in Section 6.1.3. One of the main issues is how to work with sampled data when all of the theory dealt with functions defined on a continuum. Other issues include finding the dual frame coefficients necessary to define the projection operators, P_{V_j} , required for representation in this frame. Also, the points $a_{n,k}$ to be used from the sets S_n must be discussed.

6.2.1 Function represented by the sampled data. All of the theory presented so far is appropriate for functions defined almost everywhere on a continuum. However, the speech we wish to work with is known only through sampled values. To use the theory, therefore, we must first determine what function we wish the sampled data to represent. Since the Laplace transform also plays an important part in the transform between $L_2(\mathbb{R}^+)$ and $H_2(\mathbb{D})$, the chosen form should also be easy to transform analytically.

Step functions will be used here. In particular, the speech represented by the sampled data will be assumed to be a step function with the sampled values being the height of evenly spaced steps. Clearly, this is not what speech really is. However, this representation (as will be seen) is very easy to handle analytically, making it desirable in this context.

The following theorem gives the Laplace transform of a function of this form at certain convenient sample points. Use is made of the Discrete Fourier Transform, the definition of which follows.

Definition 6.2.1 Fix $\Delta t \in \mathbb{R}^+$ and $N \in 2\mathbb{Z}^+$ and define $\Delta\omega \doteq \frac{2\pi}{\Delta t}$. Let $\mathbf{x} = \{x_m\}_{m=0}^{N-1} \subset \mathbb{C}$. The Discrete Fourier Transform, DFT: $\ell_2(N) \rightarrow \ell_2(N)$, of \mathbf{x} is given by

$$\text{DFT}[\mathbf{x}](k) = \sum_{m=0}^{N-1} x_m e^{-ik\Delta\omega m\Delta t}. \quad (69)$$

Theorem 6.2.2 Fix $\Delta t, \alpha \in \mathbb{R}^+$, $N \in 2\mathbb{Z}^+$. Let $f \in L_2(\mathbb{R}^+)$ be given by

$$f(t) = \sum_{m=0}^{N-1} f(m\Delta t) \mathbf{1}_{[m\Delta t, (m+1)\Delta t)}(t)$$

and $W \in L_2(\mathbb{R}^+)$ by

$$W(t) = e^{-\alpha t} \mathbf{1}_{[0, N\Delta t)}(t). \quad (70)$$

Then, for $\Delta\omega \doteq \frac{2\pi}{\Delta t}$, $k \in \{\frac{-N}{2}, \dots, -1, 0, 1, \dots, \frac{N}{2}\}$, and $\sigma \in \mathbb{R}$, we have

$$\mathcal{L}[Wf](\sigma + ik\Delta\omega) = \frac{(1 - e^{-(\alpha + \sigma + ik\Delta\omega)\Delta t})}{\sqrt{2\pi}(\alpha + \sigma + ik\Delta\omega)} \text{DFT} \left[\{f(m\Delta t) e^{-(\alpha + \sigma)m\Delta t}\}_{m=0}^{N-1} \right] (k)$$

where DFT is as defined in (69).

Proof. First, considering the transform of a single, windowed step, we have

$$\begin{aligned}
\mathcal{L}[e^{-\alpha t} \mathbf{1}_{[m\Delta t, (m+1)\Delta t)}](s) &= \frac{1}{\sqrt{2\pi}} \int_0^\infty e^{-\alpha t} \mathbf{1}_{[m\Delta t, (m+1)\Delta t)}(t) e^{-st} dt \\
&= \frac{1}{\sqrt{2\pi}} \int_{m\Delta t}^{(m+1)\Delta t} e^{-(s+\alpha)t} dt \\
&= \frac{1}{\sqrt{2\pi}(s+\alpha)} (e^{-(s+\alpha)m\Delta t} - e^{-(s+\alpha)(m+1)\Delta t}) \\
&= \frac{(1 - e^{-(s+\alpha)\Delta t})}{\sqrt{2\pi}(s+\alpha)} e^{-(s+\alpha)m\Delta t}.
\end{aligned}$$

This gives

$$\mathcal{L}[Wf](s) = \frac{(1 - e^{-(s+\alpha)\Delta t})}{\sqrt{2\pi}(s+\alpha)} \sum_{m=0}^{N-1} f(m\Delta t) e^{-(s+\alpha)m\Delta t}.$$

Letting $s = \sigma + ik\Delta\omega$, we have

$$\begin{aligned}
\mathcal{L}[Wf](\sigma + ik\Delta\omega) &= \frac{(1 - e^{-(\alpha + \sigma + ik\Delta\omega)\Delta t})}{\sqrt{2\pi}(\alpha + \sigma + ik\Delta\omega)} \sum_{m=0}^{N-1} f(m\Delta t) e^{-(\alpha + \sigma)m\Delta t} e^{-ik\Delta\omega m\Delta t} \\
&= \frac{(1 - e^{-(\alpha + \sigma + ik\Delta\omega)\Delta t})}{\sqrt{2\pi}(\alpha + \sigma + ik\Delta\omega)} \text{DFT} \left[\{f(m\Delta t) e^{-(\alpha + \sigma)m\Delta t}\}_{m=0}^{N-1} \right] (k).
\end{aligned}$$

□

Note that in the Theorem 6.2.2, we have represented the Laplace transform at certain sample points in the complex plane in terms of a DFT of the function's sampled values scaled by decaying exponentials. Despite the use of the DFT and the sampled data, this expression yields *exact* values of the Laplace transform of a function of the assumed form at the sample points $\sigma + i\Delta\omega k$ for $k = -\frac{N}{2}, \dots, \frac{N}{2}$.

6.2.2 Dual frame to a windowed frame. We are given a frame, $\{\psi_k\}_{k=1}^N$, and are working with the set of windowed frame elements $\{\phi_k\}_{k=1}^N = \{W\psi_k\}_{k=1}^N$, also a frame, where W is given by (70). We wish to know the dual $\{\tilde{\phi}_k\}_{k=1}^N$ to this new frame. Unfortunately, the dual frame of a windowed frame is not (necessarily) the same as the windowed dual frame, although in many cases, it may be close. The following theorem will be useful in determining the actual dual frame.

Theorem 6.2.3 *Let the finite set $\{\psi_k\}_{k=1}^N$ be an exact frame in some Hilbert space. Then the dual frame $\{\tilde{\psi}_k\}_{k=1}^N$ is given by*

$$\tilde{\psi}_k = \sum_{j=1}^n c_{k,j} \psi_j$$

where

$$[A^{-1}]_{k,j} = c_{k,j}$$

and the matrix A is given by

$$[A]_{k,j} = \langle \psi_k, \psi_j \rangle .$$

Proof. The dual frame, always being in the span of the frame elements, can be expressed by

$$\tilde{\psi}_k = \sum_{j=1}^n c_{k,j} \psi_j .$$

Since this frame is exact, we have by Theorem 4.1.3 that

$$\langle \tilde{\psi}_k, \psi_m \rangle = \delta_{k,m} .$$

That is

$$\sum_{j=1}^N c_{k,j} \langle \psi_j, \psi_m \rangle = \delta_{k,m} .$$

This gives

$$I = CA ,$$

where $[C]_{k,j} = c_{k,j}$, which implies that $C = A^{-1}$. That is, $[A^{-1}]_{k,j} = c_{k,j}$. □

In order to use Theorem 6.2.3, it will be necessary to determine the inner product of windowed frame elements. This is easily done (as will be seen) in the $L_2(\mathbb{R}^+)$ space. For

this reason (among others), it is necessary to find the representation in the $L_2(\mathbb{R}^2)$ space for the simple pole functions used in the representations in $H_2(\mathbb{D})$. The following theorem gives that representation.

Lemma 6.2.4 *For a pole of the form*

$$\psi(z) = \frac{(1 - |a|^2)^{1/2}}{(1 - \bar{a}z)}$$

where $|a| < 1$, $T^{-1}\psi$ is given by

$$T^{-1}\psi(t) = \frac{\sqrt{2}(1 - |a|^2)^{1/2}}{(1 + \bar{a})} e^{-(\frac{1-\bar{a}}{1+\bar{a}})t} \quad (71)$$

where T is as defined in (63).

Proof. Since $T^{-1} = \mathcal{L}^{-1}S^{-1}$, we will first look at $S^{-1}\psi$, as defined by (60).

$$\begin{aligned} S^{-1}\psi(s) &= \frac{\psi\left(\frac{1-s}{1+s}\right)}{\sqrt{\pi}(1+s)} \\ &= \frac{\frac{(1-|a|^2)^{1/2}}{(1-\bar{a}(\frac{1-s}{1+s}))}}{\sqrt{\pi}(1+s)} \\ &= \frac{(1 - |a|^2)^{1/2}}{\sqrt{\pi}((1+s) - \bar{a}(1-s))} \\ &= \frac{(1 - |a|^2)^{1/2}}{\sqrt{\pi}((1-\bar{a}) + s(1+\bar{a}))} \\ &= \frac{(1 - |a|^2)^{1/2}}{\sqrt{\pi}(1+\bar{a})(s + (\frac{1-\bar{a}}{1+\bar{a}}))}. \end{aligned}$$

Applying the inverse Laplace transform operator, defined in (62), to this result, we get

$$\begin{aligned} T^{-1}\psi(t) &= \mathcal{L}^{-1}S^{-1}\psi(t) = \frac{1}{i\sqrt{2\pi}} \int_C S^{-1}\psi(s) e^{st} ds \\ &= \frac{1}{i\sqrt{2\pi}} \int_C \frac{(1 - |a|^2)^{1/2}}{\sqrt{\pi}(1+\bar{a})(s + (\frac{1-\bar{a}}{1+\bar{a}}))} e^{st} ds \\ &= \frac{\sqrt{2}(1 - |a|^2)^{1/2}}{(1 + \bar{a})} e^{-(\frac{1-\bar{a}}{1+\bar{a}})t}. \end{aligned}$$

□

6.2.3 Inner products with windowed frame elements. In practice, we will be required to find the inner product with the windowed frame elements. Note that for real-valued windowing functions, $W \in L_2(\mathbb{R})$, we get $\langle f, Wg \rangle = \langle Wf, g \rangle$ for all $f, g \in L_2(\mathbb{R})$. For our purposes, one implication of this is that the window may be applied to the data rather than to the frame element. For our frame elements $\{\psi_{n,k}\}$, we have $\langle g, \psi_{n,k} \rangle = (1 - |a_{n,k}|^2)^{1/2} g(a_{n,k})$ for $g \in H_2(\mathbb{D})$; that is, the inner product with one of our frame elements samples the value of the function at the sample point $a_{n,k}$. By Theorem 6.2.2, (59), and (63), we have exact values for $TWf \in H_2(\mathbb{D})$ at certain sample points, which makes this theorem very useful provided the points $\{a_{n,k}\}$ include those sample points.

6.2.4 Representation of frame elements, $\psi_n B_n$. Much of the theoretical work dealt with frame elements $\psi_n B_n$ of the form

$$\psi_n(z) = \frac{(1 - |a_n|^2)^{1/2}}{(1 - \overline{a_n}z)} \quad (72)$$

and

$$B_n(z) = \prod_{k=1}^{n-1} \frac{(a_k - z)}{(1 - \overline{a_k}z)}. \quad (73)$$

As shown in Chapter V, $\psi_n B_n \in \text{span}\{\psi_k\}_{k=1}^n$. For practical (i.e., computer) applications, it is desirable to use the expression $\psi_n B_n = \sum_{k=1}^n c_k \psi_k$. The following lemma gives the values of the constants c_k in that representation.

Lemma 6.2.5 *For ψ_n and B_n as in (72) and (73), with $a_n \neq a_k$ for all $n \neq k$, we have*

$$\psi_n B_n = \sum_{k=1}^n b_k \psi_k$$

where

$$b_n = \prod_{j=1}^{n-1} \frac{(1 - \overline{a_n}a_j)}{(\overline{a_j} - \overline{a_n})}$$

and where for $k = 1, \dots, n-1$,

$$b_k = \frac{(1 - |a_n|^2)^{1/2}(1 - |a_k|^2)^{1/2}}{(1 - \overline{a_k}a_n)} \prod_{j=1, j \neq k}^n \frac{(1 - \overline{a_k}a_j)}{(\overline{a_j} - \overline{a_k})}.$$

Proof. This proof is strictly algebraic in nature. Since $a_n \neq a_k$ for all $n \neq k$, we have that $\psi_n B_n$ can be expanded according to

$$\psi_n B_n = \frac{(1 - |a_n|^2)^{1/2}}{(1 - \bar{a}_n z)} \prod_{j=1}^{n-1} \frac{(a_j - z)}{(1 - \bar{a}_j z)} = \sum_{j=1}^n b_j \frac{(1 - |a_j|^2)^{1/2}}{(1 - \bar{a}_j z)} = \sum_{j=1}^n b_j \psi_j .$$

Multiplying both sides by the quantity $(1 - \bar{a}_n z)$, we have

$$(1 - |a_n|^2)^{1/2} \prod_{j=1}^{n-1} \frac{(a_j - z)}{(1 - \bar{a}_j z)} = b_n (1 - |a_n|^2)^{1/2} + (1 - \bar{a}_n z) \sum_{j=1}^{n-1} b_j \psi_j .$$

Evaluating this expression at $z = \frac{a_n}{|a_n|^2}$, this gives

$$\begin{aligned} b_n &= \prod_{j=1}^{n-1} \frac{(a_j - \frac{a_n}{|a_n|^2})}{(1 - \bar{a}_j \frac{a_n}{|a_n|^2})} \\ &= \prod_{j=1}^{n-1} \frac{(1 - a_j \bar{a}_n)}{(\bar{a}_j - \bar{a}_n)} . \end{aligned}$$

The same technique can be used to show the value of b_k for $k = 1, \dots, n-1$. □

6.2.5 Choice of points $\{a_{n,k}\}$. As mentioned previously, the set of points $\{a_{n,k}\}$, used in (54) and (55) to define our frame, should include the set $\{x_n + i\Delta\omega k\}_{k=-\frac{N}{2}}^{\frac{N}{2}}$ for each chosen x_n , under the mapping $z \mapsto \frac{1-z}{1+z}$. By Lemma 6.1.4, we know that for each x_n , these points are evenly spaced under the pseudo-hyperbolic metric, ρ . Therefore, it is necessary to add to this set only enough points so that the separation requirements of Theorem 3.1.4 are met.

6.3 The computer program

The design of a computer program based on the frame developed in Section 6.1 is discussed. Designing this application program involved making additional assumptions and simplifications. The main points of interest pertaining to the points of correspondence between theory and application are described below. Brief summaries of some of the heuristics employed are given also.

The main simplification of concern is the choice of basis functions. The sets chosen by this application are a subset of those required by Theorem 3.6.4. This is not necessarily

unreasonable for this application, however, since only a small number of basis elements are to be retained in any case. The choice of basis elements is discussed below, followed by discussions of other heuristics and approximations. Taken as a whole, the remainder of this section presents a very rough sketch of the design of the program.

6.3.1 Basis set selection. As seen in Section 6.1, for each offset time used in the creation of the frame, a frame for $L_2(\mathbb{R})$ is required. For this application, it was decided to use the same frame for each offset time, regardless of the underlying data to be represented. This frame is of the form given in Theorem 5.2.10.

As shown in Lemma 3.6.3, for our choice of basis functions, $\psi_{n,k}$, we know that $\langle f, \psi_{n,k} \rangle = (1 - |a_{n,k}|)^{1/2} f(a_{n,k})$. That is, the basis function *samples* the function at the *sample point* $a_{n,k}$. Theorem 3.1.4 gives the constraints under which the sample points are chosen.

Section 6.1.5 gives curves S_n from which the sample points are to be chosen. However, to find the sampled values at arbitrary points of these curves is computationally expensive. So, computationally tractable subsets of these curves, based on the calculations shown in Theorem 6.2.2, are used instead. The computationally tractable subsets used by the program consist of points along a horizontal segment in the complex plane, for which the sample values can be easily computed (given Theorem 6.2.2). These points are mapped via the mapping $z \mapsto \frac{1-z}{1+z}$ onto the right-half of curves of the form S_n described in Section 6.1.5. Depending on the settings of the program, the left-half of the curve can either be ignored or filled-in with points generated by other horizontal segments.

6.3.2 Determination of offset times and analysis window sizes. There are two methods by which this program can determine the offset times and sizes of the analysis windows; data-dependent and data-independent. In either case, the maximum analysis window size is specified.

In the data-independent method, the analysis windows are evenly spaced in time. The desired number of analysis windows to overlap each data point, n is used to determine the analysis window size, with the size being determined as the largest multiple of n not greater than the maximum analysis window size. One window starts at the first sample data point, which determines the offset times of the remaining windows. Enough analysis windows are generated so that each sample data point is included in n analysis windows.

In the data-dependent method, the program uses a heuristic algorithm (described in Appendix C) to estimate where glottal pulses begin and places analysis windows starting

at those locations. An additional window is added which starts at the first data point. Following this, additional windows (if necessary) are placed to ensure that every data point is contained in at least n analysis windows. Finally, the lengths of the analysis windows are determined such that every data point is contained in exactly n analysis windows. This results in analysis windows which are of varying lengths and are unevenly spaced. Potentially, many of these windows are of lengths much less than the maximum analysis window length, depending on the vocal pitch, n , and the maximum analysis window size.

6.3.3 A parameter for internal rescaling. In the representation given in Theorem 3.6.4, a basis is given which requires sets of sample points in the complex unit disk, \mathbb{D} . In the simplest case these sample points are elements of torus-shaped, closed subsets of \mathbb{D} arranged about the origin. With the transform given in (59), the point $s = 1$ is mapped to the origin. That is, the point at the origin corresponds to the decaying exponential e^{-t} . Sample points taken from closed, torus-shaped subsets of \mathbb{D} about the origin correspond to decaying exponentials of both higher and lower decay rates.

Note that in the above, the units of t are not given. If the time units are assumed to be seconds, one sees a much slower decay rate than that observed in the impulse response of the vocal tract. That is, the decay rate seen in a frame element, assuming a time unit of, e.g., seconds, is not necessarily a good match for speech. Because of this, it is desirable to rescale the units so that an exponential of a decay rate more representative of that seen in the impulse response of the vocal tract corresponded to the point at the origin. To do this, an additional variable, *spread*, has been added to the program. This variable corresponds to an internal (to the program) multiplication of the sampling rate.

To summarize, *spread* can be considered as a “knob” to be turned as far as the operation of the program is concerned. Tweaking it is encouraged.

6.3.4 Basis selection. For this application we desire a compact approximation. That is, for a given example of speech, a reasonably close approximation is desired which is built from a reasonably small number of basis elements. This requires some selection criteria for the basis elements.

The method used in the application program is to choose a fixed (user input) number of basis elements for each of the offset times. The selection of basis elements for each time increment is independent of that for the other time increments.

For each offset time, the basis elements to be used are chosen via a heuristic very similar to the orthogonal matching pursuit described in [24]. In the heuristic used here, the

basis elements are chosen iteratively. After each selection, the projection onto the space spanned by the basis elements chosen thus far (for that offset time only) is found. The residual found by subtracting the projection from the original is used in the selection of the next basis element. This selection is based on the magnitudes of the inner products of the candidate basis elements with the signal to be represented, weighted by a factor designed to favor basis elements which are further (in the pseudo-hyperbolic metric) from those already chosen. (There is reason to believe that this selection criteria may yield a perceptually better projection.)

6.3.5 Approximation coefficients. Once the basis elements for the approximation are chosen for each time increment, it is necessary to find the coefficient associated with each one to represent the projection of the signal onto the span of the chosen basis elements. This representation is found using the iterative approximation given in Theorem 4.3.4.

The projections onto the basis elements chosen for each offset time is done via matrix inversions. These results are then used in the iterative algorithm, when the number of iterations used is a user input.

Since the inner product between non-overlapping basis elements is zero, iterating with non-overlapping analysis windows has no effect, in theory, on the inverse frame computation. However, such iteration is sometimes of use in this implementation, to improve numeric accuracy. In certain cases, the matrix inversions are unstable due to the poles being chosen too close together, resulting in a near-singular matrix. In this case, the inverse matrix is approximated by the inverse matrix for the non-windowed basis functions since that inverse is known exactly. This approximate inverse is usually close enough to the true inverse so that iterations of the inverse frame approximation yield a good result.

6.4 Summary

Presented in this chapter was an application of the results of Chapters III, IV, and V. A frame tailored to speech representation in $L_2(\mathbb{R})$ was constructed using frames for $H_2(\mathbb{D})$. The necessary constraints and bounds were proven to enable the use of the iterative method given in Theorem 4.3.4. The design of a computer program which finds representations in such a frame is discussed.

Of particular note, the frame elements of this speech frame have the useful property of sampling the value of the Discrete Fourier Transform of sampled speech signal, allowing for fast calculation of inner products with frame elements. This property is important in

that digitally recorded speech is already sampled, with good interpolation between sample points being problematic.

The approach taken here could be used for other types of functions; it is not restricted to speech. It should prove to be useful in other areas of signal analysis and in the representation of other types of functions, particularly where the characteristics of the function vary with the independent variable.

VII. Computer experiments

In this chapter, the computer experiments will be presented and discussed. Three different types of analyses were done – fine-scale, medium-scale, and large-scale.

In the fine-scale analysis, an in-depth look is taken at the performance of the projection algorithm for a single offset time. This analysis is done for short segments of data (64 data points or fewer), both for segments of speech and segments of non-speech signals of similar frequency content. In addition, the performance of the algorithm on harmonic speech is examined with respect to the location of the start of the glottal pulse within the analysis window.

In the medium-scale analysis, longer data segments are used. For tests involving actual speech, contiguous, harmonic speech is used from a male and a female speaker. A row of data from a digitized image and a reversed segment of harmonic speech are used as non-speech samples for this medium-scale analysis only. These samples are used to test the reconstruction algorithm of Theorem 4.3.4 as well as to examine some of the properties of the representation.

In the large-scale analysis, the algorithm is tested only on two entire sentences, one from a male speaker and one from a female speaker. The data compression possible by using this representation is examined. Additional analysis is done using the same two sentences to which Gaussian white noise has been added, to examine the noise suppression characteristics inherent in the approximation algorithm.

The recorded speech used in these tests is from the TIMIT database. This extensive corpus, a joint effort by several sites sponsored by the Defense Advanced Research Projects Agency - Information Science and Technology Office (DARPA-ISTO), is currently maintained by the National Institute of Standards and Technology (NIST). The TIMIT database contains recordings of 6300 sentences read by speakers from all major dialect regions of this country. It is indexed by a unique speaker identification code and sentence identification code for each entry.

The Arpabet notation was used notationally to identify the phonemes used in analyses on shorter signal lengths. A description of the Arpabet notation can be found in, e.g., [23].

Entropic's Signal Processing System (ESPS), written by the Entropic Research Laboratory, Inc., was used to display and manipulate much of the data used in these analyses.

All analysis on actual speech used two recordings from the TIMIT database. Where shorter segments are needed for testing, they are extracted from these two sentences. The female voice was speaker *fcm0* saying sentence *sa1* (“She had your dark suit in greasy wash water all year.”). The male voice was speaker *mcm0* saying sentence *sx194* (“They enjoy it when I audition.”).

The TIMIT database recordings are digitized at a sample rate of 16 kHz. Since most of the important information in human speech is contained in the frequency range 0-4 kHz, the speech was down-sampled using the function *sfconvert* of ESPS to a sampling rate of 8 kHz for the analysis.

In every case reported, *normalized L_2 error* is the L_2 error normalized by the L_2 norm of the signal. When working with signals to which noise has been added, the L_2 error is normalized by the L_2 norm of the *clean* signal.

7.1 Fine-scale analyses

The purpose of the fine-scale analyses is to examine the performance of representation based on a set of zero offset time exponentially damped sinusoids (simple pole functions), such as given in (71). This relates to the work presented in Chapter III.

The performance of the projection algorithm was examined in two ways. The first analysis compares the performance of the representation algorithm on different signals, some speech and some not speech. The second analysis examines the performance of the projection algorithm for different alignments of one or two glottal pulses within an analysis window.

7.1.1 Description of fine-scale analyses.

7.1.1.1 Performance on different types of signal. The analysis was done with eight signals. The eight signals are described below and are shown in Figure 5.

Three of these signals, the phonemes /IY/, /OY/, and /S/ are actual speech segments consisting of one glottal pulse period of harmonic speech for /IY/ (female speaker) and /OY/ (male speaker) and a segment of similar length for /S/ (female speaker). The segments /IY/ and /OY/ are zero-padded so that each segment would have 64 total data points.

Of the five non-speech signals, four of them (*blocks*, *bumps*, *doppler*, and *heavisine*) were inspired by those in [10]. These test functions have various characteristics, such as

structure, and frequency content, that seemed to be a good test of the method, so they were duplicated for use here. The fifth, *bumpstx*, is the inverse Fourier transform of *bumps*. Each signal contains 64 data points.

Blocks is a sequence of step functions of varying widths and heights. Of the four, it appears (to visual inspection) the least like speech. *Bumps* resembles the magnitude Fourier spectrum of a signal containing several well-defined frequency components. It also bears little resemblance to speech, although it lacks the discontinuities found in *blocks*. *Doppler* is a windowed, chirped, sinusoid. *Heavisine* is a sinusoid added to a step function to form discontinuities. *Bumpstx*, being the inverse Fourier transform of *bumps* is not speech, but has spectral qualities that should be well represented by the representation being tested.

To fairly compare the tests on the different samples, I evaluated the magnitude of their Fourier transforms and rescaled the signals so that the spectrum was concentrated in a range similar to that of speech. I then sampled the signals at the same rate as that for the speech. I used a data window of size similar to that of one glottal pulse. In this way, I hoped to make the comparisons on a more even foundation. The magnitude Fourier transforms of the rescaled, windowed, sampled, signals are shown in Figure 6.

Each signal was approximated using a single analysis window. That is, the approximation is a sum of exponentially damped sinusoids starting at time $t = 0$. The decay rate on the window was zero. Thirty-two poles were used for each approximation. For each signal, we compare the original signal and its approximation for increasing numbers of pole. These results are shown in Figures 7 through 22. The L_2 norm errors between the original signals and the approximations are plotted in Figure 23.

7.1.1.2 Performance for different alignments. This analysis examines the performance of the projection algorithm for different positions of the first glottal pulse within an analysis window; it is intended to show the effects of mis-alignment of the glottal pulse within the analysis window.

A single glottal pulse was repeated to create the analysis data. A periodic shift of the sampled data was used to simulate different positions of the first glottal pulse within a window. Glottal pulses were used from the phonemes /IY/ and /OY/.

Analysis windows of two (data dependent) lengths were examined. In the first case, the analysis window contains one glottal pulse; in the second, two. This resulted in window lengths of 34 and 68 samples, respectively, for the phoneme /IY/ and window lengths of 59 and 118, respectively, for the phoneme /OY/.

The program was used to find the approximation for each offset (shift of the data) and for numbers of poles from one through 20. Table 1 shows the minimum and maximum normalized L_2 errors for the approximation with each number of poles for each phoneme for an analysis window containing one and two glottal pulses. The errors for each offset for approximations with one, two, three, six, nine, and 18 poles are shown in Figures 24 through 27. Figures 24 and 25 show the results for an analysis window containing one glottal pulse for phonemes /IY/ and /OY/, respectively. Figures 26 and 27 show the same for an analysis window containing two glottal pulses.

7.1.2 Discussion of results.

7.1.2.1 Performance on different types of signal. Examining Figures 7 through 10, it can be seen that for harmonic speech (the phonemes /IY/ and /OY/), the approximation appears (a subjective judgement) to become close to the original signal with few poles, both in the time and frequency domains. This is both expected and hoped for, since one pulse cycle of harmonic speech resembles our building blocks of damped sinusoids. The phoneme /S/ (Figures 11 and 12) appears to be less well represented, both in the time and frequency domains. This is also expected, since this phoneme strongly resembles Gaussian white noise, which is not modeled well by such building blocks.

Figure 13 shows clearly some of the weak points of this representation as pertains to representation of non-speech signals, and hence, supporting my hypothesis that the representation is better suited to speech than most non-speech. *Blocks* contains sharp discontinuities and constant portions. While the approximation may appear close in an L_2 norm sense, it has lost many of the characteristics that one might wish to preserve, such as the constant portions of the signal and discontinuity locations. However, Figure 14 shows that the approximation in the frequency domain looks much better – subjectively as good as for the phonemes /IY/ and /OY/ (Figures 8 and 10).

The results for *bumps* are even worse (Figures 15 and 16). While the approximation has large wiggles in the appropriate locations, it takes many more poles to get a reasonable approximation, either in the time or the frequency domain.

The results for *bumpstr* are somewhat better, mainly due to the way that it was constructed – as the inverse Fourier transform of a function with well isolated spikes. As can be seen in Figure 17, the approximation does become visually close in the time domain rather quickly. In Figure 18, it can be seen that successive poles align with different spikes in the transform, behavior that is not always obvious with some of the other signals.

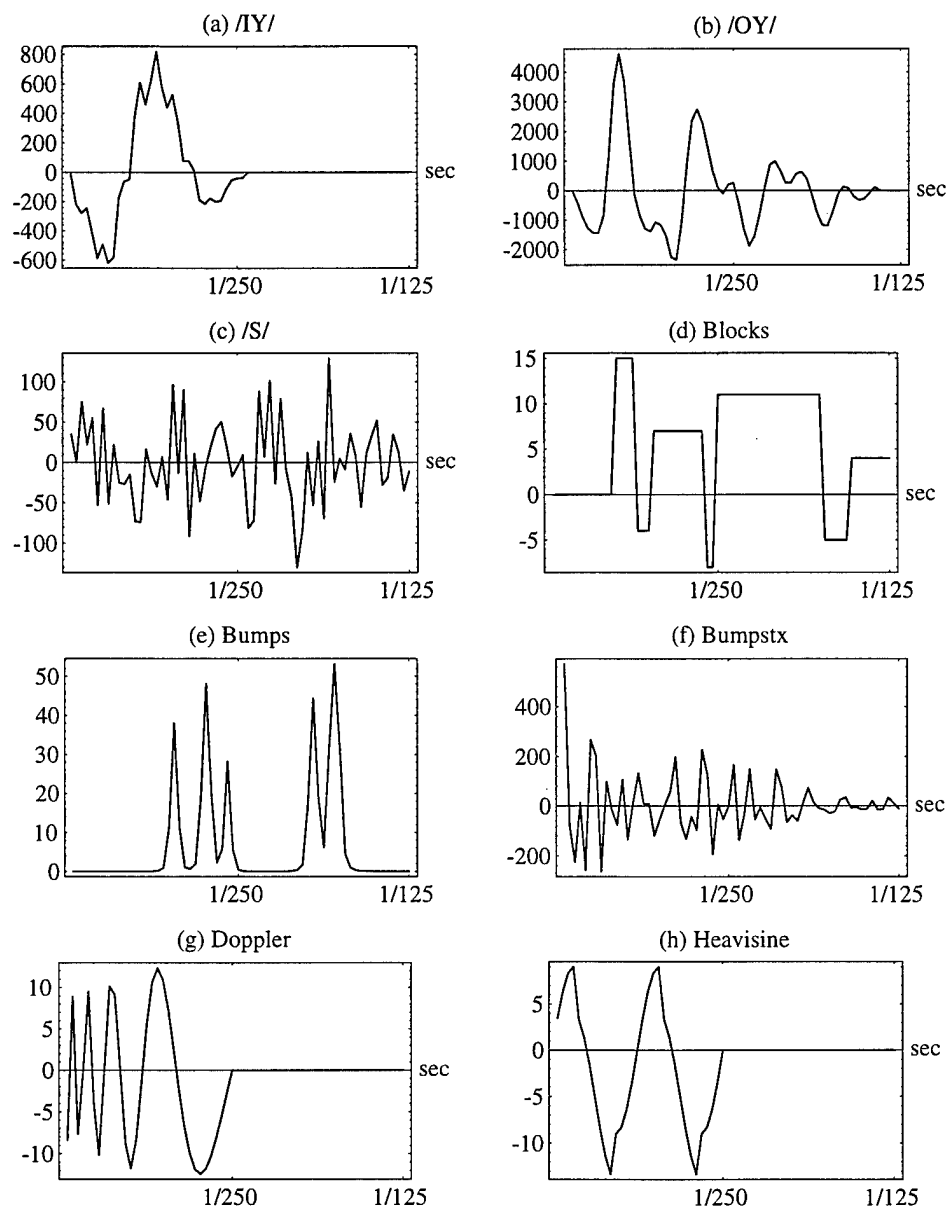


Figure 5. Data used for fine-scale analysis. (a) The phoneme */IY/*, female speaker, (b) the phoneme */OY/*, male speaker, (c) the phoneme */S/*, female speaker, (d) *blocks*, (e) *bumps*, (f) *bumpstx*, (g) *doppler*, and (h) *heavisine*.

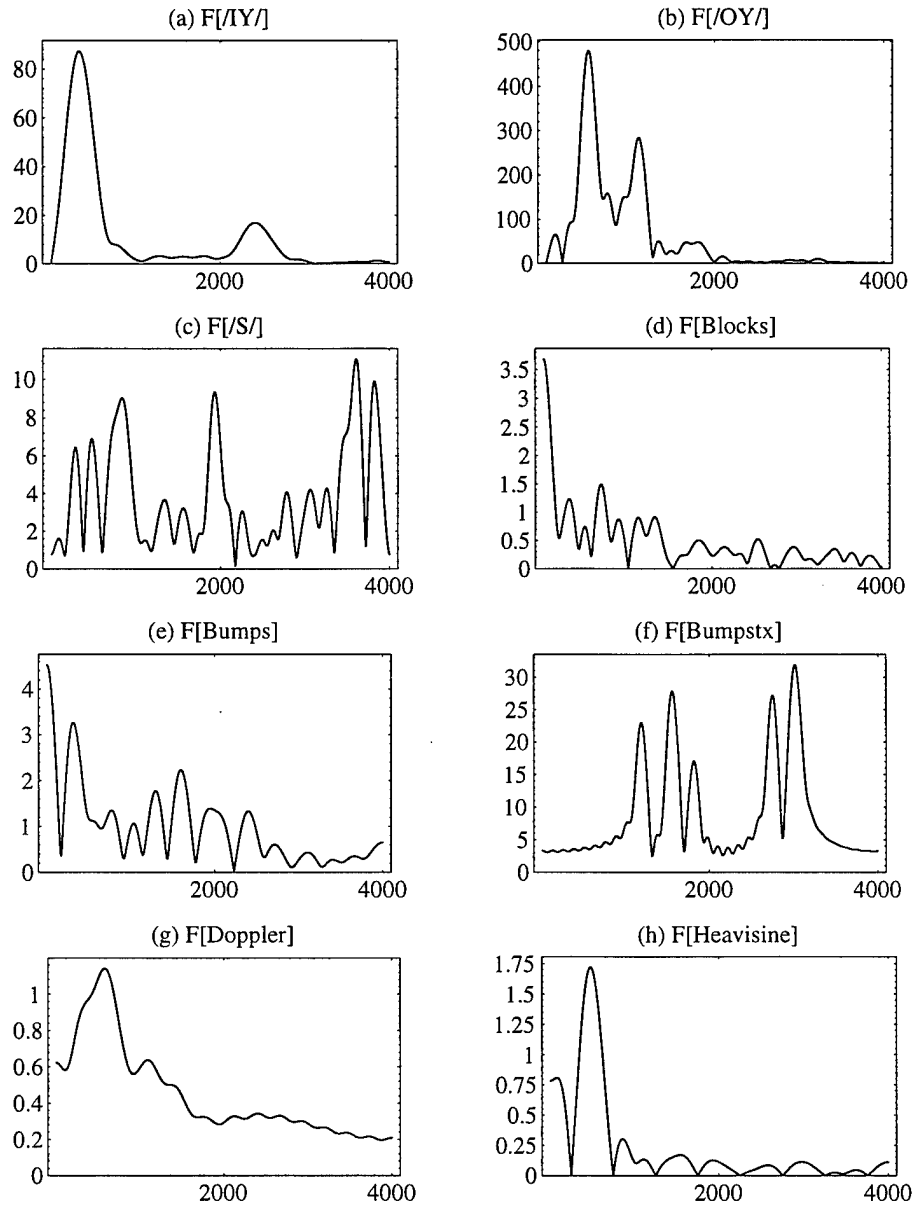


Figure 6. Fourier transform of the data used for fine-scale analysis. (a) The phoneme /IY/, female speaker, (b) the phoneme /OY/, male speaker, (c) the phoneme /S/, female speaker, (d) *blocks*, (e) *bumps*, (f) *bumpstx*, (g) *doppler*, and (h) *heavisine*.

Doppler shows more of the weaknesses of using this representation with arbitrary L_2 signals. While *doppler* is fairly smooth and has a sinusoidal appearance, its significant frequency contribution from wide range of frequencies makes it unsuitable for this representation. As seen in Figures 19 and 20, 32 poles are not sufficient to get a good approximation in either the frequency domain or the time domain.

The last signal, *heavisine*, seen in Figures 21 and 22, along with the earlier results for *blocks*, shows the inability of this representation to represent well (within one window) a discontinuity. The approximation achieved with six poles closely matches the general shape of the original signal, but shows no hint of the discontinuity. The representation appears good in the frequency domain, but enough high-frequency data is lost so that the discontinuities are smoothed.

As seen in Figure 23, for each signal, the L_2 error decreases with each additional pole added. This is to be expected, since the approximations are found by projecting the signal onto the space spanned by the poles. Therefore, the error can not increase with the addition of each successive pole. Note that for the phonemes /IY/ and /OY/ (Figure 23 (a)-(b)), the error with one pole is significantly lower than all others except *heavisine*. Contrasting with this result is the result for the phoneme /S/ (Figure 23 (c)), for which the L_2 error with six poles exceeds that of the phonemes /IY/ and /OY/ with one pole. In fact, the L_2 error plot for /S/ is consistently higher than that of all of the other signals. This is not unexpected, given the noise-like nature of the phoneme /S/. For the other signals, which have features more suitable for approximation using this representation (i.e., more speech-like), the error plots range between those for /IY/, /OY/, and *heavisine* and that of /S/.

7.1.2.2 Performance for different alignments. As seen in Figures 24 and 26 and in Table 1, for an analysis window containing a single glottal pulse, the alignment of the glottal pulse within the analysis window makes a major impact on the closeness of the approximation for a fixed number of poles. Using the results for the phoneme /IY/ as an example, the values in Table 1 shows that to achieve the same error found when approximating with three poles in the best alignment would require 16 poles in the worst alignment.

The results for the phoneme /OY/ are even more impressive; from Table 1 it can be seen that a closer L_2 -approximation can be found with two poles, optimally aligned, than can be found with 20 poles in the worst alignment.

Further examination of Figures 24 and 25 shows that there is some flexibility as to where the window can begin and still achieve an approximation with error similar to that of the best alignment. For the phoneme /OY/ (Figure 25), this good alignment region is quite distinct, with a rapid rise in error for alignments outside this region.

When the analysis window contains two glottal pulses, the results are less dramatic. As seen in Table 1, for both phoneme /IY/ and /OY/, the error achieved with a three poles approximation with the best alignment can be matched by an eight poles approximation with the worst alignment. However, the same region of good alignment can be seen in Figure 26 and 27 as before, although it is less distinct.

While these results may appear to be significant, it is worth noting that L_2 -error is, in general, not a valid measure of perceptual closeness for speech. While I believe that the L_2 norm is more valid given the basis set (exponentially damped sinusoids) of the approximation, an exhaustive, perceptual experiment has not been conducted to confirm this.

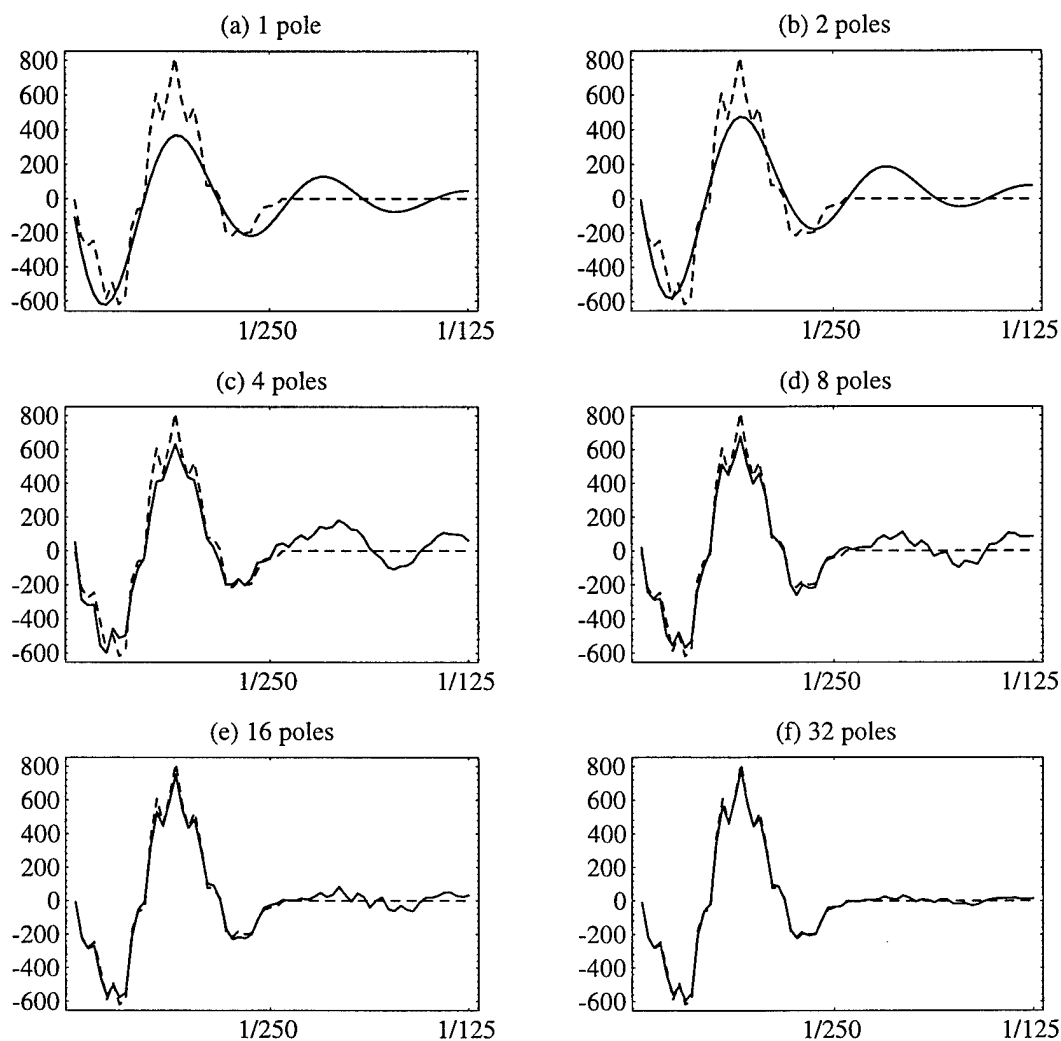


Figure 7. Approximation sequence for phoneme /IY/. (a) Approximation with one pole, (b) approximation with two poles, (c) approximation with three poles, (d) approximation with four poles, (e) approximation with five poles, and (f) approximation with six poles. In each plot, the approximation is shown (solid line) superimposed over the original data (dashed line).

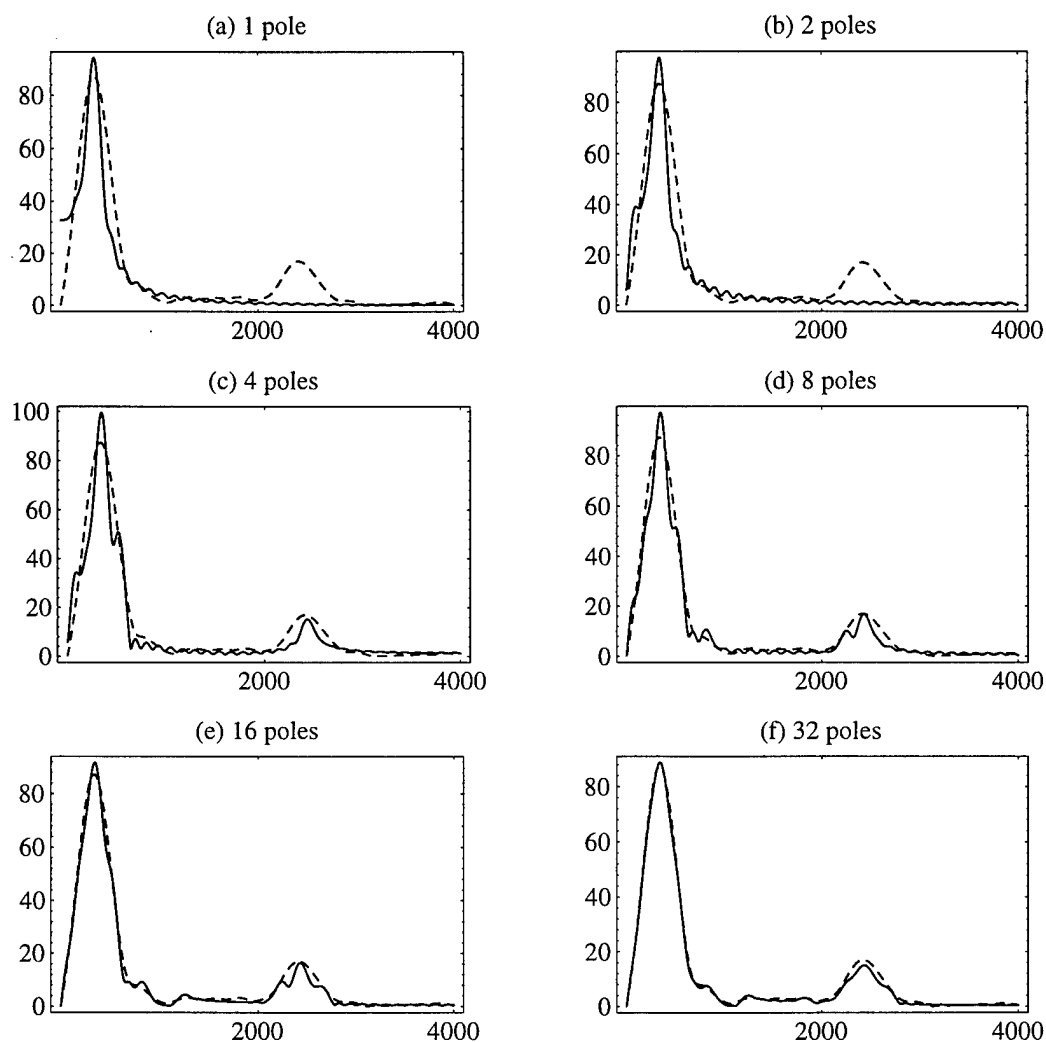


Figure 8. Fourier transform of the approximation sequence for phoneme /IY/. Fourier transforms of: (a) approximation with one pole, (b) approximation with two poles, (c) approximation with three poles, (d) approximation with four poles, (e) approximation with five poles, and (f) approximation with six poles. In each plot, the Fourier transform of the approximation is shown (solid line) superimposed over the Fourier transform of the original data (dashed line).

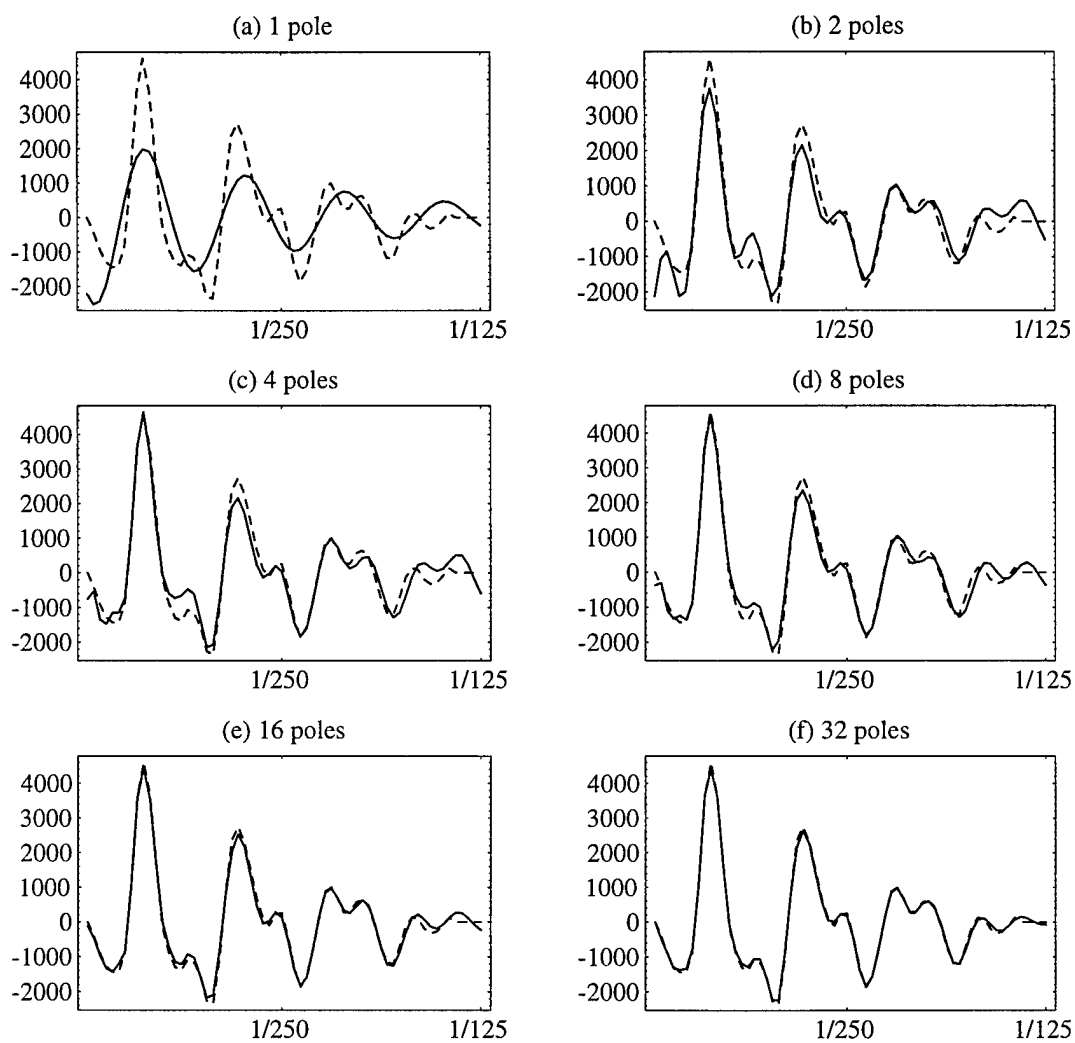


Figure 9. Approximation sequence for phoneme /OY/. Approximation with (a) one pole, (b) two poles, (c) four poles, (d) eight poles, (e) 16 poles, and (f) 32 poles. In each plot, the approximation is shown (solid line) superimposed over the original data (dashed line).

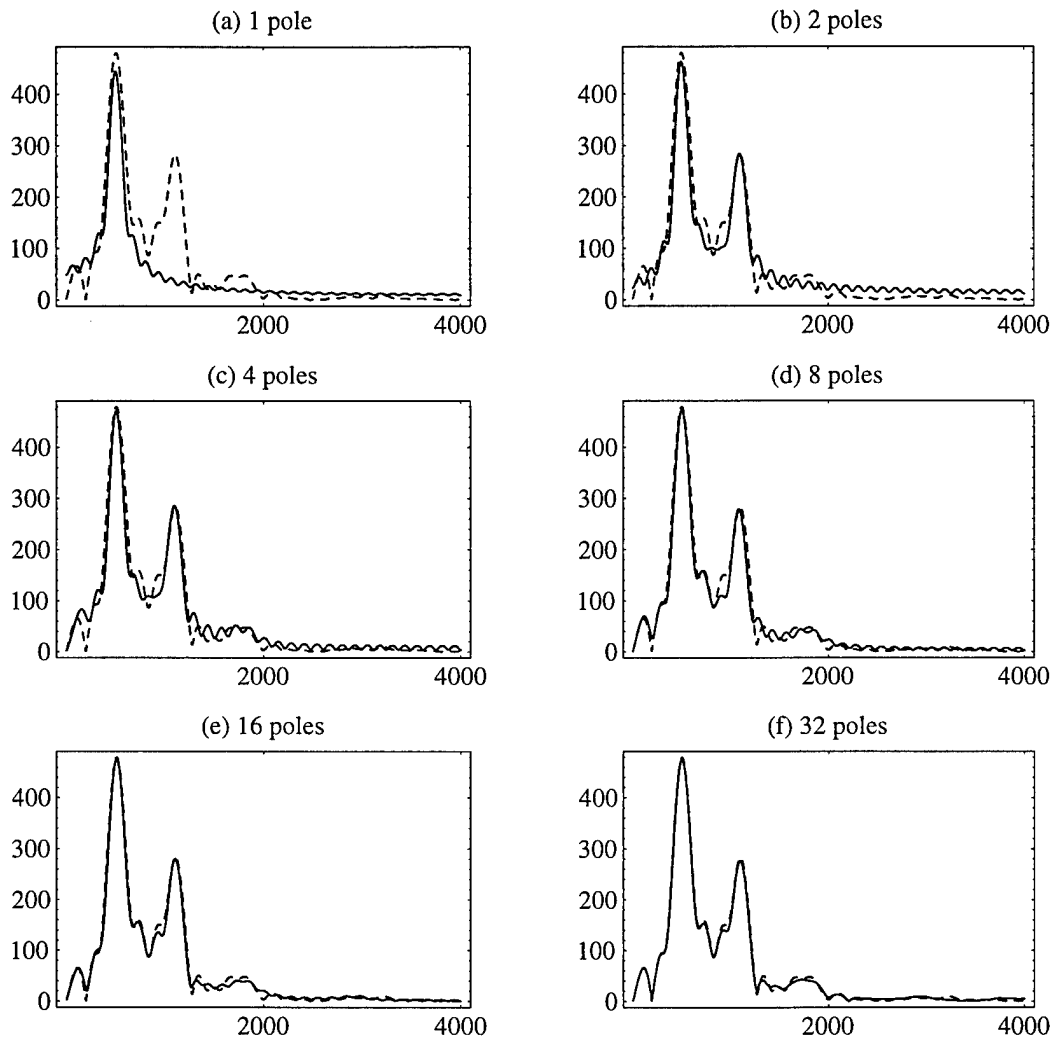


Figure 10. Fourier transform of the approximation sequence for phoneme /OY/. Fourier transform of approximation with (a) one pole, (b) two poles, (c) four poles, (d) eight poles, (e) 16 poles, and (f) 32 poles. In each plot, the Fourier transform of the approximation is shown (solid line) superimposed over the Fourier transform of the original data (dashed line).

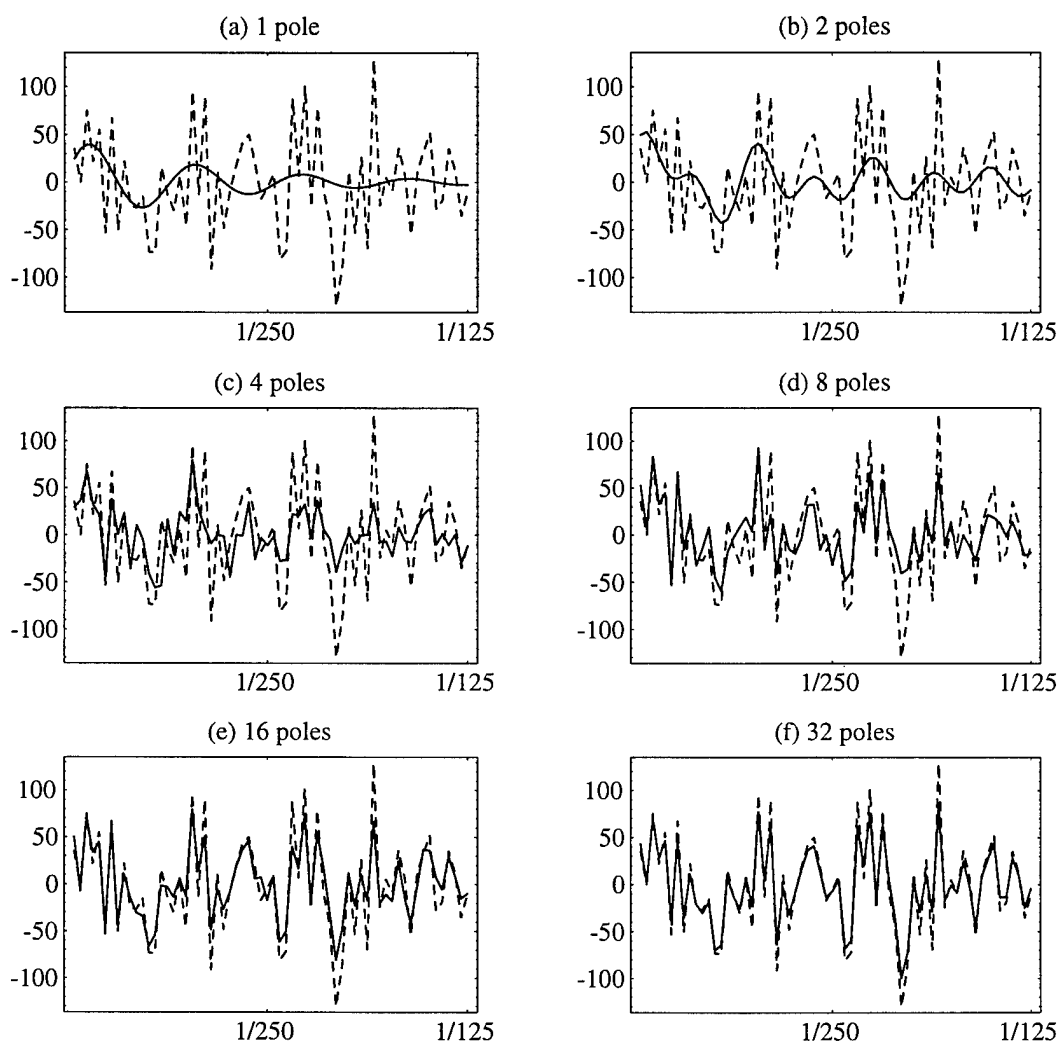


Figure 11. Approximation sequence for phoneme /S/. Approximation with (a) one pole, (b) two poles, (c) four poles, (d) eight poles, (e) 16 poles, and (f) 32 poles. In each plot, the approximation is shown (solid line) superimposed over the original data (dashed line).

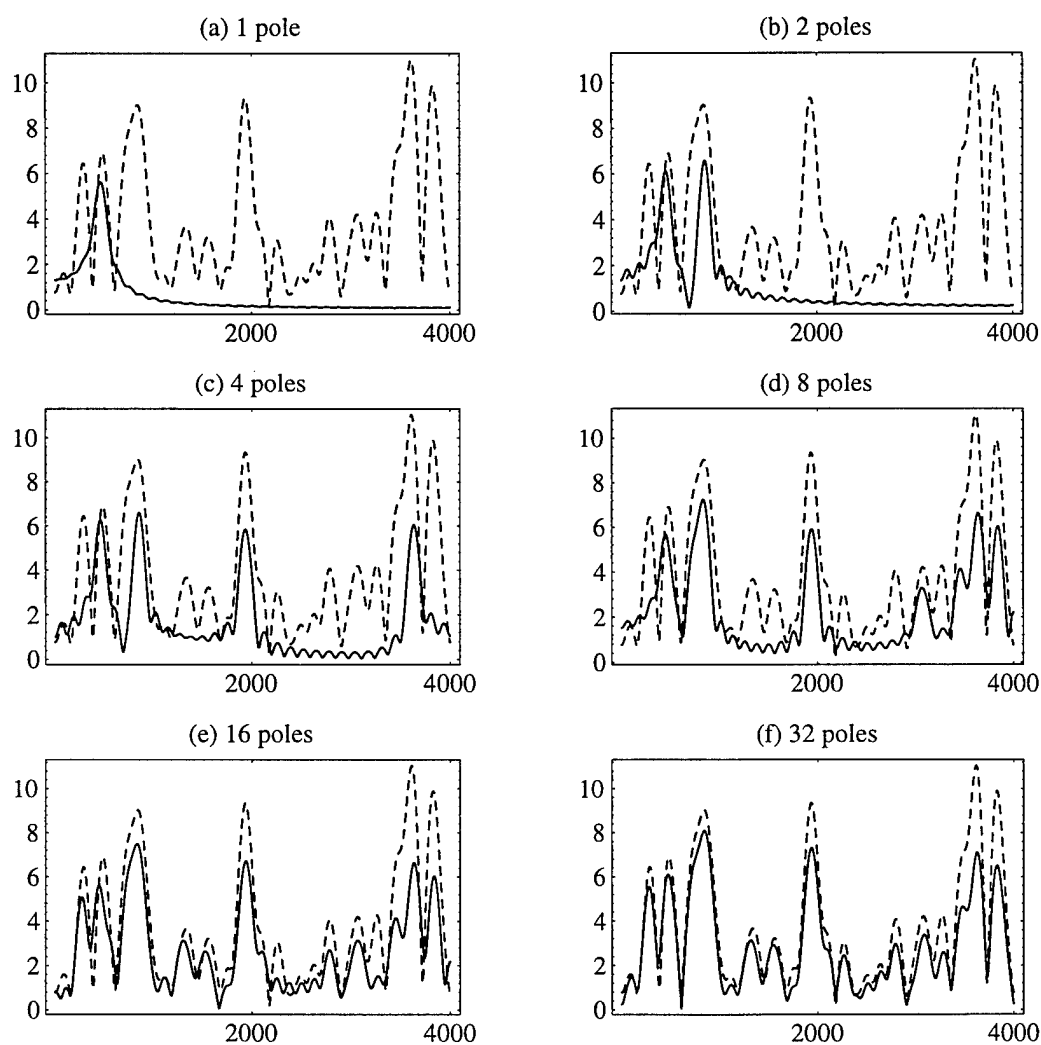


Figure 12. Fourier transform of the approximation sequence for phoneme /S/. Fourier transform of approximation with (a) one pole, (b) two poles, (c) four poles, (d) eight poles, (e) 16 poles, and (f) 32 poles. In each plot, the Fourier transform of the approximation is shown (solid line) superimposed over the Fourier transform of the original data (dashed line).

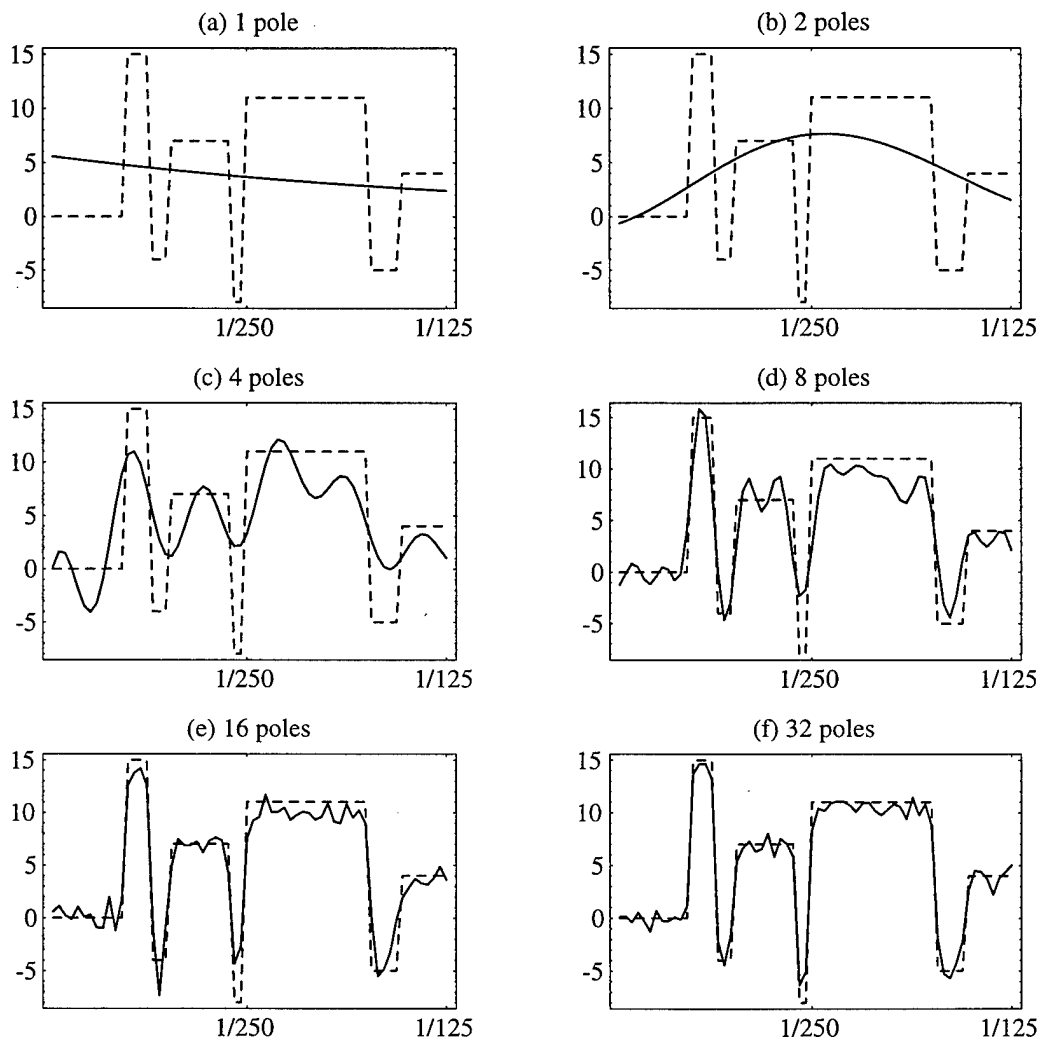


Figure 13. Approximation sequence for *blocks*. Approximation with (a) one pole, (b) two poles, (c) four poles, (d) eight poles, (e) 16 poles, and (f) 32 poles. In each plot, the approximation is shown (solid line) superimposed over the original data (dashed line).

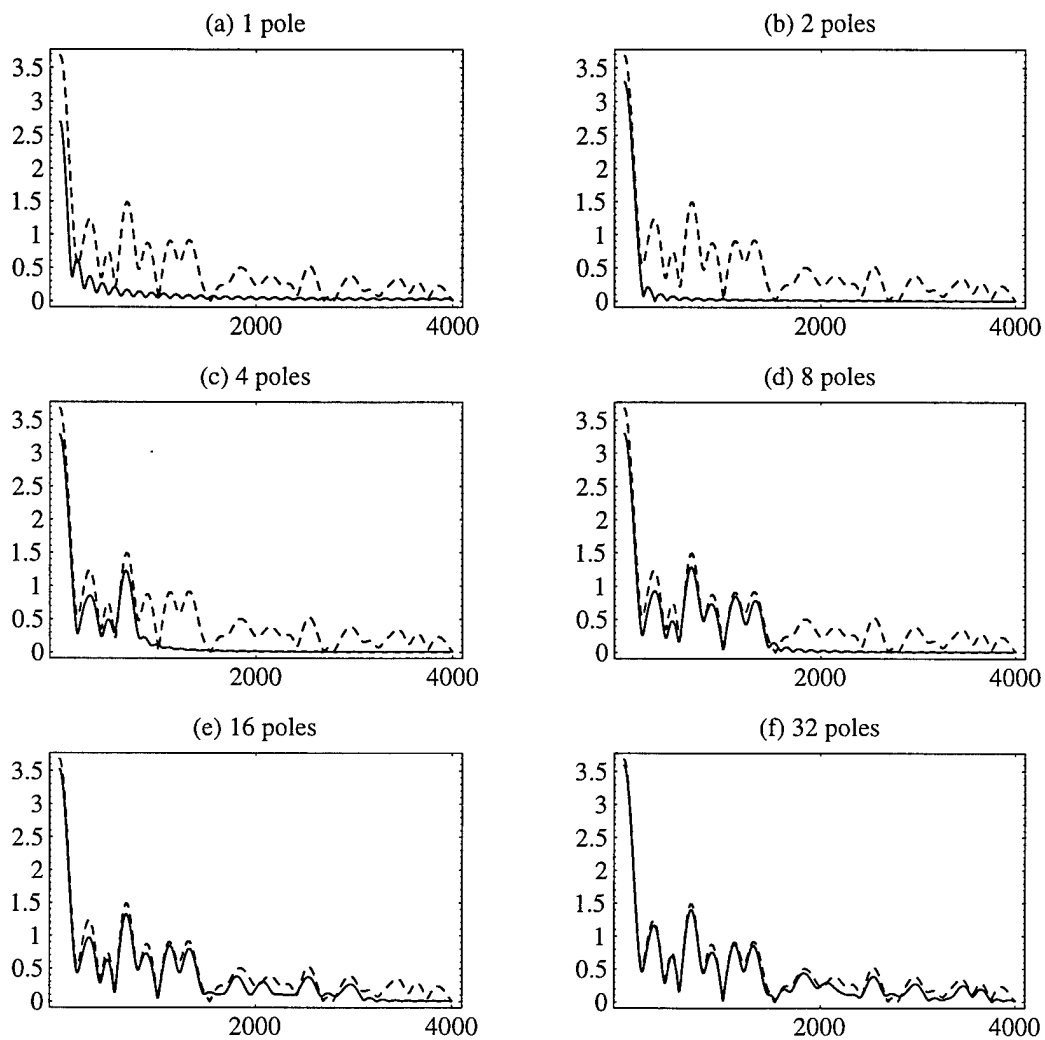


Figure 14. Fourier transform of the approximation sequence for *blocks*. Fourier transform of approximation with (a) one pole, (b) two poles, (c) four poles, (d) eight poles, (e) 16 poles, and (f) 32 poles. In each plot, the Fourier transform of the approximation is shown (solid line) superimposed over the Fourier transform of the original data (dashed line).

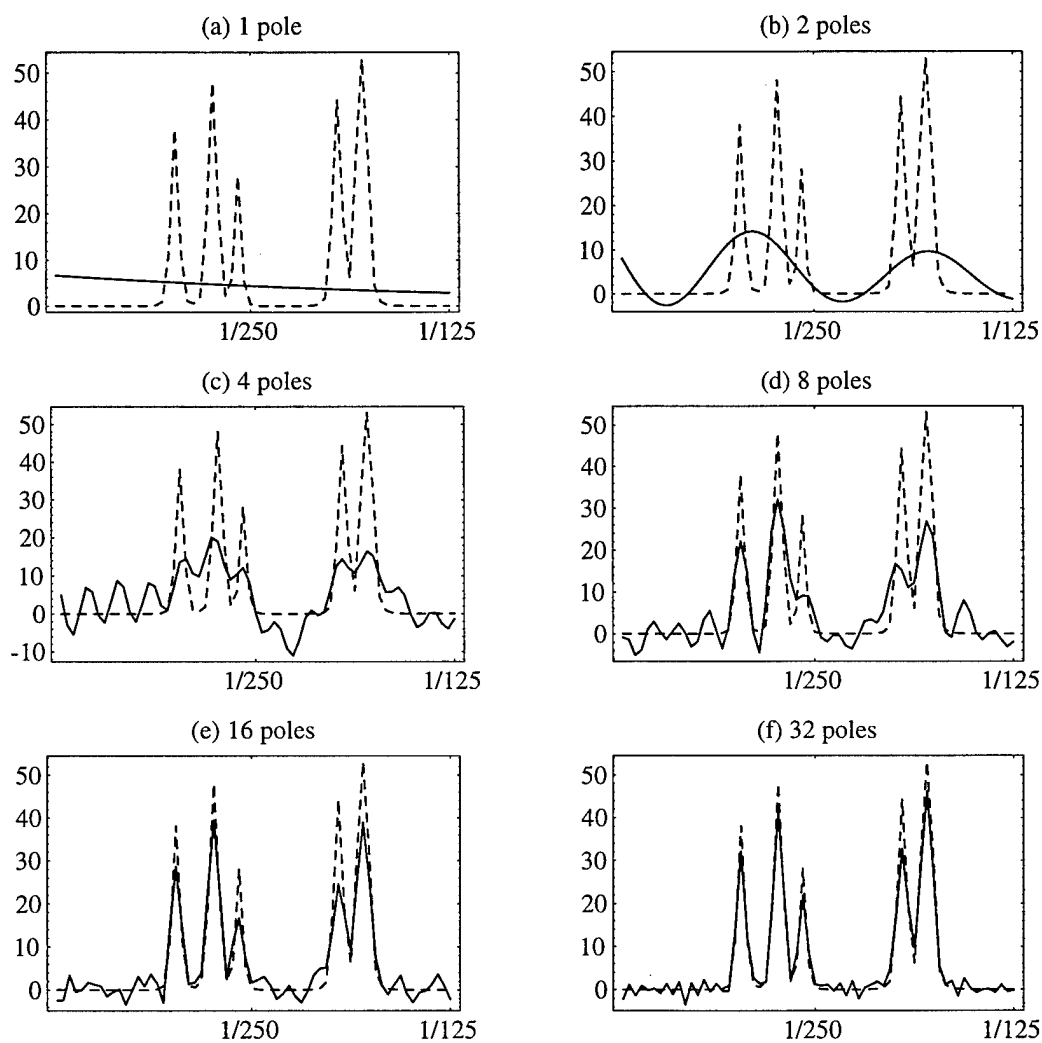


Figure 15. Approximation sequence for *bumps*. Approximation with (a) one pole, (b) two poles, (c) four poles, (d) eight poles, (e) 16 poles, and (f) 32 poles. In each plot, the approximation is shown (solid line) superimposed over the original data (dashed line).

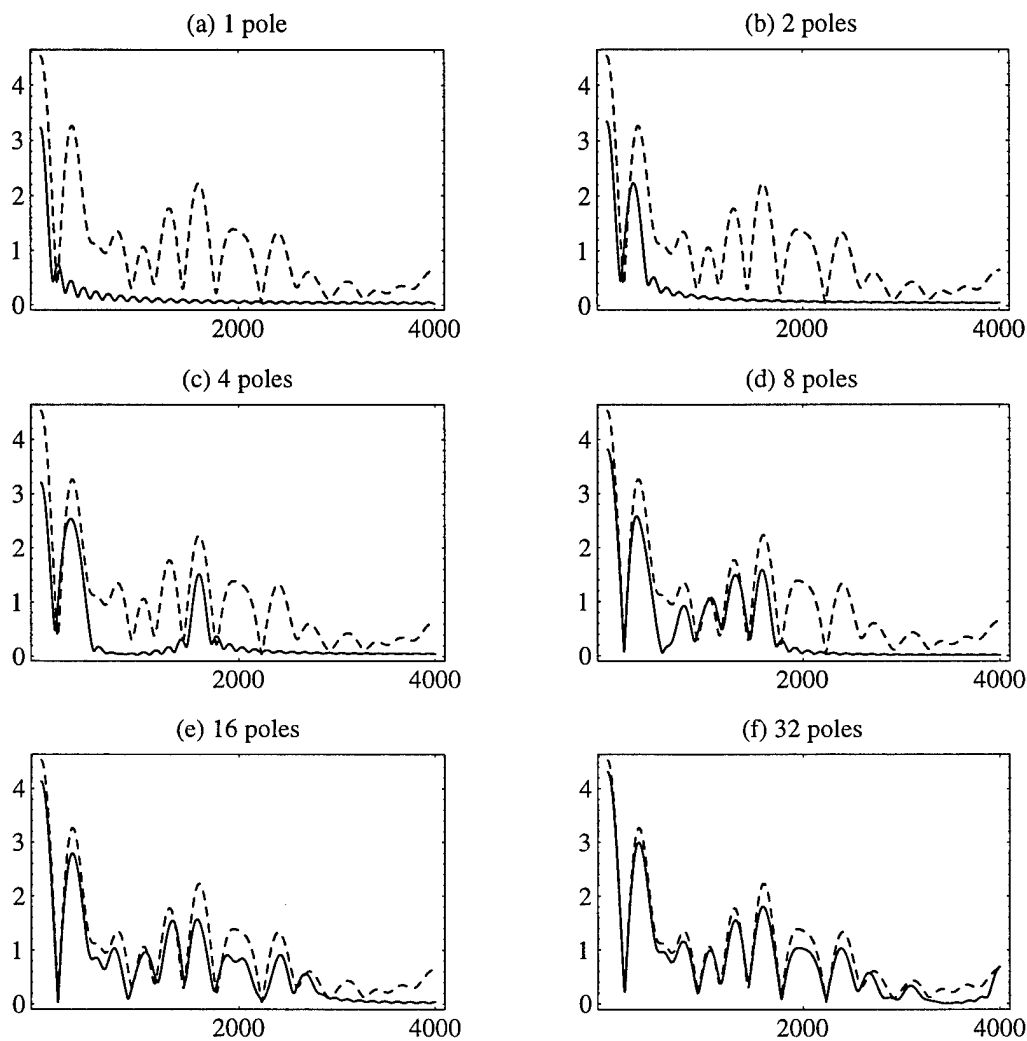


Figure 16. Fourier transform of the approximation sequence for *bumps*. Fourier transform of approximation with (a) one pole, (b) two poles, (c) four poles, (d) eight poles, (e) 16 poles, and (f) 32 poles. In each plot, the Fourier transform of the approximation is shown (solid line) superimposed over the Fourier transform of the original data (dashed line).

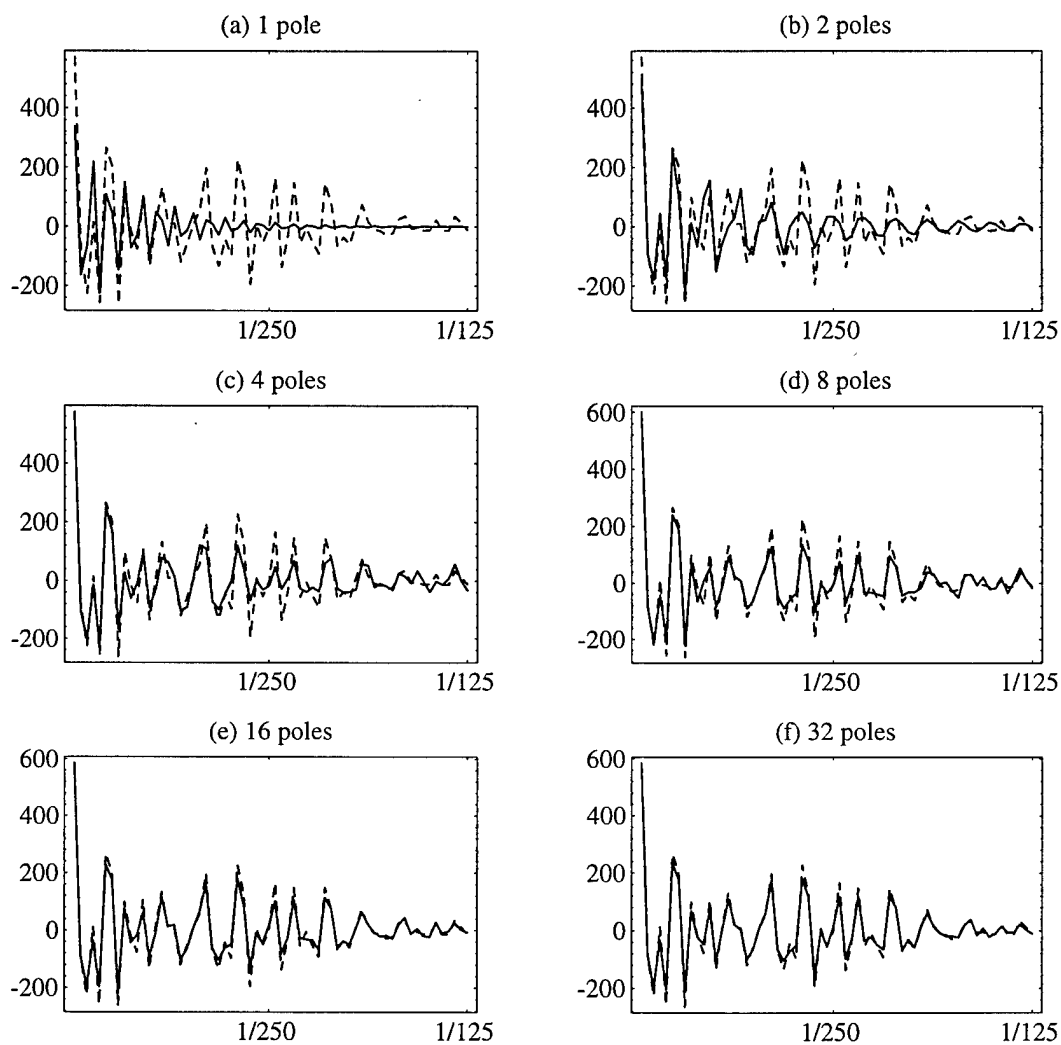


Figure 17. Approximation sequence for *bumpstx*. Approximation with (a) one pole, (b) two poles, (c) four poles, (d) eight poles, (e) 16 poles, and (f) 32 poles. In each plot, the approximation is shown (solid line) superimposed over the original data (dashed line).

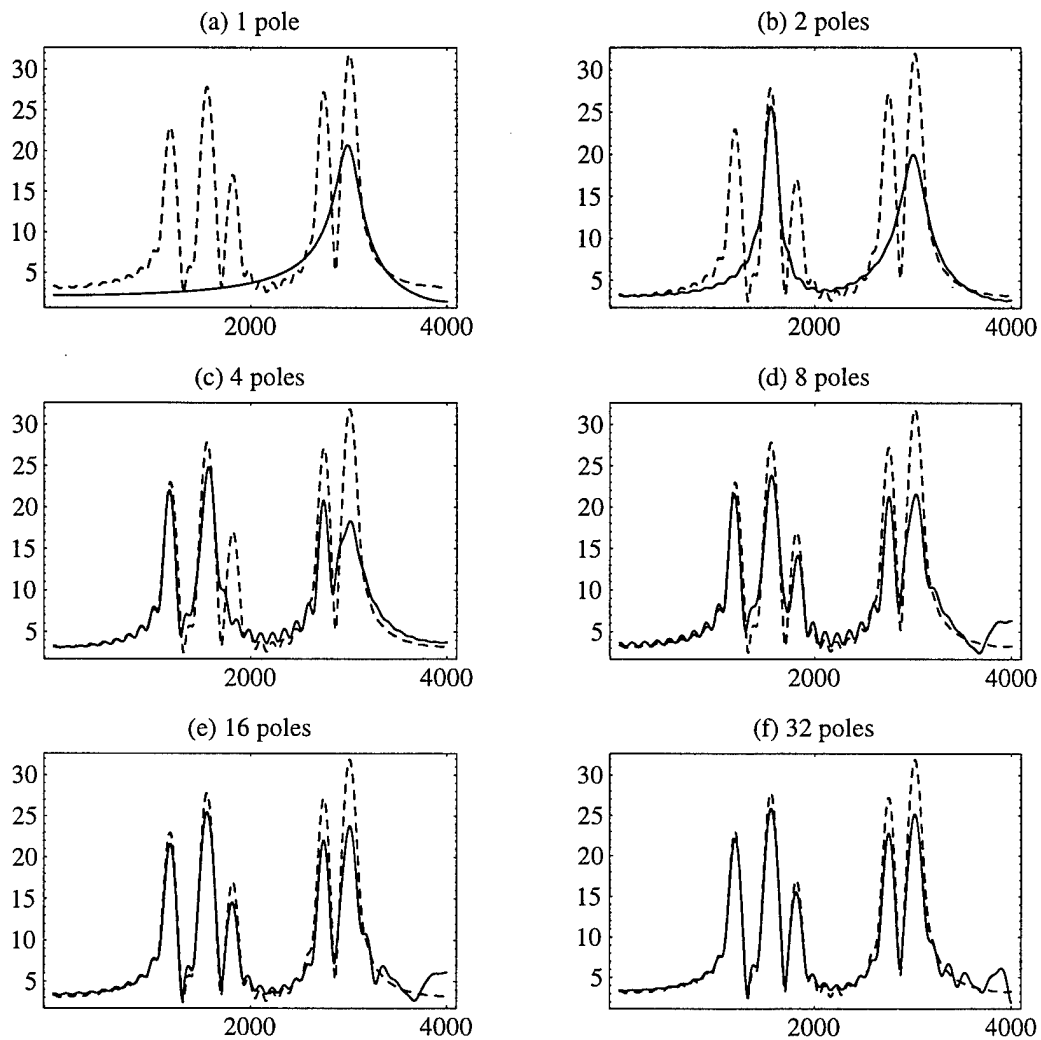


Figure 18. Fourier transform of the approximation sequence for *bumpstx*. Fourier transform of approximation with (a) one pole, (b) two poles, (c) four poles, (d) eight poles, (e) 16 poles, and (f) 32 poles. In each plot, the Fourier transform of the approximation is shown (solid line) superimposed over the Fourier transform of the original data (dashed line).

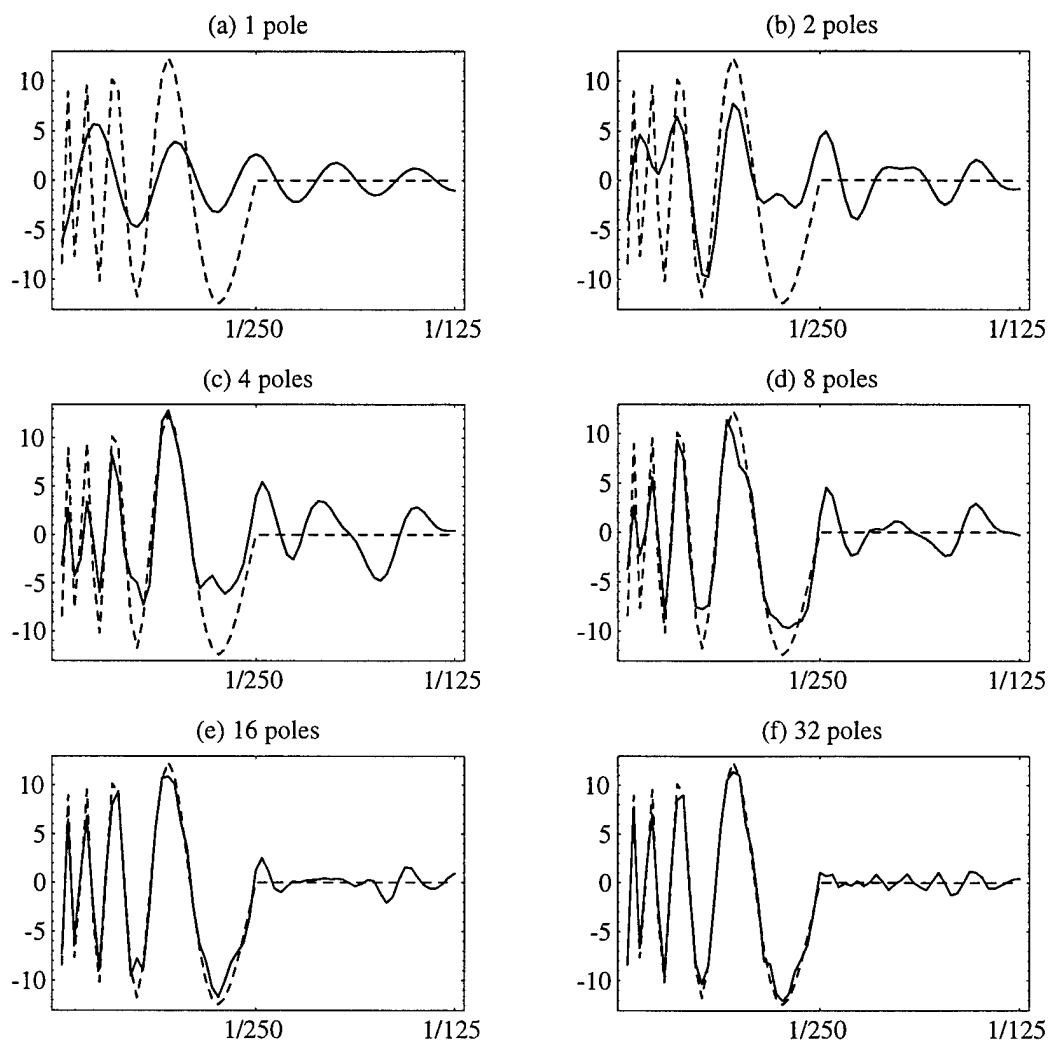


Figure 19. Approximation sequence for *doppler*. Approximation with (a) one pole, (b) two poles, (c) four poles, (d) eight poles, (e) 16 poles, and (f) 32 poles. In each plot, the approximation is shown (solid line) superimposed over the original data (dashed line).

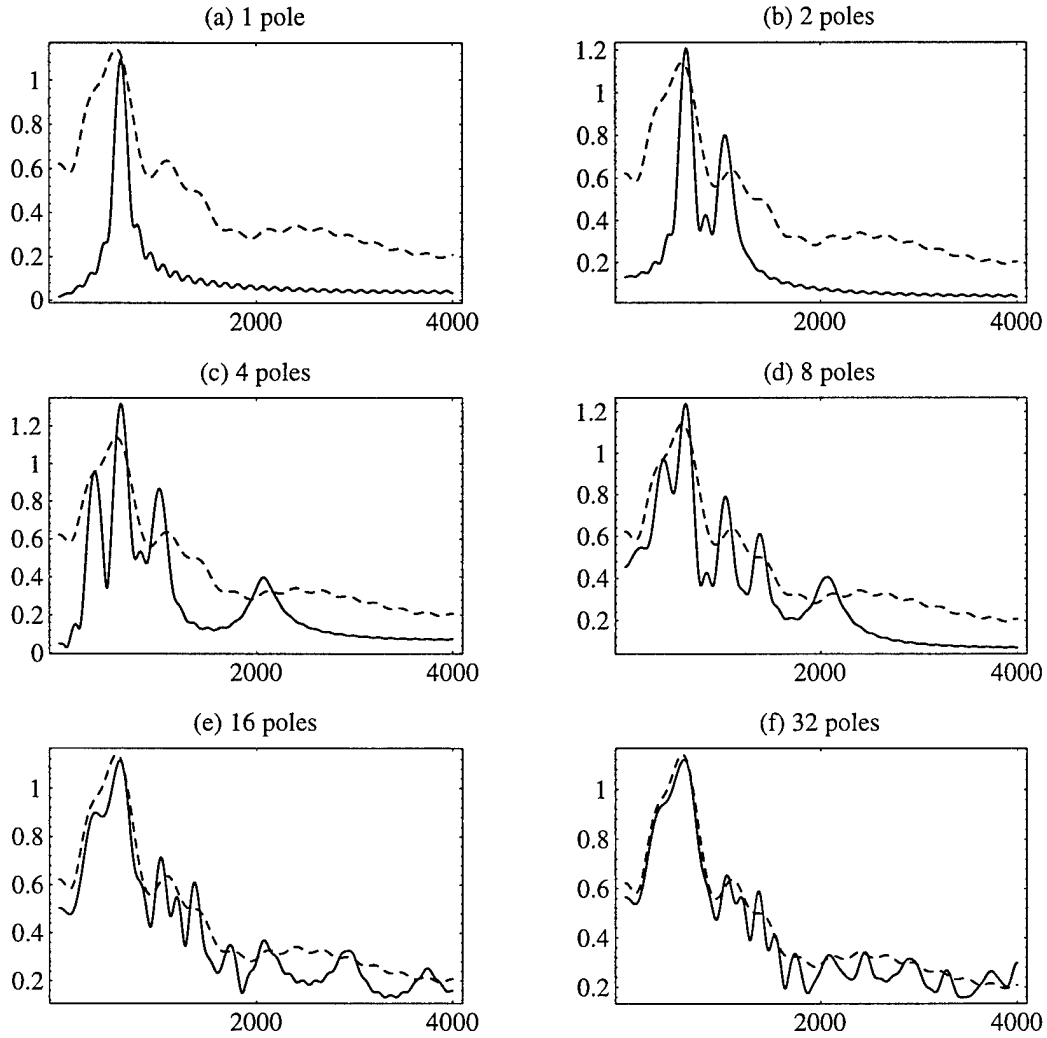


Figure 20. Fourier transform of the approximation sequence for *doppler*. Fourier transform of approximation with (a) one pole, (b) two poles, (c) four poles, (d) eight poles, (e) 16 poles, and (f) 32 poles. In each plot, the Fourier transform of the approximation is shown (solid line) superimposed over the Fourier transform of the original data (dashed line).

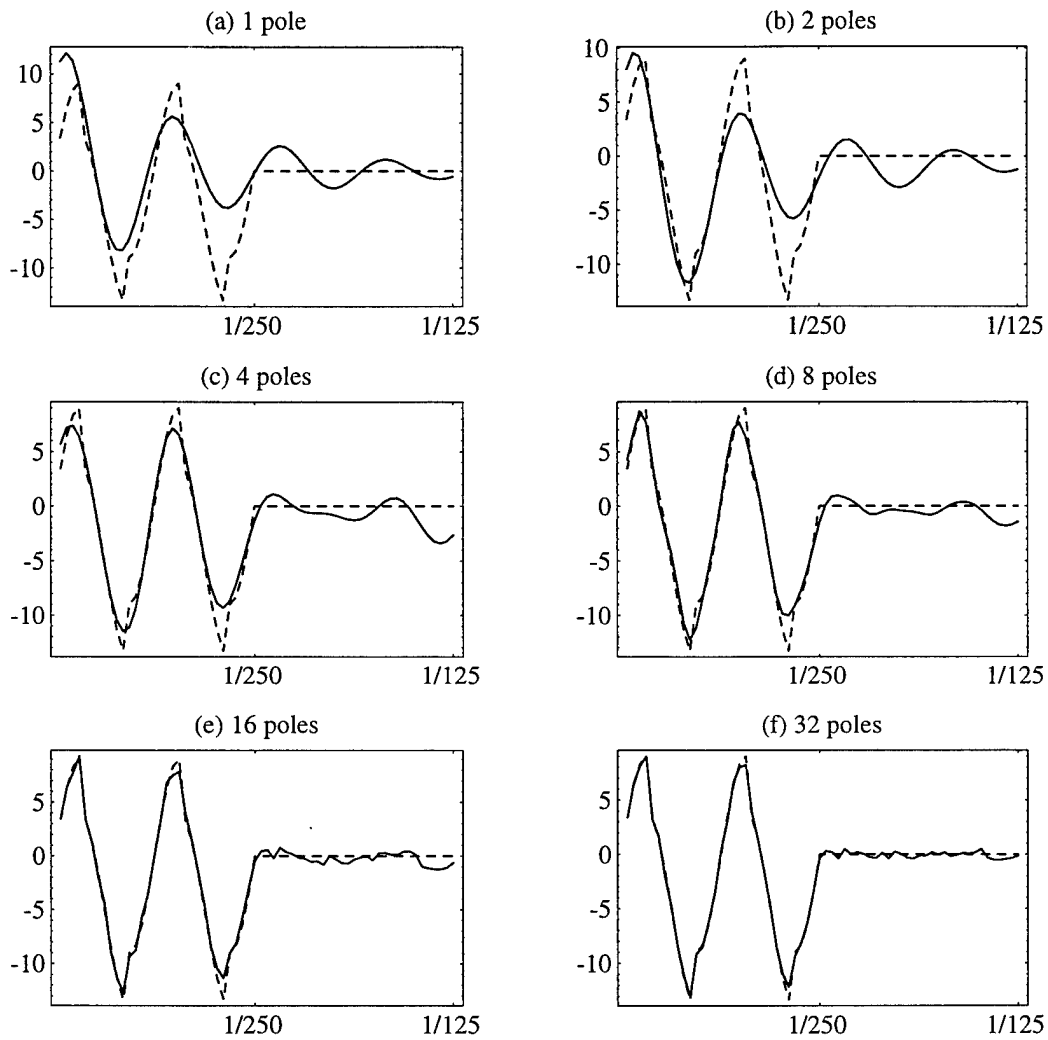


Figure 21. Approximation sequence for *heavisine*. Approximation with (a) one pole, (b) two poles, (c) four poles, (d) eight poles, (e) 16 poles, and (f) 32 poles. In each plot, the approximation is shown (solid line) superimposed over the original data (dashed line).

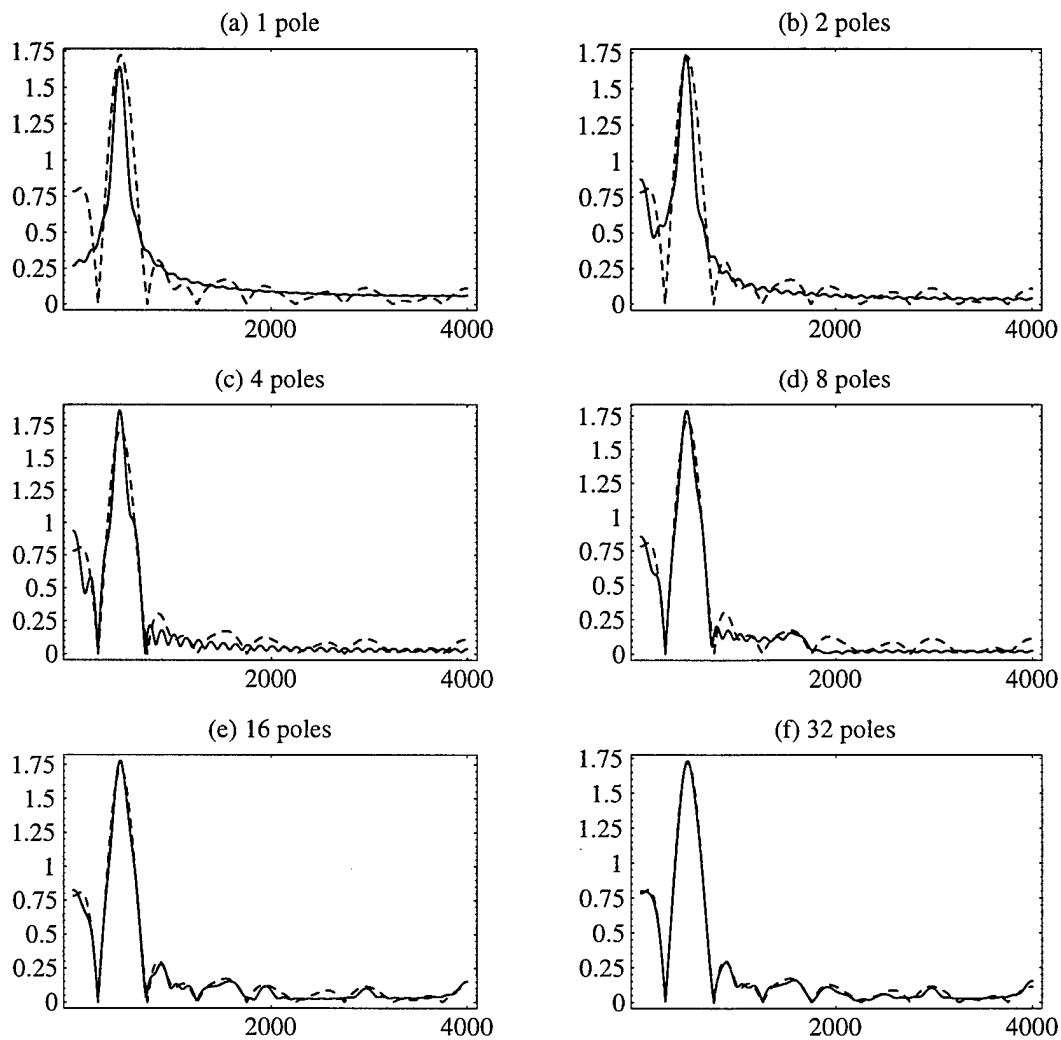


Figure 22. Fourier transform of the approximation sequence for *heavisine*. Fourier transform of approximation with (a) one pole, (b) two poles, (c) four poles, (d) eight poles, (e) 16 poles, and (f) 32 poles. In each plot, the Fourier transform of the approximation is shown (solid line) superimposed over the Fourier transform of the original data (dashed line).

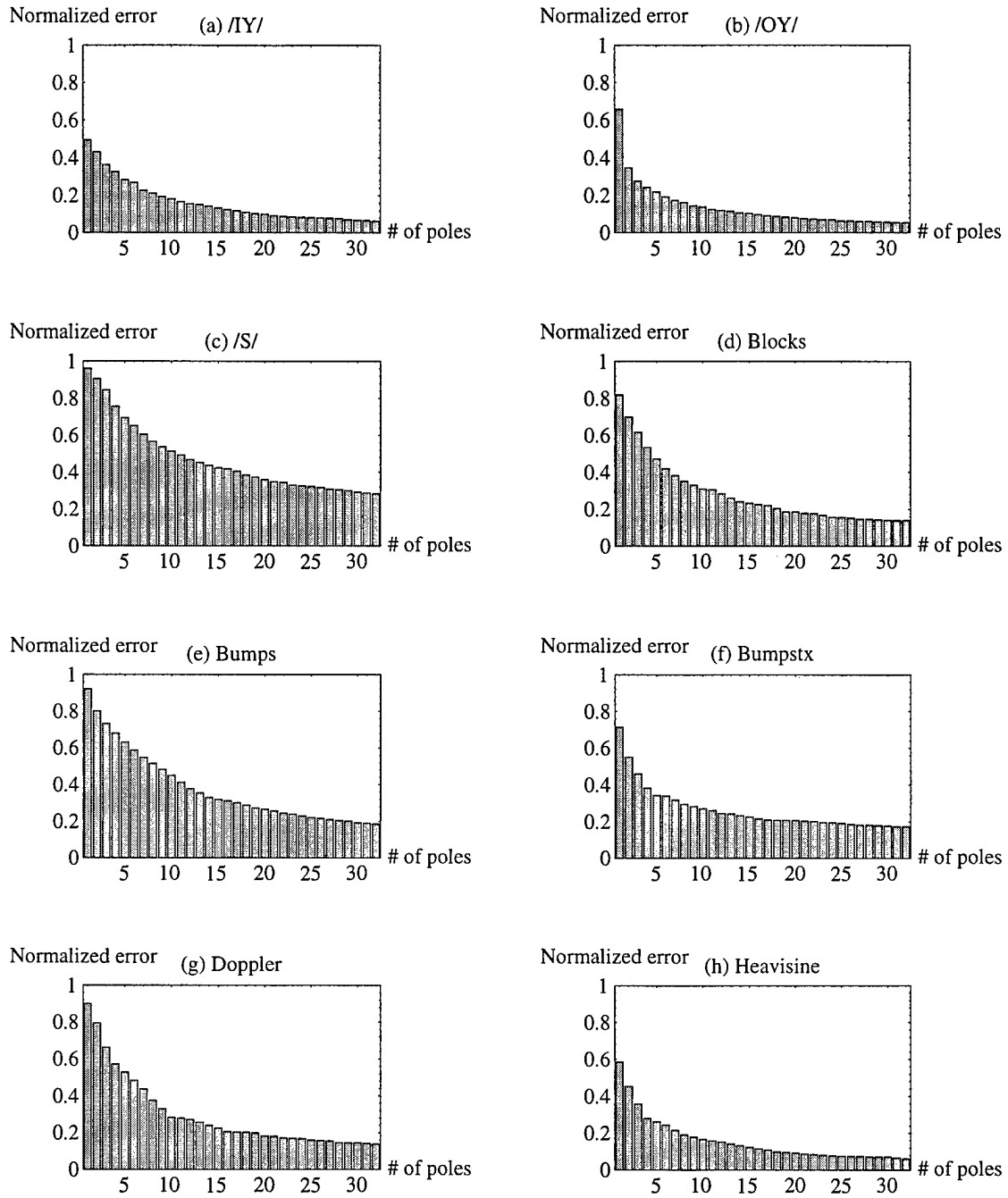


Figure 23. Number of poles vs. normalized L_2 error for each signal. The error is normalized by the L_2 norm of the original signal. (a) The phoneme /IY/, (b) the phoneme /OY/, (c) the phoneme /S/, (d) *blocks*, (e) *bumps*, (f) *bumpstx*, (g) *doppler*, and (h) *heavisine*.

# of poles	One glottal pulse per analysis window				Two glottal pulses per analysis window			
	Phoneme /IY/		Phoneme /OY/		Phoneme /IY/		Phoneme /OY/	
	Minimum Error	Maximum Error	Minimum Error	Maximum Error	Maximum Error	Minimum Error	Maximum Error	Minimum Error
1	0.460291	0.812850	0.513864	0.828856	0.646511	0.789152	0.704659	0.827021
2	0.323028	0.621919	0.229435	0.716668	0.386326	0.492282	0.561976	0.744625
3	0.268697	0.566329	0.210855	0.624579	0.324757	0.423212	0.454333	0.661916
4	0.207934	0.486123	0.192573	0.552087	0.280782	0.384953	0.414456	0.601263
5	0.173436	0.446329	0.175565	0.490591	0.236488	0.355051	0.377198	0.566798
6	0.161867	0.427236	0.162753	0.468758	0.214609	0.333163	0.348653	0.509707
7	0.157996	0.393248	0.149690	0.444034	0.200741	0.287904	0.325050	0.478742
8	0.126765	0.375314	0.137544	0.404298	0.172376	0.268204	0.303950	0.443744
9	0.119073	0.364153	0.128424	0.383311	0.162266	0.260166	0.290739	0.409024
10	0.112897	0.337523	0.116444	0.360579	0.153773	0.243383	0.268339	0.395719
11	0.110230	0.318021	0.109938	0.346475	0.141680	0.224595	0.244809	0.377138
12	0.107024	0.302431	0.103605	0.321957	0.136093	0.214414	0.231006	0.364048
13	0.096229	0.293542	0.097265	0.306701	0.124955	0.205986	0.220919	0.347784
14	0.092523	0.285065	0.092192	0.295884	0.123418	0.200360	0.208767	0.330553
15	0.088555	0.269546	0.086315	0.284046	0.119481	0.193764	0.195660	0.325168
16	0.081032	0.262443	0.082161	0.276742	0.112628	0.186706	0.188557	0.321615
17	0.079156	0.254823	0.077078	0.271640	0.105716	0.177564	0.182029	0.312791
18	0.075289	0.243101	0.074037	0.261622	0.101655	0.171892	0.174368	0.302629
19	0.072026	0.236213	0.070669	0.251509	0.096277	0.162143	0.164950	0.296547
20	0.071699	0.226527	0.069649	0.239655	0.093374	0.157936	0.157771	0.285576

Table 1. Minimum and maximum error over the different analysis window offsets for the phonemes /IY/ and /OY/ for analysis windows containing one and two pulses.

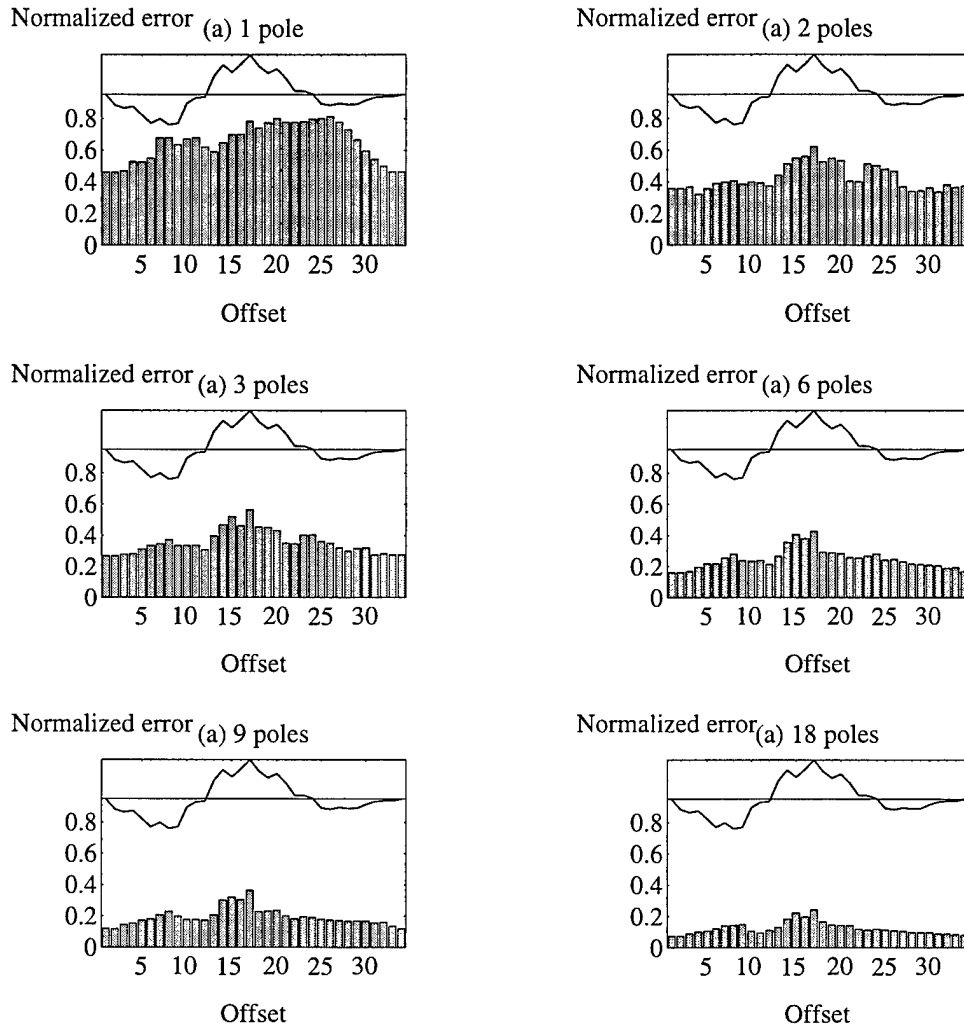


Figure 24. Data offset vs. normalized L_2 error for the phoneme /IY/ for an analysis window containing one pulse. The original data is shown over the histogram for comparative purposes. The offset used to generate a given value in the histogram is the abscissa point of the original data directly above the histogram value. The error is normalized by the L_2 norm of the original signal. Approximation using (a) one pole, (b) two poles, (c) three poles, (d) six poles, (e) nine poles, and (f) 18 poles.

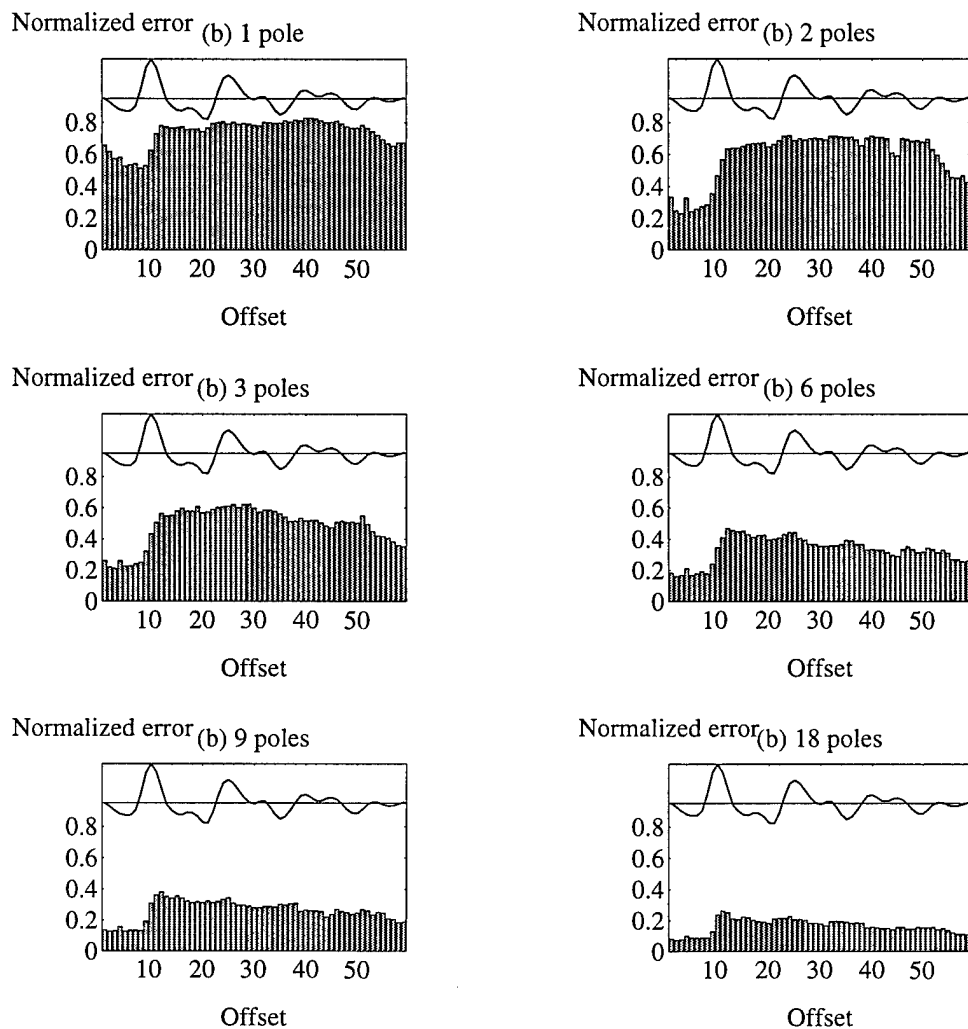


Figure 25. Data offset vs. normalized L_2 error for the phoneme /OY/ for an analysis window containing one pulse. The original data is shown over the histogram for comparative purposes. The offset used to generate a given value in the histogram is the abscissa point of the original data directly above the histogram value. The error is normalized by the L_2 norm of the original signal. Approximation using (a) one pole, (b) two poles, (c) three poles, (d) six poles, (e) nine poles, and (f) 18 poles.

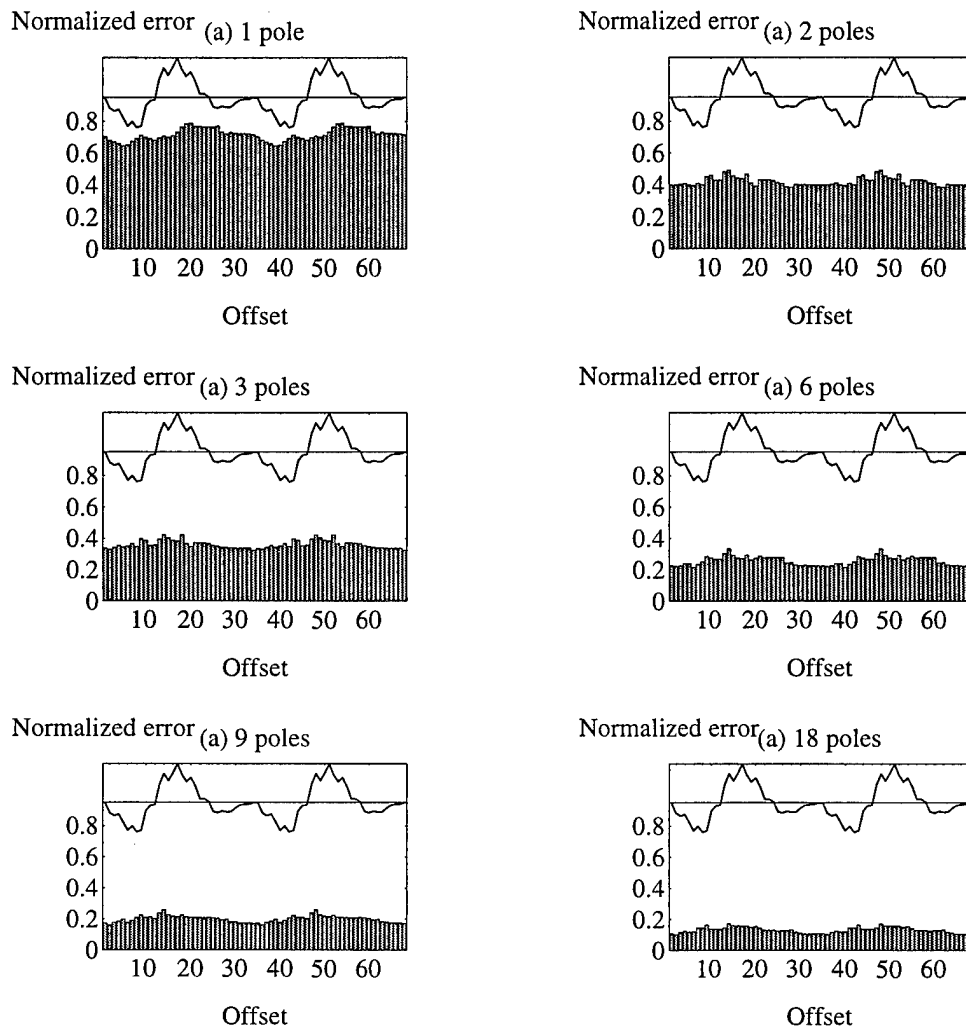


Figure 26. Data offset vs. normalized L_2 error for the phoneme /IY/ for an analysis window containing two pulses. The original data is shown over the histogram for comparative purposes. The offset used to generate a given value in the histogram is the abscissa point of the original data directly above the histogram value. The error is normalized by the L_2 norm of the original signal. Approximation using (a) one pole, (b) two poles, (c) three poles, (d) six poles, (e) nine poles, and (f) 18 poles.

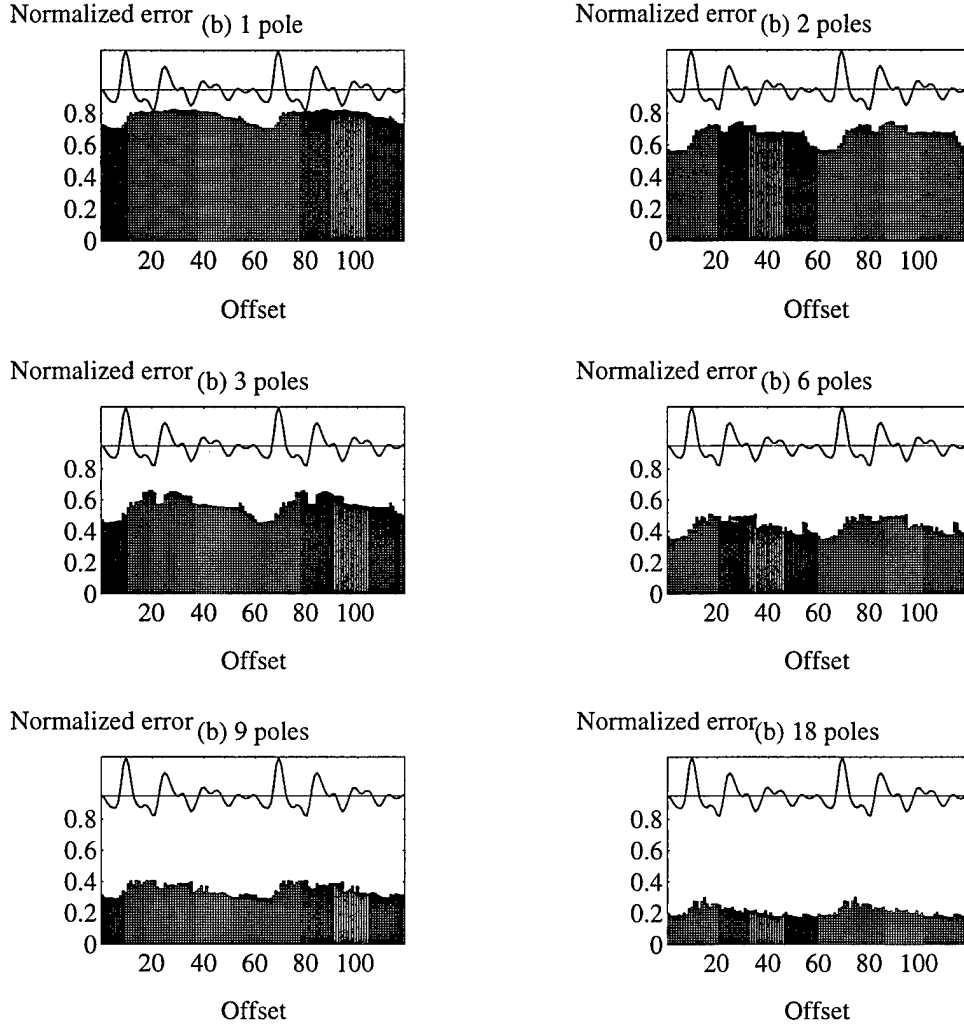


Figure 27. Data offset vs. normalized L_2 error for the phoneme /OY/ for an analysis window containing two pulses. The original data is shown over the histogram for comparative purposes. The offset used to generate a given value in the histogram is the abscissa point of the original data directly above the histogram value. The error is normalized by the L_2 norm of the original signal. Approximation using (a) one pole, (b) two poles, (c) three poles, (d) six poles, (e) nine poles, and (f) 18 poles.

7.2 *Medium-scale analyses*

The fine-scale analyses above examined the performance of the representation on the scale of a single analysis window. The goal of the medium-scale analysis is to examine the performance of the the frame described in Chapter VI, based on Theorem 4.2.4, and the algorithm to find the frame representation given in Theorem 4.3.4.

The performance of this representation is examined in two ways. First, representation of harmonic speech is analyzed. Next, representation of non-speech is analyzed. The error for differing number of basis function and overlaps between basis function is analyzed.

7.2.1 *Description of medium scale analyses.*

7.2.1.1 *Performance on harmonic speech.* Two segments of speech, the phoneme /IY/ from a female speaker and the phoneme /OY/ from a male speaker, each consisting of several glottal pulses, were used in this analysis. The program's pulse finder was used to determine the estimated starting times of the glottal pulses in the segments. Both segments and the pulse start times as identified by the program are shown in Figure 28. The spectrograms for each segment are shown in Figure 29.

Approximations were found for analysis windows overlapping by 0%, 50%, 67%, and 75%. Note that this corresponds to each data point being contained in one, two, three, and four analysis windows, respectively. For each of these cases, the analysis window decay rate was varied through 0, 25, 50, 75, and 100. Approximations using three, six, 10, and 32 poles per glottal pulse were found for each case.

The data-dependent analysis window selection method was used. That is, the starting points of the glottal pulses were used as the starting points of the analysis windows, with an additional analysis window starting at the first sample point was added to the the set. To prevent additional analysis windows from being inserted between glottal pulses for the cases of 67% and 75% overlapping windows, the maximum length of the analysis window was set to 256 sample data points. This was done for the sake of fair comparisons between the cases of differing overlap amounts.

The same analysis window start points are used for each of the different analysis window overlap amounts; the window length is simply adjusted to give desired overlap amount. Additional windows are added starting before the signal start time as needed to achieve the desired overlaps at the start of the segment. All analysis window selection was done automatically by heuristic algorithms in the program, as described in Section 6.3

and Appendix C. The analysis window selection is independent of the window decay rate, the number of poles to be chosen, and the number of iterations to be performed of the reconstruction approximation.

The segment containing the phoneme /IY/ consists of 343 sample points and was determined to contain nine glottal pulses, yielding a basic set of 10 analysis windows. The segment containing the phoneme /OY/ consists of 512 sample points and was determined to contain eight glottal pulses, for a basic set of nine analysis windows. For the cases of analysis window overlaps of 50%, 67% and 75%, one, two, and three additional analysis windows were added, respectively, to give the desired amount of overlap. Each additional analysis window begins at a time before the first sampled data point. The candidate poles were the same for every case, and were chosen automatically as described in Section 6.3.

The program was run for all combinations of the cases. The poles chosen in each case are shown graphically in Figures 31 through 38.

The program was set to use 11 iterations (numbered 0 through 10) of the approximation given in Theorem 4.3.4 to determine the approximation of the speech segment. The error after each iteration of the approximation process was found. The error for each case is shown graphically in Figures 39 through 46.

7.2.1.2 Performance on non-speech signals. In this analysis, the performance on two non-speech signals is examined. The performance is compared to that with the phoneme /OY/, which was the same segment used previously. A single row of a digitized image, *Lenna*, was used as the first non-speech signal. The second is reversed speech, that is, sampled speech in reverse order. For this sample, the same data points as are in the control sample (the phoneme /OY/) are used, in reverse order. Since non-speech does not necessarily have a glottal pulse structure that could be profitably used by the program, evenly spaced analysis windows of length 128 sample points with 50% overlap between segments are used in this analysis. Due to some unexpected results to be described below, the program was also run for the case of analysis windows aligned with the glottal pulses, with 50% window overlap and an analysis window maximum length of 128 samples to give additional data for comparison. The segments used by the program are shown in Figure 30. The analysis window decay rate was varied through 0, 25, 50, 75, and 100. Approximations for three, six, 10, and 32 poles were found for each case. All data segments contained 512 data points and nine analysis windows were used.

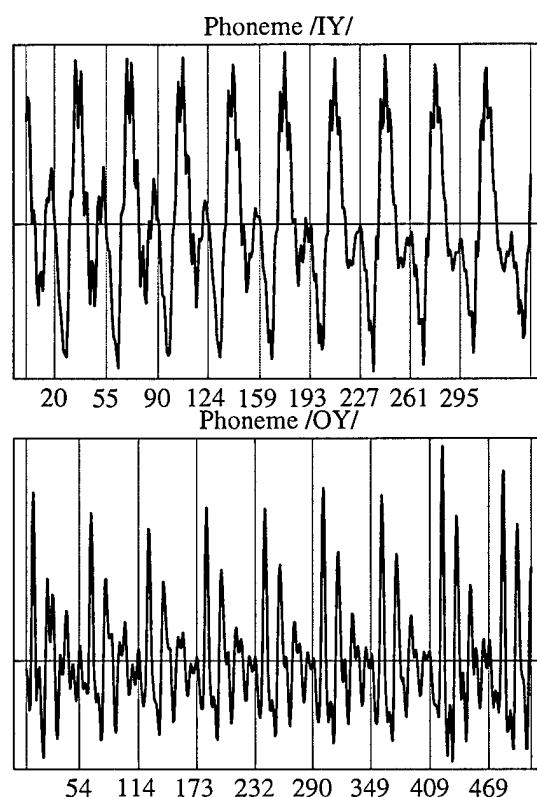


Figure 28. Data segments used in medium-scale analysis. The estimated starting points of the glottal pulses, as determined by the program, are shown by the vertical grid lines. Additional vertical grid lines were placed to clearly delineate the starting points and ending points of the segments. Note that the heuristic pulse-finding algorithm (described in Appendix C) may not perform well near the beginnings and ends of segments, as can be seen near the end of the segment of the phoneme /IY/, due to insufficient data.

The program was run for all combinations of the cases. The program was set to use 11 iterations (numbered 0 through 10) of the approximation given in Theorem 4.3.4 to determine the approximation of the speech segment. The error after each iteration of the approximation process was found. The error for each case is shown graphically in Figures 47 through 50. The minimum errors for each signal for each number of poles in the approximation are compared in Figure 51.

7.2.2 Discussion of results. The results for these analyses were mixed, as will be described below. On the one hand, the results for harmonic speech were not unexpected. However, the results for the representations of non-speech were unexpected, with one non-

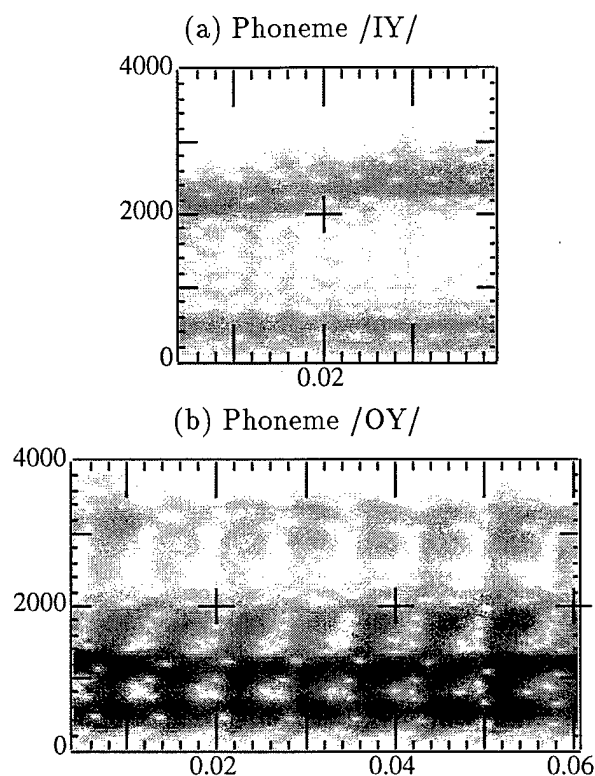


Figure 29. Spectrograms of harmonic speech segments used in medium-scale analysis. (a) Phoneme /IY/. (b) Phoneme /OY/.

speech signal being better represented than the comparison speech signal. A reasonable explanation for this occurrence is proposed.

7.2.2.1 Performance on harmonic speech. Figures 31 through 38 illustrate the behavior of the heuristic which chooses poles. Comparing these figures to the respective spectrograms in Figure 29, one can see that the poles are chosen along the formant locations first, with later poles filling in detail away from the main formants. The formant locations are especially prominent in the plots for the six pole and 10 pole approximations. In the plots for the 32 pole approximations, enough detail information has been added that a plot of poles, without magnitude information, cannot reveal the formant locations well. Examining the plots for the three pole approximations, it appears that there may be some benefit to the more rapidly decaying analysis windows in that the first two formants are more quickly filled-in.

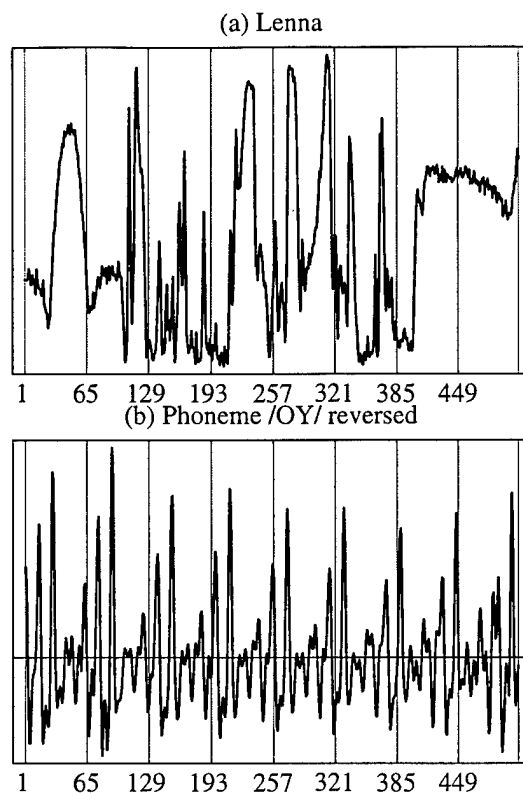


Figure 30. Non-speech data segments used in medium-scale analysis. The starting points of the analysis windows are shown by the vertical grid lines. Additional vertical grid lines were placed to clearly delineate the starting points and ending points of the segments. (a) One row of the digitized image, *Lenna*. (b) The phoneme /OY/, reversed.

Figures 39 and 46 show both the behavior of the inverse frame operator algorithm described in Theorem 4.3.4 and the circumstances under which having overlapping analysis windows gives a definite L_2 norm advantage. As can be seen in this figure, the iterative algorithm converges reasonably quickly, with only negligible improvements after five iterations.

Examination of Figures 39 through 42 reveals that, for this phoneme /IY/, having overlapping analysis windows gives a definite L_2 norm advantage with the three pole per glottal pulse approximations but a negligible improvement or even a slight degradation in the approximations with more poles per glottal pulse. Figures 43 through 46 reveal a similar story, although with this phoneme there is some noticeable advantage to having overlapping windows with the 6 poles per glottal pulse approximations.

7.2.2.2 *Performance on non-speech signals.* The results for representation of non-speech signals were not as expected. Instead of superior performance on speech as opposed to non-speech, the opposite occurred. In proposing explanations for this unexpected result, an interesting observation is made concerning longer analysis windows.

Comparing Figures 47 and 48, it can be seen that while the reversed speech was slightly less well represented with six and 10 pole approximations than the speech in the correct order, for the 32 pole approximations the difference was negligible, and for the three pole approximations, the reversed speech was actually represented better. That the reversed speech was represented so well was unexpected.

An even more unexpected result is found in comparisons between Figures 47 and 49. Here, the non-speech *Lenna* is much better represented for approximations of all tested numbers of poles. This unexpected result required further investigation. Figure 50 shows the error of approximations of the phoneme /OY/ using analysis windows aligned with glottal pulses. This figure shows data that is suggestive of much improved representation with glottal pulse alignment, but not conclusive, since to align the segments with the glottal pulses required one more analysis window, and hence, more basis elements were used for the approximations. Comparing this figure with Figures 47, 48, and 49, it can be seen that the aligned analysis windows gave a better representation of the phoneme /OY/ than the non-aligned windows, but that *Lenna* was still better represented. A comparison of the best approximations of each of the four signals is shown in Figure 51.

Because these results were so unexpected, the data were examined in more detail. Seen in Figure 52 are the data in the analysis windows used in finding the approximations to *Lenna* and /OY/. Here, it can be seen that *Lenna* appears far less regular than /OY/. However, as seen in Figure 53, the Fourier transform of the segments of *Lenna* is much simpler than that of the segments of /OY/. The implications of this is that the segments of *Lenna* may be more easily represented in our basis (in an L_2 norm sense), despite their irregular appearance.

Also revealed in Figure 53 are some short-comings of using longer analysis windows. As can be seen in the transforms of the segments of /OY/, the segments containing more data points from two glottal pulses (segments 1 through 7) have a spectrum with more detail (i.e., the more jagged appearance is due to the presence of multiple pulses in the analysis window). Segment 8, only having data from one glottal pulse, does not have this level of detail. Since the additional detail requires more poles to represent it better, longer analysis windows may be poorly represented by the same number of poles.

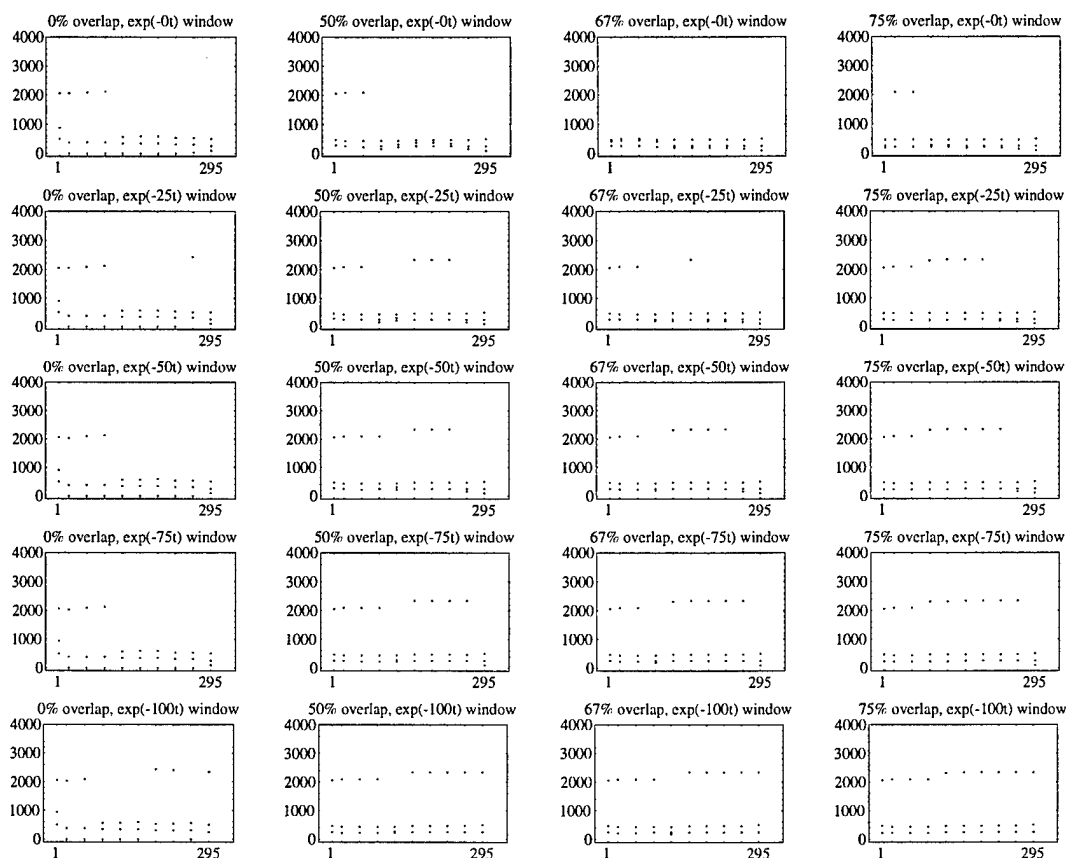


Figure 31. Poles chosen for varying window overlaps and window decay rates for the phoneme /IY/ for approximations with three poles per glottal pulse. The imaginary portion of the pole is plotted vs. the sample number of the window starting location. Only the poles determined for analysis windows with starting points within the speech segment are shown.

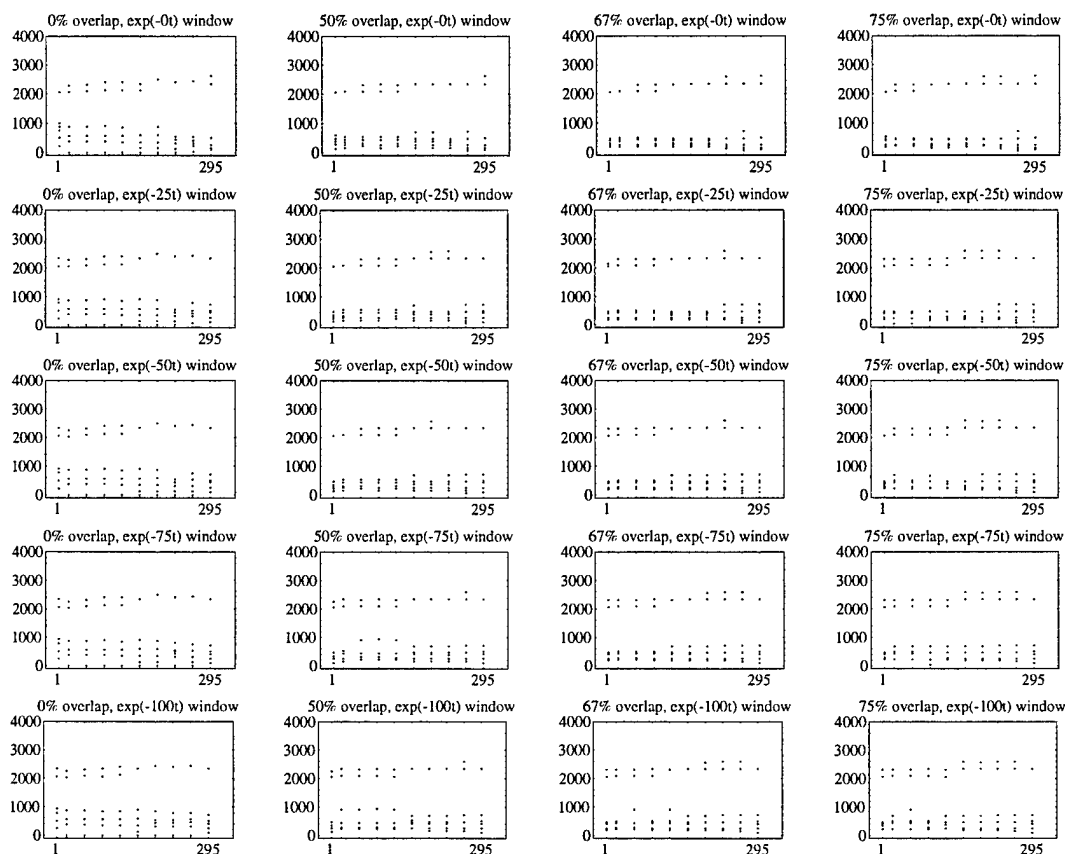


Figure 32. Poles chosen for varying window overlaps and window decay rates for the phoneme /IY/ for approximations with six poles per glottal pulse. The imaginary portion of the pole is plotted vs. the sample number of the window starting location. Only the poles determined for analysis windows with starting points within the speech segment are shown.

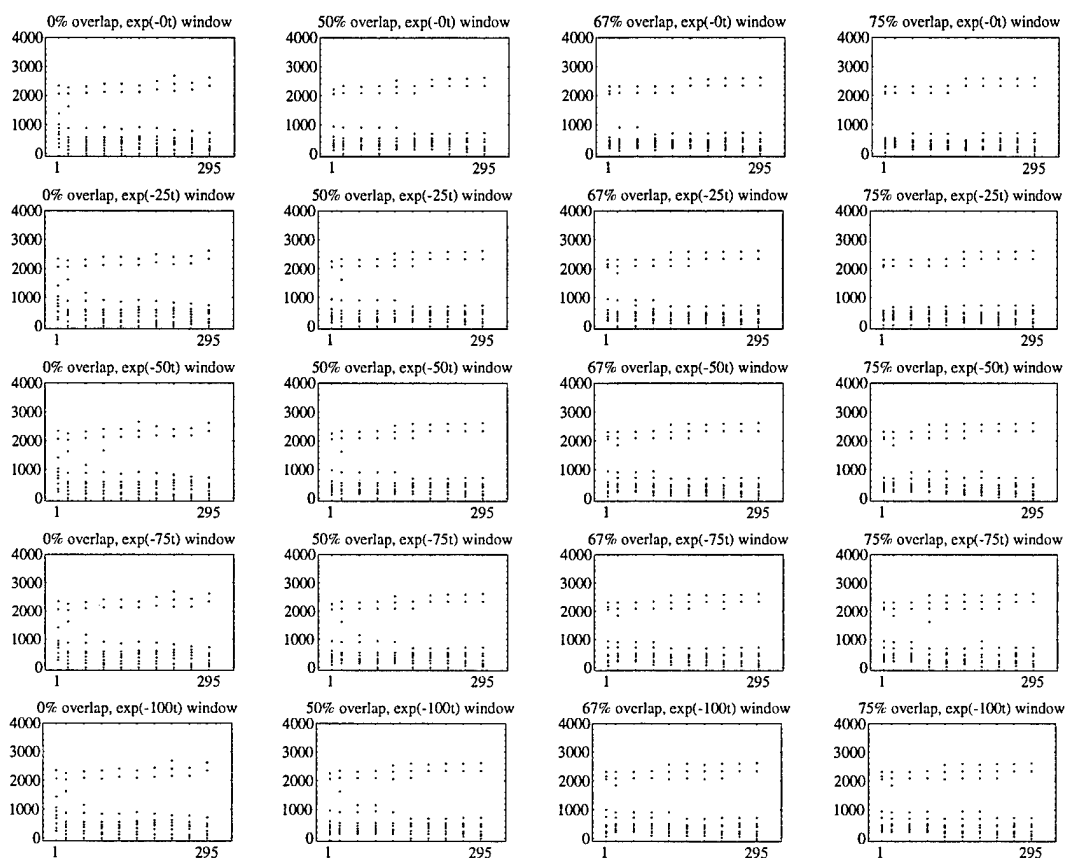


Figure 33. Poles chosen for varying window overlaps and window decay rates for the phoneme /IY/ for approximations with 10 poles per glottal pulse. The imaginary portion of the pole is plotted vs. the sample number of the window starting location. Only the poles determined for analysis windows with starting points within the speech segment are shown.

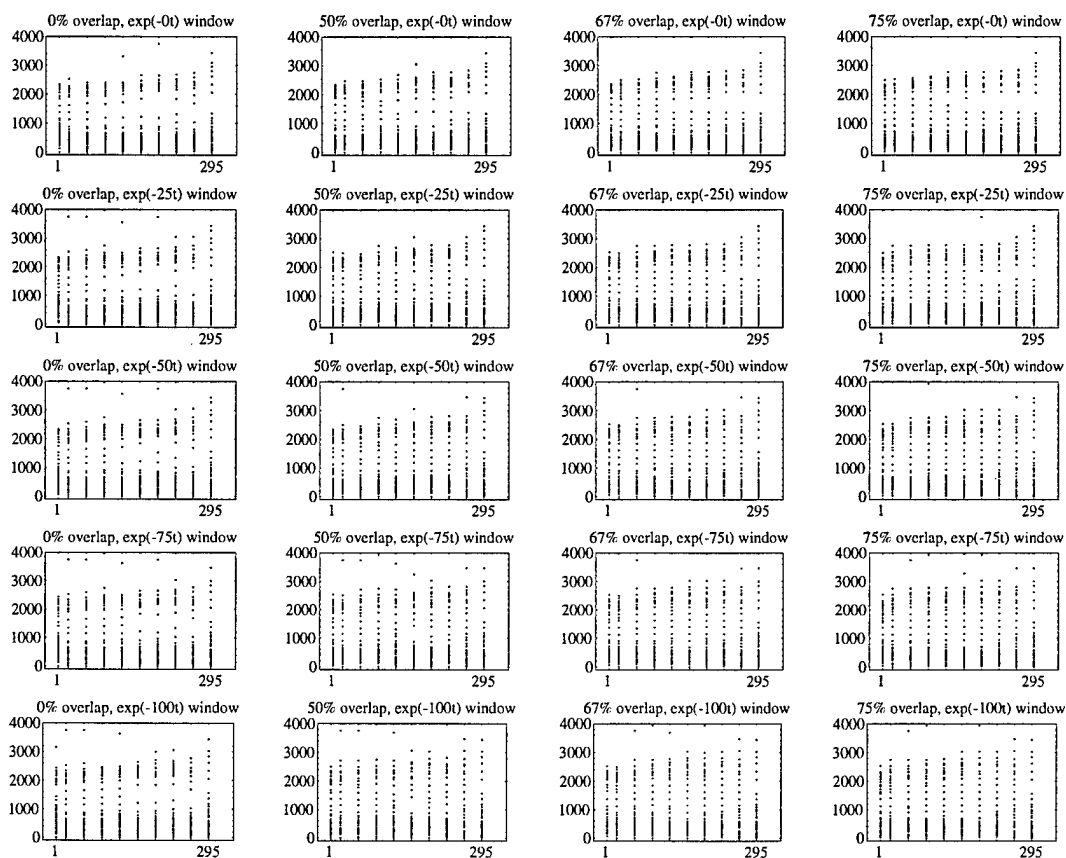


Figure 34. Poles chosen for varying window overlaps and window decay rates for the phoneme /IY/ for approximations with 32 poles per glottal pulse. The imaginary portion of the pole is plotted vs. the sample number of the window starting location. Only the poles determined for analysis windows with starting points within the speech segment are shown.

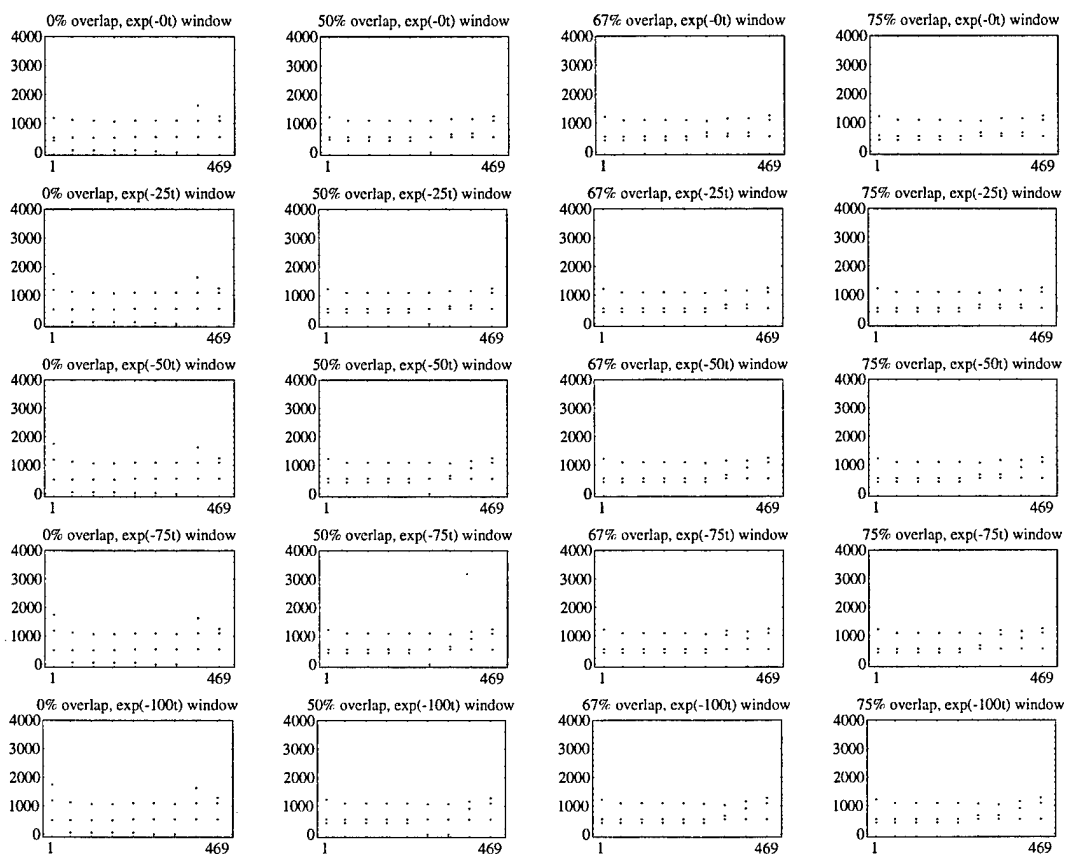


Figure 35. Poles chosen for varying window overlaps and window decay rates for the phoneme /OY/ for approximations with three poles per glottal pulse. The imaginary portion of the pole is plotted vs. the sample number of the window starting location. Only the poles determined for analysis windows with starting points within the speech segment are shown.

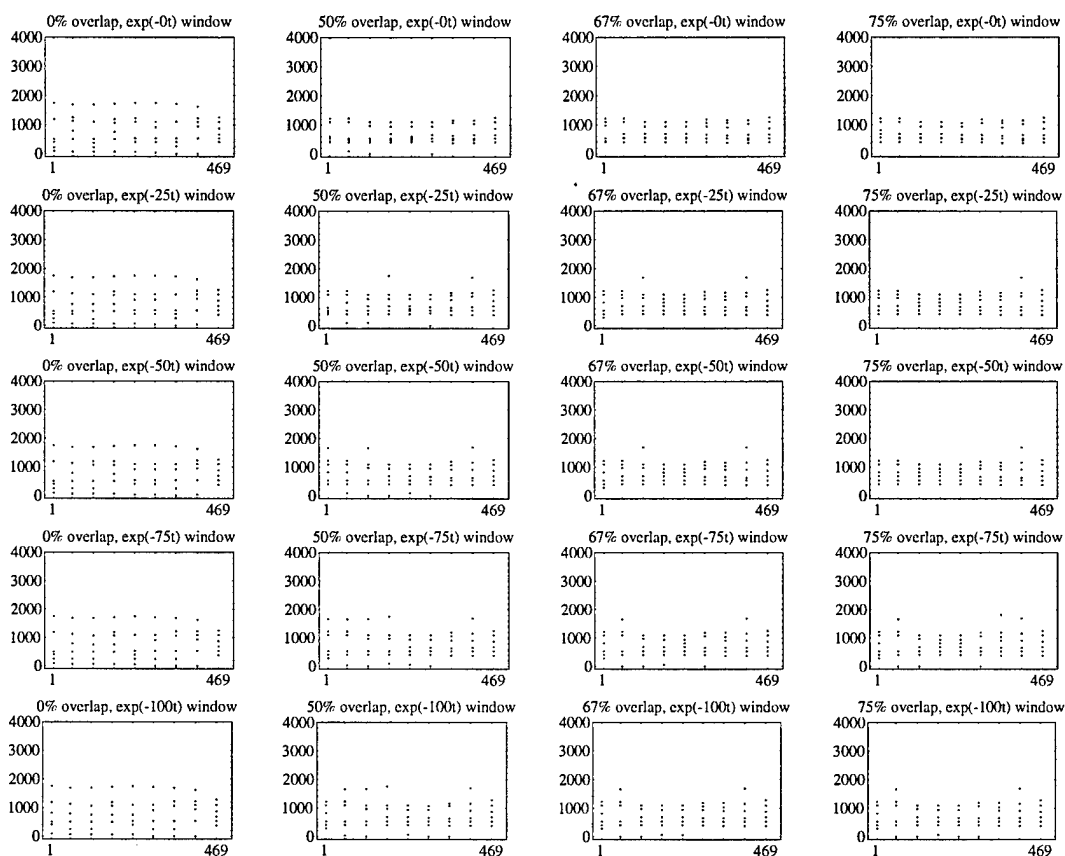


Figure 36. Poles chosen for varying window overlaps and window decay rates for the phoneme /OY/ for approximations with six poles per glottal pulse. The imaginary portion of the pole is plotted vs. the sample number of the window starting location. Only the poles determined for analysis windows with starting points within the speech segment are shown.

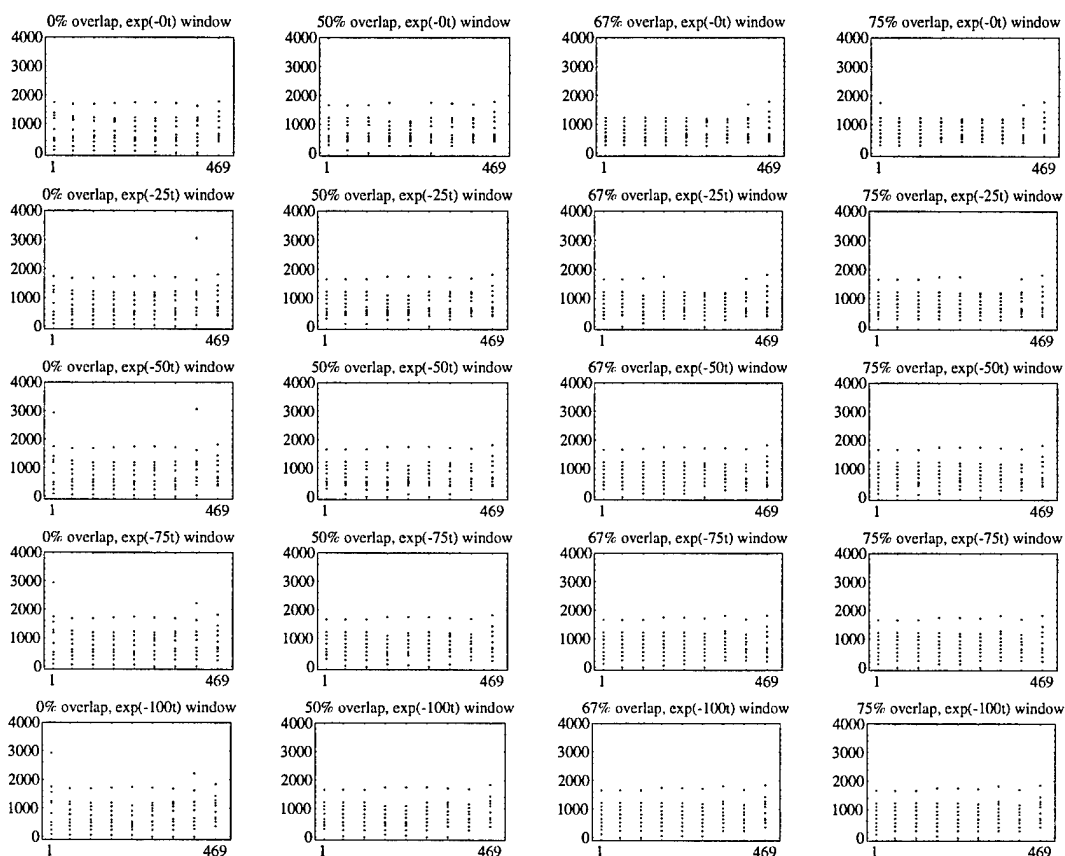


Figure 37. Poles chosen for varying window overlaps and window decay rates for the phoneme /OY/ for approximations with 10 poles per glottal pulse. The imaginary portion of the pole is plotted vs. the sample number of the window starting location. Only the poles determined for analysis windows with starting points within the speech segment are shown.

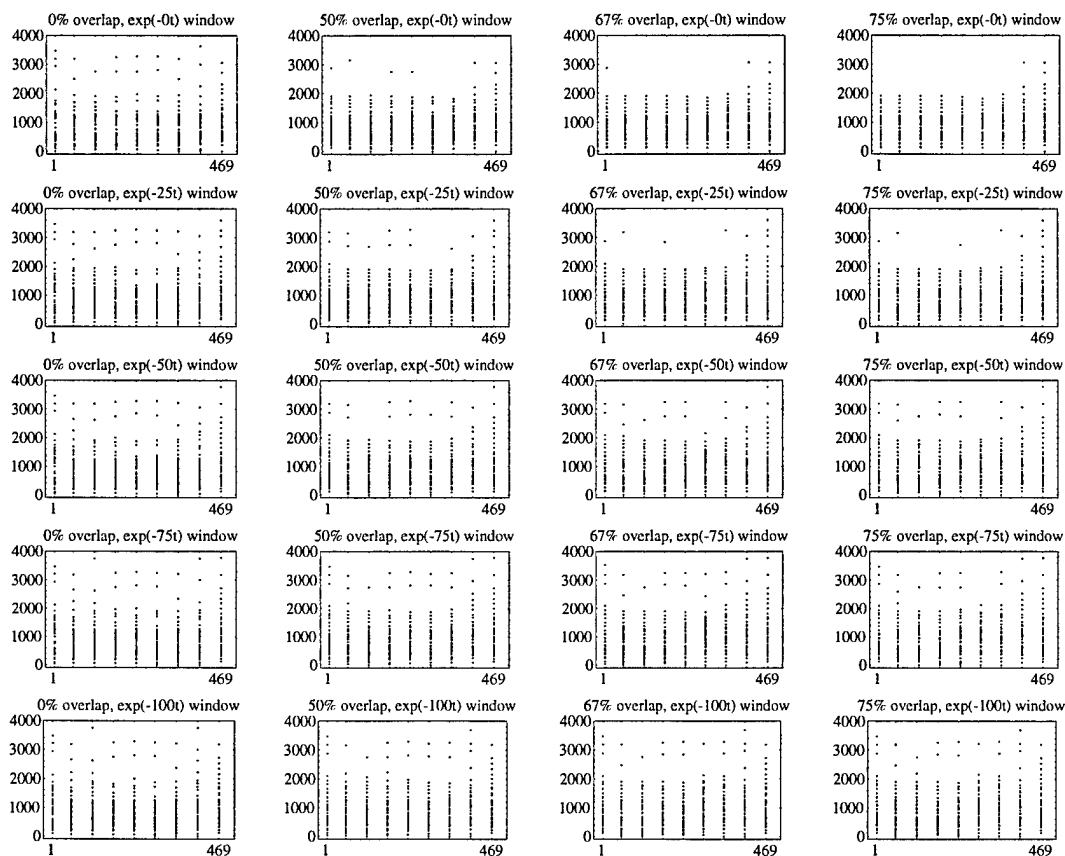


Figure 38. Poles chosen for varying window overlaps and window decay rates for the phoneme /OY/ for approximations with 32 poles per glottal pulse. The imaginary portion of the pole is plotted vs. the sample number of the window starting location. Only the poles determined for analysis windows with starting points within the speech segment are shown.

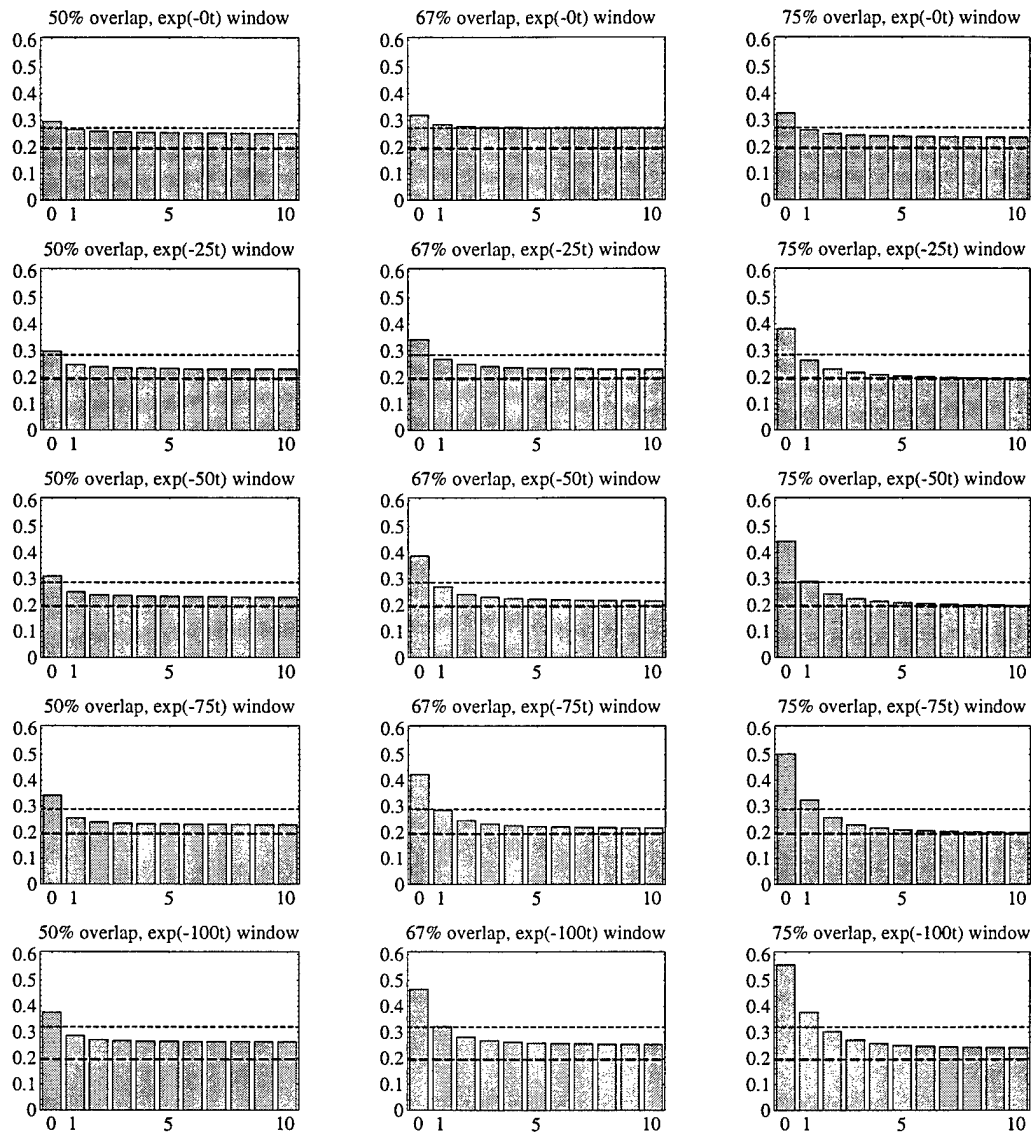


Figure 39. Number of iterations vs. normalized error for varying window overlaps and window decay rates for the phoneme /IY/ for approximations with three poles per glottal pulse. The thick dashed line marks the minimum error over all cases for a three pole approximation. For each decay rate analyzed and for window overlaps of 50%, 67% and 75%, the normalized error for the same decay rate for non-overlapping windows is shown by the thin dashed line superimposed over the bar graph.

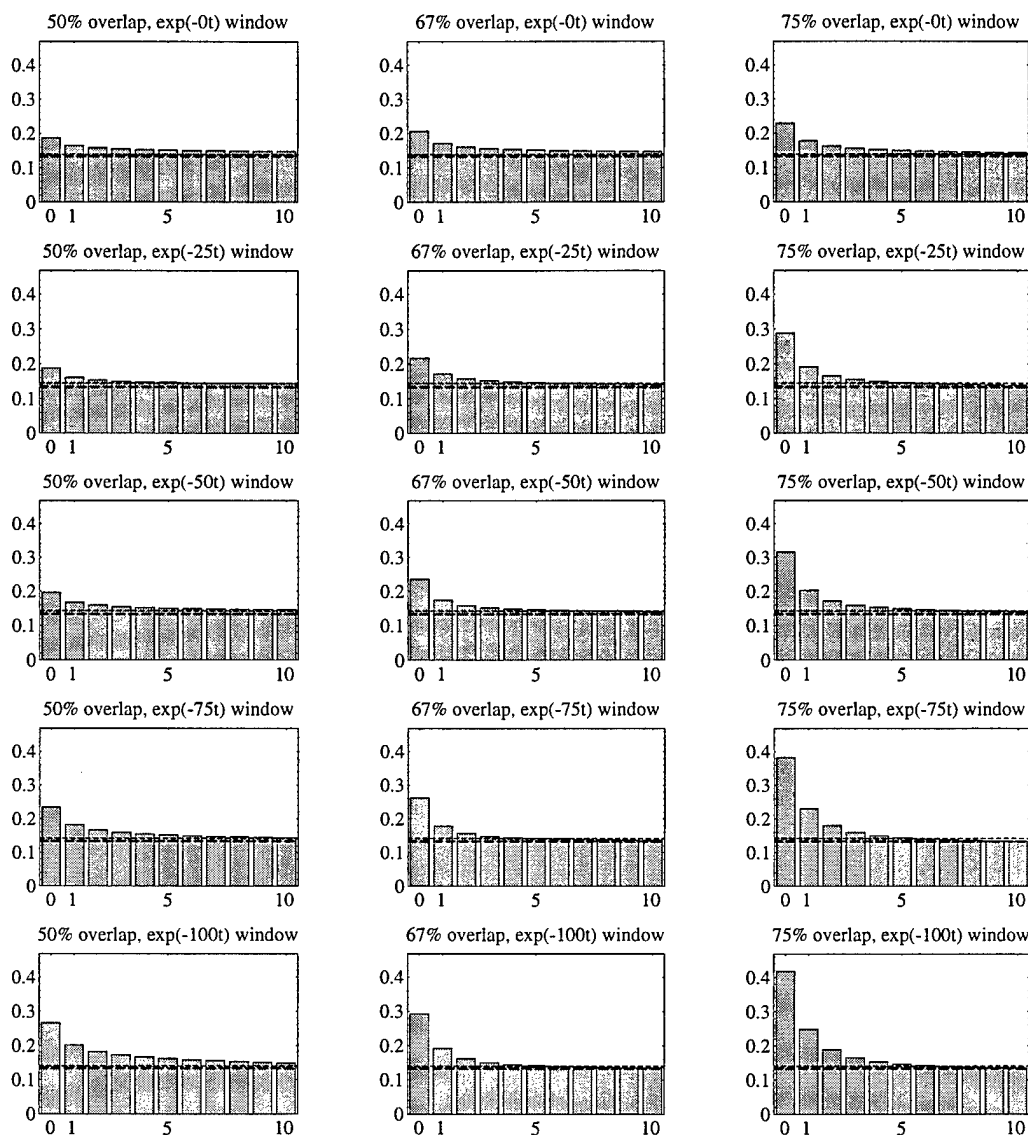


Figure 40. Number of iterations vs. normalized error for varying window overlaps and window decay rates for the phoneme /IY/ for approximations with six poles per glottal pulse. The thick dashed line marks the minimum error over all cases for a six pole approximation. For each decay rate analyzed and for window overlaps of 50%, 67% and 75%, the normalized error for the same decay rate for non-overlapping windows is shown by the thin dashed line superimposed over the bar graph.

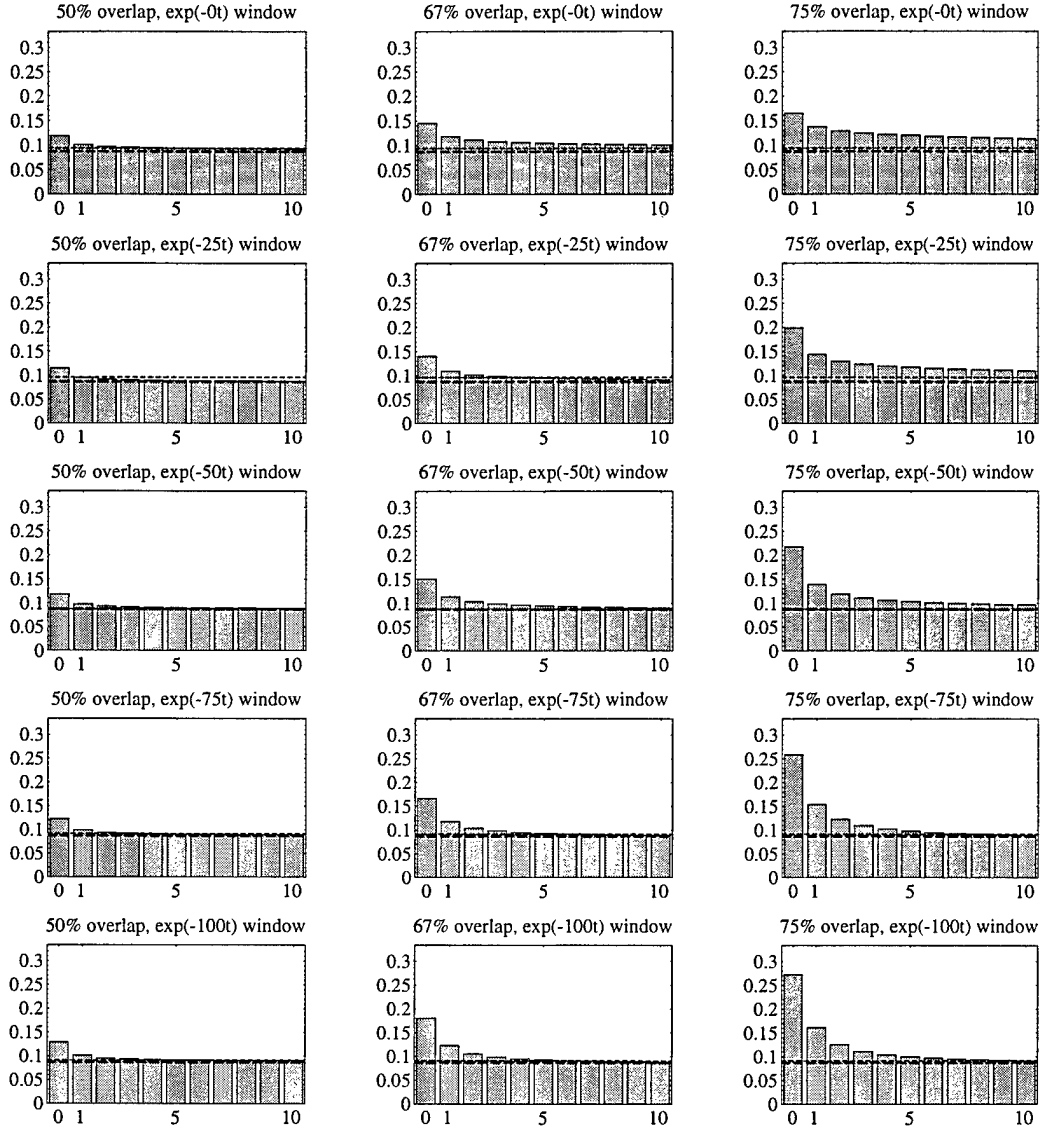


Figure 41. Number of iterations vs. normalized error for varying window overlaps and window decay rates for the phoneme /IY/ for approximations with 10 poles per glottal pulse. The thick dashed line marks the minimum error over all cases for a 10 pole approximation. For each decay rate analyzed and for window overlaps of 50%, 67% and 75%, the normalized error for the same decay rate for non-overlapping windows is shown by the thin dashed line superimposed over the bar graph.

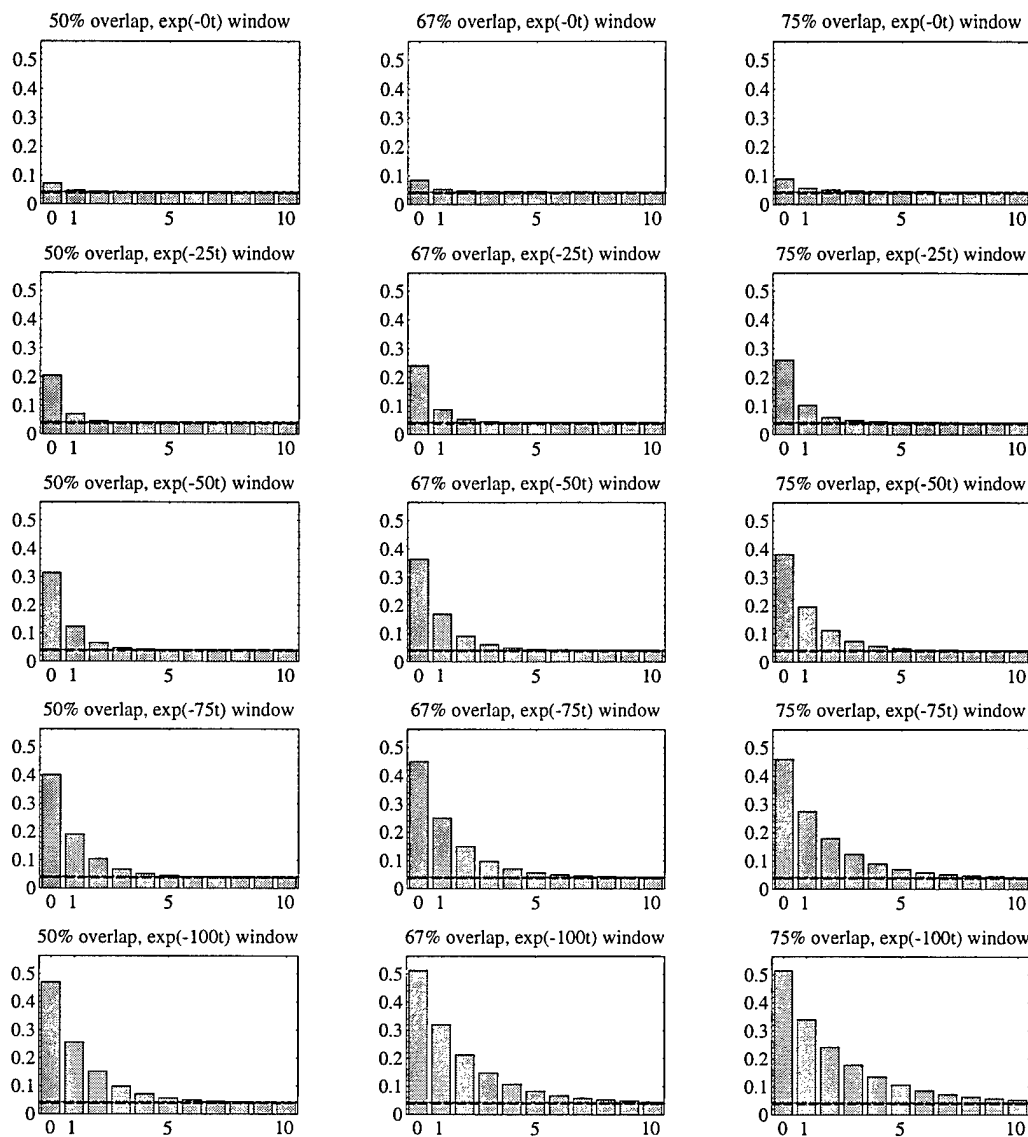


Figure 42. Number of iterations vs. normalized error for varying window overlaps and window decay rates for the phoneme /IY/ for approximations with 32 poles per glottal pulse. The thick dashed line marks the minimum error over all cases for a 32 pole approximation. For each decay rate analyzed and for window overlaps of 50%, 67% and 75%, the normalized error for the same decay rate for non-overlapping windows is shown by the thin dashed line superimposed over the bar graph.

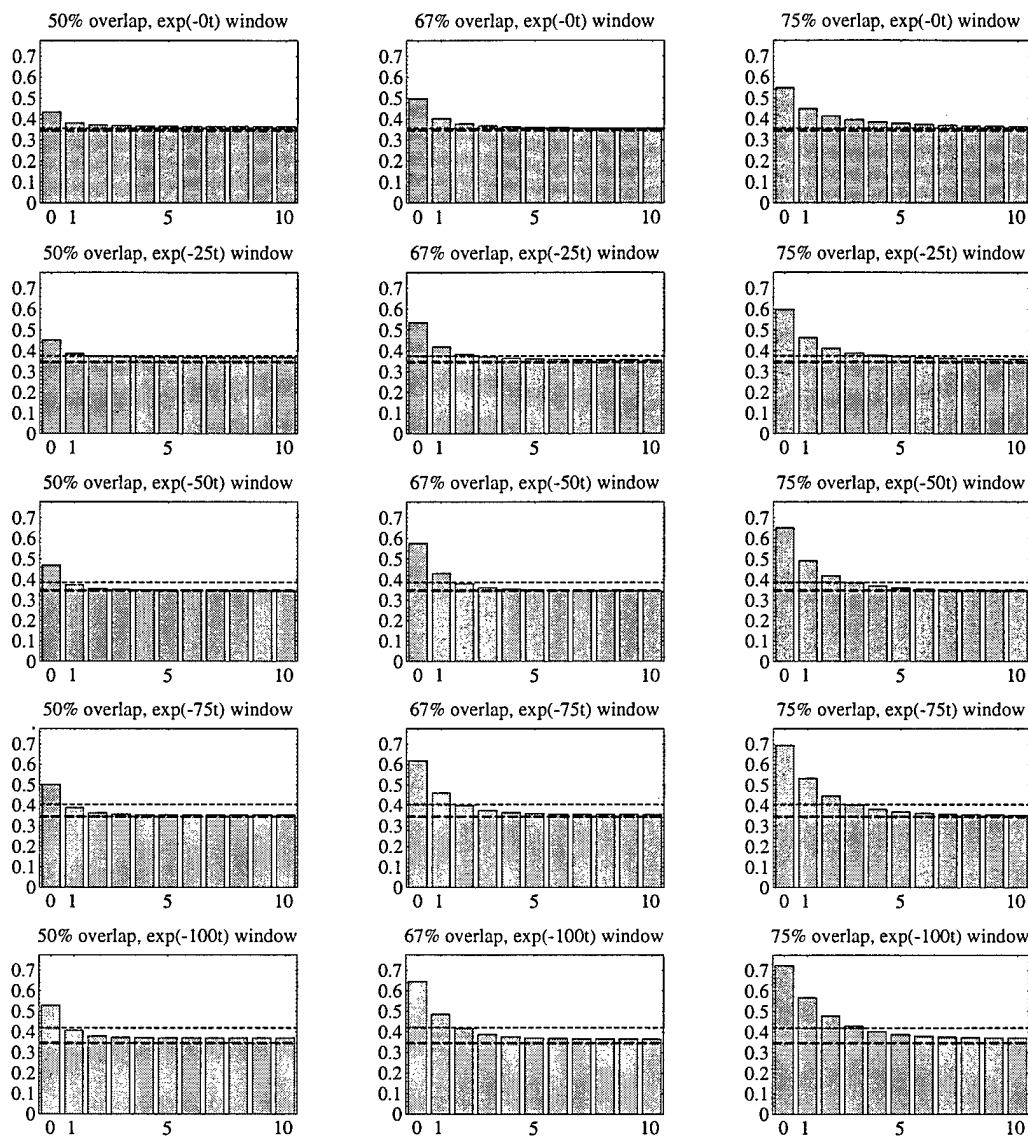


Figure 43. Number of iterations vs. normalized error for varying window overlaps and window decay rates for the phoneme /OY/ for approximations with three poles per glottal pulse. The thick dashed line marks the minimum error over all cases for a three pole approximation. For each decay rate analyzed and for window overlaps of 50%, 67% and 75%, the normalized error for the same decay rate for non-overlapping windows is shown by the thin dashed line superimposed over the bar graph.

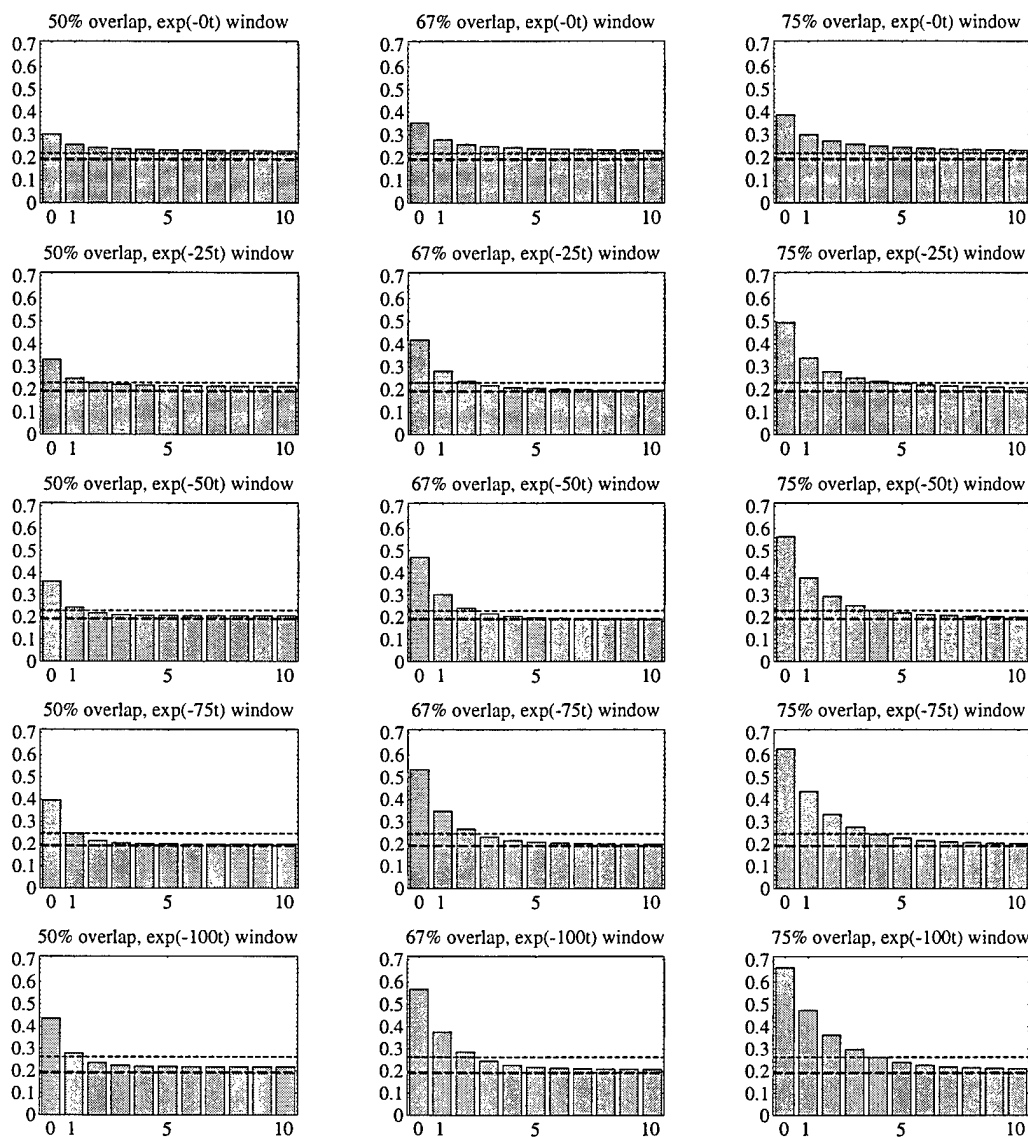


Figure 44. Number of iterations vs. normalized error for varying window overlaps and window decay rates for the phoneme /OY/ for approximations with six poles per glottal pulse. The thick dashed line marks the minimum error over all cases for a six pole approximation. For each decay rate analyzed and for window overlaps of 50%, 67% and 75%, the normalized error for the same decay rate for non-overlapping windows is shown by the thin dashed line superimposed over the bar graph.

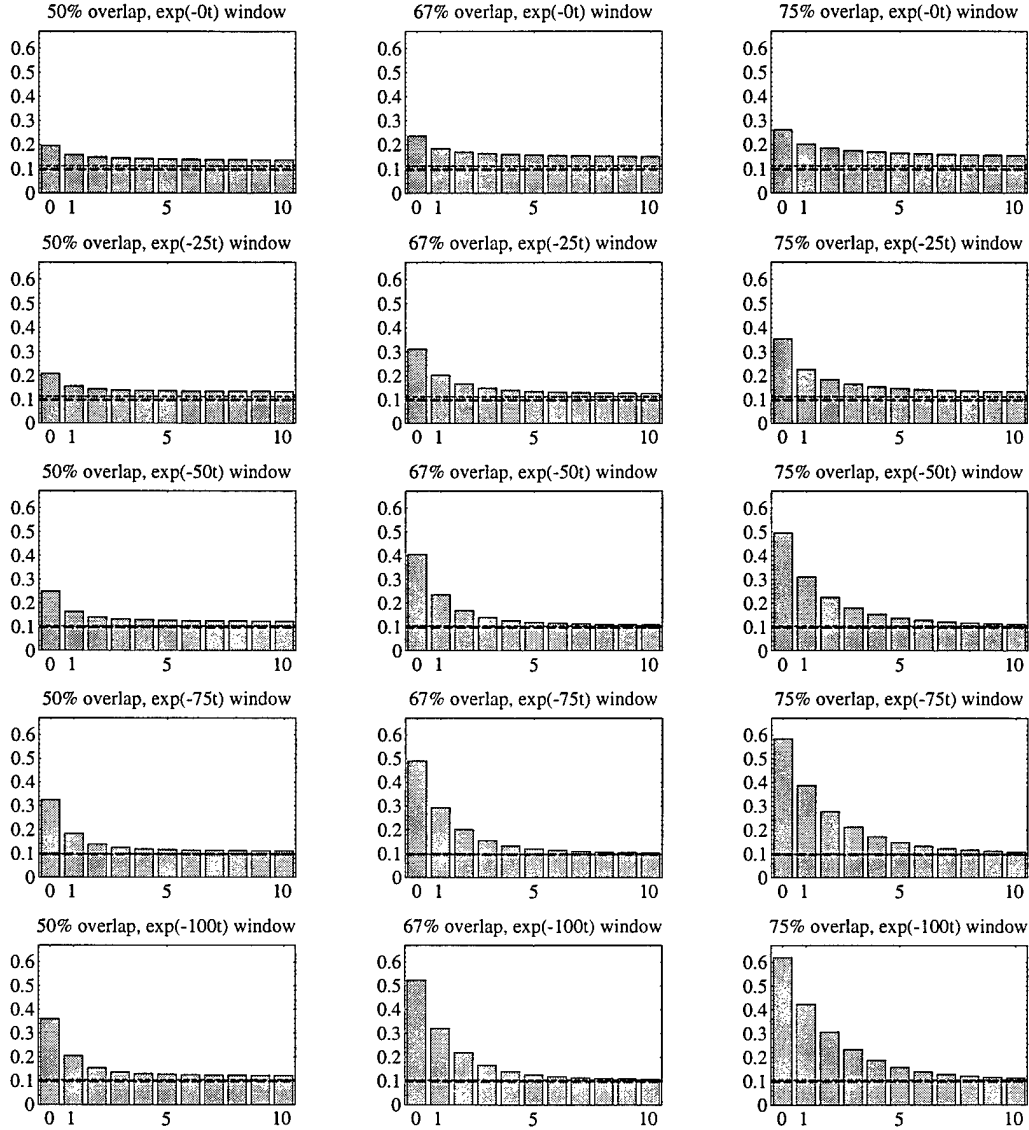


Figure 45. Number of iterations vs. normalized error for varying window overlaps and window decay rates for the phoneme /OY/ for approximations with 10 poles per glottal pulse. The thick dashed line marks the minimum error over all cases for a 10 pole approximation. For each decay rate analyzed and for window overlaps of 50%, 67% and 75%, the normalized error for the same decay rate for non-overlapping windows is shown by the thin dashed line superimposed over the bar graph.

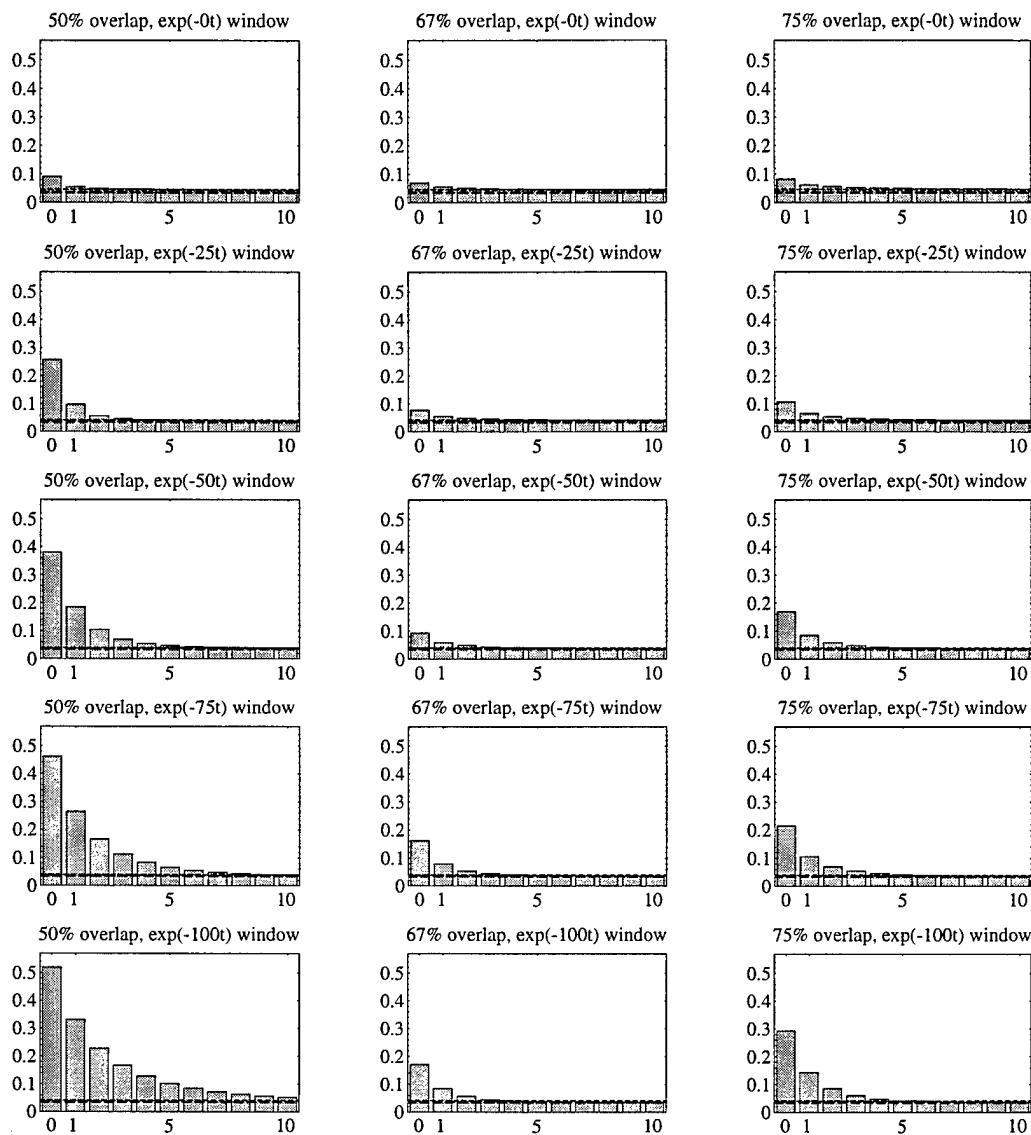


Figure 46. Number of iterations vs. normalized error for varying window overlaps and window decay rates for the phoneme /OY/ for approximations with 32 poles per glottal pulse. The thick dashed line marks the minimum error over all cases for a 32 pole approximation. For each decay rate analyzed and for window overlaps of 50%, 67% and 75%, the normalized error for the same decay rate for non-overlapping windows is shown by the thin dashed line superimposed over the bar graph.

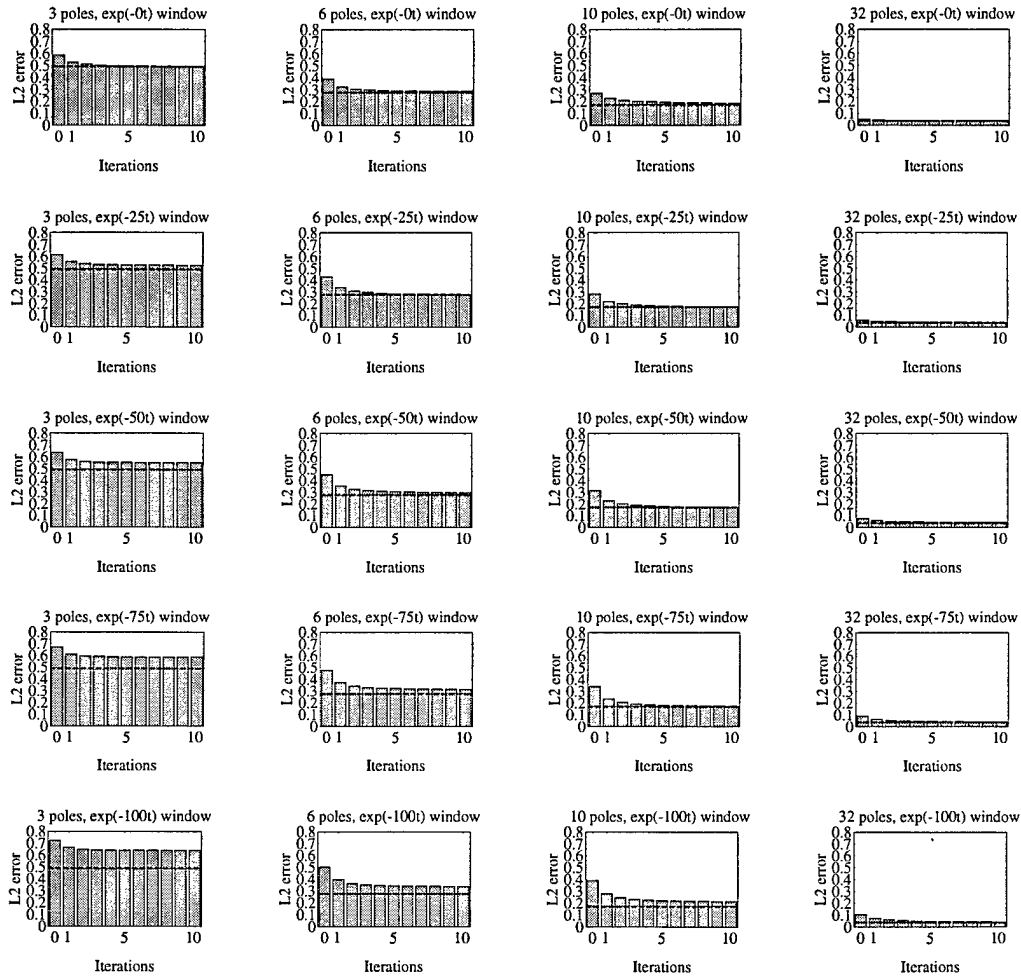


Figure 47. Number of iterations vs. normalized error for a 50% window overlap, evenly spaced analysis windows, and varying window decay rates and numbers of poles for the phoneme /OY/. The thick dashed line marks the minimum error over all cases of approximations with the same number of poles.

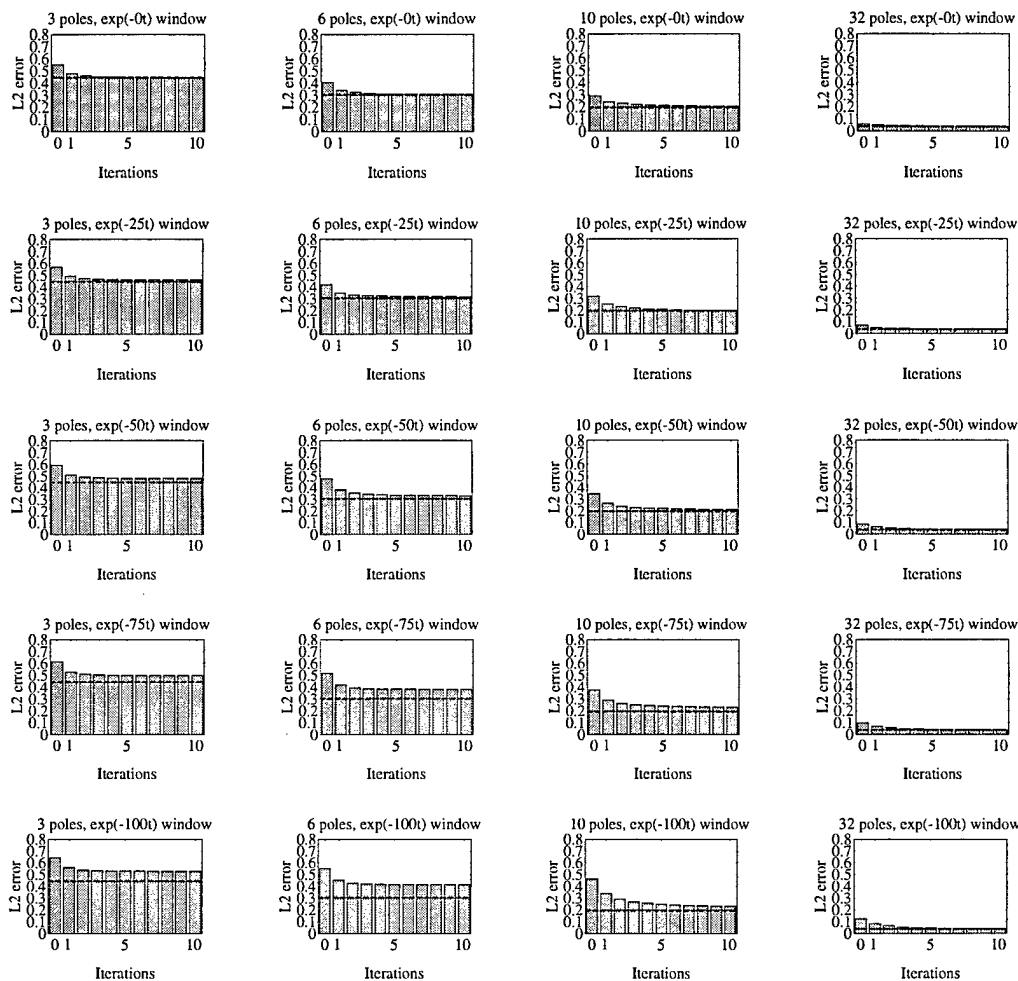


Figure 48. Number of iterations vs. normalized error for a 50% window overlap, evenly spaced analysis windows, and varying window decay rates and numbers of poles for the phoneme /OY/, reversed. The thick dashed line marks the minimum error over all cases of approximations with the same number of poles.

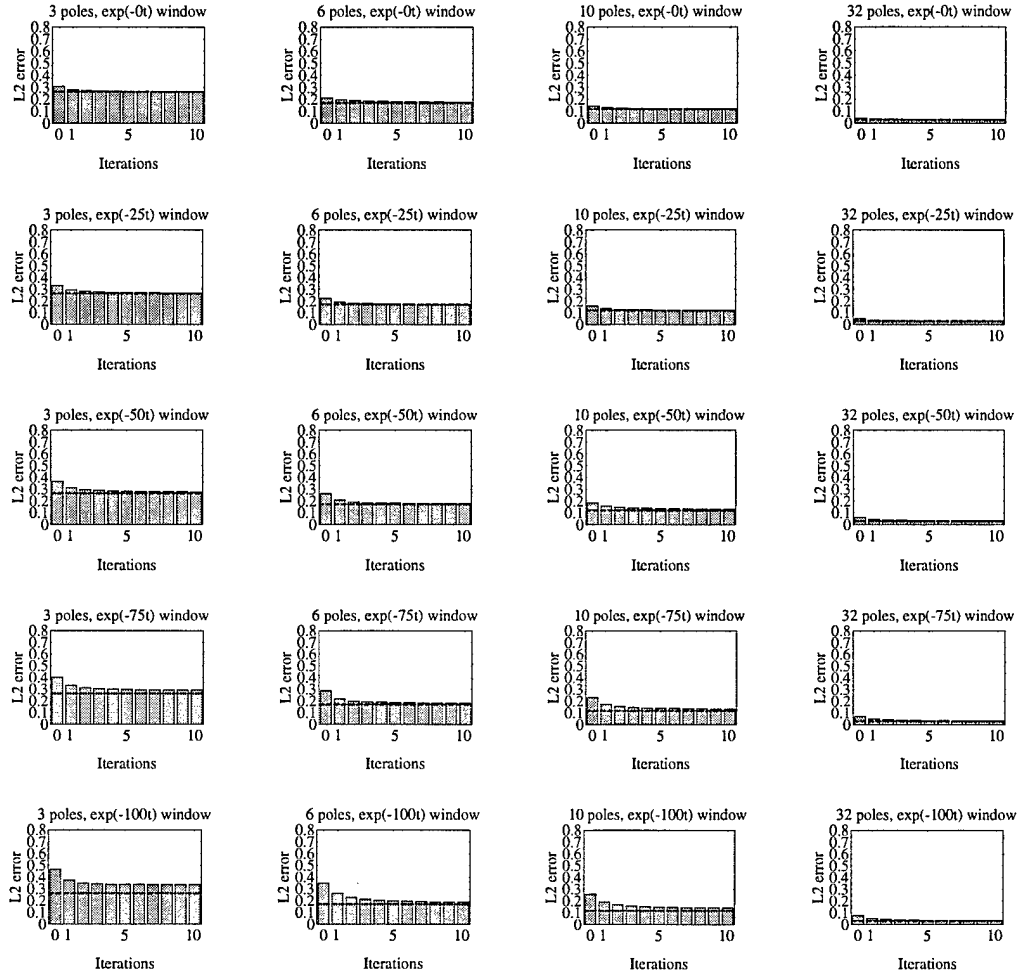


Figure 49. Number of iterations vs. normalized error for a 50% window overlap, evenly spaced analysis windows, and varying window decay rates and numbers of poles for a row of the digitized image, *Lenna*. The thick dashed line marks the minimum error over all cases of approximations with the same number of poles.

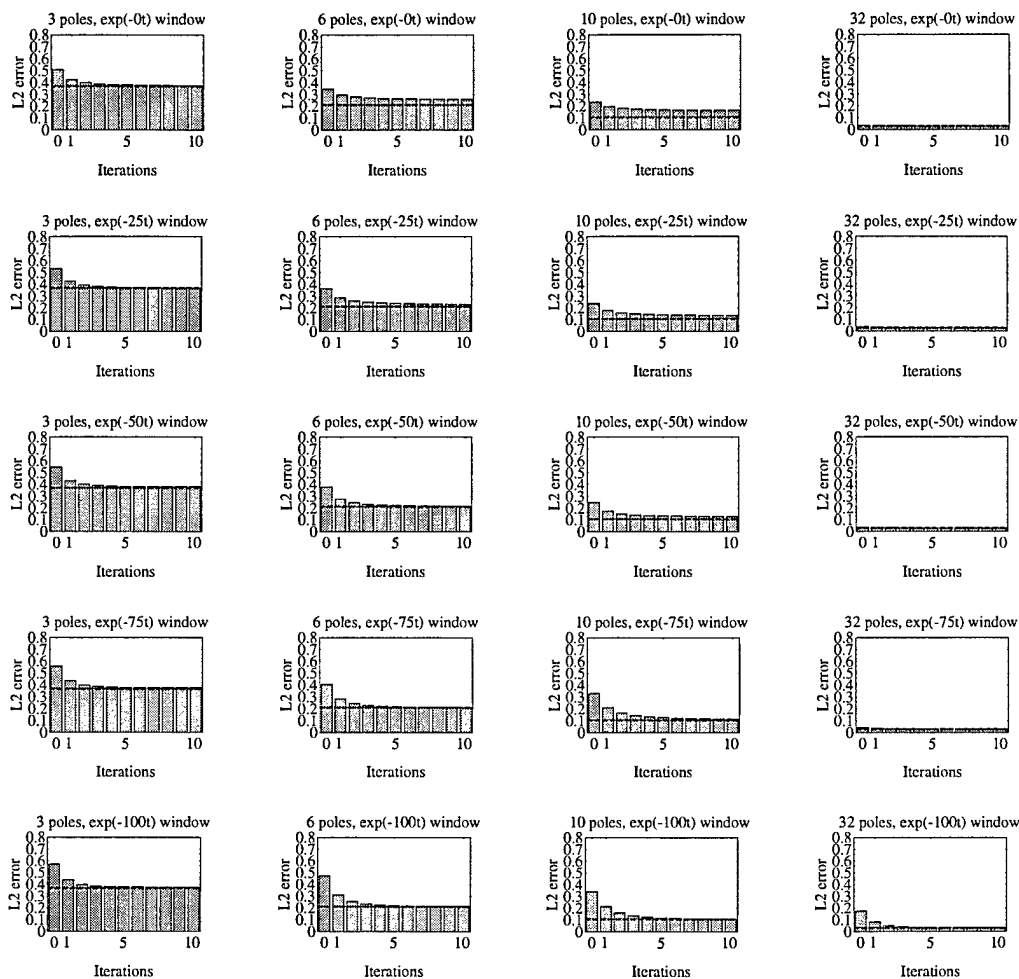


Figure 50. Number of iterations vs. normalized error for a 50% window overlap and varying window decay rates and number of poles for the phoneme /OY/ with analysis windows aligned with glottal pulses. The thick dashed line marks the minimum error over all cases of approximations with the same number of poles.

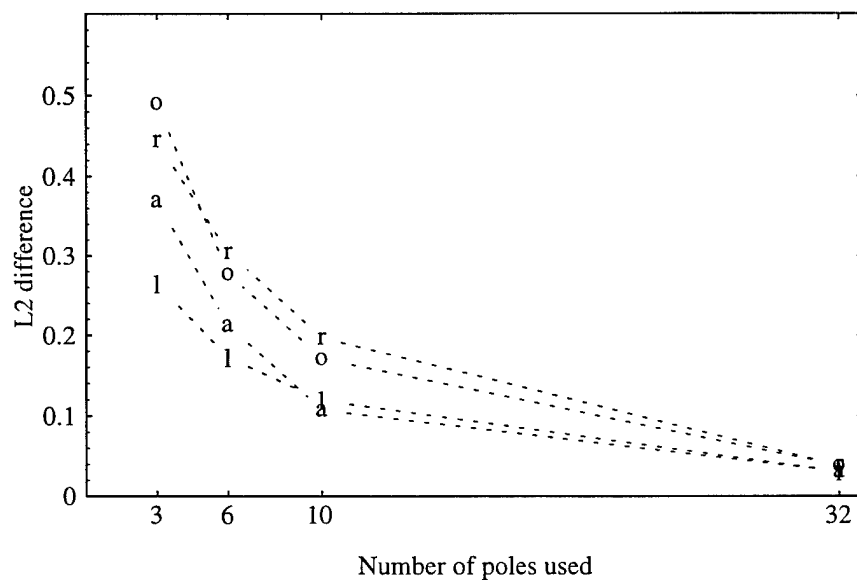
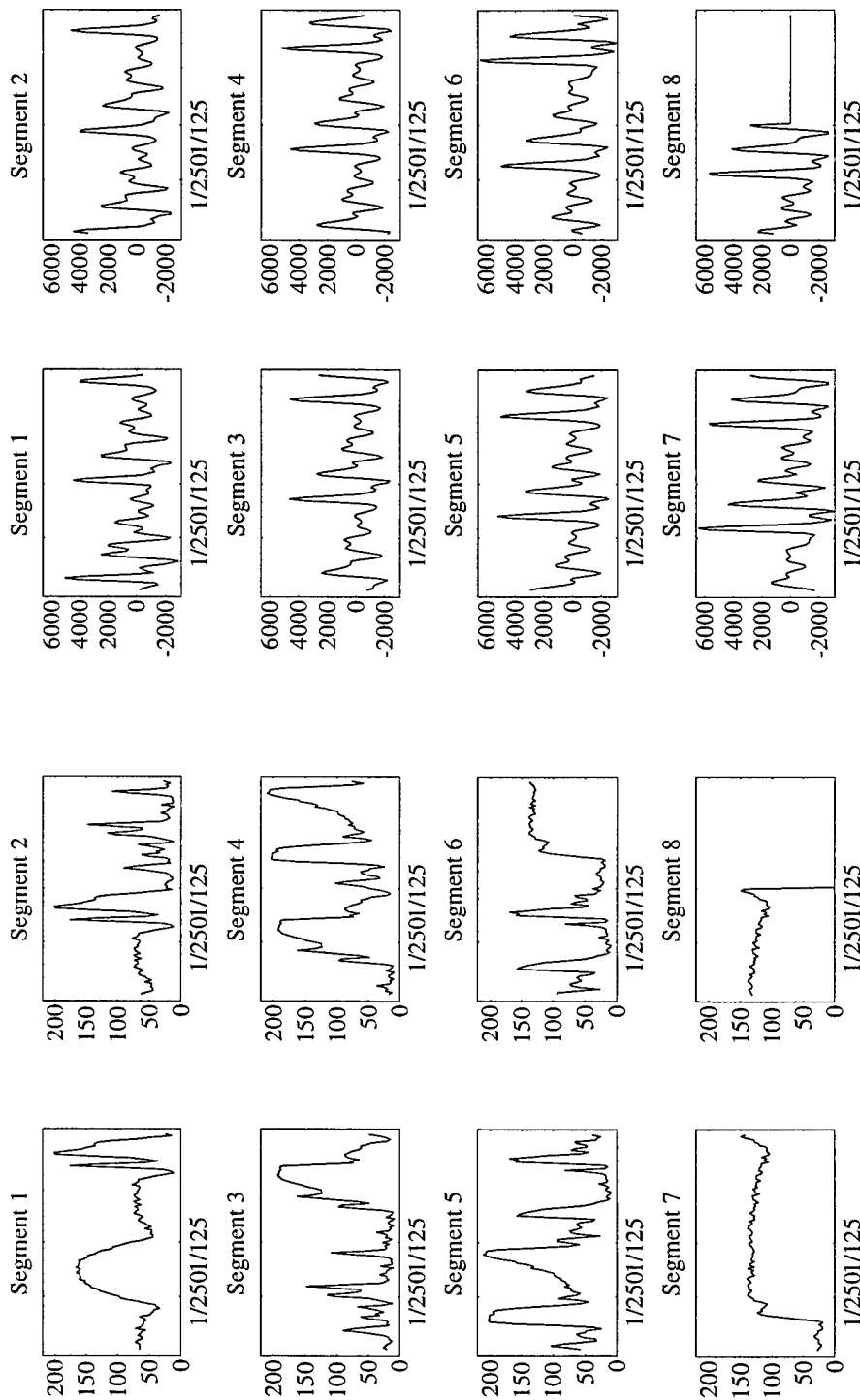


Figure 51. Normalized error for approximation of various non-speech and speech samples. For each sample and each number of poles used, the minimum error over all window decay rates is plotted. Data points denoted “o” mark the normalized error for the speech phoneme /OY/. Those denoted “r” and “l” mark the normalized error for the reversed phoneme /OY/ and the row of the digitized image *Lenna*, respectively. The data points denoted “a”, shown for comparison purposes, mark the normalized error of approximations of the phoneme /OY/ with analysis windows aligned with the glottal pulses.



(a) Segments used for signal *Lenna*

(b) Segments used for signal */OY/*

Figure 52. Non-aligned segments used in finding the approximations of *Lenna* and */OY/*. Note that these segments overlap by 50% and that the last one is zero padded. The zeroth segment, padded before with zeros, is not shown. Shown are the segments used for the approximations for (a) *Lenna* and (b) */OY/*.

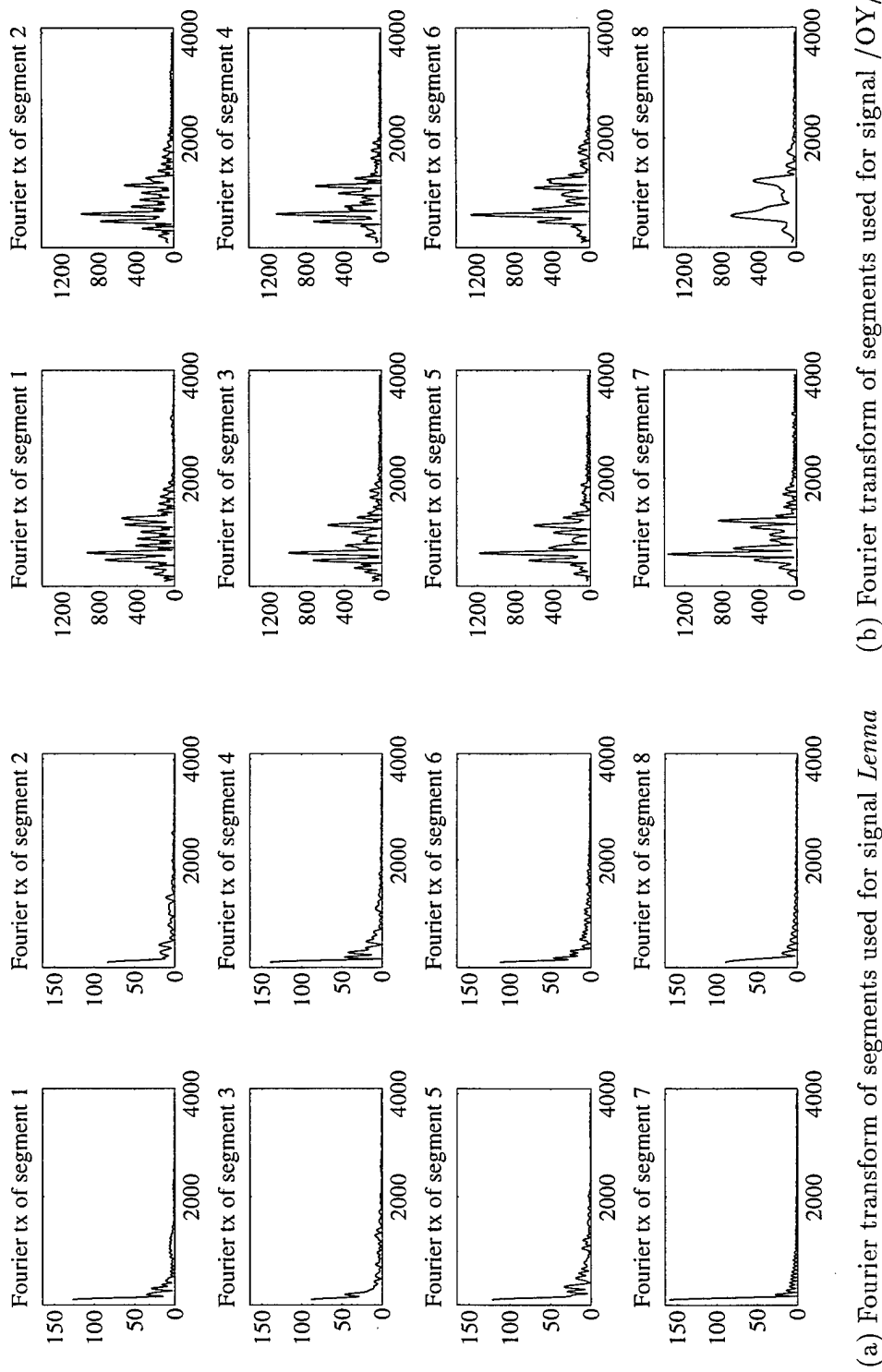


Figure 53. Fourier transforms of on-aligned segments used in finding the approximations of *Lenna* and *OY*. Note that these segments overlap by 50% and that the last one is zero padded. The zeroth segment, padded before with zeros, is not shown. Shown are the Fourier transforms of segments used for the approximations for (a) *Lenna* and (b) *OY*.

7.3 Large-scale analysis

The fine and medium scale analyses examined aspects of the mathematics and heuristics on a small scale – too small for listening tests. However, in speech processing, the only test for accuracy generally accepted as reliable is listening tests. In addition, the results of the previous sections were on a very limited number of phonemes. Thus there is no guarantee that the results extend to longer lengths of more varied speech. The large scale analysis done here is intended to examine both of these issues.

7.3.1 Description of large scale analyses. The purpose of this analysis is to examine the performance of the program on longer segments of digitized speech. Both clean speech and noisy speech of varying signal-to-noise-ratio (SNR) are used in this analysis. All noise is additive Gaussian white noise.

Two complete sentences from the TIMIT database, *sa1* spoken by female speaker *fcmm0* and *sx194* spoken by male speaker *mcmj0*, are used in this analysis. To create the noisy versions of these sentences, Gaussian white noise of an amplitude necessary to create the desired SNR was added to each sentence. The SNRs chosen were 10 dB, 6 dB, 3 dB and 0 dB, calculated with respect to the entire digitized sentence according to

$$\text{SNR} = 20 \log_{10} \frac{\sigma_s}{\sigma_n},$$

where σ_s and σ_n are the L_2 norms of the speech and the noise, respectively.

The spectrograms of the clean and noisy sentences are shown in Figures 54 and 55. These figures illustrate the usefulness of spectrograms, which are described more fully in Section 2.1. Details which are visible in the spectrograms of clean speech are masked in the noisy speech. As the noise levels increase, more detail is lost, corresponding to greater difficulty in understanding the underlying speech.

For the cases of clean speech and the 6 dB SNR speech, approximations with one, two, three, six, 10, and 15 poles per glottal pulse, for window decays of 0, 50, and 100, and for window overlaps of 0%, 50% and 67% were found. These results are shown in Figures 56 and 57. Since the quantitative results did not vary significantly with varying window decay rates and window overlaps, analyses on the 0 dB, 3 dB, and 10 dB SNR speech was done only for window decay rates of 0 and window overlaps of 50%. These results are shown in Figures 58 and 59. Spectrograms of representative and illustrative approximations are shown in Figures 60 through 63.

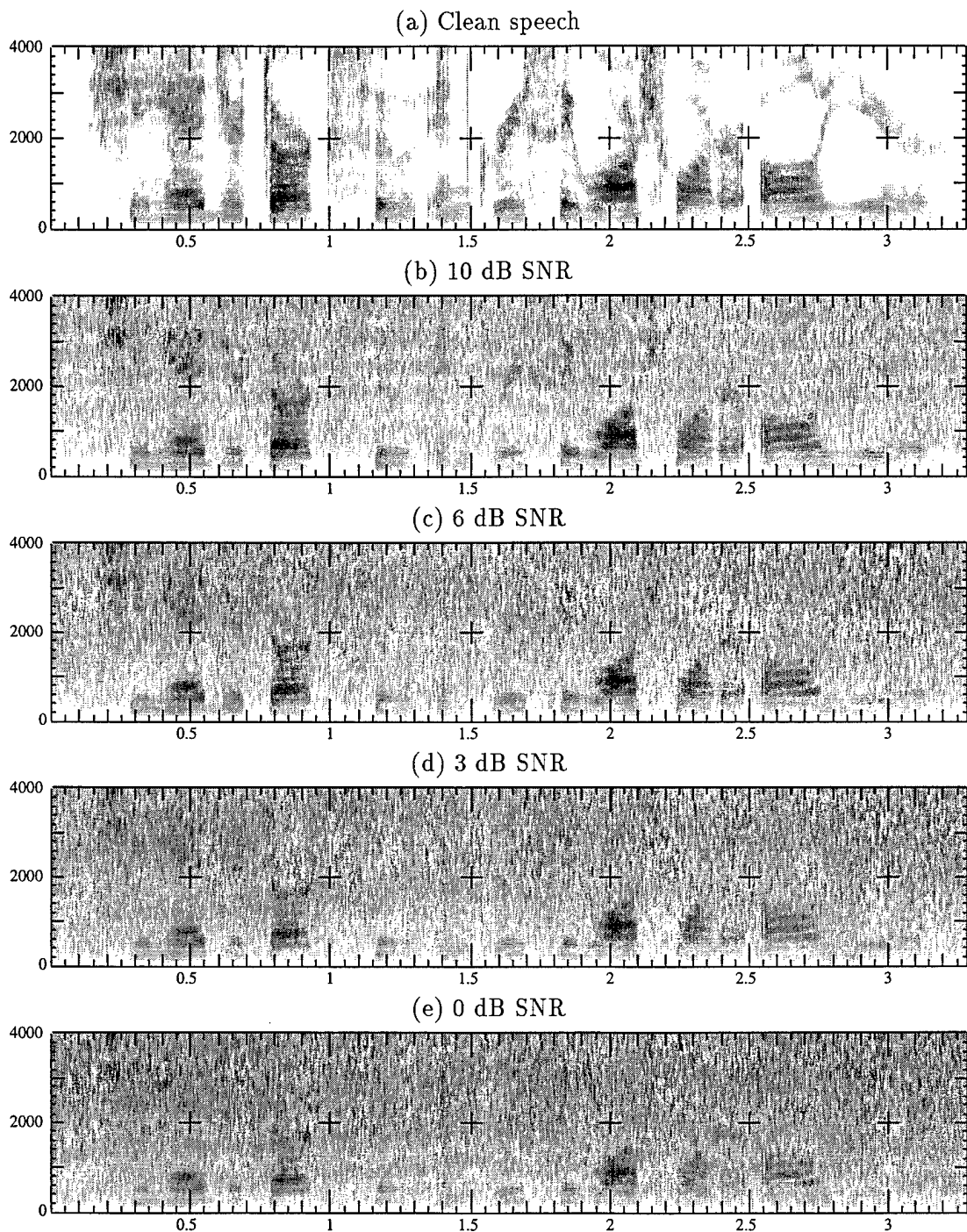


Figure 54. Spectrograms of clean and noisy speech (*sal*). (a) Clean speech. Noisy speech with a SNR of: (b) 10 dB, (c) 6 dB, (d) 3 dB, and (e) 0 dB.

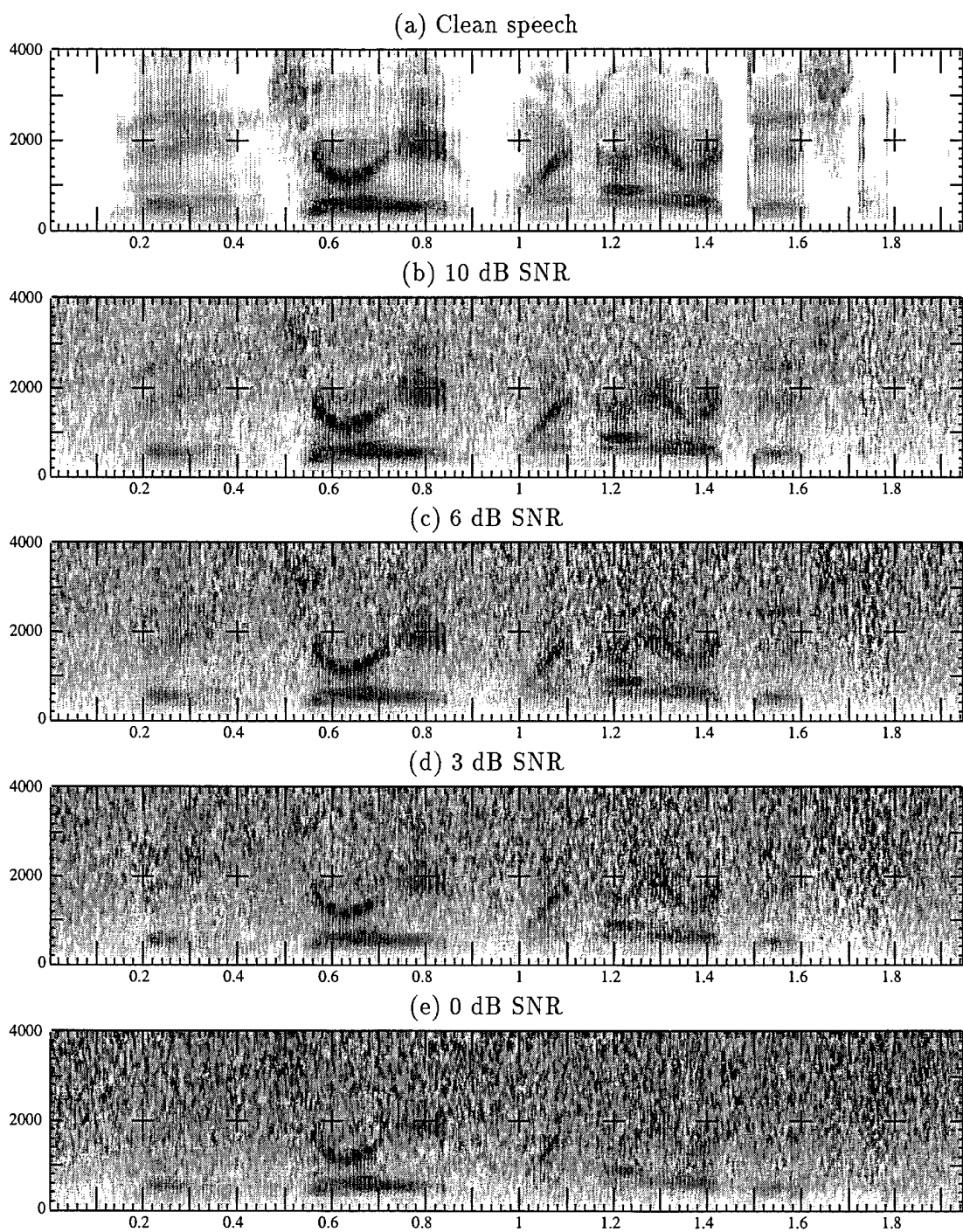


Figure 55. Spectrograms of clean and noisy speech (*sx194*). (a) Clean speech. Noisy speech with a SNR of: (b) 10 dB, (c) 6 dB, (d) 3 dB, and (e) 0 dB.

Poles per glottal pulse	Compression ratio (sentence <i>sa1</i>)	Compression ratio (sentence <i>sx194</i>)
1	24.0 : 1	27.2 : 1
2	12.0 : 1	13.6 : 1
3	8.0 : 1	9.1 : 1
6	4.0 : 1	4.5 : 1
10	2.4 : 1	2.7 : 1
15	1.6 : 1	1.8 : 1

Table 2. Compression ratios for approximations based on different numbers of poles per glottal pulse.

The ratios of compression achieved with each each approximation are shown in Table 2. This is a ratio of *numbers required*, not a ratio of *bits required*. This ratio was computed by dividing the number of samples in the segment by twice the number of poles required for the entire approximation. The factor of two accounts for the fact that both the identity of the poles being used and the coefficients of corresponding to these poles must be retained. The locations of the glottal pulses are not included in this number.

Rigorous listening tests require a trained panel of listeners, which was not available for our study. For this reason, the only extensive listening tests performed were informal ones by one untrained, but knowledgeable, listener. The goals of these tests were to listen for any unexpected auditory phenomena and to validate results.

7.3.2 Discussion of results. The results of the large-scale analyses are, overall, encouraging. Tests show that approximations based on the frame developed in Chapter IV can be used to represent speech. Such approximations based on lower numbers of poles per glottal pulse have inherent noise suppression characteristics, and yet are able to well represent fricatives (best described as colored noise) when being used to approximate clean speech. While it requires a significant number of poles to get a good approximation to speech, an intelligible approximation is achievable with far fewer.

The results are presented in three sections below. The first deals with numeric results. These results are analyses of the L_2 norm differences between signals and approximations. The next section deals with differences visible in spectrograms, which reveals some of the implications of the algorithms. The numeric and spectrogram results must be considered

suggestive until verified with listening tests. The results of some rudimentary listening tests are presented in the last section.

Note that because the pole selection algorithm is a heuristic, a better heuristic, perhaps one based on physiological considerations, might improve the results presented herein.

7.3.2.1 Numeric results. Examining Figures 56 and 57, one can see that as the number of basis elements in the approximation increases, the difference between the signal and the approximation of it decreases monotonically. This occurs in both the noisy and clean signal approximations. This is expected, since with more basis functions, the approximation should improve, whether or not the original data was clean or noisy. The results for differing analysis window decay rates and overlaps were very similar, although some audible qualitative differences were noted, as we shall discuss below.

Some more interesting behavior is seen in these figures in comparing the approximation of the noisy signal to the clean signal. For the cases of one, two, three, and six poles per glottal pulse in the approximation, the approximation of the noisy signal is closer (in L_2 norm) to the clean signal than to the noisy signal on which it is based. For the cases with 10 poles per glottal pulse, sufficient basis functions are used that the approximations of the noisy signal are closer to the noisy signal than to the clean signal, which is what one would expect with an increasing number of basis functions. This behavior supports the contention that this representation can more easily represent speech than most non-speech (in this case, Gaussian white noise).

Figures 58 and 59 show even more interesting results. As with the previous case, the approximation to the noisy speech is initially closer (in L_2 norm) to the clean speech than to the noisy speech on which it was based. For each SNR examined, the point at which the approximation to the noisy speech becomes closer to the noisy speech than to the clean occurs somewhere between six and 10 poles per glottal pulse.

Of more importance in these figures is the point at which the approximation to the noisy speech most closely resembles (in an L_2 norm sense) the clean speech. It appears that this minimal point depends on the level of noise, with the SNR and the number of poles in the minimal approximation being positively correlated. This result has some important implications to speech de-noising techniques.

An additional result, also expected, seen in Figures 58 and 59 is that for large SNR, until sufficiently many poles are added to the approximation, the noisy signal is a better

approximation to the clean one than either the noisy or the clean approximation. However, for a low SNR, even an approximation (of noisy or clean signal) based on one pole per glottal pulse is closer, in L_2 norm, to the clean signal than is the noisy one.

7.3.2.2 Spectrogram results. Examining the spectrograms in Figures 60, the first thing to be noted is that increasing numbers of poles in the approximation corresponds to a spectrogram that more closely represents the original. With one pole per glottal pulse, only one formant is clearly picked up. With two poles, two formants are visible in some places while in others the second pole contributed towards further refinement of first formant. Even with three poles per glottal pulse, the second formant is not completely filled-in and is mostly missing where it was of low amplitude. This clearly identifies an instance in which further refinements of the pole-picking heuristic is likely to produce an audible improvement in the results.

The spectrograms of Figure 61 are an illustration of the noise-suppressing characteristics of these approximations. In the areas with a strong formant structure, the first several poles of the approximation go towards refining the formant structure. The noise in these portions of the approximation do not become apparent in the spectrograms until after a large number of poles has been used.

An especially nice example of the effect Gaussian noise has on fricatives in these approximations can be seen in comparing the spectrograms of Figures 60 and 61. Following the development with additional poles of the fricatives /JH/ (“j” in “enjoy”) and /SH/ (“t” in audition), located in intervals (0.47,0.53) and (1.62,1.72), respectively, one can see in Figure 60 for clean speech, even with one pole per glottal pulse is enough to begin filling in the higher frequency noise that represent the fricative. However, for approximations to noisy speech, as in Figure 61, the colored noise of the fricative is not well represented, seemingly being masked by the Gaussian white noise added to the signal.

Figure 62 is a comparison of the spectrograms of six poles per glottal pulse approximations of clean and noisy speech for various SNRs. As can be seen here, with increasing levels of noise, the poles in the approximation are less likely to be used in refining the formant structure and more likely to go towards representing the noise.

Figure 63 is included to show the effects of the amount of overlap between analysis windows. In particular, comparing the spectrograms of the approximations to the spectrogram of the original, particularly in the areas of harmonic speech, one can see vertical striations marking the edges of the analysis windows. These striations are most prominent

for the approximation with non-overlapping windows and least apparent in the windows overlapping by 67%. It is thought that these striations may represent the static-like distortion, discussed below, reported in approximations with fewer poles and non-overlapping analysis windows.

7.3.2.3 Perceptual results. These tests are qualitative, not quantitative, in nature, and there is a strong subjective component to the results. As a reminder, these listening tests were not done with a trained panel, but rather a single knowledgeable, but untrained, test subject. Also, these were not blind tests in that the subject knew a great deal about the expected results. Therefore, these results may vary somewhat from those with other test subjects.

General quality. General listing tests were performed to evaluate the quality of the approximations. While the results for lower numbers of poles per glottal pulse were generally better than expected, the results for higher numbers of poles per glottal pulse were slightly disappointing in that the approximations were not of as high quality as hoped. Tests on varying overlaps between analysis windows indicated an advantage to fixed-size, overlapping windows over non-overlapping windows.

Surprisingly, even the approximations based on one pole per glottal pulse sound speech-like. While a naive subject would not be able to understand such an approximation, it can be understood if one knows the text of the sentence. Approximations based on two poles per glottal pulse are borderline in intelligibility, and those based on three poles per glottal pulse are definitely intelligible. However, despite being intelligible, these approximations do not sound good because of distortions introduced by the linear approximation operation.

A surprising result was that, for clean speech, a single pole per glottal pulse was sufficient to give a good rendering of the fricative /SH/ in the sentence *sz194*. This is surprising because this sound has very little harmonic nature and is best described as colored Gaussian noise. However, in speech to which noise had been added, approximations with a single pole per glottal pulse do not capture this fricative at all. Spectrograms of some of the approximations where it is apparent are shown in Figures 60 and 61, where the fricative /SH/ occurs during the time duration (1.62,1.71).

Comparing the qualities of approximations of the two sentences, the listener suggested that an approximation based on six poles per glottal pulse of the sentence *sa1*

was comparable in quality to an approximation based on 10 poles per glottal pulse of the sentence *sz194*. Also, an approximation of *sa1* based on 10 poles per glottal pulse was comparable in quality to one of *sz194* with 15 poles per glottal pulse. The reasons for this disparity are not known.

The distortion present in the approximations based on lower numbers of poles has a tonal quality, like random, short duration tones. The descriptions of it vary. One person said that it sounded like a child playing a xylophone in the background. Another said that it sounded like the music from several merry-go-rounds playing simultaneously. Regardless, as the number of poles in the approximation increase, this distortion is reduced.

In approximations of noisy speech, with increasing poles, the distortion is reduced as the representation of the noise improves, leading to a trade-off between tonal distortion and accurately reproduced noise. This trade-off will be discussed in more detail below.

As an additional note, in these tests there was a difference in quality of the distortion in approximations of female speech (*sa1*) and male speech (*sz194*). That on the female speech was noted to be more “whistly” and that on the male, more “garbly.” Since only two speakers were used, this is too small of a sample to generalize this observation. Possible explanations include pitch and formant location differences, with the female’s voice having both higher pitch and formants in higher frequencies, possibly leading to the distortions being concentrated in a higher frequency range.

Quality of speech segments. The listener also listened to short segments of the approximations to determine which segments were most easily represented by the approximations.

For sentence *sa1*, the segments “wash water” and “all year” were captured almost perfectly in the six-pole approximation, with the 10 pole approximation being only slightly better. However, of the tests performed, it required the 10 pole approximation to get a good rendering of “dark suit” and the 15 pole approximation for a good rendering of “she had.”

Segments of the sentence *sz194* required higher-pole approximations to achieve good quality. The segments “they en” and “joy it” (excerpted from “they enjoy it”) had noticeable degradation in the six pole approximation, but were captured fairly well in the 10 pole approximation. The degradation noticeable in the six pole approximation of the segment “dition” (excerpted from “audition”) is not as noticeable in the 10 pole approximation.

The “garbly” degradation is audible in both the six pole and 10 pole approximations of the segment “I au” (excerpted from “I audition”).

An additional perceptual comment was that, in these shorter segments, the distortion in the approximations was often not objectionable. In longer segments, the same distortion became annoying.

Best approximations to noisy speech. Figures 58 and 59 indicate that for a given level of noise, there is a best number of poles per glottal pulse, such that the L_2 difference between the approximation and the clean speech was minimized. Listening tests were performed to test the hypothesis that this best approximation sounds better than the other approximations. Comparisons were also done between approximations of speech with differing noise levels with similar L_2 differences from the clean speech.

As seen in Table 3, the results of the listening tests comparing approximations of noisy speech follow are as expected. In every case but one, the approximation identified as sounding best was the closest or second closest in L_2 norm to the clean signal. This implies some perceptual validity to the L_2 norm in such comparisons.

As can be noted from Figures 58 and 59 and Table 3, the L_2 norm differences between the clean speech and approximations based on one pole per glottal pulse of both clean and noisy speech are very close. Perceptually, this is also true, with the one pole approximations being deemed of equal quality regardless of the noise level (of those used in our tests) of the original signal. Note that, while perceived as speech-like, these approximations are not intelligible.

The tests comparing approximations with similar L_2 differences revealed a weakness of using the L_2 norm to predict perceptual differences. The three pole approximation of the 3 dB SNR *sa1* was judged to be the same quality as the two pole approximation to the 10 dB SNR *sa1*, which was expected. However, the six pole approximation to the 10 dB SNR *sa1* was much more intelligible than the one pole approximation to the 6 dB SNR *sa1*, despite the latter being slightly closer to the clean speech in L_2 norm. This shows that even among the approximations used here, the L_2 norm is not always a reliable indicator of perceptual differences.

Overlapping analysis windows. Listening tests were performed to determine the advantage, if any, of using overlapping analysis windows. It was found that

there is little advantage to using overlapping analysis windows when working with approximations of clean speech, but that they produce better sounding results when working with noisy speech.

In clean speech, it was found that non-overlapping windows produces an approximation with a static-like distortion, which was reduced with increasing numbers of poles in the approximation. Overlapping analysis windows produced a “talking in a megaphone” distortion, with windows overlapping by 67% having more distortion than those overlapping by 50%. Again, this distortion decreased with increasing numbers of poles in the approximation. So, the difference between overlapping and non-overlapping analysis windows appears to be a choice between types of distortion.

For noisy speech, however, having overlapping analysis windows improved overall quality. For example, the 10 pole approximation to the sentence *sx194* with a noise level of 6 dB SNR was deemed awful, while the 50% and 67% overlapping windows produced a much better result.

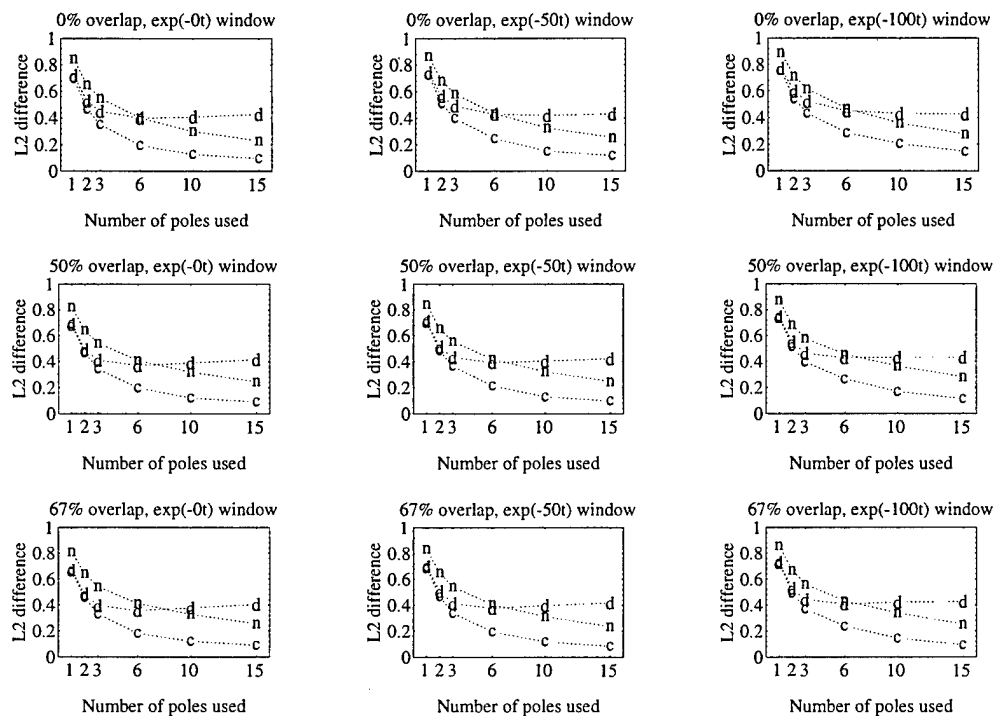


Figure 56. Normalized error for speech approximations (*sal*), for clean speech and 6 dB SNR Gaussian white noise-added speech for varying window overlaps, decay rates, and numbers of poles used. Data points denoted “c” mark the normalized difference between the clean speech and the approximation to clean speech. Similarly, “n” marks difference between noisy speech and the approximation of the noisy speech. “d” marks the difference between the original clean speech and the approximation to the noisy speech.

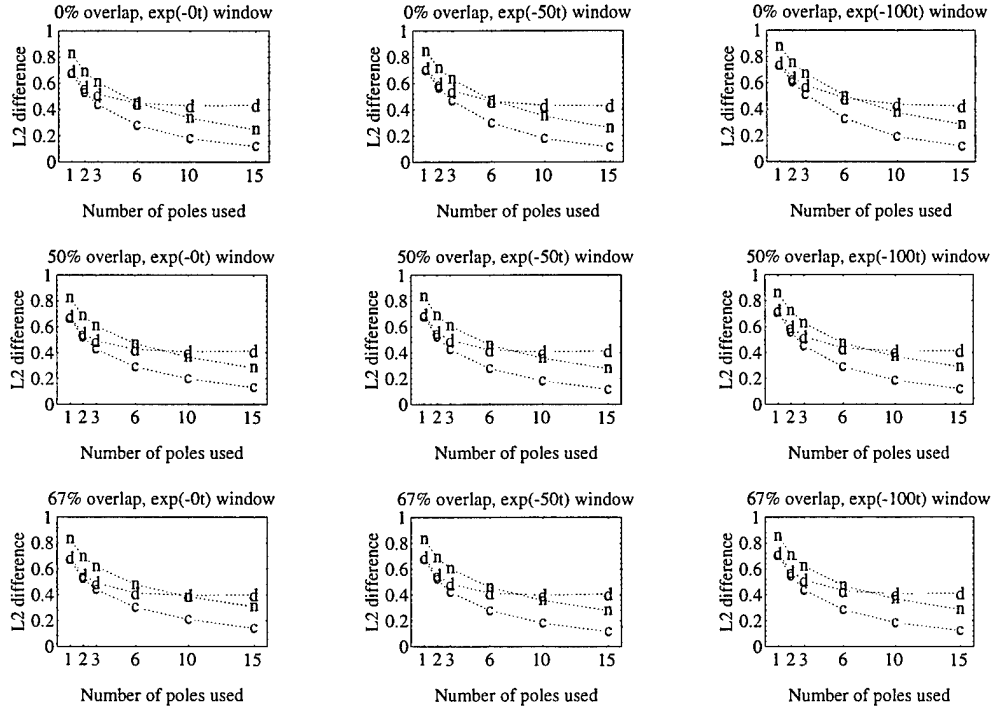


Figure 57. Normalized error for speech approximations (*sz194*), for clean speech and 6 dB SNR Gaussian white noise-added speech for varying window overlaps, decay rates, and numbers of poles used. Data points denoted “c” mark the normalized difference between the clean speech and the approximation to clean speech. Similarly, “n” marks difference between noisy speech and the approximation of the noisy speech. “d” marks the difference between the original clean speech and the approximation to the noisy speech.

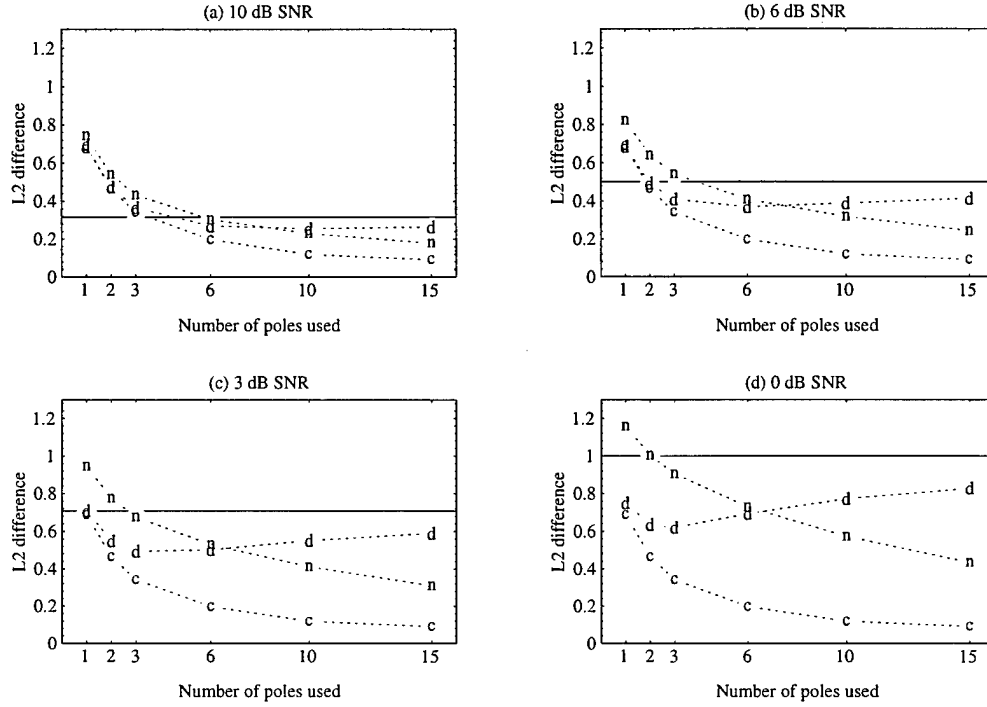


Figure 58. Normalized error for speech approximations (*sal*), for varying SNR Gaussian white noise-added speech for analysis window overlaps of 50%, window decay rates of 0, and varying numbers of poles used. Data points denoted “c” mark the normalized difference between the clean speech and the approximation to clean speech. Similarly, “n” marks difference between noisy speech and the approximation of the noisy speech. “d” marks the difference between the original clean speech and the approximation to the noisy speech. The horizontal line marks the L_2 difference between the clean and noisy signal in each case. The SNR of the data used are (a) 10 dB, (b) 6 dB, (c) 3 dB, and (d) 0 dB.

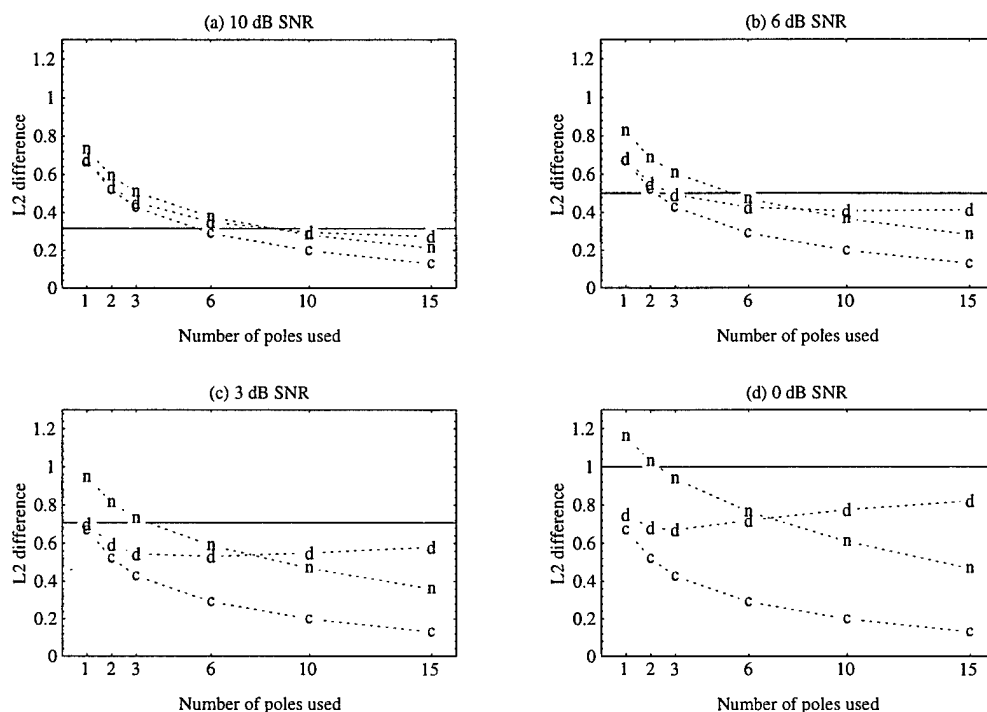


Figure 59. Normalized error for speech approximations (*sz194*), for varying SNR Gaussian white noise-added speech for analysis window overlaps of 50%, window decay rates of 0, and varying numbers of poles used. Data points denoted “c” mark the normalized difference between the clean speech and the approximation to clean speech. Similarly, “n” marks difference between noisy speech and the approximation of the noisy speech. “d” marks the difference between the original clean speech and the approximation to the noisy speech. The horizontal line marks the L_2 difference between the clean and noisy signal in each case. The SNR of the data used are (a) 10 dB, (b) 6 dB, (c) 3 dB, and (d) 0 dB.

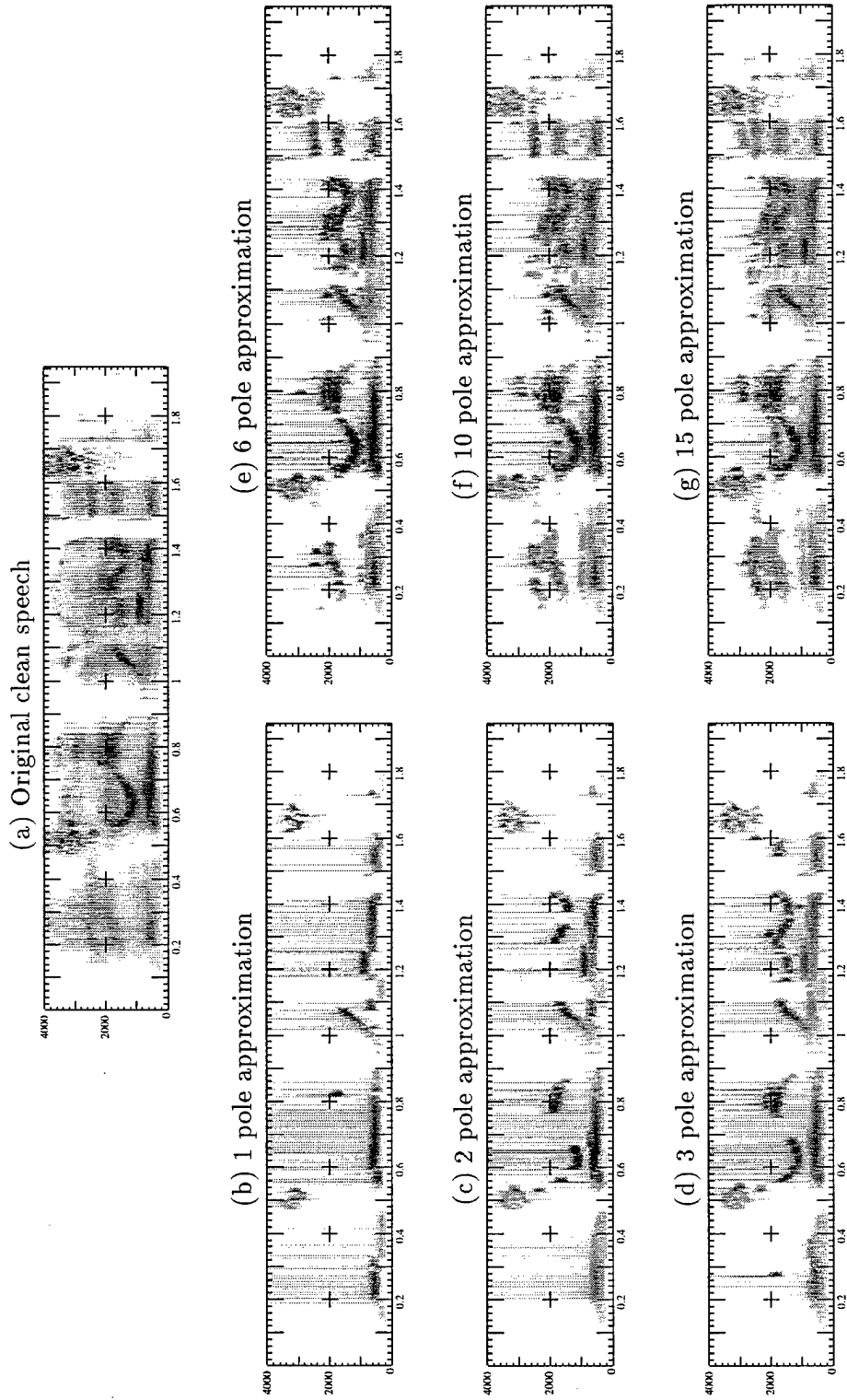


Figure 60. Spectrograms of approximations of clean speech (*sx194*). Shown are the spectrogram of (a) clean speech, and spectrograms of the approximations with (b) one pole, (c) two poles, (d) three poles, (e) six poles, (f) 10 poles, and (g) 15 poles per glottal pulse.

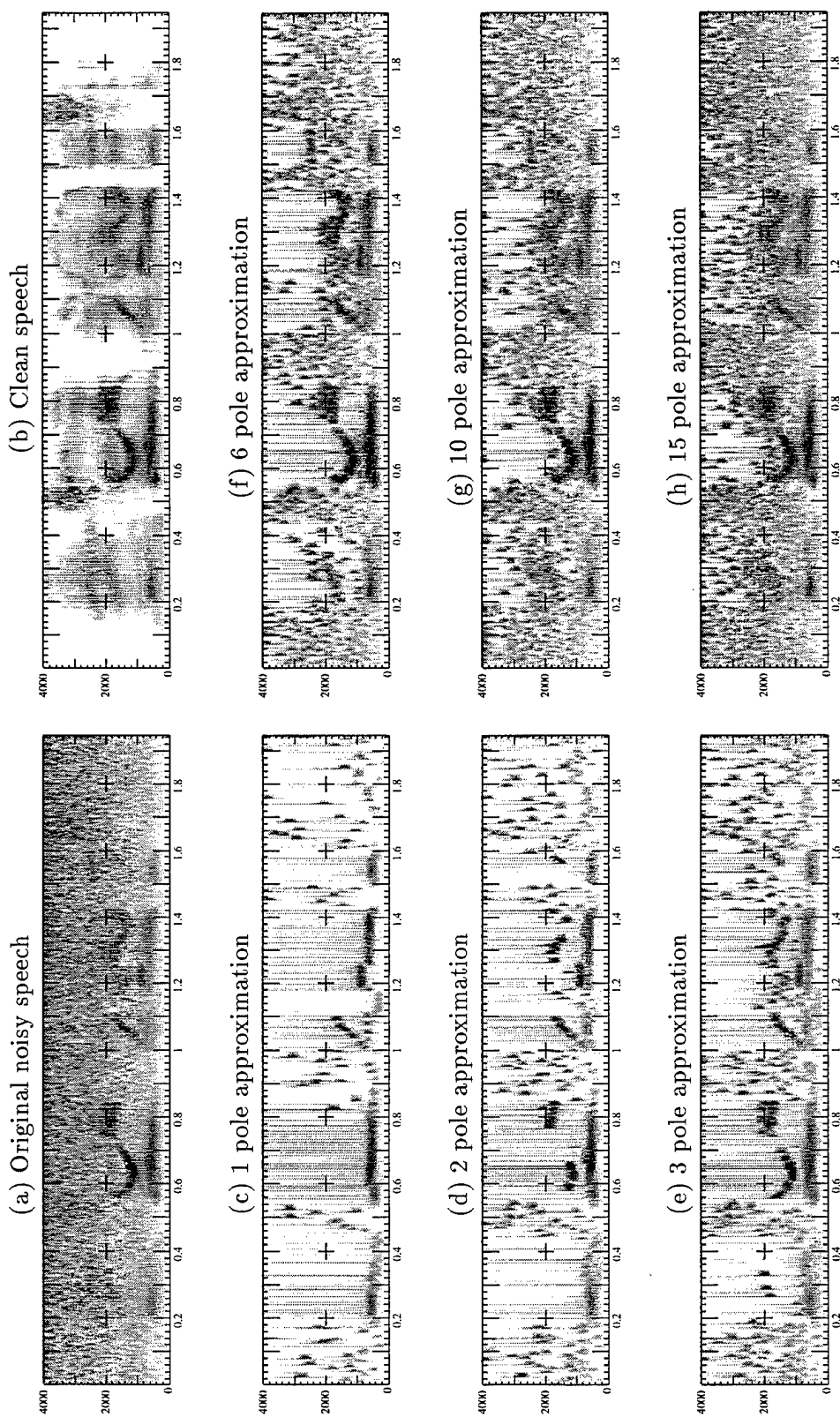


Figure 61. Spectrograms of approximations of noisy speech (SNR 6 dB, *sr194*). Shown are the spectrograms of the (a) noisy speech, on which the approximations are based, and the (b) clean speech, and the spectrograms of the approximations with (c) one pole, (d) two poles, (e) three poles, (f) six poles, (g) 10 poles, and (h) 15 poles.

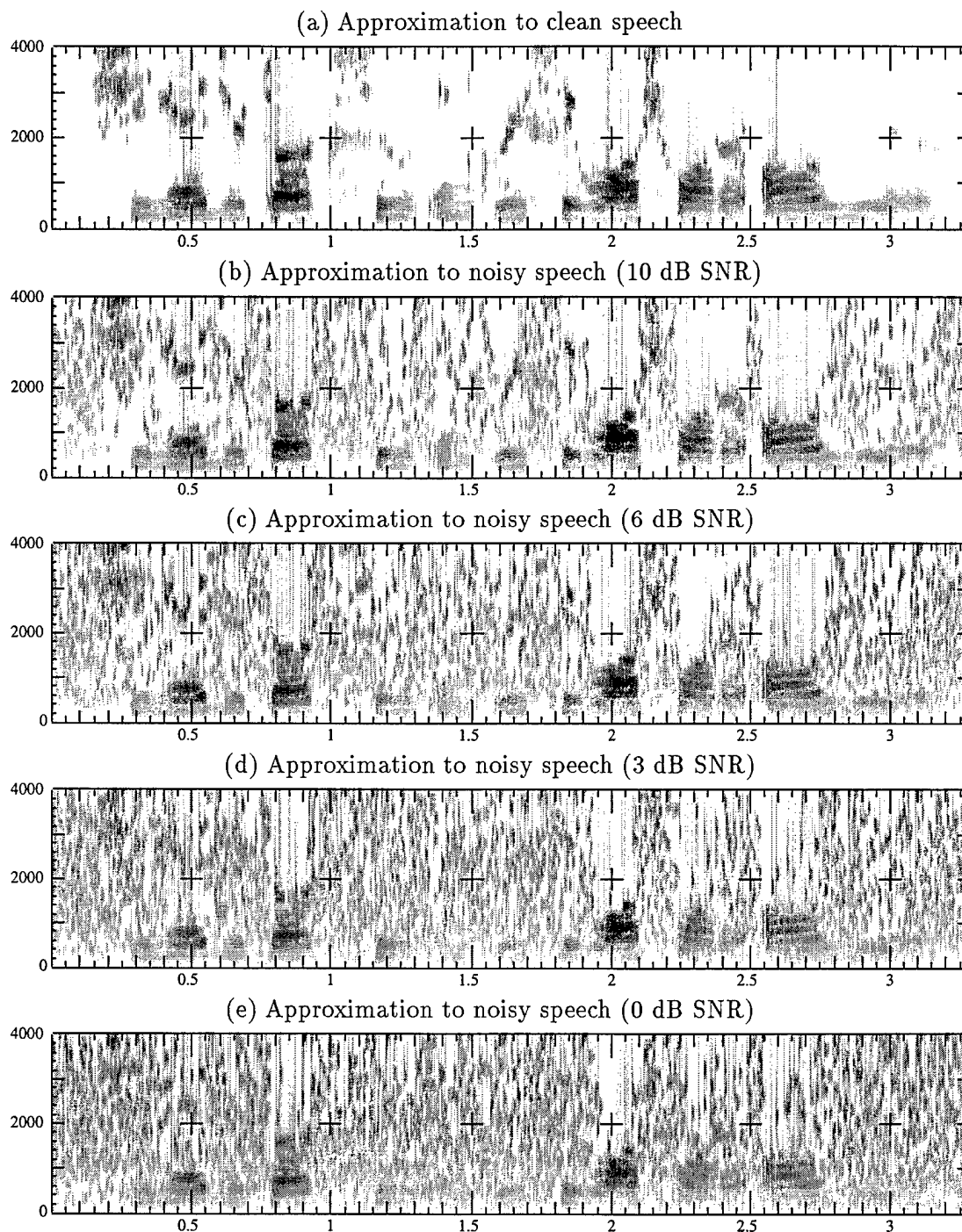


Figure 62. Spectrograms of approximations of speech with different levels of Gaussian white noise *sal*). Each approximation is with six poles per glottal pulse. Shown are the spectrogram of (a) the approximation of clean speech, and the spectrograms of the approximations of noisy speech with a SNR of (b) 10 dB, (c) 6 dB, (d) 3 dB, and (e) 0 dB.

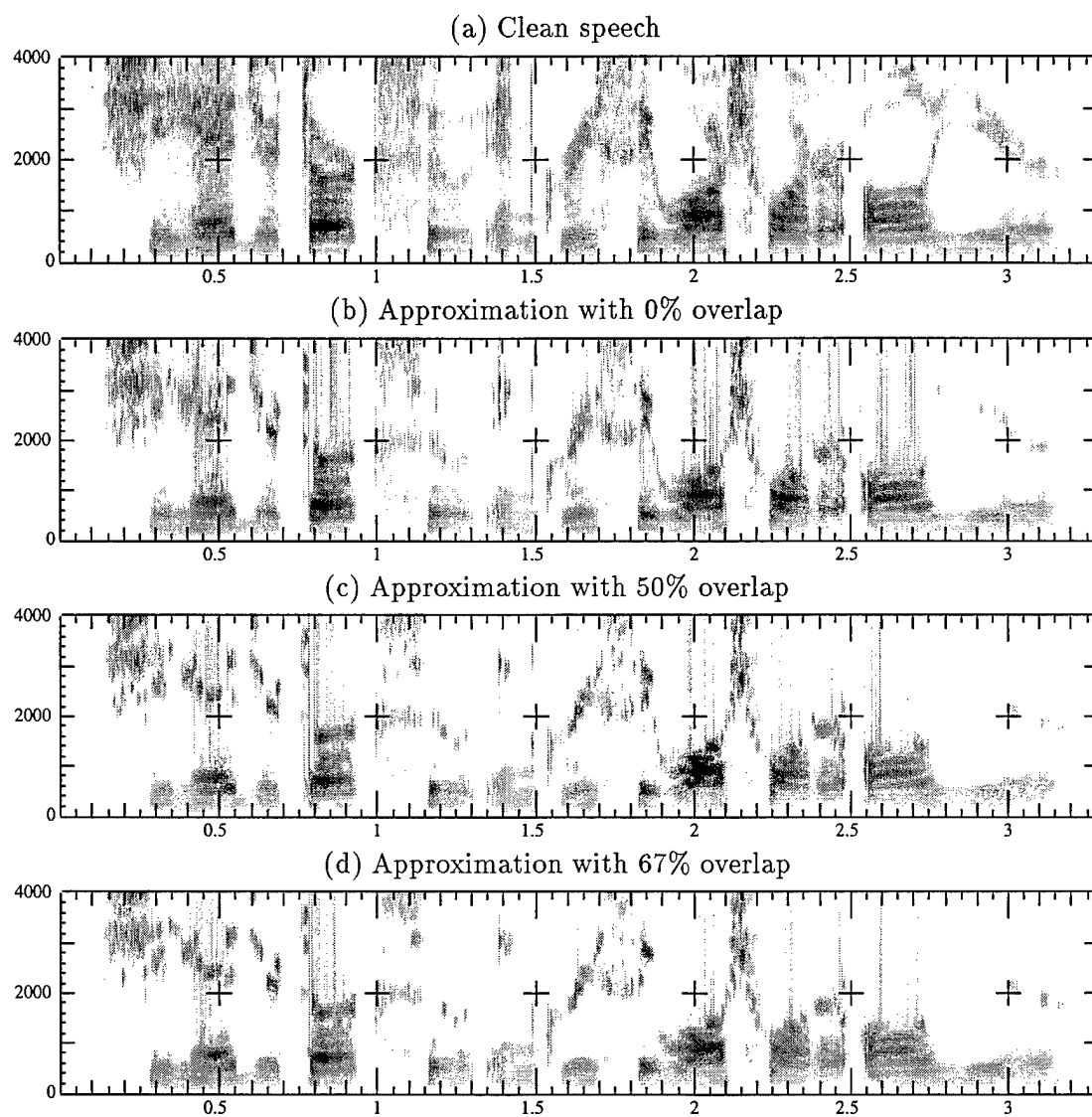


Figure 63. Spectrograms of approximations of clean speech with differing window overlaps (*sa1*). All approximations are with six poles. Shown are (a) clean speech, and approximations based on (b) 0%, (c) 50%, and (d) 67% overlap between analysis windows.

Sentence <i>sa1</i>					
Poles per glottal pulse	Clean speech	10 dB SNR	6 dB SNR	3 dB SNR	0 dB SNR
1	0.687702	0.685619	0.685046	0.709586	0.750175
2	0.464619	0.474355	0.492053	0.548095	0.635339
3	0.342174	0.365598	0.409262	+ 0.493598	+* ⁴ 0.620351
6	0.197260	0.270047	+* ² 0.368374	* ³ 0.502714	0.692969
10	0.119157	+* ¹ 0.255672	0.389134	0.551639	0.772717
15	+* 0.090360	0.264063	0.414692	0.589132	0.827508

Sentence <i>sr194</i>					
Poles per glottal pulse	Clean speech	10 dB SNR	6 dB SNR	3 dB SNR	0 dB SNR
1	0.669009	0.675625	0.681489	0.700375	0.749570
2	0.520508	0.532727	0.550816	0.593328	0.681335
3	0.427633	0.453797	0.493363	0.544308	+* ⁸ 0.671220
6	0.290861	0.350330	* ⁶ 0.426135	+* ⁷ 0.531198	0.719564
10	0.198787	* ⁵ 0.295894	+ 0.408046	0.549081	0.775857
15	+* 0.129461	+ 0.274082	0.413903	0.580043	0.821027

Listener's comments	
1	"10 poles" slightly better. "15 poles" has too much noise.
2	"6 poles" significantly better than "3 poles"; better, but not significantly, than "10 poles."
3	"6 poles" very slightly better than "3 poles," possibly because "6 poles" sounds louder.
4	"3 poles" better than "2 poles." "6 poles" has too much noise.
5	"10 poles" slightly better, but leaning more towards "15 poles" than "6 poles."
6	"6 poles" slightly better, but leaning more towards "10 poles" than "3 poles."
7	"6 poles" noticeably better than others.
8	"3 poles" slightly better than others.

Table 3. L_2 difference between clean speech and approximations of clean speech and approximations of noisy speech with varying SNR. The approximation preferred out of the set of approximations of a sentence with a given level of noise is marked by the symbol "*." For easy comparison, the approximations with the lowest L_2 norm from the clean speech are marked with the symbol "+."

7.4 Summary

While the results achieved in these experiments were very good and, in general, matched expectations, there were some unexpected results also.

For the fine-scale analyses, it was found that short segments of harmonic speech are represented better (lower L_2 error with fewer poles) than similar segments of non-harmonic speech and non-speech-like signals. It was also found that the alignment of the speech segment within the window made a noticeable difference in performance of the representation, with the worst alignments requiring many more poles to achieve the same accuracy as for the best alignments. These results were as expected.

The medium-scale analysis produced some expected and some unexpected results. The iterative algorithm used to find the frame representations, given in Theorem 4.3.4, was found to converge quickly, with only negligible improvements after 5 iterations – a desired result. Examining the representations of harmonic speech, it was found that there is sometimes an advantage (lower error with fewer poles) to having overlapping analysis windows. However, comparing the representations of harmonic speech to those of signals other than harmonic speech, some disturbing anomalies were observed. First, the accuracy of the representation of reversed speech was on par with that of the speech in the correct order. Second and more disturbing, a distinctly non-speech signal was better represented than harmonic speech. Further investigation suggested that this is due to the uncomplicated nature of the Fourier transform of this non-speech signal.

While the results of the fine- and medium-scale analyses were suggestive, the results of the large-scale analysis are the most meaningful since they involved listening tests. It was found that approximation in this representation has inherent noise-suppression characteristics – that is, the speech is represented more naturally than the noise. Specifically, low order approximations of noisy speech were found to be both numerically and perceptually closer to the clean speech than to the speech corrupted by noise. For representations of speech corrupted by noise, it was found that the L_2 norm difference between the representation and the clean speech corresponded well with the perceptual difference, lending support to the hypothesis that, *when using this frame for representations*, the L_2 norm can be used as a reliable predictor of perceptual differences.

VIII. Conclusions

This work presented new results from several areas of mathematics, applied to the problem of mathematical speech representation. Representations in $H_p(\mathbb{D})$ were used to develop frames in $H_2(\mathbb{D})$. These frames were then used in the construction of frames for $L_2(\mathbb{R})$ suitable for use in speech processing. A generalization of the frame operator was presented which allows for combinations of iterative and exact solutions of frame representations to be used.

The Carleson inequality proven in Theorem 3.1.4 allows for bounds on sums of sampled values of elements of the Hardy spaces $H_p(\mathbb{D})$, $1 < p < \infty$, where the sampling locations are allowed to lie in closed subsets of \mathbb{D} of more general shapes, rather than on the simple concentric circles in \mathbb{D} in previous theorems. This relaxation of the locations of the sampling points allows this theorem to be used to create more versatile representation theorems. Theorem 3.6.1 is an example of such a representation theorem for elements of the Hardy spaces.

Similar to mathematical bases, mathematical frames are used to obtain representations in Hilbert spaces. Frames for $H_2(\mathbb{D})$ were found in Theorems 5.2.7 and 5.2.10 based on Theorem 3.6.1. These frames are suitable for a wide variety of representation applications in \mathbb{D} . They are suitable for representation in other spaces via transforms, which was how they were used in this work. Exact forms of projections into these frames are also determined.

A composite mathematical frame for $L_2(\mathbb{R})$ was developed in Theorem 4.2.4 which was shown to be useful in representing digitally recorded speech. It should be particularly useful in signal processing applications where phenomena of varying time duration and of changing characteristics are frequently found.

Of particular use in a wide range of applications far beyond those of this paper is the generalization of the frame operator presented in Theorem 4.3.1, together with the iterative method for finding representations given in Theorem 4.3.4. This provides a sound basis for combining exact and iterative methods of determining frame expansion coefficients to enable faster calculations.

The utility of the mathematics developed here was shown via an application to speech representation. A frame especially suitable for speech representation was developed based on the adaptive $L_2(\mathbb{R})$ frame of Theorem 4.2.4. The frame for $L_2(\mathbb{R}^+)$ used as a building block in this speech frame was a transform of an $H_2(\mathbb{D})$ frame.

A computer program was written which could adaptively fit a composite frame to a specific example of speech and project the speech onto this frame. This frame, rather than being for all of $L_2(\mathbb{R})$, was instead for a finite-dimensional subspace of $L_2(\mathbb{R})$, allowing approximations to speech to be found. The sampling points of the $H_2(\mathbb{D})$ frame used in the construction were chosen such that they corresponded with exactly known points of the Laplace transform of the windowed signal to be represented. Tests on clean and noisy speech and non-speech signals showed the usefulness of the constructed frame in speech representation.

Appendix A. A Space of Speech

A.1 Abstract Speech Space

Presented in this section is an abstract metric space designed to contain useful representations of speech. “Useful” in this context means that differences as measured by the metric are well correlated with perceptual differences as perceived by a listener. Additionally, the coordinates of this space have some physiological meaning.

A.1.1 Desired characteristics of the space. We want an abstract metric space, (S, d) , where S is a set and d is a metric, such that the set represents speech well. The space is abstract in that the exact makeup of the set S and the metric d are not known, although the characteristics they must satisfy are quantified. Concrete examples of this space, where the makeup of the space is fully specified, can be used for applications.

Definition A.1.1 *A metric defined on a set S is a function $d : S \times S \rightarrow [0, \infty)$ such that*

1. $d(s_1, s_2) \geq 0$ and $d(s_1, s_1) = 0$ for all $s_1, s_2 \in S$,
2. $d(s_1, s_2) = 0$ iff $s_1 = s_2$ for all $s_1, s_2 \in S$,
3. $d(s_1, s_2) = d(s_2, s_1)$ for all $s_1, s_2 \in S$, and
4. $d(s_1, s_3) \leq d(s_1, s_2) + d(s_2, s_3)$ for all $s_1, s_2, s_3 \in S$.

A **pseudo-metric** is such a function for which conditions 1), 3), and 4) hold, and a **quasi-metric** (a.k.a **skew-metric**) is such a function for which conditions 1), 2), and 4) hold.

The space should represent speech well in that the metric d will provide a good quantifier of the perceptual differences between instances of speech represented in the space. The set S should be as small as possible, and yet it is desirable for *any* one-speaker-at-a-time speech to be exactly representable in it. Additionally, it is desirable that the set S exhibit mathematical structure (e.g., algebraic structure, convexity, etc.) Also, the representation should be “natural” in that speech is more compactly represented in the space than non-speech.

Because speech synthesis researchers have been enjoying success, a logical inspiration for S could be a variant of the speech production model.

The metric or pseudo-metric d may actually be one of a class of metrics/pseudo-metrics defined on S . This map, d , should be able to quantify (as much as possible)

perceivable differences. This will make d suitable for “quality” type discriminations: two sounds that are very close under d will be perceived by a human listener to be indistinguishable.

Many spaces will meet the desired characteristics. Below, an abstract speech space is developed based on the simple speech production model discussed in Section 2.1.2, in which the constraints that must be met are discussed. The set upon which this space is based is convex. Elements of this space can be “produced” into speech by a non-linear map, S , which is defined. Concrete speech spaces can be created from this abstract space by further quantifying its elements.

A.1.2 Description of the Abstract Speech Space, (S, d) . The speech space defined here, denoted by (S, d) , is a four-component Cartesian-product set $S = G \times A \times P \times V$ with an associated metric, d . The component set G contains characterizations of the glottal excitation source shape, A contains characterizations of the amplitude of the voice, P contains characterizations of the fundamental pitch of the voice, and V contains characterizations of the vocal tract response. Each of the component sets, G , A , P and V , is described in detail below.

Since the speech production process is finite of duration, it is desirable to model the interval on which “speech production” happens to be a finite interval \mathbb{I} , although the effects of speech production can be considered to be infinite in duration, if so desired. Without loss of generality, the interval \mathbb{I} may be assumed to be $\mathbb{I} = [0, T]$ for some terminal time T .

This space is related to the simple speech production model (Figure 4) in the following way. The system response of the linear system “vocal tract” is represented by the component set V . The glottal excitation source is represented by the three component sets G , A , and P .

Breaking the glottal excitation into three component parts, G , A , and P , effectively separates the excitation into three components for which there exist extensive measurements of human sensitivity [16]. For instance, it is known that the human ear cannot detect small pitch changes below a certain threshold. Therefore, “small” changes in the P -component (“small” to be quantified in the development of the metrics) should be difficult to detect (i.e., should not degrade quality). Likewise, “small” amplitude changes, represented in the A -component, should be difficult to detect. Experience with linear prediction coding (LPC) has shown that the human auditory system is not extremely sen-

sitive to small changes in LPC coefficients; I suspect that this can be extended to “small” differences in a vocal tract response.

Under the assumption that “small” changes in any of these components are imperceptible to the human ear, and that any glottal excitation can be represented with them, it seems likely that good metrics could be developed based on this representation.

This decomposition of the glottal excitation into component parts is related to that in [26], where the frequency content (which is closely related to pitch) is manipulated separately, and is similar to that in [17], where the *instantaneous waveform* is related in concept to the glottal excitation source shape used here, except that there it is not normalized for pitch.

A.1.2.1 Glottal excitation shape. For voiced speech, the glottal excitation resembles roughly a periodic signal, where the shapes of the pulses and the period varies with time. Suppose, however, that one were to freeze the vocal cord and air flow parameters at time t , and examine the glottal excitation produced by this configuration. This *instantaneous glottal excitation* at time t would be a periodic signal. If then, one were to examine how the instantaneous glottal excitation varied within one pitch cycle with time, it might be possible to put constraints on the rate of shape change that would model the constraints imposed by physiology.

Based on this idea, I define the glottal excitation source shape set, G , as a set of real valued functions on $\mathbb{I} \times \mathbb{R}$ which are periodic with period one in the second coordinate. For voiced speech, each period (in the second coordinate) represents one glottal pulse, with the first coordinate representing how the pulse shape is changing with time. For unvoiced speech, what a “period” represents is less clear, but the turbulence producing the unvoiced excitation will still be modeled in this manner. Because it is desirable for the speech map, S , to be defined on the whole space, it is necessary (due to the energy normalization which will be seen in the definition of S) for the 0 function to be excluded. At the same time, it is desirable to maintain convexity, to preserve useful space structure for projections into the space. Therefore, the set G will further be constrained to functions that, for all t , have a positive mean in the second coordinate. That is,

$$\inf_{t \in \mathbb{I}} \int_0^1 g(t, \tau) d\tau > 0.$$

Also, we wish to add some constraints which reflect physiological realities on the set G . The exact constraint will vary with the particular instantiation chosen. However, the

constraint functional, ϕ_G , must be convex if we wish the subset of convex set G defined by $\{g \in G : \phi_G(g) \leq K\}$ to also be convex, where K is some positive constant. That is,

$$\phi_G(\alpha g_1 + (1 - \alpha)g_2) \leq \alpha \phi_G(g_1) + (1 - \alpha)\phi_G(g_2) \quad \forall g_1, g_2 \in G, 0 \leq \alpha \leq 1.$$

Since it will be necessary to energy-normalize elements of G to “produce” speech, the set G will have to be restricted to functions that satisfy

$$\int_0^1 |g(t, \tau)|^2 d\tau < \infty \quad \forall t \in \mathbb{I}.$$

Due to the normalization to be done later, this may be further restricted to

$$\int_0^1 |g(t, \tau)|^2 d\tau \leq 1 \quad \forall t \in \mathbb{I}.$$

Additionally, for the speech map, \mathbf{S} , to be well-defined, it will be necessary to bound the elements of G . That is,

$$\sup_{(t, \tau) \in \mathbb{I} \times [0, 1]} |g(t, \tau)| < \infty.$$

The set G can be defined as

$$\begin{aligned} G = \{g: \mathbb{I} \times \mathbb{R} \rightarrow \mathbb{R} \mid & g(t, \tau) = g(t, \tau + 1) \quad \forall (t, \tau) \in \mathbb{I} \times \mathbb{R}, \\ & \int_0^1 |g(t, \tau)|^2 d\tau \leq 1 \quad \forall t \in \mathbb{I}, \\ & \phi_G(g) \leq K_G, \\ & \sup_{(t, \tau) \in \mathbb{I} \times [0, 1]} |g(t, \tau)| < \infty, \text{ and} \\ & \inf_{t \in \mathbb{I}} \int_0^1 g(t, \tau) d\tau > 0\}. \end{aligned}$$

Figure 64(a) shows a simplified example of a “voiced” element of one such set. To show convexity of the set G , the following proposition is necessary.

Proposition A.1.2 *The set G , as defined above, is a convex subset of $L^2(\mathbb{I} \times [0, 1])$.*

Proof. By its construction, G is convex. Also, $\int_0^1 |g(t, \tau)|^2 d\tau \leq 1$ for all $t \in \mathbb{I}$ and \mathbb{I} compact implies $g \in L^2(\mathbb{I} \times [0, 1])$. \square

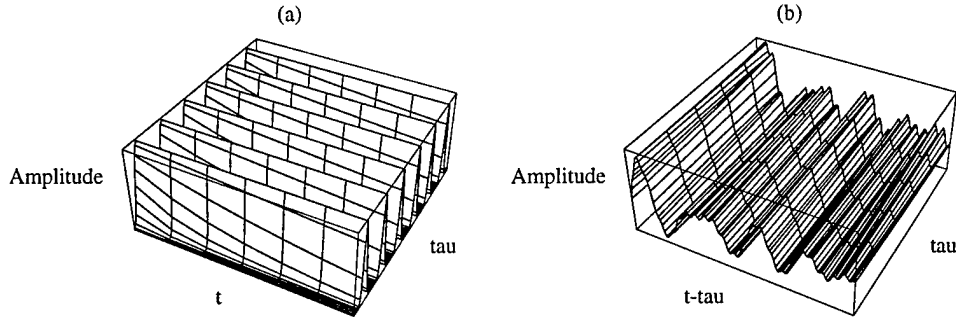


Figure 64. (a) A simplified example of a time varying glottal excitation shape. (b) A simplified example of a time-varying impulse response.

A.1.2.2 The amplitude, A . To represent the time varying amplitude of speech, another coordinate, A , is necessary. Clearly, since the human voice is amplitude and energy limited, it is possible to bound the amplitude above by a_{max} and below by 0. Also, as with the set G above, we will want to apply some convex measure of rate of change to elements of A , denoted ϕ_A .

The set A can be represented as

$$A = \{a \in L^2(\mathbb{I}) : 0 \leq a(t) \leq a_{max} \forall t \in \mathbb{I}, \phi_A(a) \leq K_A\}.$$

By its definition, it is clear that A is a convex subset of $L^2(\mathbb{I})$.

A.1.2.3 The fundamental pitch, P . The perceived pitch of the human voice is usually the pulse repetition rate of the glottal pulses (for voiced speech). The pitch coordinate, P , represents the time varying, instantaneous pitch of the speech. For unvoiced speech, this value is less intuitively definable, but the pitch component will still be used. As with the amplitude A , the pitch may be bounded above and below by p_{max} and 0, respectively, and bounded by a suitably chosen rate of change functional, ϕ_P .

The set P can be represented by

$$P = \{p \in L^2(\mathbb{I}) : 0 \leq p(t) \leq p_{max} \forall t \in \mathbb{I}, \phi_P(p) \leq K_P\}.$$

Again, by its definition, it is clear that P is a convex subset of $L^2(\mathbb{I})$.

A.1.2.4 The vocal tract response, V . The vocal tract response, V , is the time-varying system response of the vocal tract. The “system response” can be simply defined as the response of the system to an impulse (Dirac delta) at some time. Since this is a time varying system, the system response depends on the time at which the impulse occurs as well as the time at which the system output is examined.

In this model, for $v \in V$, $v(t, \tau)$ represents the response of the system (vocal tract) at time t to an impulse at time τ . Since the vocal tract is being modeled as a causal system, $v(t, \tau) = 0$ for all $t < \tau$. Also, as with the set G , the impulse response must have finite energy for each time t and there must be a convex functional ϕ_V to govern the acceptable rate of change.

The set V can be defined as

$$V = \{v: \mathbb{R} \times \mathbb{I} \rightarrow \mathbb{R} \mid v(t, \tau) = 0 \forall t < \tau \\ \int_{\tau}^{\infty} |v(t, \tau)|^2 dt \leq \frac{1}{T} \forall \tau \in \mathbb{I} \\ \phi_V(v) \leq K_V\}.$$

Figure 64(b) shows an example of such a time-varying impulse response from a candidate set. Again, to show convexity of the set S , the following proposition is required.

Proposition A.1.3 *The set V , as defined above, is a convex subset of $L^2(\mathbb{R} \times \mathbb{I})$.*

Proof. By its construction, V is convex. Also, $\int_{\tau}^{\infty} |v(t, \tau)|^2 dt = \int_0^{\infty} |v(t, \tau)|^2 dt \leq \frac{1}{T}$ for all $\tau \in \mathbb{I}$ and \mathbb{I} compact implies $v \in L^2(\mathbb{R} \times \mathbb{I})$. \square

A.1.2.5 Mathematical representations of physiological constraints on rate of change. Clearly, there are physiological constraints on how fast the components of the vocal tract can change, which should translate into constraints on the elements of each of the coordinate sets, G , A , P , and V . Depending on the exact set S chosen for instantiation, these constraints can be specified in a number of ways. As discussed above, however, these constraint functionals should be convex (on the convex set on which they are defined). That is, for $X \in \{G, A, P, V\}$,

$$\phi_X(\alpha x_1 + (1 - \alpha)x_2) \leq \alpha \phi_X(x_1) + (1 - \alpha)\phi_X(x_2) \quad \forall x_1, x_2 \in X, 0 \leq \alpha \leq 1.$$

One example of a class of suitable functionals would be the norms defined on the Sobolev spaces, which are defined in \mathbb{R} by [1]

$$\begin{aligned}\|x\|_{m,p} &= \left| \sum_{\alpha=0}^m \|D^\alpha x\|_p^p \right|^{1/p} \quad 1 \leq p < \infty \\ \|x\|_{m,\infty} &= \max_{0 \leq \alpha \leq m} \|D^\alpha x\|_\infty ,\end{aligned}\tag{74}$$

where $D^0 x(t) = x(t)$, $D^\alpha x(t) = \frac{d^\alpha}{dt^\alpha} x(t)$, and $\|\cdot\|_p$ denotes the L^p norm. These are easily shown to be convex functionals. However, they require differentiability, which may not be desirable in every case. Possibly more suitable are subsets of the class of Lipschitz functions [7], in that rates of change of functions in these classes is bounded without requiring in that differentiability.

Definition A.1.4 *Let $f: X \rightarrow Y$ and let p and q be metrics defined on X and Y , respectively. The function f is called a Lipschitz function if there exists a constant $M > 0$ such that $q(f(x), f(y)) \leq Mp(x, y)$ for all $x, y \in X$.*

If one were to consider the subset of the set of Lipschitz functions defined by setting a maximal value for M (called the Lipschitz constant) in the above definition, perhaps this subset would be of use. In addition, there are many other suitable functions. The correct choice depends on the particular sets chosen.

A.1.2.6 Properties of the set S . The following proposition can be easily proven.

Proposition A.1.5 *Let A and B be Hilbert spaces with inner products $\langle \cdot, \cdot \rangle_A$ and $\langle \cdot, \cdot \rangle_B$, respectively. Then, the Cartesian space $A \times B$ is a Hilbert space with inner product $\langle \cdot, \cdot \rangle_{A \times B}$ defined by*

$$\langle (f_A, f_B), (g_A, g_B) \rangle_{A \times B} = \langle f_A, g_A \rangle_A + \langle f_B, g_B \rangle_B .$$

Proposition A.1.6 *The set $S = G \times A \times P \times V$, as defined above, is convex subset of the Hilbert space $L^2(\mathbb{I} \times \mathbb{R}) \times L^2(\mathbb{I}) \times L^2(\mathbb{I}) \times L^2(\mathbb{R} \times \mathbb{I})$.*

Proof. By its construction, S is indeed a subset of the Hilbert space in question. The convexity of S is easily seen by the convexity of its component sets. \square

A.1.2.7 Speech production from elements of S . The “speech production process” used herein is a non-linear map, $\mathbf{S}: S \rightarrow L^2(\mathbb{R}^+)$. Since all speech is of finite energy (finite support and finite amplitude), the set of all speech is a subset of $L^2(\mathbb{R}^+)$.

The action of \mathbf{S} on each element of S is defined as

$$\mathbf{S}[g, a, p, v](t) = \int_0^{\min\{t, T\}} x[g, a, p](\tau) v(t, \tau) d\tau ,$$

where the glottal excitation $x: G \times A \times P \rightarrow L^2(\mathbb{I})$ is defined by

$$x[g, a, p](t) = a(t) N_G[g](t, w[p](t)) , \quad (75)$$

where $N_G: G \rightarrow L^2(\mathbb{I} \times \mathbb{R})$ is defined by

$$N_G[g](t, \tau) = \frac{g(t, \tau)}{|\int_0^1 |g(t, \zeta)|^2 d\zeta|^{1/2}} ,$$

and $w: P \rightarrow L^2(\mathbb{I})$ is defined by

$$w[p](t) = \int_0^t p(\tau) d\tau .$$

Observe, $w[p]$ is non-decreasing, since p is nonnegative.

Before operator \mathbf{S} is shown to be well-defined, some preliminary results are proven. All norms of the form $\|\cdot\|_X$ are L^2 norms on the indicated set, X .

Lemma A.1.7 *For every $g \in G$, $\sup_{(t, \tau) \in \mathbb{I} \times [0, 1]} |N_G[g](t, \tau)| < \infty$.*

Proof. Recall $\inf_{t \in \mathbb{I}} \int_0^1 g(t, \tau) d\tau > 0$ and define ϵ by

$$\begin{aligned} \epsilon &\doteq \inf_{t \in \mathbb{I}} \int_0^1 g(t, \tau) d\tau \\ &\leq \int_0^1 g(t, \tau) d\tau \\ &\leq \left| \int_0^1 |g(t, \tau)|^2 d\tau \right|^{1/2} . \end{aligned}$$

This gives

$$\sup_{(t, \tau) \in \mathbb{I} \times [0, 1]} |N_G[g](t, \tau)| = \sup_{(t, \tau) \in \mathbb{I} \times [0, 1]} \left| \frac{g(t, \tau)}{|\int_0^1 |g(t, \zeta)|^2 d\zeta|^{1/2}} \right|$$

$$\begin{aligned}
&\leq \sup_{(t,\tau) \in \mathbb{I} \times [0,1]} \left| \frac{g(t,\tau)}{\epsilon} \right| \\
&= \frac{1}{\epsilon} \sup_{(t,\tau) \in \mathbb{I} \times [0,1]} |g(t,\tau)| < \infty .
\end{aligned}$$

□

Lemma A.1.8 *The map $x: G \times A \times P \rightarrow L^2(\mathbb{I})$, as defined in (75), is well-defined.*

Proof. Fix $(g, a, p) \in G \times A \times P$. By definition of A , $a \in A$ implies $|a(t)| \leq K_A$ for all $t \in \mathbb{I}$. Also, $g \in G$ implies $\sup_{(t,\tau) \in \mathbb{I} \times [0,1]} |N_G[g](t, \tau)| = M < \infty$. Therefore,

$$|a(t)N_G[g](t, \tau)| \leq MK_A \quad \forall (t, \tau) \in \mathbb{I} \times [0, 1] ,$$

which implies

$$\|x[g, a, p]\|_{\mathbb{I}} \leq \left(\int_0^T |MK_A|^2 dt \right)^{1/2} = T^{1/2} MK_A < \infty .$$

Therefore, $x[g, a, p] \in L^2(\mathbb{I})$ for all $(g, a, p) \in G \times A \times P$. □

We are now prepared to prove the main theorem.

Theorem A.1.9 *The map $S: S \rightarrow L^2(\mathbb{R})$, as defined above, is well-defined.*

Proof. What we must show is that for all $(g, a, p, v) \in S$, we have $s \doteq S[g, a, p, v] \in L^2(\mathbb{R}^+)$. Recall, $v \in V$ satisfies

$$\int_{\mathbb{R}^+} |v(t, \tau)|^2 dt \leq \frac{1}{T} \quad \forall \tau \in \mathbb{I} . \tag{76}$$

Hence,

$$\int_{\mathbb{I}} \int_{\mathbb{R}^+} |v(t, \tau)|^2 dt d\tau = \int_{\mathbb{I} \times \mathbb{R}^+} |v(t, \tau)|^2 d(t, \tau) = \|v\|_{\mathbb{I} \times \mathbb{R}}^2 \leq 1 ,$$

by Fubini's Theorem. Since

$$s(t) = \int_0^{\min\{t, T\}} x(\tau) v(t, \tau) d\tau ,$$

we have that

$$\begin{aligned}
|s(t)| &\leq \int_0^{\min\{t,T\}} |x(\tau)| |v(t,\tau)| d\tau \\
&\leq \int_{\mathbb{I}} |x(\tau)| |v(t,\tau)| d\tau \\
&\leq \left(\int_{\mathbb{I}} |x(\tau)|^2 d\tau \right)^{1/2} \left(\int_{\mathbb{I}} |v(t,\tau)|^2 d\tau \right)^{1/2} \\
&= \|x\|_{\mathbb{I}} \left(\int_{\mathbb{I}} |v(t,\tau)|^2 d\tau \right)^{1/2}
\end{aligned}$$

which gives

$$\begin{aligned}
\|S[g, a, p, v]\|_{\mathbb{I}^+} &= \left(\int_{\mathbb{I}^+} |s(t)|^2 dt \right)^{1/2} \leq \|x\|_{\mathbb{I}} \left(\int_{\mathbb{I}^+} \int_{\mathbb{I}} |v(t,\tau)|^2 d\tau dt \right)^{1/2} \\
&= \|x\|_{\mathbb{I}} \|v\|_{\mathbb{I} \times \mathbb{I}} \\
&\leq \|x\|_{\mathbb{I}}
\end{aligned}$$

with another application of Fubini's Theorem. Therefore, $S[g, a, p, v] \in L^2(\mathbb{R}^+)$ for all $(g, a, p, v) \in S$. \square

Note that for any particular space, it is possible that not all examples of speech can be represented. However, for any example of speech, there exists some specific space from which it can be produced. Also, unless carefully constructed, any given space may contain multiple representations of the same example of speech. This is undesirable, since then any metric on the space will show equivalent elements to be dissimilar sounding. If, for some reason, such a space is useful despite the multiple representations, it will probably be necessary to work with a pseudo-metric instead of a metric.

A.1.2.8 The class of metrics, d. One way to define a metric on a Cartesian product of sets is to base it on metrics of the component sets. That is, an obvious family of metrics for S is given by

$$\begin{aligned}
d((g_1, a_1, p_1, v_1), (g_2, a_2, p_2, v_2)) &= \alpha_G d_G(g_1, g_2) + \alpha_A d_A(a_1, a_2) \\
&\quad + \alpha_P d_P(p_1, p_2) + \alpha_V d_V(v_1, v_2),
\end{aligned}$$

where d_G, d_A, d_P , and d_V are metrics on G, A, P , and V , respectively, and $\alpha_G, \alpha_A, \alpha_P, \alpha_V > 0$ are weighting factors. Such a function is clearly a metric on the set S .

Note that the energy normalization done in the speech production process on the G and V components effectively defines equivalence classes within the set S . Therefore, a suitable pseudo-metric might be given by

$$\begin{aligned} d_{ps}((g_1, a_1, p_1, v_1), (g_2, a_2, p_2, v_2)) = & \alpha_G d_G(N_G[g_1], N_G[g_2]) + \alpha_A d_A(a_1, a_2) \\ & + \alpha_P d_P(p_1, p_2) + \alpha_V d_V(N_V[v_1], N_V[v_2]) . \end{aligned}$$

A.1.2.9 Space short comings and additional work needed. This model is suitable for characterizing speech where the excitation is solely from the area of the vocal cords. This describes vowels and some consonants (e.g., l, r, y) well, but does not describe the important classes of fricatives (e.g., s, sh, z, f) or plosives (e.g., p, b, t). To handle these sounds in a natural way would require a Cartesian space, S , with additional coordinates, and would be less mathematically tractable.

One approach is to assume no more than one additional constriction (the source of turbulence for fricatives). Then consider the impulse responses before and after the constriction, with the glottal excitation affected by both impulse responses and the additional turbulence only affected by the second. For a time-invariant system, this could be represented mathematically by

$$s(t) = (f[x_1 * v_1] * v_2)(t) ,$$

where x_1 is the glottal excitation, v_1 and v_2 represent the vocal tract responses before and after the constriction, respectively, and f is a nonlinear function which changes some of the signal from before the constriction into “turbulence” (i.e., wideband noise). This model collapses to the simple model discussed previously for the appropriately chosen f and v_2 .

A.2 Linear System Background

Much work has been put into modeling the vocal tract as a linear system. Most approaches use the frozen time approximation to the time-varying system which, while a good approximation for most portions of speech, is inappropriate for rapid transitions. These areas, however, are often extremely important in making determinations of identities of consonants. Therefore, it is appropriate to examine approximations which are based on time-varying systems.

The work presented in this section is closely related to the speech space presented in Section A.1 through the mapping S . By fixing the components g , a , and p , this mapping can be considered to be a linear operator on $v(t, \cdot) \in L_2(\mathbb{R}^+)$.

Section A.2.1, below, will review linear systems briefly and introduce the class of linear systems which we will be using to represent the speech process. Approximations to this class of linear system will also be discussed.

Section A.2.2 presents speech as the product of a time-varying, linear system. Based on some of the characteristics of speech, a “ τ -varying poles” model of speech is presented.

A.2.1 Linear Systems. This section is an introduction to linear systems, as we intend to use the term. The general (time-varying) case will be discussed, as well as the special case of time invariant systems.

A.2.1.1 General Linear Systems. Because the work presented here is of a mathematical nature, linear systems will be presented as mathematical entities to facilitate future discussion.

Definition A.2.1 *Let X and Y be linear spaces over the field F . A linear mapping is a mapping $A: X \rightarrow Y$ for which*

$$A[\alpha_1 x_1 + \alpha_2 x_2] = \alpha_1 A x_1 + \alpha_2 A x_2$$

for all $x_1, x_2 \in X$, $\alpha_1, \alpha_2 \in F$.

Definition A.2.2 *Let R_x and R_y be linear spaces over \mathbb{R} and let X be a linear space of functions of the form $x: \mathbb{R} \rightarrow R_x$ and let Y be a linear space of functions of the form $y: \mathbb{R} \rightarrow R_y$. Let $A: X \rightarrow Y$ be a linear mapping. Then, the equation*

$$Ax = y$$

describes a linear system with “input” $x \in X$ producing “output” $y \in Y$. Such a linear system is called causal if whenever $x(t) = 0$ for all $t \leq \tau$, $Ax(t) = 0$ for all $t \leq \tau$. Such a linear system is called time invariant if

$$Ax(t + \tau) = Ax_\tau(t)$$

for all $t, \tau \in \mathbb{R}$ where $x_\tau(t) \doteq x(t + \tau)$. All linear systems which are not time invariant are called *time-varying linear systems*.

A.2.1.2 Analysis of Linear Systems. Given a linear system, there are many questions which may be asked. For example, one may wish to examine the relation between input x and output y for a given system, S . While (in general) y can be easily determined for a given x , the opposite is generally not true. More difficult yet is when neither x nor S is known with much precision, and yet some best S and x must be found for some known y . This describes the process of analyzing recorded speech.

Below, three specific examples of linear systems are given. In each case, the mapping A is representable as an integral.

Impulse Response. Suppose that for a given linear system described by the linear mapping $A: X \rightarrow Y$, one has an input x and wishes to know the output y . This would be given by

$$y = Ax .$$

One common way to solve this problem is to solve for the *impulse response* of the system. That is, determine v (if possible) such that

$$Ax(t) = \int_0^t v(t, \tau)x(\tau) d\tau ,$$

where, for simplicity, A is assumed to be causal and to produce 0 output before time 0.

Transfer Function. In a time-invariant linear system, the impulse response, $v(t, \tau)$, can be simplified to a function h , defined by $h(t - \tau) \doteq v(t, \tau)$ where, due to the time-invariant nature of the system, this relation holds true for any choice of $\tau \in \mathbb{R}^+$.

The output from such a system is given by

$$\begin{aligned} y(t) &= \int_0^t v(t, \tau)x(\tau) d\tau \\ &= \int_0^t h(t - \tau)x(\tau) d\tau \\ &= [h * x](t) . \end{aligned}$$

Using the fact that

$$[h * x](t) = \mathcal{L}^{-1}[\mathcal{L}[h]\mathcal{L}[x]](t),$$

where \mathcal{L} represents the well known Laplace transform, this gives

$$y(t) = \mathcal{L}^{-1}[HX](t),$$

where $H(s) \doteq \mathcal{L}[h](s)$ and $X(s) \doteq \mathcal{L}[x](s)$. The function H is often called the *transfer function* of the linear system.

Zadeh's System Function. Zadeh's system function [8] can be thought of as a transfer function for time-varying linear systems. A brief development of it, showing its similarity in concept to the transfer function is given here.

Assume that a linear system describable by a mapping $A: X \rightarrow Y$ has associated with it an impulse response v . The output y from this system for a given input x is given by

$$y(t) = \int_{-\infty}^{\infty} x(\tau)v(t, \tau) d\tau,$$

which, assuming causality and (for simplicity) that the system produces only 0 output for $t < 0$, becomes

$$y(t) = \int_0^t x(\tau)\tilde{v}(t, t - \tau) d\tau,$$

where \tilde{v} is defined by $\tilde{v}(t, \tau) \doteq v(t, t - \tau)$. Then, for each t , $y(t)$ is given by

$$\begin{aligned} y(t) &= \int_0^t x(\tau)\tilde{v}_i(t - \tau) d\tau \\ &= [x * \tilde{v}_i](t) \end{aligned}$$

where $\tilde{v}_i(\cdot) \doteq \tilde{v}(t, \cdot)$. Applying the Laplace transform, we find

$$y(t) = \mathcal{L}^{-1}[XZ_i](t)$$

where X and Z_t are the Laplace transforms of x and \tilde{v}_t , respectively. Defining a function $Z: T \times \mathbb{C}^+ \rightarrow \mathbb{C}$ by $Z(t, s) \doteq Z_t(s)$, we have Zadeh's system function, given by

$$\begin{aligned} Z(t, s) &= Z_t(s) = \mathcal{L}[\tilde{v}_t](s) \\ &= \int_0^\infty \tilde{v}(t, \xi) e^{-s\xi} d\xi \\ &= \int_0^\infty v(t, t - \xi) e^{-s\xi} d\xi \\ &= \int_{-\infty}^t v(t, \tau) e^{-s(t-\tau)} d\tau . \end{aligned}$$

The last form is the one usually given as Zadeh's system function. This gives for y ,

$$\begin{aligned} y(t) &= \mathcal{L}^{-1}[X(\cdot)Z_t(\cdot)](t) \\ &= \mathcal{L}^{-1}[X(\cdot)Z(t, \cdot)](t) . \end{aligned}$$

This last form shows the similarity in concept to the transfer function used for the time-invariant case.

A.2.1.3 Linear Systems Describable by Integral Transforms. In Section A.1, a mapping S was introduced that maps elements of a speech space into "speech" (that is, the $L_2(\mathbb{R}^+)$ representation of speech). This mapping can also be considered an element of the class of linear systems described below. This class, which I believe will be of particular use in representing the speech process, is describable by the linear operator $S_v: L^2(\mathbb{R}^+) \rightarrow L^2(\mathbb{R}^+)$, where S_v is defined by

$$S_v x(t) = \int_0^t x(\tau) v(t, \tau) d\tau ,$$

where $v \in V$ and

$$V = \{v \in L^2(\mathbb{R}^+ \times \mathbb{R}^+) : v(t, \tau) = 0 \ \forall t < \tau\} .$$

In words, the set V represents a rather large set of causal, time-varying, impulse responses.

Theorem A.2.3 *The operator $S_v: L^2(\mathbb{R}^+) \rightarrow L^2(\mathbb{R}^+)$, as defined above, is well-defined.*

Proof. It is sufficient to show that $\|S_v x\| < \infty$ for arbitrarily chosen $v \in V$ and $x \in X$. First,

$$\begin{aligned} |S_v x(t)|^2 &= \left| \int_0^t v(t, \tau) x(\tau) d\tau \right|^2 \\ &\leq \left(\int_0^t |v(t, \tau)| |x(\tau)| d\tau \right)^2 \\ &\leq \int_0^t |v(t, \tau)|^2 d\tau \int_0^t |x(\tau)|^2 d\tau \\ &\leq \|x\|^2 \int_0^t |v(t, \tau)|^2 d\tau . \end{aligned}$$

Next,

$$\begin{aligned} \int_0^T |S_v x(t)|^2 dt &\leq \|x\|^2 \int_0^T \int_0^t |v(t, \tau)|^2 d\tau dt \\ &\leq \|x\|^2 \|v\|^2 . \end{aligned}$$

Since this is true for any chose of $T \in \mathbb{R}^+$, we have

$$\int_0^\infty |S_v x(t)|^2 dt \leq \|x\|^2 \|v\|^2 < \infty .$$

□

Corollary A.2.4 *For all $v \in V$, S_v is a bounded linear operator.*

Proof.

$$\|S_v\| = \sup_{\|x\| \neq 0} \frac{\|S_v x\|}{\|x\|} \leq \frac{\|x\| \|v\|}{\|x\|} = \|v\| .$$

□

By varying $v \in V$, we may define a set, L , of linear systems indexed on v . That is,

$$L = \{S_v : L^2(\mathbb{R}^+) \rightarrow L^2(\mathbb{R}^+) : v \in V, S_v x(t) = \int_0^t x(\tau) v(t, \tau) d\tau\} .$$

This is a very large set of linear systems. In fact, it will be shown that the closure of the set of ranges of operators in this set is all of $L_2(\mathbb{R}^+)$. The significance of this with

regard to speech is that any example of speech can be produced by some such operator, assuming (quite reasonably) that speech is an element of $L_2(\mathbb{R}^+)$.

Let $\mathcal{R}_L = \bigcup_{v \in V} \mathcal{R}(S_v)$, where $\mathcal{R}(S_v)$ denotes the range of the operator S_v . Define E by

$$E = \{s \in L_2(\mathbb{R}^+) : s(t) = 0 \text{ for } t \in [0, \epsilon] \text{ for some } \epsilon > 0\}.$$

Lemma A.2.5 $\overline{E} = L_2(\mathbb{R}^+)$.

Proof. By construction, $E \subset L_2(\mathbb{R}^+)$. Therefore, to conclude the proof, all that is necessary is to show that for $f \in L_2(\mathbb{R}^+)$ arbitrarily chosen, there exists a sequence $\{f_n\}_{n=1}^\infty$, $f_n \in E$, such that $f_n \rightarrow f$.

Given $f \in L_2(\mathbb{R}^+)$, construct $\{f_n\}_{n=1}^\infty$ according to

$$f_n(t) = \begin{cases} f(t) & t > \frac{1}{n} \\ 0 & \text{otherwise} \end{cases}.$$

Clearly, $f_n \in E$ for each $1 \leq n < \infty$.

To show $f_n \rightarrow f$, it is only necessary to note that $|f(t) - f_n(t)|^2$ converges pointwise almost everywhere to 0 on the interval $[0, 1]$, that $|f(t) - f_n(t)|^2$ is bounded above by $|f(t)|^2$, and that

$$\int_{\mathbb{R}^+} |f(t) - f_n(t)|^2 dt = \int_0^{\frac{1}{n}} |f(t)|^2 dt \rightarrow 0,$$

as $n \rightarrow \infty$. Therefore, $f_n \rightarrow f$, and hence, $f \in \overline{E}$. □

Lemma A.2.6 $E \subset \mathcal{R}_L$.

Proof. Let $s \in E$. Thus there exists $\epsilon > 0$ such that $s(t) = 0$ for $t \in [0, \epsilon]$. To complete the proof, we exhibit an $x \in L_2(\mathbb{R}^+)$ and $v \in L_2(\mathbb{R}^+ \times \mathbb{R}^+)$ such that $s = S_v x$.

Define x by

$$x(t) = \begin{cases} \frac{1}{\sqrt{\epsilon}} & 0 \leq t < \epsilon \\ 0 & \text{otherwise} \end{cases}$$

and define v by

$$v(t, \tau) = v_1(t)v_2(\tau)$$

where

$$v_1(t) = s(t)$$

and

$$v_2(t) = \begin{cases} \frac{1}{\sqrt{\epsilon}} & 0 \leq t < \epsilon \\ 0 & \text{otherwise} \end{cases}.$$

Clearly $x \in L_2(\mathbb{R}^+)$. Examining $\|v\|$, we see

$$\begin{aligned} \|v\|^2 &= \int_{\mathbb{R}^+ \times \mathbb{R}^+} |v(t, \tau)|^2 d(t, \tau) \\ &= \int_{\mathbb{R}^+ \times \mathbb{R}^+} |v_1(t)v_2(\tau)|^2 d(t, \tau) \\ &= \int_0^\infty \int_0^\infty |v_1(t)|^2 |v_2(\tau)|^2 d\tau dt \\ &= \int_0^\infty |v_1(t)|^2 \int_0^\infty |v_2(\tau)|^2 d\tau dt \\ &= \int_0^\infty |v_1(t)|^2 \int_0^\epsilon \frac{1}{\epsilon} d\tau dt \\ &= \int_0^\infty |v_1(t)|^2 dt \\ &= \int_0^\infty |s(t)|^2 dt \\ &= \|s\|^2 < \infty. \end{aligned}$$

Therefore, $v \in L_2(\mathbb{R}^+ \times \mathbb{R})$. We now show that $s = S_v x$. We have

$$\begin{aligned} S_v x(t) &= \int_0^t x(\tau)v(t, \tau) d\tau \\ &= v_1(t) \int_0^t x(\tau)v_2(\tau) d\tau. \end{aligned}$$

Examining the case where $t \in [0, \epsilon]$ we see that $v_1(t) = s(t) = 0$, and so $S_v x(t) = 0 = s(t)$.
Examining the case where $t \in [\epsilon, \infty)$, we get

$$\begin{aligned} \int_0^t x(\tau) v_2(\tau) d\tau &= \int_0^\epsilon \frac{1}{\epsilon} d\tau \\ &= 1 \end{aligned}$$

and so $S_v x(t) = v_1(t) = s(t)$. Therefore, $s \in \mathcal{R}(S_v) \subset \mathcal{R}_L$. \square

Theorem A.2.7 $\overline{\mathcal{R}_L} = L_2(\mathbb{R}^+)$.

Proof. $E \subset \mathcal{R}_L \subset L_2(\mathbb{R}^+)$ and $\overline{E} = L_2(\mathbb{R}^+)$, which implies $\overline{\mathcal{R}_L} = L_2(\mathbb{R}^+)$. \square

A.2.1.4 Approximations to S_v . Here, it will be shown that approximations to v yield equally close approximations to S_v .

Theorem A.2.8 Fix $\epsilon > 0$ and let $v \in V$ and $\tilde{v} \in L_2(\mathbb{R}^+ \times \mathbb{R}^+)$ be such that $\|v - \tilde{v}\|^2 \leq \epsilon$. Then, $\|S_v - S_{\tilde{v}}\|^2 \leq \epsilon$.

Proof.

$$\begin{aligned} \|S_v - S_{\tilde{v}}\|^2 &= \sup_{\|x\| \leq 1} \|S_v x - S_{\tilde{v}} x\|^2 \\ &= \sup_{\|x\| \leq 1} \int_0^\infty |S_v x(t) - S_{\tilde{v}} x(t)|^2 dt \\ &= \sup_{\|x\| \leq 1} \int_0^\infty \left| \int_0^t x(\tau) v(t, \tau) d\tau - \int_0^t x(\tau) \tilde{v}(t, \tau) d\tau \right|^2 dt \\ &= \sup_{\|x\| \leq 1} \int_0^\infty \left| \int_0^t x(\tau) (v(t, \tau) - \tilde{v}(t, \tau)) d\tau \right|^2 dt \\ &= \sup_{\|x\| \leq 1} \int_0^\infty |S_{(v-\tilde{v})} x(t)|^2 dt \\ &= \sup_{\|x\| \leq 1} \|S_{(v-\tilde{v})} x\|^2 \\ &= \|S_{(v-\tilde{v})}\|^2 \\ &\leq \|v - \tilde{v}\|^2 \\ &\leq \epsilon. \end{aligned}$$

\square

Therefore, any approximation \tilde{v} to v also yields an equally close approximation $S_{\tilde{v}}$ to S_v . This statement is important because it allows us to approximate S_v by approximating v .

A.2.1.5 Approximations to v . We now explore ways to approximate $v \in V$ since we know that such results can be used to approximate S_v .

I wish to show that my set V can be approximated by a more restricted set \tilde{V} . Let P be a countable basis for $L^2(\mathbb{R}^+)$ and define \tilde{V} by

$$\tilde{V} = \{v: L_2(\mathbb{R}^+ \times \mathbb{R}^+) \mid v(t, \tau) = \begin{cases} p_\tau(t - \tau) & t \geq \tau \\ 0 & \text{otherwise} \end{cases}, \\ p_\tau \in \text{span}(P) \text{ for a.e. } \tau \in \mathbb{R}^+\}$$

Theorem A.2.9 For V and \tilde{V} as defined above, $V \subset \overline{\tilde{V}}$.

Proof. To prove this theorem, we need to show that for any nonzero $v \in V$ and any $\epsilon > 0$, we can find $\tilde{v} \in \tilde{V}$ such that $\|v - \tilde{v}\|^2 < \epsilon$. So, fix $v \in V$ and $\epsilon > 0$.

Since $v \in L^2(\mathbb{R}^+ \times \mathbb{R}^+)$, we have that $v(\cdot, \tau) \in L^2(\mathbb{R}^+)$ for a.e. choice of τ . Also, $v(t, \tau) = 0$ for all $t < \tau$. Therefore, $v_\tau \doteq v(\cdot - \tau, \tau)$ can be approximated by some $p_\tau \in \text{span}(P)$ such that

$$\|v_\tau - p_\tau\|^2 \leq \frac{\epsilon \|v_\tau\|^2}{\|v\|^2},$$

Defining $\tilde{v}(t, \tau)$ by

$$\tilde{v}(t, \tau) \doteq \begin{cases} p_\tau(t - \tau) & t \geq \tau \\ 0 & \text{otherwise} \end{cases}$$

for a.e. τ , we see that

$$\begin{aligned} \|v - \tilde{v}\|^2 &= \int_0^\infty \int_0^\infty |v(t, \tau) - \tilde{v}(t, \tau)|^2 dt d\tau \\ &= \int_0^\infty \|v_\tau - p_\tau\|^2 d\tau \\ &\leq \int_0^\infty \frac{\epsilon \|v_\tau\|^2}{\|v\|^2} d\tau \end{aligned}$$

$$\begin{aligned}
&\leq \frac{\epsilon}{\|v\|^2} \int_0^\infty \int_0^\infty |v(t, \tau)|^2 dt d\tau \\
&\leq \frac{\epsilon}{\|v\|^2} \|v\|^2 \\
&\leq \epsilon .
\end{aligned}$$

Since \tilde{v} defined in this way is an element of \tilde{V} , this proves the theorem. \square

A.2.2 Linear System Representation of Speech.

A.2.2.1 Speech as the Output of a Linear System. As proven in Theorem A.2.7, the closure of the range of the linear operator $S_v: L_2(\mathbb{R}^+) \rightarrow L_2(\mathbb{R}^+)$ is all of $L_2(\mathbb{R}^+)$, where S_v is defined by

$$S_v x(t) = \int_0^t x(\tau) v(t, \tau) d\tau ,$$

where $v \in V$ and where

$$V = \{v \in L_2(\mathbb{R}^+ \times \mathbb{R}^+) : v(t, \tau) = 0 \forall t < \tau\} .$$

Making the quite reasonable assumption that any given example of speech, s , is an element of $L_2(\mathbb{R}^+)$, we have now established that speech can be produced by such a linear system. Therefore, a linear system that can produce that example of speech for an appropriate input (excitation) can be approximated as shown in Theorems A.2.8 and A.2.9.

However, the linear systems that represent speech have additional characteristics, which can be incorporated into a representation. Below, we will discuss a “ τ -varying poles” model of the impulse response of speech. Following that, the form that Zadeh’s system function takes for the τ -varying poles model will be examined briefly.

A.2.2.2 Rational Functions. Rational functions are often used to represent the Laplace transform of time-invariant impulse responses. Indeed, they are the logical representation for certain classes of time-invariant linear systems.

A rational function $f: \mathbb{C} \rightarrow \mathbb{C}$ can be expressed in the form

$$f(s) = \frac{\sum_{m=1}^M (s - z_m)^{j(m)}}{\sum_{m=1}^N (s - p_m)^{k(m)}} .$$

The p_m 's are called *poles* of f and the z_m 's are called *zeros* of f . The function f is analytic everywhere in \mathbb{C} except at the poles.

A.2.2.3 “ τ -Varying Pole” Representation of Speech. When one performs a windowed Fourier analysis of a sample of voiced speech for a short duration window, one sees results similar to those one would see from the output of a time-invariant linear system describable by a system function consisting of a low-order rational function. Particularly, a time-invariant linear system which may be modeled by a system function with 3-4 poles and at most 1 zero can be found to produce similar (in a frequency analysis sense) results to the speech. Performing a windowed Fourier analysis on a slightly shifted window produces results that can be modeled by a simple pole-zero model with the poles and zeros in slightly different locations. One implication of this is that the vocal tract behaves like a slowly varying linear system.

This also is the impetus to model the vocal tract as a linear system with “ τ -varying poles.” That is, the impetus to model the vocal tract as a system which, if frozen at any instance in time, has a transfer function modeled by a rational function. So, an impulse at time τ produces output identical to that of some time-invariant system modeled by a rational function. At different times τ , the equivalent time invariant system has different poles and zeros. Here, this will be referred to as a “ τ -varying pole” model of speech production.

Such a system is represented by an impulse response of the form

$$v(t, \tau) = \mathcal{L}^{-1}[F(\cdot, \tau)](t - \tau)$$

where

$$F(s, \tau) = \frac{\sum_{i=0}^M \beta_i(\tau) s^i}{\sum_{i=0}^N \alpha_i(\tau) s^i}$$

where the coefficients of the rational function vary with τ . This function, F , will be referred to as the “frozen time system function.” One implication of this form is that the system response, $v(t, \tau)$, for an impulse at some fixed time τ depends only on the values of the α_i s and the β_i s at time τ , and is totally independent of their values at other times.

Note the difference between the frozen time system function with τ -varying poles and Zadeh's system function with time-varying poles. In the first case, the poles are in the

function transformed with respect to the first variable, whereas, with Zadeh, the transform is with respect to the second variable.

If the frozen time system function representation were “perfect,” then it would be possible to examine the configuration of the vocal tract at time τ and from that configuration, determine the impulse response, $v(\cdot, \tau)$, for an impulse at that time. However, intuitively one can see that this is not so. Since the excitation takes a non-zero time to propagate through the vocal tract, and the vocal tract is an unpredictable (i.e., past speech does not determine future speech), time-varying, physical system, the system response $v(\cdot, \tau)$ will be affected by configurations (changes) at times greater than τ .

However, that does not mean that the above model cannot be used. The system response, by its definition, must incorporate the effects, if any, of the subsequent system changes. So the question becomes, can the system responses typical of the vocal tract be approximated well by the above model?

I believe so, since the amplitude of response of the vocal tract to an impulse drops off very quickly relative to the rate of change in the vocal tract. For a fixed-configuration vocal tract, the pole-zero model has been shown to be good. Given the slow rate of change of the vocal tract and the rapid decrease in response, it is possible that for a given τ , a pole-zero model can be found that will be a good approximation of the transfer function of the time-varying vocal tract to an impulse at time τ .

Appendix B. Additional proofs

B.1 Additional proofs from Chapter III

Proof (Lemma 3.3.1). To show the first part of the lemma, note that if $\partial B(a, \delta) \subset \overline{K(a, r)}$ then $B(a, \delta) \subset \overline{K(a, r)}$. The set $\partial B(a, \delta)$ is given by

$$\partial B(a, \delta) = \{z \in \mathbb{C} : z = a + \delta e^{i\theta}, \theta \in [0, 2\pi)\}.$$

Therefore, what we want is the largest δ such that $\rho(a, a + \delta e^{i\theta}) \leq r$. That is

$$\rho(a, a + \delta e^{i\theta}) = \frac{\delta}{|1 - |a|^2 - \bar{a}\delta e^{i\theta}|} \leq r,$$

which implies

$$\delta \leq r|1 - |a|^2 - \bar{a}\delta e^{i\theta}|.$$

The right-hand side is minimized by choosing $\theta = \arg a$, giving

$$\delta \leq r(1 - |a|^2 - |a|\delta),$$

which brings us to

$$\delta \leq \frac{r(1 - |a|^2)}{1 + |a|r}.$$

The second part of the lemma is shown in a similar way. Solving for $\rho(a, a + \delta e^{i\theta}) \geq r$, we see

$$\rho(a, a + \delta e^{i\theta}) = \frac{\delta}{|1 - |a|^2 - \bar{a}\delta e^{i\theta}|} \geq r,$$

which leads to

$$\delta \geq r|1 - |a|^2 - \bar{a}\delta e^{i\theta}|.$$

The right-hand quantity is maximized by choosing $\theta = \pi + \arg a$, giving

$$\delta \geq r(1 - |a|^2 + |a|\delta),$$

and leading to

$$\delta \geq \frac{r(1 - |a|^2)}{1 - |a|r}.$$

□

Proof (Lemma 3.3.2). It is easily seen that $\rho(0, re^{i\theta}) = r$ for all $r \in [0, 1]$ and $\theta \in [0, 2\pi)$, which implies $K(0, r) = B(0, r)$. From Lemma 3.2.4, we have that for all $z \in \mathbb{D}$, that $\rho(0, z) = \rho(\phi_a(0), \phi_a(z)) = \rho(a, \phi_a(z))$. Therefore, $K(a, r)$ is the image of the set $B(0, r)$ under the transform ϕ_a .

To show that this image is the set described above in the statement of the lemma, we will show that the boundaries of the sets are the same. For all $\theta \in [0, 2\pi)$, we have $re^{i\theta} \in \partial B(0, r)$, which implies $\phi_a(re^{i\theta}) \in \overline{K(a, r)}$. The boundary of the set $B(\tilde{a}, \tilde{r})$ is given by the set of points z such that $|\tilde{a} - z| = \tilde{r}$. Examine the quantity $|\tilde{a} - \phi_a(re^{i\theta})|$. If this quantity is equal \tilde{r} , then we will know that $\partial K(a, r) = \partial B(\tilde{a}, \tilde{r})$.

$$\begin{aligned} |\tilde{a} - \phi_a(re^{i\theta})| &= \left| a \left(\frac{1 - r^2}{1 - r^2|a|^2} \right) - \frac{a - re^{i\theta}}{1 - \bar{a}re^{i\theta}} \right| \\ &= \left| \frac{r(1 - |a|^2)(e^{i\theta} - ar)}{(1 - r^2|a|^2)(1 - \bar{a}re^{i\theta})} \right| \\ &= \frac{r(1 - |a|^2)}{1 - r^2|a|^2} \left| \frac{e^{i\theta}(1 - are^{-i\theta})}{(1 - \bar{a}re^{i\theta})} \right| \\ &= \frac{r(1 - |a|^2)}{1 - r^2|a|^2} \left| \frac{(1 - \bar{a}re^{i\theta})}{(1 - \bar{a}re^{i\theta})} \right| \\ &= \frac{r(1 - |a|^2)}{1 - r^2|a|^2} = \tilde{r}. \end{aligned}$$

Therefore, $\partial K(a, r) = \partial B(\tilde{a}, \tilde{r})$. Since $K(a, r)$ and $B(\tilde{a}, \tilde{r})$ are both convex, this gives that $K(a, r) = B(\tilde{a}, \tilde{r})$. □

Proof (Lemma 3.3.3). Because $\rho(e^{i\theta}w, e^{i\theta}z) = \rho(w, z)$ for all $\theta \in \mathbb{R}$, $w, z \in \mathbb{D}$, without loss of generality, we may assume that $w \in \mathbb{R}^+$. Then, it is easily shown that $\rho(w, z) = \rho(w, \bar{z})$. That is, $K(w, \delta)$ is symmetric about the real axis. This implies that if there is a unique $z \in \mathbb{D}$ for which the maximal value $|z|$ is obtained, then $z \in \mathbb{R}$. Examination of the shape of $\overline{K(w, \delta)}$, which is a closed disk, reveals that there is either a unique $z \in \mathbb{D}$ such that the maximal value of $|z|$ is achieved, or else it is achieved for all

$z \in \partial K(w, \delta)$. In either case, a point z which obtains the maximum value $|z|$ will be on $\mathbb{R} \cap \partial K(w, \delta)$.

Since $z, w \in \mathbb{R} \cap \mathbb{D}$, we have

$$\rho(z, w) = \frac{|w - z|}{1 - wz}.$$

Assume $\rho(w, z) = \delta$ and $z > w$, to get

$$\delta = \frac{z - w}{1 - zw},$$

which implies one candidate for z is z_1 , defined by

$$z_1 \doteq z = \frac{\delta + w}{1 + \delta w}.$$

Next assume $\rho(w, z) = \delta$ and $z < w$, to get

$$\delta = \frac{w - z}{1 - zw},$$

which implies a second candidate for z is z_2 , defined by

$$z_2 \doteq z = \frac{w - \delta}{1 - \delta w}.$$

This gives two candidate values for z . In the case where $0 \leq z_2 < w$, we have that $|z_2| < |z_1|$. Examining the case where $z_2 < 0$, we see that

$$\begin{aligned} |z_2| = -z_2 &= \frac{\delta - w}{1 - \delta w} \\ &= \frac{(\delta - w)(1 + \delta w)}{(1 - \delta w)(1 + \delta w)} \\ &= \frac{\delta - \delta w^2 + w(\delta^2 - 1)}{(1 - \delta w)(1 + \delta w)} \\ &\leq \frac{\delta - \delta w^2 + w(1 - \delta^2)}{(1 - \delta w)(1 + \delta w)} \\ &= \frac{(\delta + w)(1 - \delta w)}{(1 - \delta w)(1 + \delta w)} \\ &= \frac{(\delta + w)}{(1 + \delta w)} = |z_1|. \end{aligned}$$

Therefore, the maximal value of $|z|$ subject to the constraint that $\rho(w, z) \leq \delta$ is given by

$$|z| = \frac{\delta + |w|}{1 + \delta|w|}.$$

To determine the value of z corresponding to this $|z|$ for a specific w , note that $w = |w|e^{i \arg w}$, which implies $e^{i \arg w} = \frac{w}{|w|}$. Using this, we see that

$$\rho(|w|, |z|) = \rho(|w|e^{i \arg w}, |z|e^{i \arg w}) = \rho(w, |z|\frac{w}{|w|}).$$

Therefore, the z corresponding to the maximal value of $|z|$ subject to the constraints is given by

$$z = \frac{w}{|w|} \left(\frac{\delta + |w|}{1 + \delta|w|} \right).$$

□

Proof (Lemma 3.3.4). If $b \in K(a, r/2)$ then $\rho(a, b) < r/2$. Next, $a \in B(z, \frac{r(1-|z|^2)}{4})$ implies

$$|a - z| < \frac{r(1 - |z|^2)}{4}$$

which in turn implies

$$\begin{aligned} \rho(a, z) &= \frac{|a - z|}{|1 - \bar{a}z|} < \frac{r(1 - |z|^2)}{4|1 - \bar{a}z|} \\ &< \frac{r(1 - |z|)(1 + |z|)}{4(1 - |a||z|)} \\ &< \frac{r(1 - |z|)(1 + |z|)}{4(1 - |z|)} \\ &< \frac{r(1 + |z|)}{4} \\ &< \frac{r}{2}. \end{aligned}$$

Since ρ is a metric, this gives

$$\rho(b, z) < \rho(b, a) + \rho(a, z) \leq r$$

which implies $b \in K(z, r)$. □

Proof (Lemma 3.3.5). Assume $|a| > \delta$. Since $\rho(a, 0) = |a|$, this implies $0 \notin K(a, \delta)$. Denote by b one (of the two) points on $\partial K(a, \delta)$ where $\partial K(a, \delta)$ is tangent to a line through 0. Since line $\overline{0b}$ is tangent to $\partial K(a, \delta)$ (a circle), the line $\overline{b\tilde{a}}$ is perpendicular to the line $\overline{0b}$, where (from Lemma 3.3.2) \tilde{a} is the center of the circle $\partial K(a, \delta)$. The length of line segment $\overline{b\tilde{a}}$ is given by the radius of $\partial K(a, \delta)$, which is (also from Lemma 3.3.2) $\tilde{r} = \frac{\delta(1-|a|^2)}{1-\delta^2|a|^2}$. Using the usual trigonometric calculations, this gives

$$\begin{aligned} \Delta\theta &= 2 \arcsin \left(\frac{\tilde{r}}{|\tilde{a}|} \right) \\ &= 2 \arcsin \left(\frac{\delta}{(1-\delta^2)} \frac{(1-|a|^2)}{|a|} \right) \\ &\leq 2 \arcsin \left(\frac{2\delta}{(1-\delta^2)} \frac{(1-|a|)}{|a|} \right). \end{aligned}$$

Since $\frac{1-|a|}{|a|} \rightarrow 0$ as $|a| \rightarrow 1$ and $\sin x \approx x$ as $x \rightarrow 0$, we have that there exists $r \in (0, 1)$ such that for $\frac{C}{4} > 1$,

$$\begin{aligned} \Delta\theta &\leq rC \left(\frac{\delta}{(1-\delta^2)|a|} \right) (1-|a|) \\ &\leq C \left(\frac{\delta}{(1-\delta^2)} \right) (1-|a|) \end{aligned}$$

for all $a \in \mathbb{D}$ such that $r < |a|$. □

Proof (Lemma 3.3.6). For the first inequality, fix a and consider the quantity $\frac{1}{1-|a||z|}$. Clearly this quantity is maximized when $|z|$ is maximized. By Lemma 3.3.3, we know that subject to the constraint that $\rho(a, z) < r$, that $|z| \leq \frac{r+|a|}{1+r|a|}$. Therefore, for all $z \in \mathbb{D}$ such that $\rho(a, z) \leq r$, we have

$$\begin{aligned} \frac{1}{1-|a||z|} &\leq \frac{1}{1-|a| \left(\frac{r+|a|}{1+r|a|} \right)} = \frac{1+r|a|}{1-|a|^2} \\ &\leq \frac{1+r}{1-|a|^2} \\ &\leq \frac{2}{1-|a|^2}. \end{aligned}$$

For the second inequality, note that by Lemma 3.3.2, we have

$$\frac{1}{m(K(a, r))} = \frac{(1 - r^2|a|^2)^2}{r^2(1 - |a|^2)^2}.$$

From an intermediate step in the proof of Lemma 3.3.6, we have that given our constraints on $\rho(a, z)$,

$$\frac{1}{1 - |a||z|} \leq \frac{1 + r|a|}{1 - |a|^2},$$

which gives that

$$\begin{aligned} \frac{1 - |a|^2}{r^2(1 - |a||z|)^2} &\leq \frac{(1 - |a|^2)(1 + r|a|)^2}{r^2(1 - |a|^2)^2} \\ &= \frac{(1 - r|a|)(1 + |a|)(1 - |a|)(1 + r|a|)^2}{(1 - r|a|)r^2(1 - |a|^2)^2} \\ &\leq \frac{2(1 - r|a|)^2(1 + r|a|)^2}{r^2(1 - r|a|)(1 - |a|^2)^2} \\ &\leq \frac{2}{(1 - r)} \frac{(1 - r^2|a|^2)^2}{r^2(1 - |a|^2)^2} \\ &\leq \frac{2}{(1 - r)} \frac{1}{m(K(a, r))}. \end{aligned}$$

□

Proof (Lemma 3.3.7). Given

$$m(K(a, r)) = \frac{r^2(1 - |a|^2)^2}{(1 - r^2|a|^2)^2}$$

and

$$m(K(a, \epsilon r)) = \frac{\epsilon^2 r^2(1 - |a|^2)^2}{(1 - \epsilon^2 r^2|a|^2)^2},$$

we have

$$\begin{aligned} \frac{m(K(a, r))}{m(K(a, \epsilon r))} &= \frac{(1 - \epsilon^2 r^2|a|^2)^2}{\epsilon^2(1 - r^2|a|^2)^2} \\ &= \frac{(1 - \epsilon r|a|)^2(1 + \epsilon r|a|)^2}{\epsilon^2(1 - r|a|)^2(1 + r|a|)^2} \end{aligned}$$

$$\begin{aligned}
&\leq \frac{(1 - \epsilon r|a|)^2(1 + r|a|)^2}{\epsilon^2(1 - r|a|)^2(1 + r|a|)^2} \\
&= \frac{(1 - \epsilon r|a|)^2}{\epsilon^2(1 - r|a|)^2} .
\end{aligned}$$

Since the derivative of this quantity w.r.t. $|a|$ is strictly positive in the range $0 \leq |a| < 1$, we know that the supremum occurs on the boundary ($|a| = 1$). This gives

$$\frac{m(K(a, r))}{m(K(a, \epsilon r))} \leq \frac{(1 - \epsilon r)^2}{\epsilon^2(1 - r)^2} ,$$

which implies

$$\frac{1}{m(K(a, \epsilon r))} \leq \frac{(1 - \epsilon r)^2}{\epsilon^2(1 - r)^2} \frac{1}{m(K(a, r))} ,$$

□

Proof (Lemma 3.3.8). Assume

$$\rho(z, w) = \frac{|z - w|}{|1 - \bar{z}w|} < \frac{1}{3} .$$

This implies

$$\begin{aligned}
3|z - w| &< |1 - \bar{z}w| \\
&= |1 - \bar{z}(z - (z - w))| \\
&= |1 - |z|^2 + \bar{z}(z - w)| \\
&\leq (1 - |z|^2) + |z||z - w| ,
\end{aligned}$$

which implies

$$(3 - |z|)|z - w| < (1 - |z|)(1 + |z|) ,$$

which in turn gives

$$|z - w| < (1 - |z|) .$$

□

Proof (Lemma 3.3.9). For the first inequality, fix $w \in \mathbb{D}$. We then have

$$m(K(w, r)) = \frac{r^2(1 - |w|^2)^2}{(1 - r^2|w|^2)^2}.$$

The quantity $\frac{1}{m(K(z, r))}$ can be maximized by minimizing $m(K(z, r))$. This in turn is done by maximizing $|z|$ subject to the constraint that $\rho(w, z) \leq \delta$. By Lemma 3.3.3, we have that

$$|z| \leq \frac{\delta + |w|}{1 + \delta|w|},$$

which implies

$$\begin{aligned} m(K(z, r)) &\geq \frac{r^2 \left(1 - \left(\frac{\delta + |w|}{1 + \delta|w|}\right)^2\right)^2}{\left(1 - r^2 \left(\frac{\delta + |w|}{1 + \delta|w|}\right)^2\right)^2} \\ &= \frac{r^2(1 - |w|^2)^2(1 - \delta^2)^2}{((1 + \delta|w|)^2 - r^2(\delta + |w|)^2)^2}. \end{aligned}$$

Thus, we have

$$\begin{aligned} \frac{m(K(w, r))}{m(K(z, r))} &\leq \frac{((1 + \delta|w|)^2 - r^2(\delta + |w|)^2)^2}{(1 - \delta^2)^2(1 - r^2|w|^2)^2} \\ &= \frac{((1 - r^2\delta^2) + 2|w|(\delta - r^2\delta) + |w|^2(\delta^2 - r^2))^2}{(1 - \delta^2)^2(1 - r^2|w|^2)^2} \\ &\leq \frac{((1 - r^2\delta^2) + 2|w|(1 - r^2\delta^2) + |w|^2(1 - r^2\delta^2))^2}{(1 - \delta^2)^2(1 - r^2|w|^2)^2} \\ &= \frac{(1 - r^2\delta^2)^2(1 + |w|)^4}{(1 - \delta^2)^2(1 - r^2|w|^2)^2} \\ &\leq \frac{16(1 - r^2\delta^2)^2}{(1 - \delta^2)^2(1 - r^2)^2}. \end{aligned}$$

Therefore,

$$\frac{1}{m(K(z, r))} \leq \frac{16(1 - r^2\delta^2)^2}{(1 - \delta^2)^2(1 - r^2)^2} \frac{1}{m(K(w, r))}$$

whenever $\rho(w, z) < \delta$.

For the second inequality, fix $z \in \mathbb{D}$. To minimize the quantity $\frac{1}{|1 - \bar{w}z|}$, we maximize $|1 - \bar{w}z|$ subject to the constraint that $\rho(z, w) \leq \delta$. With reasoning similar to that in

Lemma 3.3.3, we see that such a w will be a multiple of z , that is, $w = x \frac{z}{|z|}$ for some $x \in \mathbb{R}$. Solving for x subject to the constraint, we have

$$\begin{aligned} \delta = \rho(z, w) &= \left| \frac{z - \frac{z}{|z|}x}{1 - \overline{z}\frac{z}{|z|}x} \right| \\ &= \frac{|z| \left| 1 - \frac{x}{|z|} \right|}{1 - |z|x} \\ &= \frac{\pm |z| \left| 1 - \frac{x}{|z|} \right|}{1 - |z|x}. \end{aligned}$$

this gives for x ,

$$x = \frac{|z| \pm \delta}{1 \pm \delta |z|}.$$

Examining both values, we find that the maximizer of $|1 - \overline{w}z|$ is $x = \frac{|z| - \delta}{1 - \delta |z|}$, giving

$$\begin{aligned} \frac{1}{|1 - \overline{w}z|} &\geq \frac{1 - \delta |z|}{1 - |z|^2} \\ &\geq \frac{1 - \delta}{1 - |z|^2}. \end{aligned}$$

Therefore

$$\frac{1}{1 - |z|^2} \leq \left(\frac{1}{1 - \delta} \right) \frac{1}{|1 - \overline{w}z|}.$$

□

B.2 Proof of Theorem 3.6.1

First, the following lemma will be needed in the proof of Theorem 3.6.1.

Lemma B.2.1 *Let $E \subset X$ be a convex set and let $T: X \rightarrow Y$ be a linear transform. Then, the image of the set E under the mapping T , denoted $T[E]$, is convex.*

Proof. Let $y_1, y_2 \in T[E]$ and let $0 \leq \alpha \leq 1$. What is necessary to show is that $\alpha y_1 + (1 - \alpha)y_2 \in T[E]$.

Since $y_1, y_2 \in T[E]$, there exist $x_1, x_2 \in X$ such that $y_1 = Tx_1$ and $y_2 = Tx_2$. Since E is convex, we have $\alpha x_1 + (1 - \alpha)x_2 \in E$. Examining $T(\alpha x_1 + (1 - \alpha)x_2)$, we see that

$$\begin{aligned} T(\alpha x_1 + (1 - \alpha)x_2) &= \alpha Tx_1 + (1 - \alpha)Tx_2 \\ &= \alpha y_1 + (1 - \alpha)y_2 \in T[E]. \end{aligned}$$

Since y_1, y_2 , and $0 \leq \alpha \leq 1$ were arbitrarily chosen, this implies that $T[E]$ is convex. \square

Proof (Theorem 3.6.1). The proof is an elaboration of that in [33], which itself is a adaptation of that in [5].

(1 \Rightarrow 2) Assume 1 is true. Suppose there exists $f \in X_1$ such that $mf \notin \overline{E_{1,p}}$. Since $E_{1,p}$ is the image of a convex set, that is, the unit ball of $\ell_{1,p}$ intersected with the set of finitely non-zero sequences, under a linear transform, by Lemma B.2.1, it is convex, implying $\overline{E_{1,p}}$ is convex also. Then, by the Hahn-Banach separation theorem, there exists $\Phi \in X^*$ such that for all $h \in \overline{E_{1,p}}$, $|\Phi(h)| < \gamma \leq m|\Phi(f)|$. Since it is true for all $h \in \overline{E_{1,p}}$, it is certainly true for $x_n \in E_{p,1}$ of the form $x_n = \sum_{k=1}^{k(n)} \lambda_{n,k} u_{n,k}$ where $\sum_{k=1}^{k(n)} |\lambda_{n,k}|^p \leq 1$. Evaluating $\Phi(x_n)$, we have

$$\Phi(x_n) = \sum_{k=1}^{k(n)} \lambda_{n,k} \Phi(u_{n,k}).$$

Observe that this is in the form of a functional $\lambda_n = \{\lambda_{n,k}\}_{k=1}^{k(n)}$ operating on the sequence $\{\Phi(u_{n,k})\}_{k=1}^{k(n)}$. Choose λ_n so that it is aligned with the sequence $\{\Phi(u_{n,k})\}_{k=1}^{k(n)}$ and $\sum_{k=1}^{k(n)} |\lambda_{n,k}|^p = 1$. Then

$$\begin{aligned} \Phi(x_n) &= \sum_{k=1}^{k(n)} \lambda_{n,k} \Phi(u_{n,k}) = \left(\sum_{k=1}^{k(n)} |\lambda_{n,k}|^p \right)^{1/p} \left(\sum_{k=1}^{k(n)} |\Phi(u_{n,k})|^q \right)^{1/q} \\ &= \left(\sum_{k=1}^{k(n)} |\Phi(u_{n,k})|^q \right)^{1/q} < \gamma \leq m\|\Phi\|. \end{aligned}$$

Since this is true for all n , this implies that

$$\sup_n \left(\sum_{k=1}^{k(n)} |\Phi(u_{n,k})|^q \right)^{1/q} < \gamma \leq m\|\Phi\|$$

which is a contradiction of 1. Therefore, $mX_1 \subset \overline{E_{1,p}}$.

To prove the other half of 2, let $x \in E_{1,p}$, where $x = \sum_{n=1}^N \sum_{k=1}^{k(n)} \lambda_{n,k} u_{n,k}$ and where $\sum_{n=1}^N \left(\sum_{k=1}^{k(n)} |\lambda_{n,k}|^p \right)^{1/p} \leq 1$. Computing $\|x\|$, we have that

$$\begin{aligned}
\|x\| &= \sup_{\substack{\Phi \in X^* \\ \|\Phi\| \leq 1}} |\Phi(x)| \\
&= \sup_{\substack{\Phi \in X^* \\ \|\Phi\| \leq 1}} \left| \sum_{n=1}^N \sum_{k=1}^{k(n)} \lambda_{n,k} \Phi(u_{n,k}) \right| \\
&\leq \sup_{\substack{\Phi \in X^* \\ \|\Phi\| \leq 1}} \sum_{n=1}^N \left| \sum_{k=1}^{k(n)} \lambda_{n,k} \Phi(u_{n,k}) \right| \\
&\leq \sup_{\substack{\Phi \in X^* \\ \|\Phi\| \leq 1}} \sum_{n=1}^N \left(\sum_{k=1}^{k(n)} |\lambda_{n,k}|^p \right)^{1/p} \left(\sum_{k=1}^{k(n)} |\Phi(u_{n,k})|^q \right)^{1/q} \\
&\leq \left[\sum_{n=1}^N \left(\sum_{k=1}^{k(n)} |\lambda_{n,k}|^p \right)^{1/p} \right] \sup_{\substack{\Phi \in X^* \\ \|\Phi\| \leq 1}} \left[\sup_n \left(\sum_{k=1}^{k(n)} |\Phi(u_{n,k})|^q \right)^{1/q} \right] \\
&\leq M \sup_{\substack{\Phi \in X^* \\ \|\Phi\| \leq 1}} \|\Phi\| \leq M.
\end{aligned}$$

Therefore, $x \in MX_1$. Since this is true for each $x \in E_{1,p}$, it is also true for each $x \in \overline{E_{1,p}}$, and so $\overline{E_{1,p}} \subset MX_1$.

(2 \Rightarrow 3)

Assume 2. Let $f_0 \in X$ and fix $\epsilon > 0$. Since $mX_1 \subset \overline{E_{1,p}}$, there exists $h_0 \in E_{1,p}$, $h_0 = \sum_{n=1}^{N(0)} \sum_{k=1}^{k(n)} \lambda_{0,n,k} u_{n,k}$ with $\sum_{n=1}^{N(0)} \left(\sum_{k=1}^{k(n)} |\lambda_{0,n,k}|^p \right)^{1/p} \leq 1$, such that for $f_1 = f_0 - \frac{\|f_0\|}{m} h_0$, $\|f_1\| < \epsilon/2$.

Repeat this process to get for each j , $h_j = \sum_{n=1}^{N(j)} \sum_{k=1}^{k(n)} \lambda_{j,n,k} u_{n,k} \in E_{1,p}$ such that for $f_{j+1} = f_j - \frac{\|f_j\|}{m} h_j$, $\|f_{j+1}\| \leq \epsilon/2^{j+1}$.

Since for each n , $f_0 = f_{n+1} + \sum_{j=0}^n \frac{\|f_j\|}{m} h_j$, and $\lim_{n \rightarrow \infty} \|f_n\| = 0$, we have that

$$f_0 = \lim_{n \rightarrow \infty} \sum_{j=0}^n \frac{\|f_j\|}{m} h_j.$$

Defining x_n by

$$\begin{aligned}
 x_n &= \sum_{j=0}^n \frac{\|f_j\|}{m} h_j \\
 &= \sum_{j=0}^n \frac{\|f_j\|}{m} \sum_{i=1}^{N(j)} \sum_{k=1}^{k(i)} \lambda_{j,i,k} u_{i,k} \\
 &= \sum_{i=1}^{\max\{N(j):j=1,\dots,n\}} \sum_{k=1}^{k(i)} \left(\sum_{j=0}^n \frac{\|f_j\|}{m} \lambda_{j,i,k} \right) u_{i,k} .
 \end{aligned}$$

Defining the transform $T: \ell_{1,p} \rightarrow X$ by

$$T\{\lambda_{n,k}\} = \sum_{n=1}^{\infty} \sum_{k=1}^{k(n)} \lambda_{n,k} u_{n,k} ,$$

we see that

$$\begin{aligned}
 x_n &= T\left\{ \sum_{j=0}^n \frac{\|f_j\|}{m} \lambda_{j,i,k} \right\} \\
 &= T\gamma_n
 \end{aligned}$$

where

$$\gamma_n = \left\{ \sum_{j=0}^n \frac{\|f_j\|}{m} \lambda_{j,i,k} \right\} .$$

Now, if we can show that $\{\gamma_n\}_{n=1}^{\infty}$ is a Cauchy sequence in $\ell_{1,p}$, we will have that it converges to a limit sequence, denoted λ_{ϵ} .

Examining $\|\gamma_n - \gamma_{n-1}\|_{1,p}$, we see that

$$\begin{aligned}
 \|\gamma_n - \gamma_{n-1}\|_{1,p} &= \left\| \left\{ \sum_{j=0}^n \frac{\|f_j\|}{m} \lambda_{j,i,k} \right\} - \left\{ \sum_{j=0}^{n-1} \frac{\|f_j\|}{m} \lambda_{j,i,k} \right\} \right\|_{1,p} \\
 &= \left\| \left\{ \frac{\|f_n\|}{m} \lambda_{n,i,k} \right\} \right\|_{1,p} \\
 &= \frac{\|f_n\|}{m} \|\{\lambda_{n,i,k}\}\|_{1,p} \\
 &\leq \frac{\|f_n\|}{m}
 \end{aligned}$$

$$\leq \frac{1}{2^n} \frac{\epsilon}{m}.$$

Therefore,

$$\begin{aligned} \|\gamma_n - \gamma_{n'}\|_{1,p} &\leq \|\gamma_n - \gamma_{n-1}\|_{1,p} + \|\gamma_{n-1} - \gamma_{n-2}\|_{1,p} + \dots + \|\gamma_{n'+1} - \gamma_{n'}\|_{1,p} \\ &\leq \frac{\epsilon}{m} \sum_{i=n'+1}^n \frac{1}{2^i} \\ &\leq \frac{1}{2^{n'}} \frac{\epsilon}{m} \sum_{i=1}^{n-n'} \frac{1}{2^i} \\ &\leq \frac{1}{2^{n'}} \frac{\epsilon}{m}. \end{aligned}$$

Since this value depends only on n' , and decreases with increasing n' , $\{\gamma_n\}_{n=1}^\infty$ is a Cauchy sequence in a complete space, and hence converges to some $\lambda \in \ell_{1,p}$ with

$$\|\lambda\|_{1,p} \leq \frac{\|f_0\| + \epsilon}{m}.$$

Since ϵ was arbitrarily chose, this implies that

$$\inf_{\lambda \in \Lambda(E,f)} \|\lambda\|_{1,p} \leq \frac{\|f\|}{m}$$

for all $f \in X$.

(3 \Rightarrow 1)

Assume 3. Let $\Phi \in X^*$ and let $f_n = \sum_{k=1}^{k(n)} \lambda_{n,k} u_{n,k}$ where $\sum_{k=1}^{k(n)} |\lambda_{n,k}|^p = 1$ for each n and where the sequence $\{\lambda_{n,k}\}_{k=1}^{k(n)}$ (when treated as a functional) is aligned with the sequence $\{\Phi(u_{n,k})\}_{k=1}^{k(n)}$. Clearly, $f_n \in E_{1,p}$. Then,

$$\begin{aligned} |\Phi(x_n)| &= \left| \sum_{k=1}^{k(n)} \lambda_{n,k} \Phi(u_{n,k}) \right| = \|\{\lambda_{n,k}\}_{k=1}^{k(n)}\| \|\{\Phi(u_{n,k})\}_{k=1}^{k(n)}\| \\ &= \left(\sum_{k=1}^{k(n)} |\lambda_{n,k}|^p \right)^{1/p} \left(\sum_{k=1}^{k(n)} |\Phi(u_{n,k})|^q \right)^{1/q} \\ &= \left(\sum_{k=1}^{k(n)} |\Phi(u_{n,k})|^q \right)^{1/q}. \end{aligned}$$

However, for all $x \in X$,

$$|\Phi(x)| \leq \|\Phi\| \|x\|,$$

which implies

$$|\Phi(x_n)| = \left(\sum_{k=1}^{k(n)} |\Phi(u_{n,k})|^q \right)^{1/q} \leq \|\Phi\| \|x_n\| \leq M \|\Phi\|.$$

This gives the right-hand inequality of 1.

Now, fix $\epsilon > 0$ and choose $f \in E_{1,p}$ such that $\|f\| \leq 1$ and $|\Phi(f)| > \|\Phi\| - \epsilon$. By 3, there exists $\lambda \in \ell_{1,p}$ such that $\sum_{n=1}^N \left(\sum_{k=1}^{k(n)} |\lambda_{n,k}|^p \right)^{1/p} \leq \frac{\|f\|}{m} + \epsilon \leq \frac{1}{m} + \epsilon$. Then,

$$\begin{aligned} \|\Phi\| - \epsilon &< |\Phi(f)| \\ &< \left| \Phi \left(\sum_{n=1}^N \sum_{k=1}^{k(n)} \lambda_{n,k} u_{n,k} \right) \right| \\ &< \left| \sum_{n=1}^N \sum_{k=1}^{k(n)} \lambda_{n,k} \Phi(u_{n,k}) \right| \\ &< \sum_{n=1}^N \left(\sum_{k=1}^{k(n)} |\lambda_{n,k}|^p \right)^{1/p} \left(\sum_{k=1}^{k(n)} |\Phi(u_{n,k})|^q \right)^{1/q} \\ &< \left(\sum_{n=1}^N \left(\sum_{k=1}^{k(n)} |\lambda_{n,k}|^p \right)^{1/p} \right) \sup_n \left(\sum_{k=1}^{k(n)} |\Phi(u_{n,k})|^q \right)^{1/q} \\ &< \left(\frac{1}{m} + \epsilon \right) \sup_n \left(\sum_{k=1}^{k(n)} |\Phi(u_{n,k})|^q \right)^{1/q} \end{aligned}$$

which gives

$$\frac{\|\Phi\| - \epsilon}{\left(\frac{1}{m} + \epsilon \right)} < \sup_n \left(\sum_{k=1}^{k(n)} |\Phi(u_{n,k})|^q \right)^{1/q}.$$

Since ϵ was arbitrarily chosen, this gives that

$$m\|\Phi\| \leq \sup_n \left(\sum_{k=1}^{k(n)} |\Phi(u_{n,k})|^q \right)^{1/q}.$$

□

Appendix C. Heuristic algorithm for finding glottal pulses

Presented in this section is the algorithm which was used in the computer application described in Chapter VII to estimate the glottal pulse starting locations in samples of speech. Unfortunately, an error was found in the implementation of algorithm at a date too late to allow for the computer results to be reexamined. However, I feel that based on the nature of the error (the weighting function varied slightly from that shown below) and the fact that the performance did not change significantly on a small test case, that no significant changes would be seen with the corrected version of the computer application.

The algorithm presented here is strictly heuristic. It is based on some observations made during various classroom projects, modified by trial-and-error. It has not been tested on a wide variety of speech or speakers.

In creating this algorithm, the primary concern was to have a method by which the approximate locations of glottal pulses could be found automatically (i.e., by computer), in speech corrupted by noise as well as in clean speech. Of course, it was desired that the performance be reasonably reliable, but since this dissertation did not hinge on this algorithm, it was only necessary that it perform acceptably on the speech samples with which I was working. The determination of what constitutes acceptable behavior was based on my estimate of where the glottal pulses were probably starting. No attempt has been made to verify that my estimate of these locations was accurate.

There are two steps in this algorithm. The first step creates, from the speech signal, a signal in which the approximate glottal pulse start times can be seen easily by inspection, appearing as local minima of the signal. The second step finds these local minima within a reasonably sized local time windows.

The intent of the first step is to create, from the speech signal s , a new signal, s_1 , in which the pitch periods can more easily be seen and hence, from which the approximate glottal pulse start points can be extracted. This step uses a weighting function, w , described by

$$w(t) = \begin{cases} \left(\frac{128}{20} + 800(t - t_o) \right) e^{-250(t-t_o)} & -\frac{1}{125} \leq (t - t_o) \leq -\frac{1}{125} + \frac{1}{800} \\ e^{-250(t-t_o)} & -\frac{1}{125} + \frac{1}{800} \leq (t - t_o) \leq -\frac{1}{800} \\ -800(t - t_o)e^{-250(t-t_o)} & -\frac{1}{800} \leq (t - t_o) \leq 0 \\ 0 & \text{otherwise} \end{cases}$$

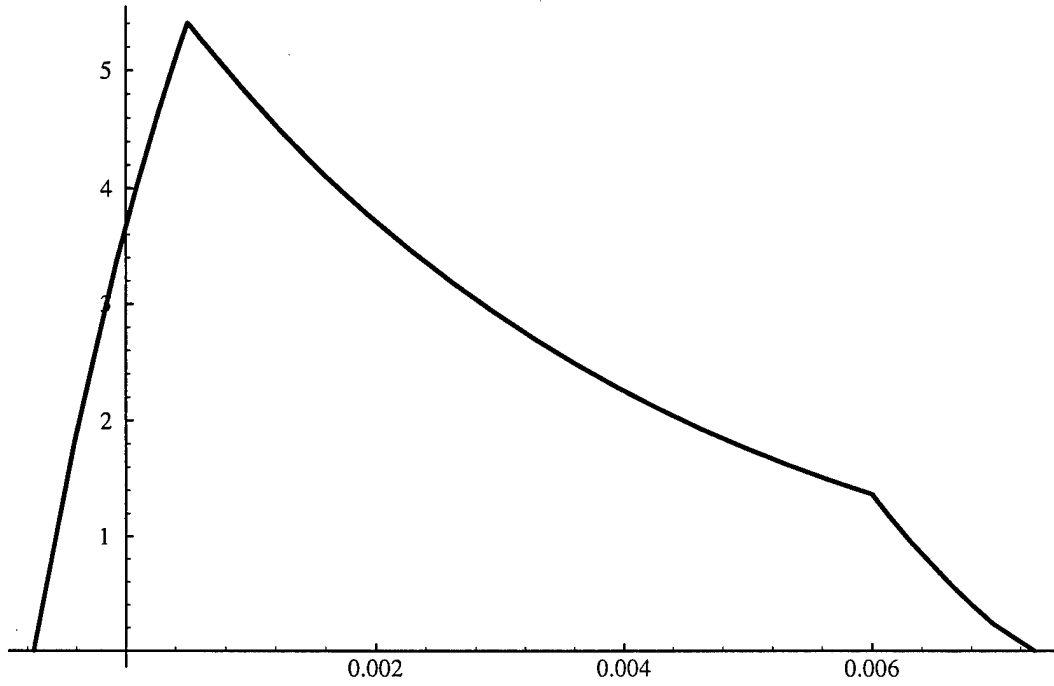


Figure 65. Weighting Function used in Glottal Pulse Finding Heuristic Algorithm

where $t_o = \frac{29}{4000}$ is an offset value used for alignment purposes. The weighting function, w , is plotted in Figure 65.

The operation performed in the first step of the algorithm is

$$s_1(t) = \int_{-\infty}^{\infty} |s(\tau)w(t - \tau)|^2 d\tau .$$

This can also be considered a convolution, as in

$$s_1 = |s|^2 * w^2 .$$

The second step of the algorithm consists of finding relative minima in the signal resulting from the first step. These relative minima roughly correspond to the starting points of glottal pulses. The minima are located in windows of width 3/500 seconds, asymmetrically centered about each time. This can best be described by the boolean-

valued function, s_2 , given by

$$s_2(t) = \begin{cases} \text{True} & s_1(t) = \min \{s_1(t + \tau) : \tau \in [-\frac{1}{500}, \frac{2}{500}]\} \\ \text{False} & \text{otherwise} \end{cases} . \quad (77)$$

Times t for which $s_2(t)$ are true are the estimated start times of glottal pulses.

While the result of the second step is well behaved for most true speech signals, it fails in the case of some non-speech signals, specifically, in the case of constant functions, where $s_2(t) = \text{True}$ for every time t . To avoid the practical aspects of problem, it is desirable to modify this definition so that $s_2(t) = \text{True}$ only if $s_1(t) < s_1(t - \delta t)$ for every sufficiently small $\delta t > 0$. This results in no peaks being estimated to be in constant portions of the signal.

Note that given the constants in the algorithm described above, glottal pulses which are spaced roughly 2/500 second apart or less (corresponding to a vocal pitch of around 250 Hz or greater) will confuse the algorithm. That is, some pulses will be detected and others not. An example of an occurrence of this is seen below in Figure 67.

Shown in Figure 66 are results from this algorithm on a sample of the phoneme /IY/ from a female speaker and a sample of the phoneme /OY/ from a male speaker. Both samples were of clean (not corrupted by noise) speech. The pitch of the female speaker's voice is close to 250 Hz – almost too high to be appropriate for use with this heuristic algorithm. The estimated starting points are marked by vertical grid lines.

As seen in this Figure, the signal resulting from the first step of this algorithm shows clear minima where one might guess the true glottal pulse starting locations to be. Note that the glottal pulses too close to the end points of the sample will be missed by the algorithm. Although the pitch of the female speaker's voice was high, the algorithm still was able to estimate reliably the glottal pulse starting locations.

Figure 67 shows the results of the algorithm on the same phoneme samples corrupted with Gaussian white noise of 10 dB, 6 dB, 3 dB, and 0 dB Signal-to-Noise Ratios (SNR). The glottal pulses estimated based on the corrupt speech are marked with solid vertical grid lines, while those estimated based on the clean speech are marked by dashed vertical grid lines for comparison.

The effects of the increasing noise levels can be seen easily, especially in the results for the phoneme /IY/. With increasing noise levels, the minima become less apparent,

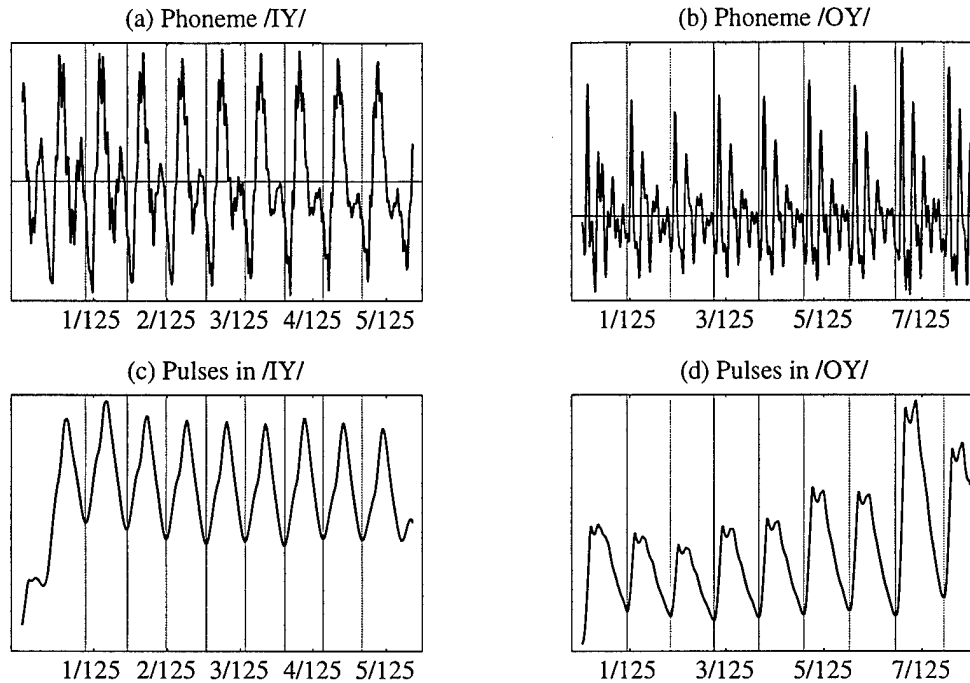


Figure 66. Glottal Pulses Found in Samples of Clean Speech. Vertical grid lines mark the estimated locations of glottal pulses as found by the algorithm. (a) A segment of the phoneme /IY/. (b) A segment of the phoneme /OY/. (c) The result of the first step of the algorithm on the phoneme /IY/. (d) The result of the first step of the algorithm on the phoneme /OY/.

making automatic detection problematic. Also, the addition of noise causes the minima of the signal resulting from the first step to vary in location somewhat. For the phoneme /OY/, from a lower pitched (male) speaker, this resulted in some small variations in the estimated glottal pulse starting location. For the phoneme /IY/, from a higher pitched (female) speaker, this variation was enough to cause the second step of the algorithm to miss some glottal pulses completely.

I believe that the algorithm could be easily modified to work better on higher pitched voices, however, this work has not yet been done. One possible approach would be to reduce the window size used in the definition of s_2 , defined in (77).

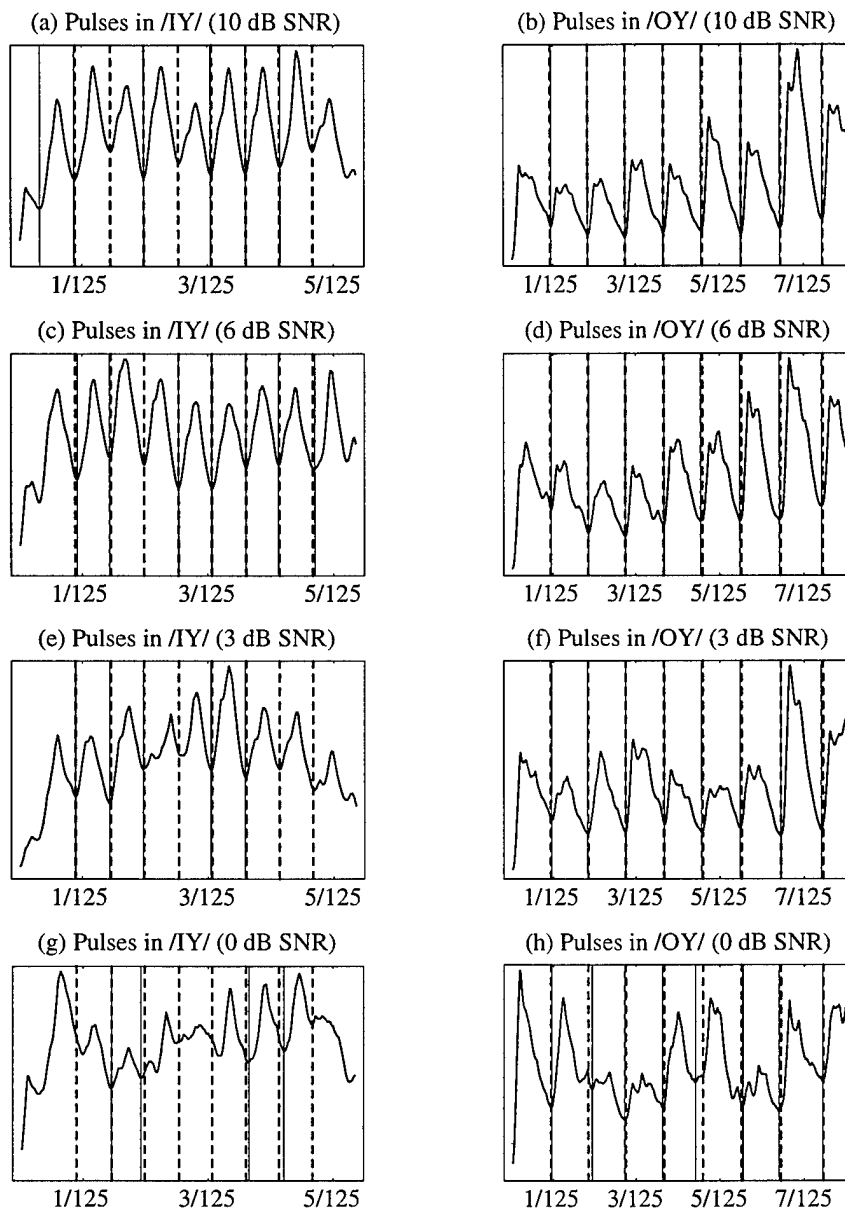


Figure 67. Glottal Pulses Found in Samples of Noisy Speech. Shown is the result of the first step of the algorithm on speech corrupted with varying amounts of noise. Solid vertical grid lines mark the estimated locations of glottal pulses as found by the algorithm. Dashed vertical grid lines mark the pulse locations found for the clean sample of speech. Results for (a) phoneme /IY/, 10 dB SNR noise, (b) phoneme /OY/, 10 dB SNR noise, (c) phoneme /IY/, 6 dB SNR noise, (d) phoneme /OY/, 6 dB SNR noise, (e) phoneme /IY/, 3 dB SNR noise, (f) phoneme /OY/, 3 dB SNR noise, (g) phoneme /IY/, 0 dB SNR noise, and (h) phoneme /OY/, 0 dB SNR noise.

Bibliography

1. Adams, Robert A. *Sobolev Spaces*. Pure and Applied Mathematics, 65, New York: Academic Press, 1975.
2. Ahlfors, Lars V. *Complex Analysis* (2nd Edition). New York: McGraw-Hill Book Company, 1966.
3. Baer, Thomas and Brian C. J. Moore. "Effects of spectral smearing on the intelligibility of sentences in noise," *Journal of the Acoustical Society of America*, 94(3):1229–1241 (September 1993).
4. Benedetto, John J. and William Heller. *Mathematical Notes*, 10, Supplement 1, chapter Irregular Sampling and the Theory of Frames, I, 103–125. Princeton, NJ: Princeton University Press, 1990.
5. Bonsall, F. F. "A General Atomic Decomposition Theorem and Banach's Closed Range Theorem," *The Quarterly Journal of Mathematics, Oxford Second Series*, 42:9–14 (1991).
6. Cheng, Yan-Ming and Douglas O'Shaughnessy. "On 450-600 b/s Natural Sounding Speech Coding," *IEEE Transactions on Speech and Audio Processing*, 1(2):207–220 (April 1993).
7. Conway, John B. *Functions of One Complex Variable* (2nd Edition). Graduate Texts in Mathematics, 11, New York: Springer-Verlag New York, 1978.
8. D'Angelo, Henry. *Linear Time Varying Systems: Analysis and Synthesis*. The Allyn and Bacon series in Electrical Engineering, Boston: Allyn and Bacon, 1970.
9. Daubechies, Ingrid. *Ten Lectures on Wavelets*. CBMS-NSF Regional Conference Series in Applied Mathematics, 61, Philadelphia, PA: Society for Industrial and Applied Mathematics, 1992.
10. Donoho, David L. and Iain M. Johnstone. "Adapting to Unknown Smoothness via Wavelet Shrinkage," *Journal of the American Statistical Association*, 90(432):1200–1224 (1995).
11. Duffin, R. J. and A. C. Schaeffer. "A Class of Nonharmonic Fourier Series," *Transactions of the American Mathematical Society*, 72:341–366 (March 1952).
12. Duren, Peter L. *Theory of H^p Spaces*. Pure and Applied Mathematics, 38, New York: Academic Press, 1970.
13. Gupta, Sunil K. and Juergen Schroeter. "Pitch-synchronous frame-by-frame and segment-based articulatory analysis by synthesis," *Journal of the Acoustical Society of America*, 94(5):2517–2530 (November 1993).
14. Hayashi, Shinji and Nobuhiko Kitawaki. "An objective quality assessment for bit-reduction coding of wideband speech," *Journal of the Acoustical Society of America*, 92(1):106–113 (July 1992).
15. Helmsberg, Gilbert. *Introduction to Spectral Theory in Hilbert Space*. North-Holland Series in Applied Mathematics and Mechanics, 6, New York: Wiley, 1969.

16. Kewley-Port, Diane and Charles S. Watson. "Formant-frequency discrimination for isolated English vowels," *Journal of the Acoustical Society of America*, 95(1):485-496 (January 1994).
17. Kleijn, W. Bastiaan. "Encoding Speech Using Prototype Waveforms," *IEEE Transactions on Speech and Audio Processing*, 1(4):386-399 (October 1993).
18. Krishnamurthy, Ashok K. "Glottal Source Estimation Using a Sum-of-Exponentials Model," *IEEE Transactions on Signal Processing*, 40:682-686 (March 1992).
19. Leek, Marjorie R. and Van Summers. "The effect of temporal waveform shape on spectral discrimination by normal-hearing and hearing-impaired listeners," *Journal of the Acoustical Society of America*, 94(4):2074-2082 (October 1993).
20. Luecking, Daniel H. "Representation and Duality in Weighted Spaces of Analytic Functions," *Indiana University Mathematics Journal*, 34(2):319-336 (1985).
21. Moore, Brian C. J. *An Introduction to the Psychology of Hearing* (3rd Edition). Academic Press, 1989.
22. Ninness, Brett and Fredrik Gustafsson. "A Unifying Construction of Orthonormal Bases for System Identification," *IEEE Transactions on Automatic Control*, 42(4):515-21 (April 1996).
23. Parsons, Thomas W. *Voice and Speech Processing*. McGraw-Hill Series in Electrical Engineering, CAD/CAM, Robotics, and Computer Vision, New York: McGraw-Hill, 1986.
24. Pati, Y. C., et al. "Orthogonal Matching Pursuit: Recursive Function Approximation with Applications to Wavelet Decomposition." *Conference Record of the Twenty-Seventh Asilomar Conference on Signals, Systems and Computers* 1. 40-44. 1993.
25. Quackenbush, Schuyler R., et al. *Objective Measures of Speech Quality*. Prentice Hall Advanced Reference Series, Edglewood Cliffs, NJ: Prentice-Hall, 1988.
26. Quatieri, Thomas F. and Robert J. McAulay. "Shape Invariant Time-Scale and Pitch Modification of Speech," *IEEE Transactions on Signal Processing*, 40(3):497-510 (March 1992).
27. Savic, Michael, et al. "Co-channel Speaker Separation Based on Maximum-Likelihood Deconvolution." *Proceedings of the ICASSP, Vol 1*. 25-28. 1994.
28. Teas, Donald C. *Foundations of Modern Auditory Theory, I*, chapter 7. New York: Academic Press, 1970. Jerry V. Tobias, editor.
29. ter Keurs, Mariken, et al. "Effects of spectral envelope smearing on speech reception. I," *Journal of the Acoustical Society of America*, 91(5):2872-2880 (May 1992).
30. ter Keurs, Mariken, et al. "Effects of spectral envelope smearing on speech reception. II," *Journal of the Acoustical Society of America*, 93(3):1547-1552 (March 1993).
31. Tobias, Jerry V., editor. *Foundations of Modern Auditory Theory, I*. New York: Academic Press, 1970.
32. Tonndorf, Juergen. *Foundations of Modern Auditory Theory, I*, chapter 6. New York: Academic Press, 1970. Jerry V. Tobias, editor.

33. Ward, N. F. Dudley and Jonathan R. Partington. "Rational Wavelet Decompositions of Transfer Functions in Hardy-Sobolev Classes," *Mathematics of Controls, Signals, and Systems*, 8(3):257-78 (1995).

REPORT DOCUMENTATION PAGE			Form Approved OMB No. 0704-0188	
Public reporting burden for this collection of information is estimated to average 1 hour per response, including the time for reviewing instructions, searching existing data sources, gathering and maintaining the data needed, and completing and reviewing the collection of information. Send comments regarding this burden estimate or any other aspect of this collection of information, including suggestions for reducing this burden, to Washington Headquarters Services, Directorate for Information Operations and Reports, 1215 Jefferson Davis Highway, Suite 1204, Arlington, VA 22202-4302, and to the Office of Management and Budget, Paperwork Reduction Project (0704-0188), Washington, DC 20503.				
1. AGENCY USE ONLY (Leave blank)		2. REPORT DATE 5 June 1998		3. REPORT TYPE AND DATES COVERED Doctoral Dissertation
4. TITLE AND SUBTITLE Representations, Approximations and Algorithms for Mathematical Speech Processing			5. FUNDING NUMBERS	
6. AUTHOR(S) Laura R. C. Suzuki, Major, USAF				
7. PERFORMING ORGANIZATION NAME(S) AND ADDRESS(ES) Department of Mathematics and Statistics Air Force Institute of Technology 2950 P Street, Bldg 640 Wright-Patterson AFB, OH 45433-7765			8. PERFORMING ORGANIZATION REPORT NUMBER AFIT/DS/ENC/98J-1	
9. SPONSORING/MONITORING AGENCY NAME(S) AND ADDRESS(ES) Dr. Jon Sjogren AFOSR/NM 110 Duncan Ave B115 Bolling AFB, DC 20332-8050			10. SPONSORING/MONITORING AGENCY REPORT NUMBER	
11. SUPPLEMENTARY NOTES				
12a. DISTRIBUTION AVAILABILITY STATEMENT Approved for public release; distribution unlimited			12b. DISTRIBUTION CODE	
13. ABSTRACT (Maximum 200 words) Representing speech signals such that specific characteristics of speech are included is essential in many Air Force and DoD signal processing applications. A mathematical construct called a frame is presented which captures the important time-varying characteristic of speech. Roughly speaking, frames generalize the idea of an orthogonal basis in a Hilbert space. Specific spaces applicable to speech are $L_2(R)$ and the Hardy spaces $H_p(D)$ for $p > 1$ where D is the unit disk in the complex plane. Results are given for representations in the Hardy spaces involving Carleson's inequalities (and its extensions), frames and hybrid frames, as well as $L_2(R)$. Examples of different speech signals are given and the representations via frames are applied to demonstrate its robustness and adaptiveness, while using very few coefficients in the approximation. Thus, the processing, transmitting and storing of speech data could be compressed or reduced and still keep the fidelity of the signal.				
14. SUBJECT TERMS Speech modeling, Wavelets, Frames, Hardy spaces, Carleson's inequality			15. NUMBER OF PAGES 252	
			16. PRICE CODE	
17. SECURITY CLASSIFICATION OF REPORT UNCLASSIFIED	18. SECURITY CLASSIFICATION OF THIS PAGE UNCLASSIFIED	19. SECURITY CLASSIFICATION OF ABSTRACT UNCLASSIFIED	20. LIMITATION OF ABSTRACT UL	